NRC FORM 464 Part I
(6-1998)

U.S. NUCLEAR REGULATORY COMMISSION

RESPONSE TO FREEDOM OF INFORMATION ACT (FOIA) / PRIVACY ACT (PA) REQUEST

FOIA/PA	RESPONSE NUMBER
2000-0321	1

RESPONSE TYPE ☑ FINAL ☐ PARTIAL

REQUESTER: Glen Mills

DATE: SEP 12 2000

PART I. – INFORMATION RELEASED

- ☐ No additional agency records subject to the request have been located.
- ☐ Requested records are available through another public distribution program. See Comments section.
- ☐ APPENDICES: Agency records subject to the request that are identified in the listed appendices are already available for public inspection and copying at the NRC Public Document Room.
- ☑ APPENDICES: A — Agency records subject to the request that are identified in the listed appendices are being made available for public inspection and copying at the NRC Public Document Room.
- ☐ Enclosed is information on how you may obtain access to and the charges for copying records located at the NRC Public Document Room, 2120 L Street, NW, Washington, DC.
- ☐ APPENDICES: Agency records subject to the request are enclosed.
- ☐ Records subject to the request that contain information originated by or of interest to another Federal agency have been referred to that agency (see comments section) for a disclosure determination and direct response to you.
- ☐ We are continuing to process your request.
- ☐ See Comments.

PART I.A – FEES

AMOUNT *: $ 22.40

* See comments for details

- ☑ You will be billed by NRC for the amount listed.
- ☐ You will receive a refund for the amount listed.
- ☐ None. Minimum fee threshold not met.
- ☐ Fees waived.

PART I.B – INFORMATION NOT LOCATED OR WITHHELD FROM DISCLOSURE

- ☐ No agency records subject to the request have been located.
- ☐ Certain information in the requested records is being withheld from disclosure pursuant to the exemptions described in and for the reasons stated in Part II.
- ☐ This determination may be appealed within 30 days by writing to the FOIA/PA Officer, U.S. Nuclear Regulatory Commission, Washington, DC 20555-0001. Clearly state on the envelope and in the letter that it is a "FOIA/PA Appeal."

PART I.C COMMENTS (Use attached Comments continuation page if required)

On September 6, 2000, you were notified that FOIA/PA-2000-0307 request was withdrawn by the requester. At that time you indicated your desire to obtain copies of the 2 records requested under FOIA/PA-2000-0307 and you agreed to duplication processing fees in the amount of $22.40.

SIGNATURE - FREEDOM OF INFORMATION ACT AND PRIVACY ACT OFFICER

for Carol Ann Reed J. Rennie Lira

Re: FOIA/PA-2000-0321

APPENDIX A
RECORDS BEING RELEASED IN THEIR ENTIRETY
(If copyrighted identify with *)

NO.	DATE	DESCRIPTION/(PAGE COUNT)
1.	05/29/96	Memorandum to James M. Taylor from David L. Morrison, Subject: Resolution of Generic Safety Issue 15, "Radiation Effects on Reactor Vessel Supports" (3 pages)
	06/22/94	Memorandum for John T. Larkins from Joseph A. Murphy, Subect: Proposed Resolution of GSI-15, "Radiation Effects on Reactor Pressure Vessel Supports" (3 pages) (Enclosures: 206 pages)

May 29, 1996

MEMORANDUM TO: James M. Taylor
Executive Director for Operations

FROM: David L. Morrison, Director /s/ DLMorrison
Office of Nuclear Regulatory Research

SUBJECT: RESOLUTION OF GENERIC SAFETY ISSUE 15, "RADIATION EFFECTS ON REACTOR VESSEL SUPPORTS"

The purpose of this memorandum is to document the resolution of Generic Safety Issue 15 (GSI-15) "Radiation Effects on Reactor Vessel Supports." GSI-15 was originally established to evaluate the effects of neutrons of energies between 0.1 and 1 Mev in addition to those of energies > 1 MeV. The issue was determined to have a LOW priority at that time because the occupational dose increases associated with this issue far outweighed the public risk reduction. The present concern arose later over the issue that neutron irradiation at low-temperature and low-flux might embrittle reactor pressure vessel (RPV) supports more rapidly than predicted based on traditional trend bands. This newer concern has been studied extensively, and the results are documented in NUREG-1509, "Radiation Effects to Reactor Vessel Supports" (in publication). The staff position is that the findings provide a sufficient basis for the resolution of GSI-15, both for the current and for the original concerns, and that no action need be taken by licensees concerning reactor vessel supports. NUREG-1509 will be distributed to licensees and CP holders, and will also be available through the NRC Public Document Room.

Background

The present concern for RPV support integrity arose when the Oak Ridge National Laboratory found that the High Flux Isotope Reactor (HFIR) surveillance data exhibited excessive embrittlement in an environment thought to be similar to operating reactor cavities. To evaluate the problem, GSI-15 was reprioritized to consider the issue of fracture resistance of RPV supports in operating plants and to determine if the structural integrity of the supports under Design Basis Accident conditions may have been compromised. The studies addressed embrittlement of structural steels of the type used to fabricate RPV supports exposed to low-flux, low-temperature conditions simulating the HFIR environment; dosimetry experiments to measure and characterize the HFIR neutron energy spectrum; studies of the neutron flux and spectrum in an operating reactor cavity; and structural analyses to determine the consequences of support failure. The work showed the unexpectedly high embrittlement in HFIR to be caused by a relatively high gamma radiation dose rather than a high thermal neutron dose as was originally postulated. Thus,

A-1

NRC FILE CENTER COPY

DF12 1/0
RES-2D-3

9606190081 960529
CF SUBJ
RES-2D-3 CF

the experimental evidence showed first, that the excessive embrittlement in the HFIR data could be attributed to long-term, low-temperature gamma radiation and second, because the HFIR gamma radiation environment is 100 to 3,000 times greater than that in an operating reactor cavity at the peak flux plane (vessel beltline), it is clear that the HFIR surveillance data are not directly applicable to RPV supports. Finally, based on the greater accuracy of the detailed neutron and gamma radiation calculations and dosimetry measurements, it could be shown that the radiation-induced embrittlement of RPV supports could be estimated from traditional trend curves and that the level of radiation-induced increase in embrittlement is not a cause for concern for continuing plant integrity, for either the 40-year life of currently operating plants or for a 20-year license renewal period. Furthermore, the original issue of embrittlement by neutrons of energies < 1 MeV was reconsidered in light of the findings of the present study. It was clearly determined that the present findings and conclusions encompass the original issue and that no unresolved technical issues remain in this area.

Issue Resolution

The analysis conducted for resolution of GSI-15 considered both the technical findings, included in NUREG-1509, and considerations of cost/benefit for a series of options (Reference 1). One of those options, for reevaluation of RPV supports and the taking of appropriate corrective action (if any), was seen to be justified only at one extreme of the cost/benefit ratios. While it was not clear how many plants would fit those conditions (although probably very few) the reevaluation option was not justified because the radiation embrittlement concern had been essentially eliminated.

Among the technical findings noted during work on GSI-15 was the fact that there would be significant variability among plants with respect to the issue because of the great variety of RPV support designs, material properties, and fuel management procedures that affect the neutron flux and spectrum in the cavity. In order to encompass the uncertainties in the various analyses and provide an overall, conservative assessment for this issue, several structural analyses were conducted. These demonstrated that (1) even if postulating one of four RPV supports were broken in a typical PWR, the remaining intact supports would carry the reactor vessel load even under SSE seismic loads and (2) if all supports were assumed to be totally removed (i.e., broken), the short span of piping between the vessel and the shield wall could carry the load of the vessel. In summary, analyses have virtually eliminated the concern for both radiation embrittlement and for significant structural consequences from a postulated RPV support failure.

The ACRS has reviewed the Staff's work on GSI-15 and agrees with the recommendation of no action to be taken (Reference 2).

Conclusion

With the issuance of NUREG-1509 and in consideration of the other referenced documents developed in this study, Generic Safety Issue 15 is considered resolved. For further information please contact Richard E. Johnson (301-415-6758).

References

1. N. R. Anderson, R. E. Lipinski and D. L. Kelly, "Supplement to Technical Report, EGG-SSRE-9458, Cost/Benefit Analysis of GSI-15:Radiation Effects on Reactor Vessel Supports," Lockheed Idaho Technologies Company, April 1995.

2. W. J. Lindblad to J. M. Taylor, "Proposed Resolution of Generic Safety Issue 15, 'Radiation Effects on Reactor Vessel Supports,'" July 13, 1994.

cc: J. Larkins, ACRS
W. Russell, NRR
B. Sheron, NRR
A. Thadani, NRR
J. Strosnider, NRR
J. Murphy, RES
F. Cherny, RES
N. Kadambi, RES
P. Norian, RES
M. Mayfield, RES
J. Vora, RES
A. Taboada, RES

DISTRIBUTION:
Central File
GSIB c/f
LCS r/f

DOCUMENT NAME:A:\GSI-15.CZS

To receive a copy of this document, indicate in the box: "C" = Copy without enclosures "E" = Copy with enclosures "N" = No copy

OFFICE	DET/EMCB	C	DET/EMCB	C	DET/GSIB		DET/DRA		RES/DD	
NAME	RJohnson:sf		MMayfield		CSerpan		[illegible]		[illegible]	
DATE	05/14/96		05/16/96		05/14/96		05/20/96		05/31/96	
OFFICE	NRR/D									
NAME	[illegible]									
DATE	06/ /96									

OFFICIAL RECORD COPY (RES File Code) RES 2D-3

JUN 22 1994

MEMORANDUM FOR: John T. Larkins, Executive Director
Advisory Committee on Reactor Safeguards

FROM: Joseph A. Murphy, Acting Director
Division of Safety Issue Resolution
Office of Nuclear Regulatory Research

SUBJECT: PROPOSED RESOLUTION OF GSI-15, "RADIATION EFFECTS ON REACTOR PRESSURE VESSEL SUPPORTS"

Enclosed for ACRS review is the proposed resolution package for Generic Safety Issue No. 15 (GSI-15), "Radiation Effects on Reactor Pressure Vessel Supports."

GSI-15 was reprioritized in December, 1988 and designated as a high priority issue. The reprioritization was done as a result of reviews by the ACRS and the NRC staff of data from surveillance specimens exposed in the HFIR reactor at the Oak Ridge National Laboratory (ORNL). The ACRS reviewed the data and the report by ORNL that the steel samples had exhibited more rapid than expected embrittlement. Noting that the environment in HFIR was sufficiently similar to the operating conditions at reactor pressure vessel (RPV) supports, the ACRS recommended revisiting GSI-15.

The concern regarding RPV support radiation embrittlement was initiated by Virginia Electric and Power Company (VEPCO) as a Part 21 notification in a March 28, 1978 letter to James O'Reilly (NRC). GSI-15 was established to address the concern that low-temperature, low energy neutron irradiation may embrittle RPV supports more rapidly than expected. The issue was originally classified as a candidate Unresolved Safety Issue (USI) in NUREG-0705. In that document it was recommended that further studies be conducted before making a decision regarding disposition of the issue. In November 1983, the issue was evaluated and designated as LOW priority.

After the high priority designation was established, a Task Action Plan was prepared to evaluate the possibility that RPV supports may be degraded and subject to failure in the event of a design basis accident. The investigation was designed to address the loss of integrity either from a loss of fracture toughness or an increase of the ductile-brittle transition temperature (commonly: NDT).

In the course of completing the program proposed in the GSI-15 Task Action Plan, several findings emerged which contributed to the technical resolution of the issue. The technical findings and results of the staff evaluations are documented in the Enclosed NUREG-XXXX and the staff's Regulatory Analysis. Based on the evaluation, the staff has concluded that the concern for radiation embrittlement of RPV supports is minimal and no regulatory action is required. However, some of the criteria which constitute conventional wisdom can be called to question and licensees should be advised of the GSI-15 findings by the vehicle of an NRC Information Notice (copy enclosed).

9407140032 940622
CF SUBJ CF
RES-5C-4

120101

NRC FILE CENTER COPY 05

A-2 DF02

RES-5C-4

The resolution of GSI-15 is being accomplished by issuing a close-out memorandum, a Regulatory Analysis and a NUREG. Because no action on the part of licensees is being required, NRR concurrence is not needed. However, RES has drafted an IN and NRR is being asked to issue it to all licensees. Because no new requirements are being proposed, the staff plans to send the proposed resolution package to the CRGR for information, only.

The ACRS will be advised as to the NRR position on the proposed resolution as soon as it is established.

ORIGINAL SIGNED BY

Joseph A. Murphy, Acting Director
Division of Safety Issue Resolution
Office of Nuclear Regulatory Research

Enclosures: See Jacket

1). Memorandum to James M. Taylor from Eric S. Beckjord, "Resolution of Generic Safety Issue 15, 'Radiation Effects on Reactor Vessel Supports'."

2). NUREG-XXXX, "Radiation Effects on Reactor Pressure Vessel Supports," Draft dated May __, 1994.

3). Regulatory Analysis, "Resolution of Generic Safety Issue No. 15, 'Radiation Effects on Reactor Vessel Supports'."

4). NRC Information Notice 94-XX: GENERIC SAFETY ISSUE RESOLUTION - RADIATION EFFECTS ON REACTOR VESSEL SUPPORTS.

5). NUREG/CR-6117, "Neutron Spectra at Different High Flux Isotope Reactor (HFIR) Pressure Vessel Surveillance Locations," Oak Ridge National Laboratory, December, 1993.

OFFICE	DSIR/EIB	DSIR/EIB	DSIR/EIB	AD:DSIR:RES
NAME	RJohnson:jf	FCherny	CZSerpan	JAMurphy
DATE	6/7/94	6/7/94	6/7/94	6/22/94

OFFICIAL RECORD COPY

RES No.: 5C-4

JUN 2 2 1994

DISTRIBUTION:
Central File
EIB c/f
C. Heltemes
J. Murphy
C. Serpan
F. Cherny
P. Cota, NRR
E. Igne, ACRS
R. Johnson, RES

[revision as of 5-2-94]

MEMORANDUM FOR: James M. Taylor
Executive Director for Operations

FROM: Eric S. Beckjord, Director
Office of Nuclear Regulatory Research

SUBJECT: RESOLUTION OF GENERIC SAFETY ISSUE 15, "RADIATION EFFECTS ON REACTOR VESSEL SUPPORTS"

The purpose of this memorandum is to summarize the resolution of the referenced generic safety issue.

Summary

Generic Safety Issue 15 (GSI-15) was established to evaluate the concern that low-temperature, low-flux neutron irradiation might embrittle reactor pressure vessel (RPV) supports more rapidly than predicted based on traditional trend bands. The RES staff has prepared a Regulatory Analysis (Enclosure 1) and concluded that a sufficient basis exists for the resolution of GSI-15. A proposed NRC Information Notice (IN 94-XX) and a supporting NUREG report (NUREG-XXXX, to be published) were forwarded to NRR for issuance to all holders of operating licenses and construction permits to inform them of the technical findings and resolution of GSI-15. IN 94-XX and NUREG-XXXX were issued to licensees and CP holders on _____ XX, 1994.

Background

The concern for RPV support integrity increased when the Oak Ridge National Laboratory found that the High Flux Isotope Reactor (HFIR) surveillance data exhibited excessive embrittlement in an environment thought to be similar to operating reactor cavities. To evaluate the problem, GSI-15 was activated to determine the variable fracture resistance of RPV supports in operating plants and the degree to which the structural integrity of the supports under Design Basis Accident conditions may have been compromised. Initially, the study addressed embrittlement of structural steels exposed to low-flux, low-temperature conditions. Dosimetry experiments aimed at measuring the HFIR neutron energy spectrum gave anomalous results; further work showed that the cause was a relatively high gamma radiation dose. From the experimental evidence, it was concluded that (1) the excessive embrittlement in the HFIR data can be attributed to long-term, low-temperature gamma radiation; and (2) because the HFIR radiation environment is significantly different from that in the cavity of an operating reactor, including the fact that the HFIR γ flux is about 3,000 times greater than the peak γ measurement at the beltline, the HFIR surveillance data do not represent RPV support embrittlement and the safety concern is minimal.

9407140046 940622
CF SUBJ
RES-5C-4 CF

In the work on GSI-15 it was found that some RPV support steels may have as-built transition temperatures so high as to leave essentially no margin for increase by irradiation. Also, other components which would have to carry higher loads in the event of RPV support failure may undergo some degradation, including: (1) primary coolant piping; (2) large snubbers supporting primary coolant lines; (3) steam generator and primary coolant pump supports (in PWRs); and (4) PWR steam generator tubing. The degradation mode will differ depending on the component but each, in its own way, may be vulnerable to failure in a Design Basis accident. Therefore it is prudent to ensure that there is adequate fracture resistance in the RPV supports, both for the current licensing period and for those plants contemplating future license renewal. It was suggested in IN 94-XX that reevaluation of RPV supports by licensees may be warranted to ensure that the strength and fracture resistance are adequate for all anticipated transients and Design Basis accident loadings.

The option of requiring licensees to reevaluate RPV supports and take indicated corrective actions was ruled out because such actions would not be cost-effective. In the course of resolving GSI-15, a detailed cost-benefit analysis was completed by INEL, the principal technical assistance contractor. Costs and benefits varied widely. Although reevaluation could be justified at one extreme of the cost/benefit ratio, the staff had insufficient information to decide how many plants would fit those conditions (probably very few) and with the radiation embrittlement concern largely eliminated, the requirement could not be justified.

Description of Resolution

The GSI-15 technical findings and cost/benefit analysis do not support a requirement that utilities reevaluate the integrity of their RPV supports. Information Notice 94-XX and the accompanying NUREG-XXXX were sent to all holders of licenses and construction permits transmitting that information and the bases for resolution of GSI-15. IN 94-XX notes that addressees who wish to avail themselves of the information in the notice can find in NUREG-XXXX an engineering approach and criteria for RPV support reevaluation accepted by the NRC. For example, by determining the NDT shift of the RPV support steels as a function of operating time, one can ensure that the NDT never exceeds the lowest support operating temperature. Such determinations would use the initial NDT and a shift calculated on the basis of dpa for the full neutron energy spectrum. Among the technical findings noted during work on GSI-15 was the fact that plants will not be equally vulnerable because of the great variety of RPV support designs and fuel management procedures. However, irradiation of RPV supports will continue at some rate so long as the plant operates. Although the massive pressure vessel effectively screens the supports from γ exposure, the neutron flux is significant. That is, neutron irradiation would be expected to induce some loss in fracture toughness but not nearly as much as the initial interpretation of the HFIR data suggested. Support reevaluation may be particularly important for cases of license renewal beyond the initial 40 years.

Conclusion

With the issuance of Information Notice 94-XX and NUREG-XXXX, along with the documents referenced therein, Generic Safety Issue 15 is considered resolved. For further information, please contact Richard E. Johnson (301-492-3909).

Eric S. Beckjord, Director
Office of Nuclear Regulatory Research

ENCLOSURE:
REGULATORY ANALYSIS - Resolution of Generic Safety Issue No. 15, "Radiation Effects on Reactor Vessel Supports"

cc: W. Russell, NRR
B. Sheron, NRR
A. Thadani, NRR
J. Strosnider, NRR
C. Heltemes, RES
T. Speis, RES
J. Murphy, RES
C. Serpan, RES
F. Cherny, RES
N. Kadambi, RES
P. Norian, RES
M. Mayfield, RES
A. Taboada, RES
R. Johnson, RES

Received w/Ltr Dated 6/22/94

[DRAFT AS OF 6/22/94]

NUREG - XXXX

"RADIATION EFFECTS ON REACTOR PRESSURE VESSEL SUPPORTS" (GSI-15)

R. E. Johnson

R. E. Lipinski

RES-5C-4

TABLE OF CONTENTS

1. ABSTRACT
2. LIST OF ACRONYMS AND INITIALISMS
3. EXECUTIVE SUMMARY
4. INTRODUCTION
5. BACKGROUND:
   5a. General Discussion: Effects of Irradiation on Structural Steels
   5b. Stone & Webster Notification
   5c. Summary of NUREG/CR-5320
6. TECHNICAL FINDINGS FROM THE GSI-15 TASK ACTION PLAN
   6a. Review of Initial Analyses
   6b. Shippingport Neutron Shield Tank Testing
   6c. Trojan Dosimetry
   6d. Lo-E Neutron Damage Theory
   6e. HFIR Dosimetry and Gamma Radiation
7. RPV SUPPORT REEVALUATION CRITERIA
   7.a Overview
   7.b Screening criteria
      7.b.1 Configuration
      7.b.2 Materials
      7.b.3 Stresses
      7.b.4 Screening Criteria
   7.c Criteria for Reevaluation
      7.c.1 Evaluation of Current Conditions
      7.c.2 Physical Examination of Structural Elements
      7.c.3 Evaluation of the Original Design
      7.c.4 Establishing the EOL NDT Temperature
      7.c.5 Fracture Analysis of RPV Support Integrity
         7.c.5.a Fracture Toughness Approach
         7.c.5.b Transition Temperature Approach
   7.d Accurate Analysis
   7.e Structural Consequence Analysis
   7.g Illustrative Examples
   7.f Fracture Mechanics Evaluation of Pins
8. SUMMARY OF THE COST/BENEFIT ANALYSIS
9. DISCUSSION OF THE GSI-15 TECHNICAL FINDINGS
10. CONCLUSIONS
11. REFERENCES

LIST OF TABLES

Table 6-1 Summary of Analyses Related to GSI-15
Table 7-1 Compilation of NDT Temperature Results
Table 7-2 Minimum Fracture Toughness Data
Table 7-3 Classification of Wrought Grades
Table 8-1 Sensitivity Analysis Results

LIST OF FIGURES

Figure 5-1 Radial Section Through Trojan Reactor Vessel
Figure 6-1 Change of NDT Temperature as a Function of dpa
Figure 7-1 Screening Criteria
Figure 7-2 Preliminary Information
Figure 7-3 Fracture Mechanics Approach
Figure 7-4 Transition Temperature Approach
Figure 7-5 Structural Consequence Analysis

LIST OF APPENDICES: Authors and topics.

A. R. E. Gregg, et al., GSI-15 cost-benefit analysis.
B. C. A. Hrabal, BNL flux calculations; Shippingport NST.
C. E. D. McGarry, Trojan cavity dosimetry.
D. R. E. Johnson, aging embrittlement of stainless steel.
E. E. H. Ottewitte, gamma radiation effects.

ACKNOWLEDGEMENTS

The authors are pleased to recognize the many people who have been gracious in their help, support, or both in the resolution of Generic Safety Issue No. 15. Naming every contributor would take too much space; the following are cited for the special reasons given.

F. B. K. Kam, the Principal Investigator of the Technical Assistance Contract at the Oak Ridge National Laboratory, led the effort which provided the basis for resolution of the issue with a commendable efficiency of time and money. In addition to many others at ORNL, the helpful support of Dr. R. Nanstad and W. Corwin is appreciated. The invaluable outside nucleonics consultants were: Professor John Williams, Dr. Larry Greenwood and Mr. E. D. McGarry.

Thanks to the NRC staff who participated in the work including A. Taboada, M. Mayfield, T. Walker, J. Mitchell, S. Weiss and special thanks to C. Hrabal for his critical assistance. We wish to note that R. Baer, who served as Branch Chief through the early days of confounding findings, never strayed from offering support and constructive criticism. In the same vein, N. Anderson at INEL actively participated as a manager, advisor and contributor.

The support and encouragement of the NRC management, including W. Minners (ret.), J. Murphy, C. Serpan and F. Cherny is gratefully acknowledged.

1. ABSTRACT
The NRC Generic Safety Issue No. 15, (GSI-15), "Radiation Effects on Reactor Pressure Vessel Supports," was established to evaluate the concern that low-temperature, low-flux-level neutron irradiation might embrittle reactor pressure vessel supports to a significant degree and compromise plant safety.

Evaluation of the surveillance samples from the High Flux Isotope Reactor (HFIR) at the Oak Ridge National Laboratory (ORNL) led to the conclusion that the embrittlement rates of some materials used for pressurized water reactor pressure vessel (RPV) supports could be higher than expected. This disclosure raised a concern that a brittle fracture of the RPV supports could occur during the anticipated life-span of the plant. Tests of specimens from the Shippingport plant neutron shield tank (NST) failed to confirm the HFIR results.

A later study by the ORNL demonstrated that gamma radiation contributed a significant amount of the embrittlement in the HFIR surveillance specimens. However, the shielding provided by the thick steel shell of the RPV ensures that degradation of RPV supports from gamma irradiation is improbable or minimal. There is a residual concern because some of the RPV supports were constructed of steel which may have rather high nil ductility transition (NDT) temperatures so close to the minimum operating temperature as to leave essentially no margin for increase from irradiation.

This report (1) describes in some detail the technical findings resulting from the work done in accord with the GSI-15 Task Action Plan and (2) was used, in part, as the basis for technical resolution of the issue.

2. LIST OF ACRONYMS AND INITIALISMS

ACRS	Advisory Committee on Reactor Safety
AIF	Atomic Industrial Forum
AISC	American Institute of Steel Construction
AOSC	Averted on-site costs
ASME	American Society of Mechanical Engineers
ASME Code	ASME Boiler & Pressure Vessel Code, Section III, Division 1
ASTM	American Society of Testing and Materials
BNL	Brookhaven National Laboratory
BOL	beginning of life
BTC	Bolting Technology Council
CMTR	Certified Material Test Report
CP	Construction Permit
CRGR	Committee for Review of Generic Requirements
CSDS	chemical shutdown system
CVN	Charpy V-notch
dpa	displacements per atom
ECCS	emergency core cooling system
EFPY	effective-full-power-years
EOL	end-of-life
EPRI	Electric Power Research Institute
GSI	Generic Safety Issue
GL	Generic Letter
HFIR	High Flux Isotope Reactor
HSST	Heavy Section Steel Technology
HSLA	high-strength low-alloy (steel)
INEL	Idaho National Engineering Laboratory
LBLOCA	large break loss-of-coolant accident
LOCA	loss of coolant accident
LST	lowest service temperature
MPC	Materials Properties Council
MTR	materials test reactor
NDT	nil-ductility-transition
NRC	Nuclear Regulatory Commission
NRR	Office of Nuclear Reactor Regulation (NRC)
NSSS	Nuclear Steam Supply System
OBE	operating basis earthquake
ORNL	Oak Ridge National Laboratory
ORR	Oak Ridge (test) Reactor
RCL	reactor coolant loop
RCP	reactor coolant pump
RCS	reactor coolant system
RES/DSIR	Office of Nuclear Regulatory Research/Division of Safety Issue Resolution
RPS	reactor protection system
RPV	reactor pressure vessel
SBLOCA	small break loss-of-coolant accident
SCC	stress-corrosion cracking
SG	steam generator
SRP	Standard Review Plan
SRSS	square-root-sum-of-squares

SSE safe shutdown earthquake
VEPCO Virginia Electric Power Company

3. EXECUTIVE SUMMARY

Generic Safety Issue No. 15, (GSI-15), "Radiation Effects on Reactor Pressure Vessel Supports," addresses the potential for embrittlement of reactor pressure vessel (RPV) supports from exposure to low-temperature, low-flux-level neutron radiation. The initial action came in 1978 as a Part 21 notification by Virginia Power (at the time: VEPCO) that radiation might reduce the integrity of the supports to a significant degree and compromise plant safety. Although the potential for embrittlement was confirmed, GSI-15 was assigned a LOW priority. The issue was revitalized after ORNL reported unexpectedly high measured ΔNDT from HFIR surveillance specimens. GSI-15 was reprioritized and assigned a HIGH ranking. A Task Action Plan was prepared to evaluate the possibility that RPV supports may be degraded and subject to failure in the event of a design basis accident. The investigation was designed to address the loss of integrity using either the fracture toughness reduction or the NDT increase (relative to the lowest operating temperature).

In the course of completing the program proposed in the GSI-15 Task Action Plan, several findings emerged which contributed to the technical resolution of the issue. At the start of the program, the RPV supports at the Trojan plant had been identified as the most vulnerable to degradation. That conclusion achieved consensus approval. Several analyses were done with the expectation that if the Trojan supports could be shown to be acceptable the result would envelope the industry. Different engineering approaches and various degrees of sophistication were employed by the analysts. Although some confidence was drawn from the analyses to the extent that the issue did not appear to pose a serious safety threat, the results showed that there was no single method, applicable to all reactors, by which GSI-15 could be resolved.

Concurrently, efforts were made to explain the post-irradiation irregularities seen in the HFIR surveillance data by conducting other radiation experiments. Archival material (the identical steel used to construct the HFIR pressure vessel) was irradiated in test reactors along with samples of other, related, steels. The observed ΔNDTs were not significantly different from the trend band for low-temperature irradiation. Thus the steel tested in the HFIR surveillance program was not the cause of the irregularity. The availability of the neutron shield tank (NST) from the Shippingport plant afforded the opportunity to test the same grade of steel (ASTM A 212-B) as that used in the HFIR vessel after exposure to similar radiation conditions (low neutron flux and low temperature). These data, too, did not differ much from the trend band leading one to look to the conditions in the HFIR for the solution.

One seemingly important variant in the HFIR environment was the reported fifty-to-one ratio of thermal to fast neutron flux. Acting on that, with the help of models advanced by theoreticians at two National Laboratories (ANL and PNL), a new damage parameter was devised. It was a modification of the displacements per atom (dpa) parameter to include neutrons of all energies, not just those with $E > 1$ MeV. Replotting the HFIR data as functions of "dpa mod" brought most of the relevant embrittlement data within a reasonably narrow scatter band along the line of the established trend curve.

The proof of the efficacy of the "dpa mod" exposure parameter, however, was limited by the fact that the HFIR neutron energy spectrum had been determined at a single location (at a capsule containing A 212-B steel). Calculations were made for several other capsule locations but the results added more confusion than resolution. To condense the report to a minimum, the new spectrum calculations found the 50-to-1 energy ratio in error by (roughly) a factor of ten. That is, the thermal-to-fast neutron ratio was revised to the order of 5-to-1. An experiment was designed to unravel the findings but it further muddied the water: the dosimeters exhibited a variation by as much as a factor of 17 in the fast neutron flux.

When checks of the measurements ruled out experimental error, a comprehensive program of experiments and calculations was launched. The project was conducted by a team drawn from the NRC, ORNL and outside consultants from national laboratories, academia and industry. The results of the effort provided enough evidence to suggest reasons for the greater than expected HFIR surveillance data and for the dosimetry discrepancies noted above.

Key factors behind the reasons for the discrepancies are: (1) the annulus of water in the HFIR attenuates neutrons but does little to gamma radiation; (2) γ radiation will result in atomic displacements (hence: embrittlement) but will do more heating than damage; (3) because the HFIR specimens were kept at a low temperature (about 50°C or 120°F), the damage done by γ (and low-energy neutrons) was retained; and (4) because the high-energy neutron flux was so low, it took a long time (about 20 years) to accumulate a significant level of neutron fluence of $E > 1.0$ MeV. Therefore, it is suggested that the embrittlement of the HFIR surveillance specimens is a summation of the neutron flux (over the entire energy spectrum) and the γ radiation. The reported variation in fast neutron flux values among the several dosimeters occurred because those monitors sensitive to photofission or photoneutron reactions exhibited additional radioactivity induced by the significant level of γ flux.

The radiation environment in the HFIR was judged to be unique to that reactor. The RPV supports of an operating reactor are shielded from γ radiation by the six to ten inches of steel interposed by the vessel shell. Therefore, no significant γ radiation embrittlement is expected in RPV supports. Embrittlement predictions should employ the complete dpa parameter to include any contribution from low-energy neutrons.

Limited surveys of RPV supports conducted in response to the unexpectedly high HFIR embrittlement data noted that data often were too sketchy to be definitive. For some (older) reactors, the margin between the lowest operating temperature and the RPV support NDT may be so small that little, if any, margin for radiation-induced increases is available. Under such conditions, it would be prudent to perform an engineering reassessment of the RPV support integrity and evaluate any potential threat to safety.

When work began on GSI-15, it was expected that evaluation of (at least some) RPV supports would be necessary so a detailed engineering approach for assessing the structural integrity was developed. For cases wherein it is prudent to reassess the integrity of the RPV supports, the methods reported in this paper should provide adequate guidance. The approach begins with

screening criteria, continues (for those cases where it is necessary) with fracture resistance evaluation and provides a consequence analysis model for situations wherein there is insufficient data to complete a fracture analysis. Application of the consequence analysis to the Trojan plant configuration (believed to be the most vulnerable) showed that RPV support failure could be tolerated providing that other components were not degraded. Analyses demonstrated the importance of the components which would have to carry additional loads in the event of RPV support failure but some critical components have exhibited other, unique, degradation mechanisms.

One of the tasks in reaching the resolution of GSI-15 was to do a detailed cost-benefit analysis. The resulting best estimate base case led to a total calculated contribution to core damage frequency from RPV support failure of 8.8×10^{-5}/yr. Five alternative corrective measures were identified and cost estimates were made. The estimated costs varied widely. Cost-benefit ratios were calculated for a range of remaining life spans and for three cost categories: (1) without either AOSC or replacement power; (2) with AOSC but without replacement power; and (3) with both AOSC and replacement power. Benefit analysis associated with the above core damage frequency resulted in an offsite dose risk per plant of 2.9 person-rem/year. The influence on the cost-benefit ratio of variability in several parameters was investigated. The resulting cost-benefit ratios ranged from a minimum of $53/person-rem to a maximum of $3,300,000/person-rem.

The wide variability in the analysis results rendered them inconclusive and the staff could not use them to support a regulatory requirement for GSI-15. However, licensees may decide that if the integrity of their RPV supports is suspect, a reevaluation would be prudent, following the technical findings presented in this report.

4. INTRODUCTION

The reactor pressure vessel (RPV) support embrittlement problem was noted in a letter to the NRC from the Virginia Electric and Power Company (VEPCO) dated March 3, 1978, submitted in accordance with the reporting requirements of 10 CFR 21. In a letter dated March 28, 1978, VEPCO explained that the issue dealt with the low-temperature irradiation of the neutron shield tanks that support the RPV. Consideration of the effects of low energy ($E << 1.0$ MeV) neutrons might result in a large shift in the ductile-to-brittle fracture mode transition temperature.

The issue of accelerated degradation of the fracture toughness of RPV supports was revitalized by the ACRS as a result of their review of the HFIR data. The unexpectedly high ΔNDT measured by HFIR material surveillance specimens was attributed initially to a rate effect. If this were the case, certain RPV supports could be susceptible to the same phenomena. Generic Safety Issue 15 (GSI-15) was activated to investigate the possibility that some RPV supports may be subject to failure in the event of certain design basis accidents. An investigation was initiated under the assumption that the loss of fracture toughness was greater than originally believed and that the NDT could be as high as the lowest operating temperature.

Following review by the ACRS and the NRC staff, the issue of embrittlement of RPV supports (GSI-15) was re-prioritized resulting in the assignment of high priority. INEL was selected to provide technical assistance in the resolution of this issue. Review of Reference 1 disclosed that there is a need for additional information regarding the configuration of various RPV supports in order to identify those supports that are exposed to significant radiation.

It was found that the HFIR data were not good predictors of the extent of degradation of RPV supports due to neutron bombardment. Consequently, other ways of predicting support degradation were sought. Many RPV supports are constructed of material which has a wide range of properties due to the loose specifications. For example, there is evidence that the NDT of steel which meets the ASTM Specification A-36 will vary considerably.

This document contains twelve sections, the more extensive of which are further divided into subsections to facilitate quick location of specific topics. The following, Section 5, provides a background to GSI-15. Section 6 presents the technical findings resulting from the work done in accord with the Task Action Plan (TAP)[2*]. Section 7 describes RPV support reevaluation criteria that could be used by licensees in a structural integrity assessment. Section 8 contains a summary of the Cost/Benefit Analysis; Section 9 is a general discussion

* Small superscripts refer to references listed in Section 11.

of the technical findings presented in Sections 6 and 7. Section 10 contains the conclusions reached and justifications for them. Some of the completed work that was used to support the conclusions is provided in Appendices.

5. BACKGROUND

Generic Safety Issue-15 (GSI-15) "Radiation Effects on Reactor Vessel Supports" was established to address the concern that low-temperature, low energy neutron irradiation may embrittle RPV supports more rapidly than expected.

The concern regarding nil-ductility transition (NDT) temperature shift was reported by Virginia Electric and Power Company (VEPCO) as early as March 28, 1978 in a letter to James O'Reilly (NRC). In that letter VEPCO informed NRC that they are evaluating the NDT temperature shift of neutron tank and NRC will be informed about the results when they are available.

The issue was originally classified as a candidate Unresolved Safety Issue (USI) in NUREG-0705.[3] In that document it was recommended that further studies be conducted before making a decision regarding disposition of the issue. In November 1983, the issue was evaluated and designated as LOW priority.

In June 1987, the Advisory Committee on Reactor Safeguards (ACRS) reviewed the ORNL data from tests on the pressure vessel surveillance specimens exposed in the High Flux Isotope Reactor (HFIR)[1]. The conclusion reached by ORNL was that the more rapid than expected embrittlement was due to low-temperature (~120°F) low-flux irradiation (10^8-10^9 n/cm^2-sec.; E > 1 MeV). From the HFIR data, ORNL predicted more rapid than expected embrittlement in steel from low-temperature neutron irradiation[4]. Since the environmental service conditions of RPV supports were believed to be similar to those at the HFIR surveillance locations, a concern was raised regarding the rate of support embrittlement. Based on the ORNL findings, the staff reassessed the issue and in December, 1988 designated it as HIGH priority.

A survey of all operating reactors was conducted by ORNL under the Heavy Section Steel Technology (HSST) program to identify the RPV supports which might be vulnerable to embrittlement. The study, reported in NUREG/CR-5320,[4] led to the selection of two plants, by virtue of their configuration, for further study: Trojan and Turkey Point Unit 3. The selections were based on RPV support design details; both consisted of short steel columns bearing on steel cantilever beams, embedded in the concrete shield wall at the core beltline and projecting into the cavity towards the reactor vessel (Fig. 1). The configuration induces tensile stresses in the upper flange of the beam where the neutron flux is greatest; conditions conducive to brittle fracture. The ORNL investigators concluded that the minimum critical flaw sizes corresponding to the most severe credible loading condition at 32 EFPY could be small enough to be of concern for both plants.

On January 11, 1989, the Office of Nuclear Reactor Regulation (NRR) requested that the Office of Nuclear Regulatory Research (RES) initiate a program which would (1) provide a structural consequence analysis of RPV support failure; (2) perform a probabilistic fracture mechanics risk analysis of the limiting

RPV supports; and (3) gather pertinent metallurgical and mechanical information, performing tests if necessary, to demonstrate the capability of flawed RPV supports to satisfy regulatory requirements.

On March 23, 1989 at the joint Materials and Metallurgy/Structural Engineering ACRS Subcommittees Meeting, and at the full ACRS Meeting on April 6, 1989 presentations by the staff indicated that further work was needed to quantify the structural integrity of the RPV supports. The preliminary analyses available at the time failed to demonstrate that there was an immediate safety problem. Several analyses of the impact of various degrees of damage to the Trojan plant RPV supports were described and reviewed in Reference 5. A brief summary of the analyses is provided in Section 6. It should be noted that all analysts accepted the assertion that the two plants cited by ORNL, Trojan and Turkey Point Unit 3, had the most vulnerable RPV supports.

5a. General Discussion: Effects of Irradiation on Structural Steels
The initial ORNL studies[1] indicated that low-temperature, low-flux neutron irradiation may embrittle steel more rapidly than traditional trend bands would predict. The data were generated in the ORNL HFIR RPV irradiation surveillance program. ORNL concluded that the steel samples were embrittled faster than expected. Since it was believed that RPV supports were exposed to an environment similar to that at the HFIR surveillance capsules, the possibility and consequence of RPV support embrittlement needed to be considered.

Generally, an NDT temperature shift is an accepted indicator of neutron radiation damage. The NDT temperature is the temperature below which commonly observed flaws may be critical with regard
to brittle fracture initiation. The traditional procedure for predicting neutron damage uses the shift (increase) in NDT temperature expressed as a function of fast neutron fluence, i.e., neutrons having energies > 1.0 Mev. More recently, it has been noted that this method is not comprehensive because it does not include reactions from the entire neutron energy spectrum. For example, there are some neutron-atom interactions in which neutrons are absorbed leading to transmutation and attendant atomic displacements. On the other hand, some neutrons may not interact at all. As a result, the amount of damage

FIGURE 1. RADIAL SECTION THROUGH TROJAN REACTOR VESSEL SUPPORTS

(embrittlement) for a given fluence may vary with the neutron spectrum.

A more accurate method of predicting neutron damage relies on the calculated displacements per atom (dpa). The dpa parameter is an estimate of the number of atomic displacements (vacancy-interstitial pairs) per atom produced by neutron irradiation. Shortcomings in neutron damage predictions based on the dpa parameter arise because it only counts the number of radiation-induced displacements. In fact, some displaced atoms and vacancies will recombine, annihilating (annealing) the damage related to the point defects. The modified dpa parameter[6], discussed in some detail in a later section, accounts for a broader base of atomic-level damage.

Both fluence and dpa, as measures of radiation damage, must be accompanied in practice by dosimetry calculations or measurements and experimental determinations of the related NDT shift.

5b. Stone & Webster Notification

Sometime in late 1977, Stone and Webster Engineering Corporation (S&W) approached the Virginia Electric and Power Company (known at the time as "Vepco") with a potential irradiation embrittlement problem related to the North Anna Units 3 and 4 neutron shield tanks (NSTs). At North Anna and plants of similar design the NST is the RPV support. S&W, the NST designer, had concluded that there might be a shift in the NDT temperature to a higher value than previously expected. On February 27, 1978, Vepco made a report to the NRC under the provisions of 10 CFR 50.55(a) citing the concern for the effect of radiation on the NDT of the NSTs. In Vepco letter Serial No.117 to the NRC Region II Director, dated March 3, 1978, information regarding the deficiency was submitted in accord with the provisions of 10 CFR 21. Vepco letter Serial No. 117A, dated March 28, 1978 a 30-day report on the potential embrittlement problem.

The possibility of a larger than expected ΔNDT of the NST steel was based on state-of-the-art developments in predicting neutron embrittlement by employing damage cross-sections derived for materials with similar irradiation damage behavior to the tank material. The neutron embrittlement calculational method used had been developed at the U.S. Naval Research Laboratory by C. Z. Serpan, Jr. (now, as then, with the NRC). Neutron energy groups with less than 1.0 MeV were considered in addition to the fast neutrons. Attenuation resulted in an abundance of neutrons in the range $0.1 < E < 1.0$ MeV at the NST. Although the low energy neutrons did not create much damage individually, collectively they made an appreciable contribution which was taken as additive to that from the fast neutrons. Because the NST was the support for the reactor vessel and was a QA Category I piece of equipment, Vepco reckoned that it had to be capable of maintaining the intended functional integrity. On those grounds, Vepco concluded that the ΔNDT of the NST steel must be determined over the life of the plant to allow a proper evaluation of the integrity of the tank(s).

Briefly, the following actions were taken apropos of the licensee's notification. Vepco advised that the analysis of the shield tank ΔNDT would continue with the help of outside consultants. On June 23, 1978 members of the NRC staff met with S&W representatives; NRL personnel also attended by NRC

invitation. It was agreed that no immediate action was necessary on the part of any licensee, in large measure because actions were planned or underway which were expected to shed more light on the problem. For one thing, an experiment was underway designed to resolve the shield tank material problem by irradiating RPV support materials in a facility at ORNL which would simulate the environment in the cavity of an operating reactor (it turned out that the experiment did not meet its goals, as noted below). Also, the NRC staff planned to review the S&W neutron flux determinations and to evaluate the applicability of the damage analysis to other supports. This action took shape by, initially, adding the RPV support problem as a new and separate Task to the Unresolved Safety Issue (USI) A-12, which at the time covered all structural support problems. Within that Task, the staff selected Brookhaven National Laboratory (BNL) to provide technical assistance by independently verifying the reactor flux spectrum at the NST. Meanwhile, Vepco had noticed that the neutron flux data had been based on the wrong core geometry, had contracted with Babcock and Wilcox (B&W) to perform an updated study, and had notified the NRC of the revised results. BNL submitted a letter report dated April 23, 1979, with the results from the calculations of energy dependent neutron fluxes at the North Anna 3 and 4 NSTs. The report was in substantial agreement with the B&W results with the minor differences largely explained by differences in the energy-group structures employed. If anything, the BNL results suggested that B&W's analysis was conservative.

Faced with a problem which loomed larger, rather than going away, by virtue of the more precise calculations, the staff turned to the NRL as consultant on the effect of irradiation on A 537-B steel, the material used to fabricate the North Anna NSTs. Fortunately, the NRL had recently concluded low-temperature irradiation of A 537-B steel so the relatively easy task of accounting for the differences in flux and spectra could be handled through dpa correlations. In a letter report dated October 22, 1979, it was concluded that for the Vepco NSTs conditions at EOL, irradiation might raise the NDT to more than 105°F and might reduce the Charpy V-notch upper shelf energy to as low as 30 ft-lb.

The sum total of the evidence at hand led to the conclusion that radiation embrittlement of RPV supports posed a clear and significant threat to the overall integrity of domestic nuclear power plants. The staff recommended that the problem be addressed as a separate generic issue. The recommendation was acted on and GSI-15 was instituted.

5c. Summary of NUREG/CR-5320

The results of the ORNL investigation suggested that the damage to RPV supports from irradiation may be a significant threat to the structural integrity of light water reactors (LWRs). The data obtained from the HFIR irradiation surveillance program were interpreted as an indication that at low temperature and low flux, the embrittlement rates of steels for vessels and supports were substantially higher than previously observed. The materials used in the investigation were ASTM A 212-B, A 350-LF3, and A 105-II. The ORNL researchers established two correlation trend lines of NDT temperature shift as a function of dpa, one on log-log and one on semi-logarithmic coordinates, using data from other published reports. In both cases a curve parallel to the trend line was drawn through selected HFIR data and extrapolated to higher exposures. To the extent that the curves drawn through

the HFIR data was physically meaningful, extrapolations suggested that typical EOL exposures would result in rather large NDT increases.

The more rapid rate of embrittlement of the RPV support material was attributed to a so called "fluence-rate effect" i.e., theorizing that low energy flux causes more irradiation damage than the high energy flux. This hypothesis was contradicted (Reference 7) based on data that showed no rate effect in the fast (E > 1.0 MeV) flux range of $1x10^{10}$ to $3x10^{13}$ $n/cm^2.s$ at approximately 200°F, but the ORNL researchers disregarded that report in suggesting a rate effect rationale.

The study concluded that there is a credible possibility of a brittle fracture in RPV supports and the estimated critical flaw could be as small as 0.42 in. with small break loss-of-coolant accident (SBLOCA) loads. Also, the report noted that residual stresses from flame-cutting during construction could further reduce the critical flaw size.

The ORNL project was terminated without providing satisfactory answers to some critical questions. First, the HFIR surveillance data fell outside of the trend band established by other sources such as data from MTR radiation experiments. The ORNL investigators suggested that the large increase in NDT temperature was related to a fluence-rate effect although there are data that show no rate effect for a similar fast flux range. Second, although it was suggested that the excess embrittlement of the HFIR samples was the result of thermal-neutron radiation rather than a fluence rate effect, the idea was not exploited. Finally, although the mechanical property test results were thoroughly audited, insufficient attention was given to the dosimetry and verification of the radiation exposure, as later work under GSI-15 has shown.

6. TECHNICAL FINDINGS FROM THE GSI-15 TASK ACTION PLAN

This section contains summaries of the technical findings from the tasks in the program undertaken to resolve Generic Safety Issue-15.

6.a Review of Initial Analyses

As previously noted (Section 5), the report by ORNL of unexpected embrittlement motivated several analysts to examine the case for RPV supports. Some of that work was discussed at ACRS meetings. One of the first tasks undertaken in the effort to resolve GSI-15 was to review those analyses for commonalities and differences. That review was described in detail in Reference 5. A brief overview is provided in this section.

Eleven structural analyses of RPV support integrity have been reported. All of them evaluated the RPV supports of the Trojan Plant; one (NUREG/CR 5320, Reference 4) also evaluated Turkey Point Unit 3. Only two of the Trojan structural analyses considered radiation embrittlement. The other analyses focused on failure consequences, i.e., how the RPV and the RCS would be impacted by failure of one or more supports. The salient features of the analyses are described below and summarized in Table 1.

Note that the two reports that dealt with radiation embrittlement used fast neutron (E > 1.0 MeV) fluence as the measure of neutron exposure. Later in this report it will be shown that the high-energy neutron fluence may be

insufficient to predict radiation damage sustained at relatively low temperatures, depending on the nature of the radiation.

Two distinctly different approaches were used by those analyzing the RPV supports. One involved postulated catastrophic failure of one or more supports and prediction of the consequences of such an occurrence. The second involved examination of stresses and radiation embrittlement as the bases for predicting the possibility of a brittle fracture. It is difficult to decide which analysis is more accurate on the basis of the information presented in the reports. The complexity of the problem requires considerable engineering judgement regarding the efficacy of the liner, the possibility of the concrete support being crushed, and the possibility of shear failure of the concrete above the remaining portion of the beam.

The consequence analyses (the first group) were based on generally accepted methods. They employed recognized principles of structural mechanics, such as beams on elastic foundations or finite element analysis. However, in spite of similar assumptions, the results differed considerably. The discrepancies illustrate the sensitivity of the analyses to

Table 1 Summary of Analyses Related to GSI-15

assumptions and methodologies used. The analysis reported by BNL used information drawn from the sophisticated finite element results in the ORNL report (Reference 4). The BNL report concluded that the capacity of the fractured beam is lower than the applied load, and the beam will deform until it reaches equilibrium through load redistribution to other supports.

The following comments are in order regarding the validity of the structural consequence analysis performed by the Lawrence Livermore National Laboratory[8].

1. The analysis did not combine the dynamic loads such as SSE and LOCA which constitutes a deviation from the Standard Review Plan (SRP), Section 3.9.3, Table 1[9].
2. The consequence analysis did not consider thermal aging of cast austenitic-ferritic (duplex) stainless steels that are used for primary coolant piping in some PWRs. Those that contain significant amounts of delta ferrite may exhibit low temperature aging embrittlement.
3. The consequence analysis considered one component at a time but in reality several components may be affected simultaneously and a cumulative/interactive effect should be accounted for.

It is possible that an analysis which took cumulative effects of all the above items into consideration might indicate that the consequences of RPV support failure are more serious than what was reported.

The analytical methods used in the second group were equally complicated. Fracture mechanics is a newcomer in design and many of its methods are not codified, leaving analysts considerable freedom of choice. Compounding that uncertainty in the solution to the problem were several factors capable of profoundly affecting the results. For example, the mechanical properties, chemical composition and metallurgical condition of structural steels may vary widely from heat to heat, and frequently are not known with much certainty. Also, the location, size and orientation of flaws often can only be postulated or approximated at best. For such reasons, variability is almost certain.

Both approaches have advantages and disadvantages. Although the "postulated failure" approach rests on proven engineering theories, it depends greatly on assumptions that must reflect real conditions and on models that must predict the behavior of the structure. On the other hand, although fracture mechanics has been proven to be a rather precise method for predicting brittle fracture, complicated structures may be difficult to model and mixed-mode (elastic-plastic) fractures, common in low-strength steels, demand sophisticated material property data and a measure of judgement. It follows that in today's state of the art there is no one reliable method by which GSI-15 could be resolved.

6b. Shippingport Neutron Shield Tank Testing

Some related work pertinent to resolution of GSI-15 was performed by ANL[10]. The program was undertaken to augment the HFIR surveillance data. The goal was to test a steel similar to one of those in the HFIR program to determine the NDT shift after irradiation under similar conditions, i. e.: low neutron flux and low temperature. The results were expected to provide a comparison with both the HFIR and test reactor data thereby helping to resolve questions related to the influence of fluence rate or energy spectrum on radiation

embrittlement. The ANL investigation involved testing of specimens machined from samples of the neutron shield tank (NST) from the decommissioned Shippingport reactor to characterize the radiation-induced embrittlement. The NST was made from hot-rolled A 212 Grade B steel. The reported inner wall exposure was a (maximum) fluence of approximately 6 x 10^{17} n/cm^2 (E > 1 MeV) over a life of 9.25 EFPY while operating at about 55°C (130°F). Reference 10 indicated that the radiation embrittlement of the Shippingport NST A 212-B steel was not as severe as that reported for the HFIR surveillance samples, that they were in good agreement with the available data for irradiation at temperatures < 232°C (< 450°F), and that they are in agreement with data from MTRs and Army reactors.

The ANL investigators concluded that the accelerated embrittlement of the HFIR surveillance samples probably reflected the high proportion of thermal neutrons compared to that for the test reactors.

6.c. Trojan Dosimetry

The point has been made in preceding sections that all parties concerned (the NRC staff, contractors, consultants and industry representatives) were in general agreement that the Trojan plant presented the best case for RPV support embrittlement. The conclusion was supported by the fact that there were strucural elements at the reactor beltline under tensile loading with flame-cut holes at the maximum moment (peak tensile stress) made of steel of questionable ancestory. It was expected that by showing the RPV supports at Trojan to be certifiably safe, the rest of the industry would be acceptable. One parameter in such an analysis for which there were no data was the radiation flux at the supports. A program, under the guidance of the Materials Engineering Branch, Engineering Division, RES(NRC), was set in place to obtain dosimetry data in the Trojan reactor cavity. The results are discussed in greater detail in Appendix C.

Radiometric and solid state track recorder (SSTR) dosimeters were prepared under subcontract by the Westinghouse Electric Corporation. Four sets were placed in vertical access channels in the concrete biological shield at Trojan in 1990 prior to operating cycle 13. After 242 days of operation, the cycle ended on March 4, 1991. The location of the dosimeter trains is of some importance. The plant was designed with vertical channels in the concrtete structure to provide access to horizontal insturmentation ports. The radial location of the vertical channels was close enough to that of the flame-cut holes in the box beam flanges to make the measurements directly applicable.

Each of the four sets of dosimeters included the following. The radiometric dosimeters consisted of foils of ^{238}U, Ni, Ti, Cu and two Co-Al alloy foils; the SSTR neutron dosimeters consisted of ultra low-mass fissionable deposits of ^{235}U, ^{237}Np, and ^{238}U in contact with mica SSTRs. Additionally, bead chain flux gradient dosimeters were inserted at two locations. At the time it was expected that Trojan would continue to operate for several years.
After withdrawl from the Trojan channels, the dosimeters were shipped to the Westinghouse Waltz Mill facility for disassembly, measurement and analysis. The results of that effort were reported in Reference 11. From the measurements, a total of 52 reaction rates were obtained which had uncertainties in the 3 to 5% range. Selected ^{235}U, ^{237}Np, and ^{238}U fissionable

deposits were irradiated in standard neutron fields by NIST to benchmark the fissionable deposit mass scales. After correcting the fissionable deposit mass scales to the NIST results and setting aside the data from one of the four capsules (found to be slightly discrepant; no reason uncovered), the ratio of SSTR to radiometric fision rates exhibited an average value of 0.999 (±3.1%).

With the intention of being able to accrue exposure to neutrons over two fuel cycles, a few Charpy specimens were attached to the dosimeter trains. Because the plant did not continue to operate, the specimens were only exposed to ex-vessel radiation for one fuel cycle. The reported fluence (E > 1.0 MeV) was 10^{16} nvt. The set of specimens included A 212 and A 36 steels; the unirradiated A 36 results showed a great deal of scatter. ORNL reported that there was essentially no NDT shift which is expected for that exposure.

6.d Low Energy Neutron Damage Theory

As previously mentioned, the ORNL report[4] on the test results from the HFIR steel vessel surveillance specimens attributed the excessive NDT temperature shift to a neutron fluence-rate effect. Brief mention was made of the idea that low-energy neutrons (epithermal and thermal) may have made a significant contribution to the observed embrittlement. Citing the results of multigroup transport calculations, the document put the thermal-to-fast neutron ratio at about 50-to-one. Even granting that the average amount of damage from each low energy neutron is a small fraction of that from a fast neutron, the greater abundance would contribute to the embrittlement. That is, radiation by a neutron flux skewed strongly to the low energy end would result in more total damage than a traditional trend curve would predict. Actual conditions are complicated because the low energy neutron micromechanisms are not the same as those for fast neutrons (principally: elastic scattering). To name one example, a low energy neutron can be captured by an iron nucleus which will in time transmute to a manganese atom. The resulting energetic recoil of the manganese atom will cause damage which may contribute to embrittlement.

Low-energy neutron damage considerations by Heinisch and Greenwood led to theoretical models and a reexamination of the HFIR data by Hrabal[6]. Modified damage parameters were used to develop new correlations between radiation-induced mechanical property changes and exposure. Development of the modified damage parameters involved rather sophisticated procedures which took into account the recombination of point defects following displacement thereby taking the parameter dpa to a more physically correct level. The best results came from Greenwood's application to damage calculations of a recombination model developed by Weidersich at the Argonne National laboratory (ANL). Hrabal used the model to calculate modified values of dpa (hereinafter: "dpa mod") from revised inputs into the computer code SPECTER[12]. Neutron spectra, applicable to the specific irradiated mechanical property data surveyed, were obtained from several sources associated with the experiments.

The task resulted in the diverse data collapsing (with typical scatter) onto a single trend curve. Specifically, the data set included: HFIR surveillance results; HFIR archival A 212B steel data (irradiated in the Oak Ridge Reactor); and the initial Shippingport NST results (reported by ANL).

Although the HFIR and ORR data represented the same plate of steel, the NST steel was unrelated except for the common ASTM specification.

The analysis was expanded to include other steels; the result was that despite differences in chemistry and metallurgical condition, the data stayed reasonably close to a single trend band of property change as a function of dpa mod. Also, the A 212B data represented a range in neutron flux of a factor of 40,000 (from 2.4×10^8 to 9.6×10^{12} $n/cm^2 \cdot s$) which certainly failed to support a suggestion that the excessive embrittlement of the HFIR steel was a manifestation of a neutron fluence-rate effect.

There is another set of data which added some interesting, if not convincing, information to this task. The results of an irradiation experiment were reported in Reference 13. The purpose was to examine the effect of irradiation on several RPV support steels in conditions designed to simulate the reactor cavity environment. Eight different materials were encapsulated; irradiation was in the ORNL poolside facility. Early in the 1.6-year irradiation period, the capsule filled with water but it was not discovered until the irradiation was complete. Because the fluence target value of 5×10^{17} n/cm^2 ($E > 1$ MeV) was not reached, the authors found the results to be inconclusive. If close attention is paid to the data, however, the eight materials provide the following observations. The six wrought steels exhibited ΔNDT values of zero, i. e., the unirradiated and irradiated Charpy curves essentially superimposed. One set of Charpy specimens, representing weld heat-affected material, showed too much scatter to allow interpretation. One set of specimens, taken from a bulk weldment, showed both a shift in the NDT temperature and a decrease in the upper shelf energy. The weld metal chemical analysis reported 3.39 % Ni which was more than the nickel content of any of the other steels. We note that Odette has found that the sensitivity of steel to neutron radiation increases with the Ni content. Because the influx of water only attenuated the neutrons, shifting the distribution to the low energy region of the spectrum, it was interesting to include the data in the dpa mod analysis. Of course, six points fall on the abscissa (ΔNDT = 0.0) and contribute nothing but the high Ni weld metal lends itself to the review and was included with the other data.

Because the *dpa mod* parameter seemed to normalize the disparate data, it was thought that the HFIR problem was a matter of accumulating damage from low energy neutrons. In fact, the staff was in the process of preparing the documents for resolution of GSI-15 on that basis when confirmatory data, reviewed below, showed that the thermal-to-fast neutron ratio in HFIR was not the 50-to-1 value initially reported. Although dpa mod did not serve to resolve GSI-15, it is true that low energy neutrons will induce some damage in steel. With irradiation (or: service) temperatures below 200°F, even the relatively short-range lattice disruptions will be retained. Therefore, the low-energy neutron fluence should be included in damage predictions if accuracy is of some importance.

6.e HFIR Dosimetry and Gamma Radiation

Although the early results from application of a low-energy neutron damage theory by re-analysis of the HFIR surveillance data using the dpa mod parameter appeared to resolve the problem of the exceptionally high NDT shift, it was based on very limited data. To elaborate, the only location for which there were neutron spectrum data was for a capsule which had contained A 212 steel. To rectify that situation, the staff requested that ORNL calculate the neutron spectrum at other surveillance capsule locations, especially for those that held specimens of other grades of steel. The work was done under a change of scope order to the HSST Program. After some delays related to changes in both hardware and software at ORNL, the results indicated that the previously-reported ratio of low-to-high energy neutrons was nowhere near 50-to-one. The calculated ratio varied from 3 to 8, approximately, i.e., about one-tenth of the initial ratio.

The next stage of the investigation was dictated by the desire to resolve the question of the physically correct neutron energy spectrum by state-of-the-art dosimetry. At the request of the NRC, ORNL inserted dosimeters in the HFIR. Although this experiment was meant to follow generally accepted procedures for neutron spectra determination, the experiment (identified as "DOS1" by ORNL[14]) created a temporarily unexplained outcome. Fast neutron (E > 1 MeV) flux measurements from the activity of Np and Be monitors resulted in values approximately 17 times and 15 times, respectively, higher than the flux values derived from the Ni monitors. When careful checks of the measurements ruled out experimental errors, a comprehensive experimental program was initiated as a new, separate, contract.

The program went forward in two steps, identified as the DOS2 AND DOS3 experiments. In the DOS2 experiment the dosimeters were "bare" within the capsules whereas in the DOS3 experiment they were clad with a 4-mil Gd cover to attenuate the thermal neutron flux and prevent interference with the response of the monitors. The scope of the project consisted of neutron and gamma transport calculations, dosimetry measurements, and least-squares logarithmic adjustments of the transport calculations and dosimetry measurements to obtain optimum neutron spectra estimates. Gamma dosimeters were furnished and (after irradiation in the HFIR) counted by NIST. The γ measurements verified that the calculated gamma field deduced from 1-D neutron and γ transport calculations was adequate to determine the γ contribution to fast fission and Be radiometric monitors.

There is a relatively minor correction to Reference 14 that should be noted for those interested in precision of radiometric measurements and transport calculations. The report states that the measured value of γ dose rate was 36.4 Gy/s and that was compared to a calculated value of 36.6 Gy/s*. Because readers might miss the point, made in an appendix, the measured value should be corrected downward by about 20%. The reason for the adjustment is that the investigator at NIST converted the measured change in optical absorption in polychlorostyrene on the basis of a 20°C irradiation temperature whereas the temperature in HIFR was nominally 50°C. This fact was uncovered after the program reached completion and although the report had not been published, the calculations had been completed. Because the correction would require considerably more work to redo all of the neutron/gamma unfolding and to redo

all of the affected tables, whereas the correction was within the measurement uncertainty, the figures were allowed to stand.

The project was conducted by a team of NRC reviewers, ORNL investigators and outside consultants from national laboratories, academia and industry. Several major findings were reached.

- Discrepancies in fast neutron flux values from various monitors irradiated in the DOS1 experiment were shown to be related to photofission and photoneutron reactions in certain monitors.

- Because photo-induced reactions dominate in the Be and fast threshold fission dosimeters, those monitors are good candidates for measuring the γ dose in some radiation fields.
- Neutron flux gradients within the dimensions of the surveillance capsules in the HFIR were not consistent being nearly flat at some locations and steep at others.
- The stainless steel monitors, located in the V-notch of the Charpy specimens in the HFIR surveillance program, were shown to be adequate for fast neutron (E > 1 MeV) flux measurements.
- In HFIR, at the one location where measurements permitted the calculation to be made, the total γ dpa was about five times higher than the neutron dpa.
- The feasibility of the application of simultaneous adjustment of neutron and γ fluxes was demonstrated and although the finding had little impact on this program, the methodology would be extremely useful in future work.

Going well beyond the scope of the program reported in Reference 14, with the experimental and calculational results obtained in the DOS1, DOS2 and DOS3 programs, the mechanical property measurements from the HFIR surveillance tests can be related to dpa based on total neutron <u>and</u> gamma fluxes. It is found that the embrittlement measured as ΔNDT, previously judged excessive, falls on the same trend band as other results, Fig. 6-1. We tentatively conclude that the deviation of the HFIR data from the correlation established from experiments done under traditional conditions (e.g., in a materials test reactor) was a manifestation of the relatively large gamma radiation and the fact that the steel could retain the damage from that source because of the low (< 200°F) temperature during irradiation. The conclusion is "tentative" because it is not supported by any independent (of the HFIR surveillance results) data. Nor is it likely that the HFIR conditions will be repeated soon because one of the necessary conditions is that the γ flux be moderate, otherwise there will be so much heat generated that the submicroscopic damage

*See the NOTE on γ radiation at the end of this Chapter.

will be simultaneously annealed. That is why it took on the order of twenty years to accumulate the embrittlement reported. At the same time, of course, the concurrent neutron flux must be relatively low to avoid the annealing or annihilation from elastic collision spikes. The water annulus of about 20 inches in HFIR created just such a set of conditions; the neutrons were attenuated so that the energy spectrum was skewed to the low energy side while the gamma flux at a level typical of a nuclear reactor passed through essentially unaffected.

With respect to the RPV of an operating LWR, there are additional important mitigating factors. First, the RPV is irradiated while at a temperature of about 550°F. At that temperature, the diffusivity of steel is high enough that most of the short-range submicroscopic damage will be annealed within a few months, if not in a few weeks. Second, vessels provide shielding of not less than six, up to ten, inches of steel for the supports. That is more than enough to reduce the γ flux by several decades. Consider reported γ radiation measurements (References 15-a and -b) made in cavities of operating reactors. The B&W experiment was conducted at a plant where low-leakage core management was in effect. The recommended beltline γ flux value was 45 Gy/hr. From Reference 14, the measured γ flux in HFIR was 36.4 Gy/s, or 131,040 Gy/hr. Comparing the two values:

$$131{,}040 \text{ Gy/hr (HFIR)}/45 \text{ Gy/hr(plant)} = 2912 \simeq 3000,$$

showing the efficacy of the RPV as a shield. The Westinghouse cavity γ flux measurements were made at a 3-loop plant which had not instituted low-leakage fuel management procedures. The reported (Reference 15-b) results were 40,000 to 150,000 rad/hr (100 rad = 1 Grey). For this case we calculate the ratio in Gy/hr of the HFIR γ flux to the peak operating reactor value as:

$$131.040/1500 = 87.36 \simeq 100.$$

The calculated ratios showed: (1) that the γ flux in cavities of operating reactors is much less than that in HFIR and (2) low-leakage cores will reduce the cavity γ flux thus affording additional protection from damage to the RPV supports. Exposure to such small measured γ radiation as reported in References 15, a and b, should not induce a significant increase in embrittlement (i.e., in ΔNDT) of the RPV supports beyond that resulting from neutron irradiation.

<u>NOTE on Gamma Radiation.</u>

Gamma flux can be reported in units of Gy/sec, where Gy stands for "Greys." 1 Gy = 1 joule/ kg., the joule being the unit of work or energy, the same as ft.-lb. in English units. Since 1 joule/sec = 1 watt (unit of power), it follows that
1 Gy/sec = 1 watt/kg. That relationship points to the most common result of γ radiation: creation of heat in the body being irradiated. For a <u>SLAB</u> configuration at steady state (the surfaces maintained at constant temperature), gamma radiation induces a thermal gradient:

$$\Delta T_{max} = 1 \times 10^{-12} \phi_{\gamma} [\ \ldots\ ] \quad {}^{\circ}K \cdot cm^2 \cdot sec,$$

where: [...] is a factor incorporating physical parameters;
ϕ is in $\gamma/cm^2 \cdot sec$.

The γ flux in the equation for slab heating is expressed in dimensions similar to the common dimensions for neutron flux, i.e.: $n/cm^2 \cdot sec$, making neutron fluence n/cm^2. Another common way of expressing neutron flux is as "nvt"

where: n = neutron density, n/cm^3;
v = velocity, cm/sec;
t = time, sec.

Performing the indicated operations will result in n/cm^2. Although this Note shows some similarities in neutron and γ representations, the equivalence in damage (to steel) involves more complicated considerations of the physics of the two types of radiation including the relative damage cross-sections, the relative efficiencies of lattice displacements and the relative radiation energy spectra. Those subjects are beyond the scope of this paper.

Fig. 6-1. The change in transition temperature as a function of total radiation (neutrons plus gammas) dpa.

7. RPV SUPPORT REEVALUATION CRITERIA

7.a Overview

As a result of recent data obtained from tests of surveillance specimens representative of RPV support materials, exposed to low temperature, low flux radiation, NRC became concerned that RPV supports may be experiencing considerably more rapid embrittlement than was considered in the original support design. The data were reported in NUREG/CR 5320[4].

Licensees may wish to reassess the structural integrity of their RPV supports. This Section provides an engineering approach, including screening criteria and technical evaluation procedures, which licensees and CP holders may take as guidelines acceptable to the NRC.

The object of developing screening criteria was to identify those RPV supports which, because of their configuration, material properties, or stress level, should be free from excessive radiation embrittlement or failure under accident loading. The Criteria for Reevaluation of Reactor Pressure Vessel Supports were designed to assist licensees and CP holders by offering several alternatives for RPV support evaluation. The Criteria were augmented by flow charts and associated notes which contain specific references and acceptance criteria. Examples, one with only membrane stresses and another with both direct tension and bending, were provided to further facilitate the analysis. Combined shear and tension also was addressed.

The Criteria contain many of the provisions of the ASME Boiler and Pressure Vessel Code (ASME Code), Sections III and XI[16,17]. This material has been included in the Criteria in spite of the fact that the ASME Code has been developed for the RPV and the RPV design criteria are different from those for the supports. It is thought, however, that since the principles of fracture mechanics apply equally well to the RPV and its supports and the Criteria are offered as guidance rather than as specifications, ASME Code requirements could be incorporated profitably.

7.b Screening criteria

Reactor pressure vessel supports should be screened sequentially for evaluation, as illustrated in Figure 7-1. The procedure is designed so that vulnerability of the supports may be assessed by a process of elimination of those supports for which embrittlement does not present a problem by virtue of their configuration or state of stresses. The most vulnerable supports are considered to be those which are exposed to a relatively high fluence, which may cause a large increase in NDT temperature, have high initial NDT temperature, and have tensile stresses. Figure 7-1 illustrates that these elements are the essential criteria for screening of the RPV supports.

To achieve a useful screening evaluation, reliable and accurate information is necessary in the indicated areas of Figure 7-1. The information may be obtained from the construction and fabrication records if such records are available. According to the ASME Boiler and Pressure Vessel Code, Section III, Subsection NCA, General Requirements, such records should be maintained and be made available by licensees. Lacking information on material composition and mechanical properties, some testing may be necessary.

7.b.1 Configuration

Configuration of the supports is an important item, because it indicates if supports or support members are likely to receive the amount of radiation necessary to accelerate embrittlement. This is why it is the first item in Figure 1 to be evaluated. If the review of "as built" design drawings indicates that the supports are located in an area where irradiation is low then embrittlement due to radiation is not an issue. For example, RPVs mounted on skirts may fall in that category. Supports of other configurations also may be eliminated using the same criterion provided that low exposure to radiation is demonstrated and the initial NDT temperature is sufficiently low.

7.b.2 Materials

Materials of construction of RPV supports are also very important, because some compositions may be so sensitive to radiation that even a very low fluence may cause enough embrittlement to make brittle fracture a possibility. The NDT temperature shift will vary depending on the metallurgical condition and the chemistry of the steel (especially the copper and phosphorus content). For these reasons information pertaining to the materials used in construction of the RPV supports should be collected and analyzed. Should reliable information on the material be unavailable, some testing may be necessary.

7.b.3 Stresses

For brittle fracture to occur, it is necessary that a tensile stress be present. Following the recommendations of the ASME Code, the threshold below which NRC staff considers that brittle fracture is unlikely is 6 ksi*. However, a fracture is most likely to be triggered by an event such as a loss-of-coolant accident (LOCA) or an earthquake. Both of these events produce sudden, dynamic stresses. Also, the shift in NDT temperature is related to the rate of load application. Consequently, strain-rate should be accounted for, the load-rate should be specified, and an explanation should be provided as to how the

*The stress of 6.0 ksi was used in the Portland General Electic Co. report, "Trojan Nuclear Plant Reactor Vessel Support Design Basis and Evaluation Summary," October 24, 1988. By private communication between R. Lipinski (INEL) and B. Elliot (NRC) on October 10, 1989 it was confirmed as being in accordance with the current NRC policy.

load rates are used in the analysis. Furthermore, residual stresses resulting from fabrication processes should be considered additive to the operational stresses. Thus they may have a pronounced effect on the overall state of stress. This is specially important wherever there are heavy welds. Although post-weld stress relieving should reduce the magnitude of residual stresses, there are indications that the reduction is only partial. The residual stress orientation and the manner of inclusion in the analysis should be specified and documented.

Finally, the cumulative effect of the chemical composition of the material, the fluence effect, and the stresses should be considered in the screening criteria and the decision making rationale for the screening should be provided in accordance with the guidance outlined in Section 7.c.1.b of this document.

7.b.4 Screening Criteria

If the initial NDT of the RPV supports is well below the lowest operating temperature, and if the radiation exposure at the supports is low, and if it

can be demonstrated that the tensile stresses are less than 6 ksi, the supports should be free from radiation embrittlement, the integrity may be reasonably assured and no further investigation is required.

7.c Criteria for Reevaluation

The RPV support reevaluation process can be divided into several distinct steps as illustrated on the flow charts (Figures 7-A, 7-B, 7-C, and 7-D). A structural integrity reevaluation should include all RPV support Design Basis loading combinations as documented in the plant FSAR (for licensees) or PSAR (for CP holders).

Step One (Fig 7-A), involves an assessment of the existing condition of the supports at the time of reevaluation, comparison with the initial construction condition, and the degree of degradation predicted by the end of plant life. The assessment includes a mandatory, visual, physical condition inspection of the vital parts of the supports. Rust, cracks, or permanent deformation of any part of the RPV support should be noted as evidence that some distress has been sustained. Limited accessibility may preclude some or all of the examinations; if so, the supports should be examined by remote means. There must be assurance that the supports have not been physically degraded to such an extent that the parameters important to load carrying capacity, such as cross-sectional area, section modulus, etc., have changed substantially. If significant degradation is observed, it should be recorded and remedial measures seriously considered.

Another part of Step One is a review of the original design and safety margin. The review should include the original design methodology, the load combinations for which the supports were designed, allowable stresses and their margins with respect to the actual stresses in the members, and the codes governing the original design. If brittle fracture avoidance was part of the original design, the review should include the criteria and methodology used, sources of information, and the bases for the conclusions reached. If the codes governing the original design are different from those currently promulgated, to the extent that they are currently accepted by the NRC, the difference, if any, between the original design margin and that which would be achieved from design in accord with the current codes and standards should be determined. This information will be useful if and when one of the subsequent options is selected. Upon completing Step One, the information obtained and the conclusions reached regarding the structural integrity of RPV supports should be documented and retained.

If the RPV support assessment according to Step One fails to confirm that there is adequate fracture resistance, Step Two can be followed. As shown in Figure 7- A, the Step One path can lead to one of two alternative approaches (See Figs. 7-B, and 7-C). Details that augment specific steps in the assessment approaches are provided in the Notes which accompany each Step Two path.

1. The more certain assessment would be based on a fracture mechanics analysis aimed at showing an acceptable factor of safety between the calculated stress intensity factor, K_I, and the material toughness, K_{Ic} (Fig. 7-B). Material properties, including a K_{Ic} value applicble to the given material, temperature and radiation exposure, must be known with

some accuracy or must be conservative handbook values. Equivalently, the fracture mechanics evaluation can utilize the maximum credible flaw size (either estimated, known from related destructive evaluation, or determined by nondestructive examination) which must be less than the calculated critical flaw size by at least the same (relative) margin as would be acceptable in the K_I-to-K_{Ic} comparison.

OR

2. The assessment can be based on a transition temperature analysis wherein it is sufficient to demonstrate that there is an adequate margin between the lowest operating temperature and the NDT temperature for EOL conditions (Fig. 7-C).

The details of the assessment, especially the factor of safety resulting from the analysis, should be adequately documented.

Step Three, a more exact reevaluation, can be taken if the Step Two results fail to provide an acceptable margin against support failure. The more exact analysis can include an elastic-plastic approach and a more detailed model. A lower stress level may result and, other things being equal, a larger flaw may be tolerated. The goal is the same as before: to demonstrate that the RPV supports are not vulnerable to failure.

If the Step Three analysis cannot be done or if the results are inconclusive, a Structural Consequence Analysis can be performed (described in Section 7.e). The Consequence Analysis assumes RPV support failure with the loads shed by the supports transferred to the reactor coolant loop (RCL) piping and supports.

7.c.1 Evaluation of the Current Conditions

7.c.1.a Physical examination of structural components.
For brittle fracture to occur in the structural steels used in RPV supports, there must be significant tensile stress. Accordingly, the structural elements which should be examined with the utmost scrutiny are the ones loaded in tension. Members such as cantilever beams, brackets, hangers, and bolts fall in this category.

Physical examination of the RPV supports is an essential part of the re-evaluation. As mentioned before, the purpose of the examination is to detect visible signs of degradation of the supports, such as rust, permanent deformation of the members, corrosion, cracks, etc.

Sometimes the reactor cavity dimensions provide insfficient space for personnel to access the part being examined. If so, the examination must be done using remotely manipulated equipment. Inspections should be performed by trained and experienced personnel who are cognizant of the function of the parts, familiar with the plant, and capable of making judgements regarding the importance of any degradation. Short resumés of the inspection team members citing the education and experience of each should be provided with the inspection report (below).

7.c.1.b Inspection report.

An accurate reporting program is an essential part of the structural evaluation, ensuring the correct and efficient assessment of current conditions. An inspection report will be necessary; in many cases it may be the only basis for deciding on maintenance priorities, criteria for replacement, structural capacity, and/or replacement versus repair of supports. Consequently, the importance of the reporting system cannot be over-emphasized. The success of any RPV support inspection is dependent in great measure upon its reporting system.

The RPV support inspection report should present a systematic evaluation of the current condition of the supports as well as observations and predictions of their possible future weaknesses. To accomplish this the following approach is recommended:

a. Conduct a thorough study of all available historical information on the structure including design, "as built" drawings, and records of previous inspections.

b. Plan, organize and establish a system for recording information on the actual conditions of the supports including an organized and detailed notebook, standard forms, sketches, etc.

c. Evaluate the findings of the inspection team. This task should be delegated to experienced engineers capable of exercising judgement regarding the degree of degradation of the RPV supports. Collectively, they should have sound knowledge of key disciplines such as structural mechanics, materials, and construction practices.

d. Provide a narrative summary of the report including: an assessment of the overall condition of the structure, expert opinions on "as is" conditions, and recommendations regarding repair or replacement.

The Inspection Report should be included in the Reactor Pressure Vessel Support Evaluation Report and should provide sufficient detail to serve as the basis for decisions regarding further actions to be taken if any, i.e: that the support is acceptable as is, or that modifications should be considered.

7.c.2 Evaluation of the Original Design

Some older nuclear plants were designed to codes and standards that are significantly different from the current ones. Many of the presently-used standards were non-existent at the advent of some original designs; others have changed over time. To utilize the foundations of present-day techniques, it is necessary that the original design evaluation be based on current criteria and knowledge.

Typically, the analysis should be based on the loads developed for the specific type of nuclear-steam-supply-system (NSSS), which can be obtained either from the vendor or by a thermo-hydraulic analysis. The structural components must be capable of carrying the imposed loads. The structural design criteria for the RPV supports are included in the current issue of the Standard Review Plan (SRP)[9], augmented by the Boiler and Pressure Vessel Code, Section III[16], as appropriate. The structural analysis should address the most adverse loading conditions, including seismic, in accordance with the criteria of Regulatory Guides 1.60 and 1.61. Combining of dynamic responses should be done in conformance with the provisions of NUREG-0484, Rev. 1[18].

Original design evaluations should account for known or estimated residual stresses. Because residual stress levels vary with fabrication processes, welding procedures, and other construction details, it is important that such information be included in the analysis and be recorded in the final report. Residual stress calculations should use state-of-the-art techniques; several of which are presently available. Frequently, they employ a finite element model with required inputs of the thermal history, thermal properties of the material, Poisson's ratio and details regarding the welding process. A description of a computational model which can be used for weld-induced residual stress is contained in Reference 19.

Stress concentrations from details such as discontinuities, holes, etc., should be taken into account in establishing the state of stresses.

Having determined the stresses at the critical locations of the support system, an evaluation of the original design can be made. Structural acceptance criteria and allowable stresses can be found in Section 3.8.3, "Concrete and Steel Internal Structures of Steel or concrete Containments" of Reference 9 and Subsection NF, "Requirements for Component Supports" of Reference 16.

7.c.3 Establishing the EOL NDT Temperature

The ductile-to-brittle fracture mode transition temperature (commonly: the NDT temperature) of steel is one of the essential parameters in brittle fracture analysis. Following the ASME Code, it may be defined as the highest temperature for fracture of a standard drop-weight specimen when tested to ASTM Standard Test Method E 208-87a[20]. The NDT also can be based on the temperature at which Charpy V-notch specimens absorb a specified amount of energy. To determine the EOL NDT temperature it is necessary to know the initial, material-dependent, NDT and the anticipated shift (increase) as a function of radiation exposure.

Strain - Rate Effects It can be shown[4] that the NDT in steels such as ASTM A 36 is sensitive to the rate of load application. Since the most adverse RPV support loads may occur during an earthquake or a LOCA, strain rates associated with the dynamic loading should be addressed. Equations acceptable for this purpose are available in the current literature.[21] If the NDT was determined in accordance with Reference 20 or an equivalent procedure, no further adjustment for dynamic effects is necessary.

Metallurgical Condition of the RPV Supports Certain alloying elements, such as copper, influence the rate of radiation embrittlement. Hence, it is important that the chemical composition of the steel be known in establishing radiation effects on RPV supports. Although quantitative relationships between radiation embrittlement and alloying additions or impurities is still under development, some progress has been reported. An equation to calculate the maximum embrittlement as a function of copper content can be found in Reference 22. Also, a very informative discussion on the subject can be found in Reference 23.

Radiation-Induced NDT Shift Relationships between dpa and ΔNDT from irradiation are shown in Figure 6-1. The graph was taken from reported NRC work; further information on dpa is available in Reference 14. Figure 6-1 can be used in RPV support reevaluation using the transition temperature approach.

7.c.4 Fracture Analysis of RPV Support Integrity

If brittle fracture avoidance was not considered in the original design, two options are offered as Step Two, either of which may suffice to ensure that the RPV support system is not vulnerable to brittle fracture. On the other hand, if the original design accounted for brittle fracture, using the currently accepted or equivalent criteria, no further action is necessary.

7.c.4 a. Fracture toughness approach (Fig. 7-B)

It was pointed out in Section 7.a that the Reevaluation Criteria contain provisions from References 16 and 17 which were intended for higher operating temperatures (~550°F) than those for the RPV supports (90 - 120°F). However, the methodology taken from the Code and presented here is applicable for RPV support analyses provided that conservative relationships are used.

The fracture toughness approach requires measurement of the material fracture toughness, K_{Ic}, or determination of the critical flaw size, a_c. The sharp crack stress intensity factor, K_I, must be calculated; the methodology can be based on Appendix A, Article 3000, "Acceptance Standards for Flaw Indications" of Reference 17. The assumed reference flaw size may be as specified in Table IWB-3510-1 of Reference 17 if the material of the supports satisfies the limitations stated in Appendix G, Article G-2000 "Vessels" of Reference 16. Assuming that the RPV support stresses are known, the acceptance criteria may be based either on the allowable stress intensity factor or on the postulated flaw size using the above references. In either case they should comply with the requirements of Article 3000 "Acceptance Standards for Flaw Indications" of Reference 17. If the material toughness cannot be positively defined, a factor of safety should be defined on the basis of K_{IR} rather than K_{Ic}, K_{IR} being defined as in Appendix G, Article G-2000, "Vessels" of Reference 16. For the purpose of these criteria, the temperature (term "T" used in Article G-2000 of Reference 16) is defined as the temperature at the point under the most adverse loading conditions. RPV support evaluation using the fracture toughness approach is illustrated by the examples provided in Section 7.g.

7.c.4.b Transition temperature approach

The transition temperature approach is based on the proposition that catastrophic failure by brittle (cleavage) fracture can be avoided by maintaining the RPV support service temperature above the NDT temperature of the steel. When using the transition temperature to evaluate the support integrity, the NDT temperature at EOL should include the irradiation-induced shift. Uncertainties related to NDT determinations demand that a margin of safety be maintained between the LST and the NDT temperature such as provided in Figure 5 as a function of component thickness. Demonstration that the RPV supports are in conformance with this relationship is necessary and sufficient to preclude failure of RPV supports by brittle fracture.

7.d. Accurate Analysis

If the reevaluation as described above failed to show adequate RPV support integrity (fracture resistance), a more accurate analysis, Step Three, may be

performed. To demonstrate that the structural integrity of RPV supports is not violated, structural and thermal-hydraulic loads may be recalculated more accurately and that may result in lower stresses. Because of the inverse-square-root relationship between stress and flaw size, a decrease in stress will result in a larger critical flaw size. The analysis should comply with the current licensing criteria, design codes, and regulatory requirements.

The fluid thrust forces may be based on a model of the actual NSSS system of the plant or on the simplified methodology presented in Reference 24.

The initial NDT temperature of the RPV support material should be evaluated in accord with Fig. 6-1. The radiation-induced ΔNDT should be calculated in accord with Figure 4. Flux profiles used in the irradiation embrittlement estimate should include the zones above and below the active core. The parameter dpa should cover the full neutron energy spectrum, not just E > 1 MeV. Irradiation damage should be estimated from the upper bound correlation curve from Fig. 4.

The structural analysis should satisfy the following conditions:

1. Allowable stresses may be based on one of the following methods: (1) use a value specified in the codes and specifications approved by the NRC, (2) determine an average value from tests of samples taken from the supports, or (3) use the records of the material producer, if such are available. Certified Material Test Reports, described in Reference 16, can serve in the third method.
2. The analysis should address the simultaneous application of vertical, tangential, and radial loads to supports.
3. The load combinations that produce the maximum tensile stresses should be included in the analysis.
4. The analytical model should be developed in sufficient detail to permit quantitative definition of all significant tensile stresses. Local stresses due to (1) transfer of loads between support structure elements, (2) load line offsets within the structural members, and (3) structure discontinuities and stress concentrations must be included in the analysis.
5. Residual stresses and thermal effects should be included in the analysis.
6. The assembly preload of threaded fasteners should be included in the analysis.
7. The support loading definition should include an estimate of loading frequency (cycles/sec.) for major dynamic loads.
8. The scope of the RPV support structure analytical model should include transmission of the vessel support loads from the point of interaction with the reactor vessel to the point(s) where the load transfer to the interfacing concrete structure is complete.
9. Elastic-plastic properties of the support material may be factored into the analysis but the pertinent provisions of References 9 and 16 should be satisfied.

7.e Structural Consequence Analysis.

If the RPV support analysis, because of insufficient, or lack of, information or other reasons, is inconclusive, integrity may be assessed by performing a

structural consequence analysis. The structural consequence analysis reported by LLNL[8] should be useful as guidance in setting out to do such a task. However, the approach used by LLNL was to assume RPV support failure and focus the analysis on determining the capability of the reactor coolant loop (RCL) piping to transfer the loads shed by the RPV supports to the remaining reactor coolant system (RCS) supports. Also, LLNL examined the capacity of the RCS components and their supports to resist these loads, and examined the effects of RPV support failure on the RCL system (i.e., RPV, reactor coolant pump [RCP], steam generator [SG], and safety injection lines). With certain qualifications, the analysis concluded that the failure of Trojan RPV supports would not result in consequences of safety concern. Reference 8 can provide guidance for a similar assessment of RPV supports provided that the critical comments listed in Section 6 are addressed.

The LLNL evaluation considered two load combinations:

1. Dead load + operating pressure + SSE, and
2. Dead load + operating temperature + LOCA

Both load combinations are designated as Level D Service Limits in the ASME Code, Section III, Division 1. The analysis was performed in accordance with the provisions of Subsection NB, "Class 1 Components," in conjunction with Appendix F of that Code.

The logic for a Consequence Analysis was drawn on Figure 7-5. To perform an analysis of the RCL piping in accord with Fig. 7-5, information regarding the piping and associated loads must be obtained including the following. Information on piping should include material properties, location of piping supports, and verification of piping design details (e.g.: details such as pipe diameter and wall thickness). Static loads should be determined based on dead weight, pressure and temperature. In many situations thermal loads are self limiting, have no bearing on the analysis, and may be neglected. There are, however, cases where thermal loads result in primary stresses and those should be included. For example, in a thermal transient, an RPV support connected to another structural element by a bolted flange can induce an increase in stress in the bolts by differential thermal expansion.

Usually, the site seismic design basis, the mathematical model of the NSSS and the floor response spectra are available for the RPV supports. If not, they must be generated. The acceptable procedure for defining response spectra for seismic design of nuclear power plants is provided in Regulatory Guide 1.60[25] and Regulatory Guide 1.122[26]. Regulatory Guide 1.61[27] defines the acceptable damping values for design of nuclear facilities.

There are two acceptable methods for seismic load determinations; the response spectrum and the time history. Technical guidance regarding application of either of these methods is provided in Sections 3.7.1, "Seismic Design Parameters;" 3.7.2, "Seismic System Analysis;" and 3.7.3, "Seismic Subsystem Analysis" of Reference 9 and the associated Regulatory Guides.

Some systems qualify for leak-before-break considerations and in such cases small-break LOCA (SBLOCA) loads apply. Loads from pressure, dead weight of the RPV, thermal gradient (if applicable), LOCA (SBLOCA or LBLOCA) and SSE should be combined in accordance with the provisions of Reference 18.

From the loads as described above, stresses in the RCL piping and RPV displacements (vertical and horizontal) should be computed. Vessel displacement may adversely affect the insertability of control rods or the functionality of safety injection lines, flux monitoring systems (such as thimble tube guide lines) and instrument thimble tubes. Also, excessive RPV displacement may deform the reactor coolant pump (RCP) casing(s) and bind the impeller(s). Tilting of the RCP may disrupt the continuity of flow (coastdown) following a loss of RCP power. Coastdown allows the reactor power to be reduced before flow through the core is reduced, ensuring that localized boiling and departure from nucleate boiling do not occur. To help maintain coastdown, the RCP receives the kinetic energy necessary for coastdown from a flywheel. Tilting of the RCP may cause excessive vibration of the RCP assembly, which could lead to loss of the flywheel. Because the flywheel is massive and rotates at a high speed (1200 rpm) in normal operation, loss of flywheel integrity could generate high energy missiles. The safety consequences of such scenarios may be significant because of possible damage to the reactor coolant system, the primary containment or the engineered safety features equipment.

Another potential cause of loss of coastdown from RCP tilting is the fact that tilting of a pump assembly may cause stresses sufficient to induce deformation or failure of the bearings. In either case, malfunction of the bearings could impede or terminate coastdown.

The SG and RCP supports must be evaluated to ensure sufficient margin under the additional loads resulting from support failure.

The scenarios described above do not encompass the entire potential problem associated with integrity of RPV supports and safety of nuclear power plants. Consideration should be given to uncertainty regarding initial transition temperature of component support material such as steam generator and reactor coolant pump, degradation of material over the life of the plant, aging embrittlement of stainless steel primary coolant loop piping, degradation of large hydraulic snubbers, erosion of piping walls, to name a few. The structural consequence analysis did not consider these conditions, but the cumulative effect of these problems could aggravate consequences of RPV support failure to the point that public safety could be at risk.

If the RPV support integrity cannot be ensured by any of the alternatives described in Sections 7.c through 7.e, modifications to the supports or to the plant operation should be considered.

7.f Fracture Mechanics Procedure For Pins

Pins and clevises deserve special attention. Because of their geometry, the predominant stress may not be tension but shear or a combination of the two. Evaluation of K_{IIc} is controversial and the parameter is not routinely included in design considerations. However, some progress to find a viable and practical solution to this problem has been made.[28,29] It is recognized that tests performed on oblique cracks showed that the predominant crack extension direction was dictated by the maximum K_I value, thus reducing the value of K_{II}. Some investigators, however, obtained Mode II cracks in their experiments indicating that the that Mode II failure is probable[28]. L. Banks-Sills

expressed an opinion that "The direction of crack growth is governed by properties of the material being tested and the conditions of the crack tip. If there is 'brittle' fracture as occurs with Perspex, a crack in a Mode II field propagates between 60 and 70° with respect to the parent crack. In elastic materials, this coincides with the direction of maximum tangential stress."[28] From the above, one may conclude that material behavior in Mode II failure is not well understood. Although more work is needed in this area, it is evident that in components loaded in shear, Mode I considerations alone may be insufficient and the analysis should consder Mode I and Mode II combinations.

7.g Examples (To be provided)

8. SUMMARY OF COST-BENEFIT ANALYSIS

The cost-benefit analysis conducted in support of GSI-15 consisted of three steps. First, estimates of the core damage frequency and risk associated with RPVS failures were made; second, detailed cost estimates of potential corrective measures for damaged RPV supports were made; and third, cost/benefit ratios for implementation of any of the five identified corrective measures were calculated. Details of the analysis and presentation of the results are contained in Appendix A to this report.

8.1 Benefit Evaluation

The benefit is defined as the reduction in risk obtained by fixing the neutron embrittled RPV supports. To estimate the risk, two different scenarios were considered that could potentially fail the supports The first scenario is a safe shutdown earthquake (SSE) as an initiating event with the subsequent failure of the RPV supports. The second scenario involved a small break loss of coolant accident (SBLOCA). Typical event tree methodology was used in the generation of event trees. Initiating event frequencies were adjusted to fit the scenario of brittle failure of supports. In the case of the SSE event tree, the probability of the earthquake was reduced to correspond to the peak ground acceleration and RPV support stress level at which brittle fracture could be expected to occur. In the case of the SBLOCA, the frequency used was taken from the Sequoyah 1 PRA and reduced by a factor of 2 because it was assumed that not all break locations would produce significant loads on the RPV supports. It was assumed that, given the initiating event, the probability of support failure would be 0.5. The event trees were quantified and those event sequences which resulted in core damage were grouped into one of seven different categories. Each sequence was assigned to the offsite release category which best modeled its outcome. The offsite release categories were taken form the WASH 1400[30] reactor safety report that classifies various degrees of release from the reactor containment. For the best estimate base case considered in the analysis, the total contribution to core damage frequency resulting from RPV support failure was calculated to be 8.8×10^{-5}.

8.2 Cost Analysis

Five alternatives were considered as corrective measures to preclude RPV support failure in the event of an SSE or SBLOCA. The alternatives were as follows.

1. shielding the RPV supports from neutron radiation;

2. increasing the RPV support operating temperature above the NDT temperature;
3. replacing the RPV supports;
4. heating the RPV supports sufficiently to anneal out any embrittlement;
5. strengthening or adding additional RPV supports.

The cost estimates for the five options were developed using the guidelines of NUREG/CR-3568[31], and NUREG/CR-4627, Rev. 1,[32] and the computer code FORECAST 2.1[33] which incorporates cost evaluation information. Cost estimation involved making an evaluation of each proposed modification, identifying equipment and materials necessary to make the proposed modifications, and assessing the work area in which the proposed modifications would be made.

There was a wide variation in the estimated costs of the alternatives considered. The maximum cost per plant was $89,000,000 (alternative 3, replacing existing supports), and the minimum cost per plant was $920,000 (aternative 2, increasing the operating temperature of the supports)

8.3 Cost/Benefit Analysis

Results of the cost/benefit analysis were calculated using the dollar-to-person-rem averted ratio (DPR). The DPR is calculated as the cost of the modification divided by the offsite person-rem averted if the modification is performed. In calculating the cost, the averted onsite cost (AOSC) is subtracted from the modification cost. For the case where the occupational exposure is considered, the occupational exposure is subtracted from the averted offsite dose. For some cases the occupational exposure from making the modification exceeded the averted offsite dose which results in no net benefit. Cost/benefit calculations were made for a 10, 20, 40, and 60 year remaining life span. The remaining life span is the time left to operate the plant after the supports are assumed to become brittle. Results of the cost/benefit analysis (presented in Appendix A) are calculated for three cost categories, 1) without either AOSC or replacement power, 2) with AOSC but without replacement power, and 3) with both AOSC and replacement power.

The results of the benefit analysis indicate a per plant offsite dose risk of 2.9 person-rem/year with a calculated core damage frequency of $8.8X10^{-5}$/yr. The risk value includes all the risk associated with support failure after embrittlement occurs. It was assumed that any of the proposed options would remove 100% of the risk associated with failure of an embrittled support. This means that after the modification, the risk due to support failure is assumed to be zero.

A number of cost/benefit calculations were made using combinations of assumptions which produced a range of values to fit the various scenarios. The calculated cost benefit ratios range from $53 per person-rem (increasing the operating temperature of the supports, without replacement power, and considering 60 year life after embrittlement occurs) and $3,100,000 per person-rem (replacing supports, with averted on-site costs, with replacement power, without occupational exposure, and considering 10 years life after embrittlement).

Sensitivity studies were conducted considering 10, 20, 40, and 60 years operation after embrittlement of the supports. Cost benefit ratios were calculated both with and without consideration of occupational doses. Several supplemental cases were evaluated with more conservative estimates of failure probability to judge the sensitivity of the risk calculation results to the event probabilities in the event trees. Seven cases were evaluated:

Case 1 Increase the frequency of an SSE by a factor of ten. For most plants, this is equivalent to assuming peak ground acceleration of 0.5g earthquake and may result in RPV support failure.

Case 2 Increase offsite dose rates by a factor of 100 to simulate a plant located in an area of high population density.

Case 3 Increase the probabilities of RPV support failure and LBLOCA to 1 to show the maximum uncertainty in the RPV support failure mechanisms.

Case 4 Increase the failure probabilities of the RPV supports and the RPS to 1 and decrease the probability of a LBLOCA to 0.

Case 5 Increase the failure probabilities of ECCS and CSDS to 1 to simulate failure of these safety systems.

Case 6 Increase the probabilities of LBLOCA and ECCS failure to 1 to simulate the pressure vessel displacing sufficiently (following RPV support failure) to cause the ECCS injection lines to break or become inoperable.

Case 7 Set the failure probabilities of the RPV supports, RPS, CSDS, and ECCS and the incidence of LBLOCA to 1 which is a worst case model of complete failure of the entire reactor protection system with the exception of the containment. This scenario involves prior embrittlement of the RPV upportss and the RPV support from the primary piping. Following the initiating event, the subsequent shifting of the RPV results in failure of all core protection systems.

Table 8-1 shows the results for each case considered for one year, as well as for ten, twenty, forty and sixty years. From the sensitivity analysis the extreme values of the cost/benefit ratio can be obtained.

Table 8-1. Sensitivity Analysis Results.

CASE	CORE MELT FREQUENCY (per year)	RISK (per year) [person-rem]	RISK (10 years) [person-rem]	RISK (20 years) [person-rem]	RISKK (40 years) [person-rem]m
1	6.5×10^{-4}	21	210	420	8400
2	8.8×10^{-5}	290	2,900	5,800	12,000 0
3	1.8×10^{-4}	10	100	200	400 0
4	3.5×10^{-4}	2.7	27	54	110 0
5	6.6×10^{-4}	26	260	520	1,0000
6	8.8×10^{-4}	49	490	980	2,0000
7	1.8×10^{-3}	98	980	2,000	3,9000
Base	8.8×10^{-5}	2.9	29	58	120 0

The core melt frequencies per year were obtained by modifying the appropriate events in the sequence event trees (not shown) for the two initiating events, SSE and SBLOCA. The Base Case shows the results of the original analysis without modifications of the sensitivity analysis parameters. For other cases, to obtain Risk per year the probabilities for each sequence (PWR 7, PWR 3, and PWR 1) are multiplied by the corresponding Consequence Factors taken from NUREG/CR-2800[34]. The result is the risk per year in person-rem. The risks for 10, 20, 40, and 60 years are simply product of the risk for one year times the number of years in question.

From Table 8-1 it can be seen that the minimum benefit is Case 4, and the risk reduction is 27 person-rem for a period of ten years. The maximum benefit occurs in case 2, which gives 17,400 person rem for a period of 60 years. Using the results of the sensitivity analyses and the corresponding costs, four extreme cases of cost/benefit were calculated. The four extreme cases are:

1. Maximum cost/minimum benefit = $3,300,000/person-rem
2. Minimum cost/maximum benefit = $5,120/person-rem
3. Minimum cost/minimum benefit = $34,000/person-rem
4. Minimum cost/maximum benefit = $53/person-rem.

The above results illustrate the large variability of the results. They also indicate that all except case 4 are above $1,000/person-rem, the accepted threshold for taking any regulatory action. The minimum cost/maximum benefit of $53/person-rem (Case 4) results derived from option 2 (increasing the operating temperature of the RPV supports above the new, embrittled NDT temperature), and the cost, without replacement power is $920, 000. The corresponding benefit (the risk reduction) is 17,000 person-rem. Because the majority of the calculated cost-benefit ratios were well above the $1,000/person-rem criterion, there is little justification for taking regulatory actions. Moreover, the range of cost-benefit ratios stems from uncertainty in the values used in the analysis and, being uncertain, were of little use to the staff in reaching a regulatory position.

9. DISCUSSION OF THE GSI-15 TECHNICAL FINDINGS

It had been reported by ORNL[4] that the thermal-to-fast neutron ratio was about 50-to-1. That was enough motivation for some theoreticians to propose mechanisms for submicroscopic damage by low energy neutron radiation at low temperature in steel. Using those models, the NRC staff developed a method for evaluating the effects of low energy neutron damage in steel by a modified dpa parameter[6]. To expand the available data base, the NRC staff requested ORNL to calculate the neutron energy spectra at additional surveillance locations in the HFIR. The resulting thermal-to-fast neutron ratios were on the order of 3-to-1 to 7-to-1. That finding did three things: (1) it cast doubt on the roughly ten times larger ratio reported in Reference 3; (2) it suggested that the low-energy neutron damage theory was not the answer to the HFIR embrittlement; and (3) it set in motion a program with the goal of determining the radiation conditions in HFIR by the best experimental and calculational means available.

When the dosimetry program was completed it was concluded[14] that the accelerated embrittlement of the HFIR surveillance samples could be attributed to long-term, low-temperature gamma radiation. Also, we found that the HFIR γ flux was about 3000 times higher than the measured γ flux in the cavity of an operating reactor. The interpretation of these findings created the following picture. The physical conditions in the HFIR, with an annulus between the Be reflector and the vessel inside surface (where the surveillance capsules were located) filled with almost two feet of water attenuated the neutrons so that the flux of those with $E > 1$ MeV was reduced by orders of magnitude. At the same time, the γ flux remained almost unabated. Although the γ flux was not especially high, there was enough radiation to create submicroscopic damage in the steel. In fact, had the γ flux been very high, the γ-heating would have annihilated much of the damage. Likewise, the relatively low neutron flux kept that element of radiation from annealing out the γ-radiation damage. Also, the temperature of the steel was kept relatively low, well below 200°F, ensuring that much of the damage from γ and low-energy neutrons would be retained. Because nuclear reactor pressure vessels operate at about 550°F, the diffusivity in the steel is so much greater than at the low temperatures of the HFIR or the RPV supports that the relatively short-range crystal lattice damage from γ radiation is annealed in months, if not in weeks, even though the flux is of the same order of magnitude as found in the HFIR.

By these arguments, we see that the radiation environment in the HFIR is unique to that reactor, the embrittlement observed in the surveillance specimens can be explained on the basis of the radiation details, by using a dpa parameter that includes all radiation (the full neutron energy spectrum and the γs) the HFIR data fall on the trend band established with other data, and the HFIR surveillance data are not relevant for predicting RPV support embrittlement in operating reactors. In an operating reactor, the vessel supports are shielded from γ radiation by the vessel, itself. The steel thickness of six to ten inches is sufficient to reduce the γ flux by two, three, or four powers of ten. For this reason, no significant γ radiation embrittlement is expected in RPV supports; however, embrittlement predictions should be made on the basis of the complete dpa parameter because there may be a significant additional contribution from low-energy neutrons.

In this regard, we note that the ASTM Standard Guide for RPV supports, E 1035 (in the ASTM Book of Standards), addresses radiation considerations in the following way. The designer and owner/operator is cautioned to consider the potential for radiation embrittlement. However, it is stated that if the fluence of neutrons of energy greater than 1 MeV is no more than 10^{17} nvt, there is no need for further consideration. From the findings in the work aimed at resolution of GSI-15, it is clear that fast neutron (E > 1 MeV) fluence may not be sufficient for accurate predictions. Although neglecting all radiation but fast neutrons is probably acceptable for a fission spectrum or something close to it, other particles can do damage and if present in sufficient numbers, they should be counted, especially at low temperature.

The work which led to NUREG/CR-5320 included a survey of LWR vessel supports using the FSAR library located at the Nuclear Operations Analysis Center at ORNL. The information from the ORNL survey was supplemented by two other studies[35,36]. It was noted that in many instances the data from all sources were too sketchy to be definitive. Based on the above surveys, at least in some of the older reactors, neither the exact chemical composition nor the mechanical properties of the RPV supports is known, neither their initial nor shifted NDT temperatures can be accurately determined, and the margin between their lowest operating temperature and their NDT temperature may be less than that recommended in the ASME Code, Appendix R. There may be cases where the initial NDT was so high that little, if any, margin for radiation-induced increases is available. Under such conditions, it would be prudent to perform an engineering reassessment of the RPV support integrity and evaluate any potential threat to safety.

10. CONCLUSIONS

1. The specimens that were incorporated in the surveillance program at the HFIR exhibited more radiation-induced embrittlement than would be predicted from pre-existing trend curves.

2. After reviewing the studies and analyses undertaken by several organizations at the outset of the work on GSI-15, it was concluded that in today's state of the art there is no one reliable method of structural analysis by which the issue could be resolved.

3. Specimens cut from the decommissioned Shippingport neutron shield tank exhibited embrittlement (ΔNDT) commensurate with pre-existing trend curves even though the steel and the irradiation conditions (in terms of the neutron spectrum) were similar to those at HFIR.

4. Specimens of the same steel used in the construction of the HFIR reactor vessel (archieval material), when tested in other facilities did not repeat the excess embrittlement found in the surveillance specimens.

5. In response to the initial report that the HFIR neutron energy spectrum had about 50 times more low energy (thermal) neutrons as high energy (fast) neutrons, a model was developed to account for the complete neutron energy spectrum by modifying the dpa parameter.

6. A comprehensive dosimetry program, designed to provide data necessary to confirm the (above) low energy neutron damage model, suggested that the excess embrittlement of the HFIR specimens could be attributed to long-term, low-temperature gamma radiation.

7. Auxilliary conclusions derived from the program noted in the preceeding statement included the following:

7a. At the location in HFIR where γ flux calculations were confirmed by measurements, the γ dpa was five times higher than the neutron dpa.

7b. Discrepencies in neutron flux values from dosimeters irradiated in the HFIR were the result of photofission and photoneutron reactions triggered by the γ radiation.

7c. Be and fast threshold fission dosimeters exhibit photo-induced reactions making them good γ dose monitors in some radiation fields.

7d. Neutron flux gradients across the surveillance capsules in HFIR were not consistent from one to another.

7e. It was shown that locating stainless steel fast neutron dosimeters in Charpy specimen V-notches resulted in adequate flux measurements.

7f. It was shown that simultaneous adjustment of the neutron and γ fluxes was feasible.

8. By relating the HFIR surveillance data to an expanded dpa parameter enveloping both the neutron and γ fluxes, the HFIR ΔNDT values could be moved into the trend band derived from other data and could not continue to be considered excessive.

9. The above finding leads to the tentative conclusion that the deviation reported in the HFIR surveillance data probably was a result of the combination of a long-time exposure <u>at relatively low temperatures</u> to a radiation field with a very low density of fast neutrons and a much larger, but typical, density of gammas.

10. Because it was initially expected that it would be necessary to evaluate (at least some) RPV supports, a detailed engineering approach for assessing the structural integrity was developed.

11. As a related task, a consequence analysis based on the Trojan plant (believed to be the most vulnerable) configuration showed that RPV support

failure could be tolerated providing that other components were not degraded (see below).

12. The limited review of RPV supports in operating plants led to a conclusion that some materials of construction may have an initial NDT high enough to allow little, if any, margin for radiation-induced increases.

13. Engineering analyses demonstrated the importance of related plant components which would have to carry additional loads in the event of RPV support failure but some critical related components have exhibited other, unique, degredation mechanisms.

14. If licensees wish to reassess the integrity of their RPV supports, the methods reported in this paper should provide adequate guidance.

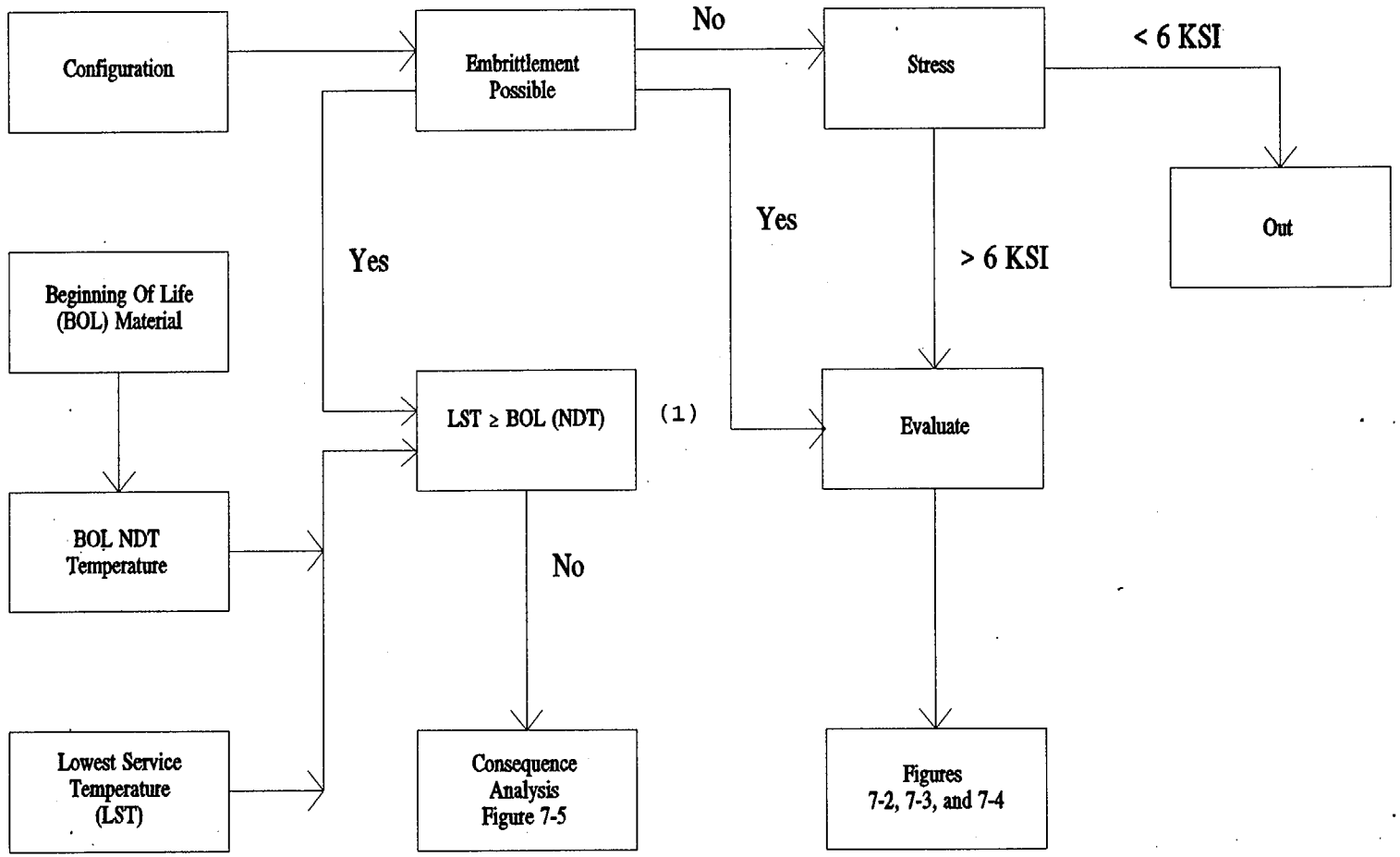

Figure 7-1 Screening Criteria

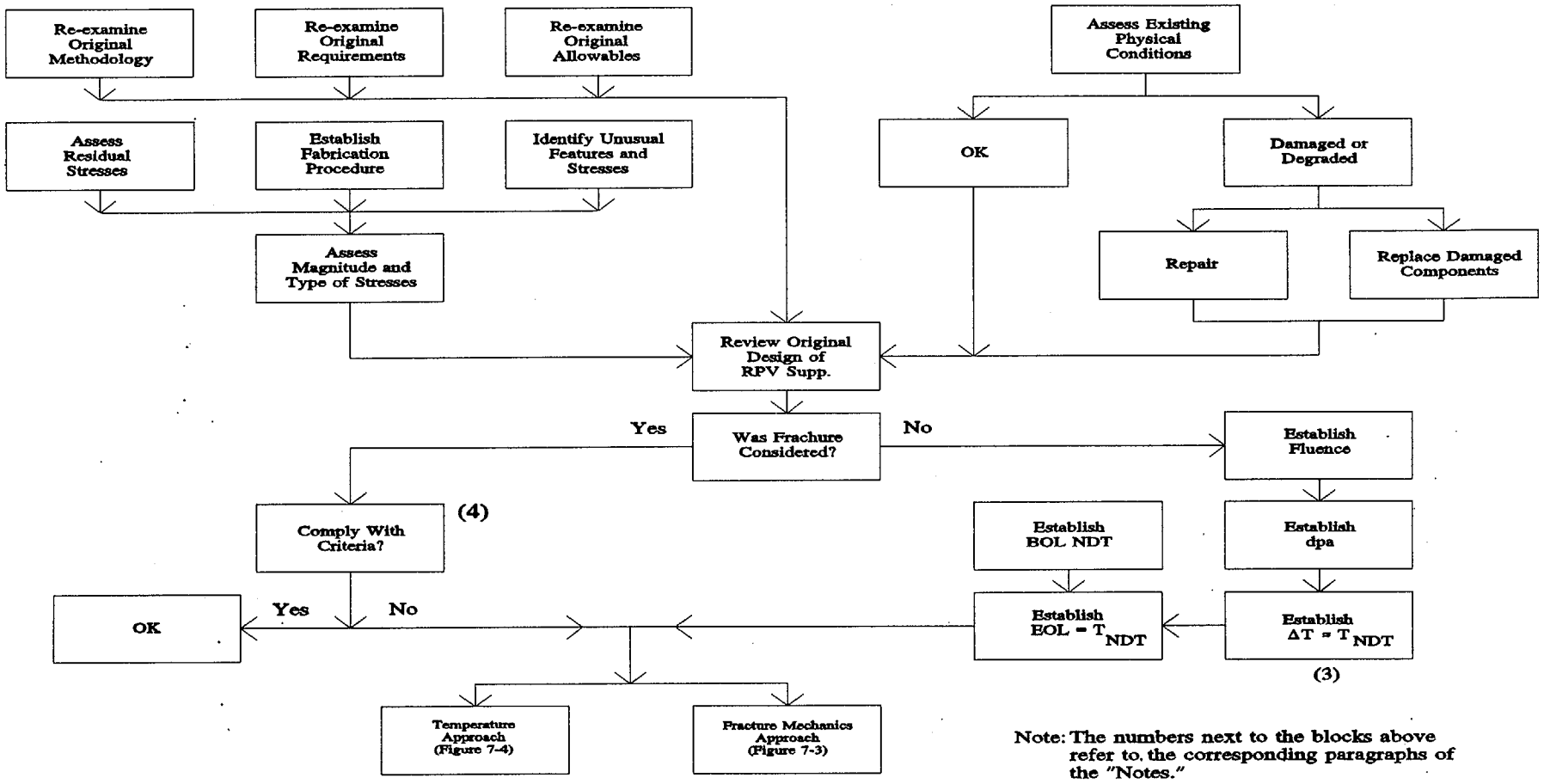

Figure 7-2 Preliminary Information

NOTES

(SEE FIG.7-1)
The safety margin between LST-T_{NDT} is established using Fig. R-1200-1 of Appendix R to Reference 17.

(SEE FIG. 7-2)

1. LST
   The lowest service temperature (LST) is defined as the minimum temperature of the most vulnerable part of the fracture-critical member at times when design basis accident loads occur. RPV support temperatures can be established either from measurements or theoretical calculations.

2. Adjustments
   2A. Irradiation
   The radiation-induced temperature shift should be based on reliable and relevant dosimetry information.
   2B. Strain-rate
   Consideration for strain-rate effects must be appropriate to the subject material. The loading rate should be estimated and its effect documented.

3. NDT Evaluation Procedure.
   List all support materials and available NDT temperature data. State the authority for material tests (e.g., Subsection NF, ASME Code Section III).
   3A. Material having minimum specified yield strength of 180 ksi or less:
   For materials in new RPV supports the NDT temperature should be determined in accordance with the provisions of ASTM E-208 (Reference 20). If Charpy V-notch testing is performed it should
   satisfy the requirements of Subsection NF, "Component Supports", Paragraphs NF 2320 and 2330 of Reference 16.
   3B. Estimated NDT
   For existing RPV supports, in case the NDT temperature cannot be determined experimentally, an estimated NDT temperature can be obtained from Table 7-1. The value of the NDT temperature, used for this purpose, should be the NDT mean plus 1.3 standard deviation.
   3C. Bolting Materials
   Code bolting materials shall meet the fracture toughness requirements of Appendix G, Subsection NC, Paragragh NC-2332.3 and Article G-4000, "Bolting," Reference 16. Those materials not specified in the Code must be analyzed in accordance with, and meet the criteria of 3A or 3B above.
   3D. Steels having minimum specified yield strength greater than 180 ksi
   Resistance to fracture under tensile loads for materials with minimum yield strength greater than 180 ksi is considered unreliable unless it can be justified by LEFM analysis. If such a justification cannot be provided, high strength materials should be assumed to have inadequate fracture toughness, and that the fracture mechanics or transition temperature options (Fig. 7-3 and 7-4) are not applicable. Structural adequacy of RPV supports should be demonstrated by means of the structural consequence analysis (Fig. 7-5).

4. The "Criteria" are those contained in Article IWB-3000 of Reference 17.

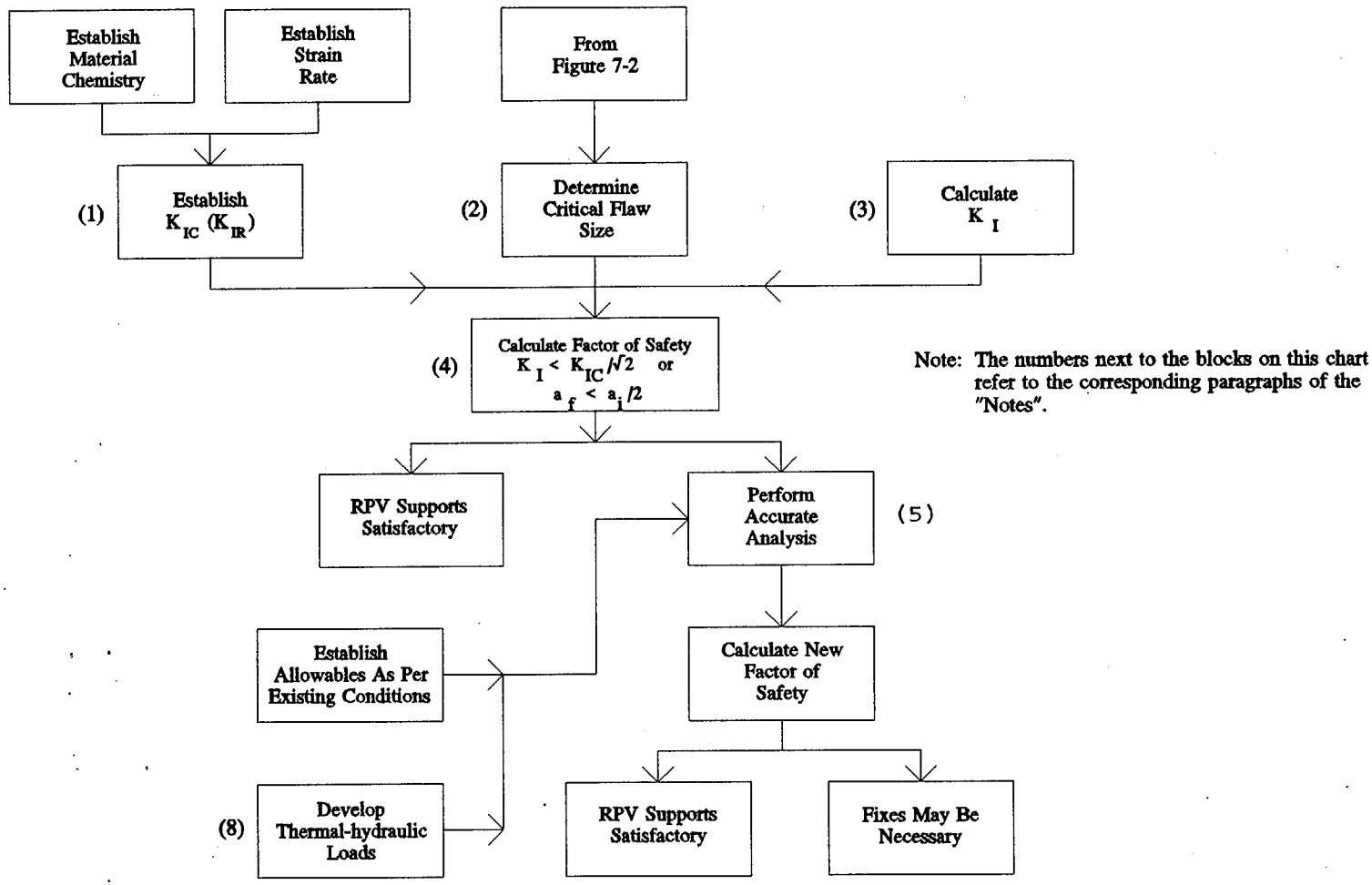

Figure 7-3 Fracture Mechanics Approach

NOTES (Fig. 7-3)

1. (a) Estimated fracture toughness by conversion of an hyperbolic tangent function fitted to Charpy data is not acceptable.
(b) Confirmation of correlations between CVN and K_{Ic} data is required.
(c) The proper determination of fracture toughness curves is based on multiple K_{Ic} tests at each of several temperatures for each class of material.
(d) Minimum Fracture Toughness values contained in Table 7-2 may be used if sufficient evidence is available to demonstrate that the material used in the RPV supports is the same as that listed in Group III in Table 4.6 of Reference 36.
(e) Where applicable, fracture toughness (K_{Ic} and/or K_{Ia}) can be obtained from the information contained in Appendix A, Figure A-4200-1 of Reference 17.

2. a) Acceptance criteria for the flaw size can be based on Subarticle IWB-3611, "Acceptance Criteria Based on Flaw Size" of Reference 17.
(b) The analysis of flaw indications should be in accordance with the provisions of Appendix A, "Analysis of Flaw Indications" of Reference 17.

3. (a) The maximum stress intensity factor K_I shall correspond to the flaw size a_f as defined in Subarticle IWB-3600 of Reference 17.
(b) If the supports are subjected to combined loading which necessitates consideration of Mode II, an appropriate fracture toughness shall be established based on the present state-of-the-art.
(c) If applicable, the reference temperature for the nil ductility transition (RT_{NDT}) may be used in conjunction with the provisions of Appendix G, Article G-2000 Reference 16.
(d) Calculate K_I using Eq. 1 in Appendix A, Article A-3000 of Reference 17.

4. Safety factors shall satisfy the criteria of Article IWB-3600 of Reference 17.

5. (a) The analysis may be performed using elastic-plastic properties of the material. The load combinations, allowable stresses and the design criteria for linear supports (consisting of shapes, beams, and columns) should conform with the provisions of Section 3.8.3, Concrete and Steel Internal Structures of Steel and or Concrete Containments," and for non-linear supports with Section 3.9.3, "ASME Code Class 1, 2, and 3 Components, Component Supports, and Core Support Structures" of Reference 9 respectively.
(b) The thermo-hydraulic loads may be based on Reference 24.

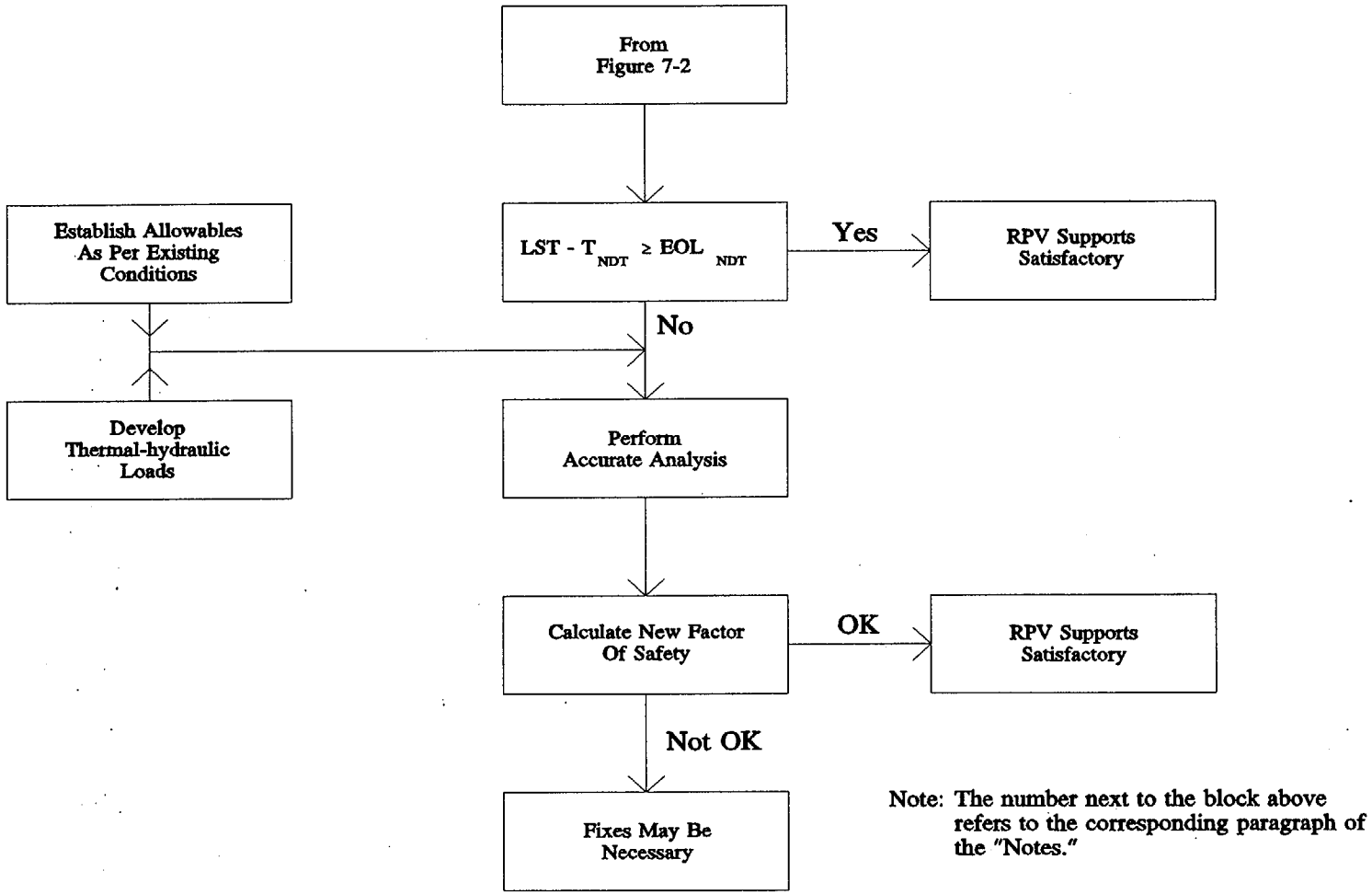

Figure 7-4 Transition Temperature Approach

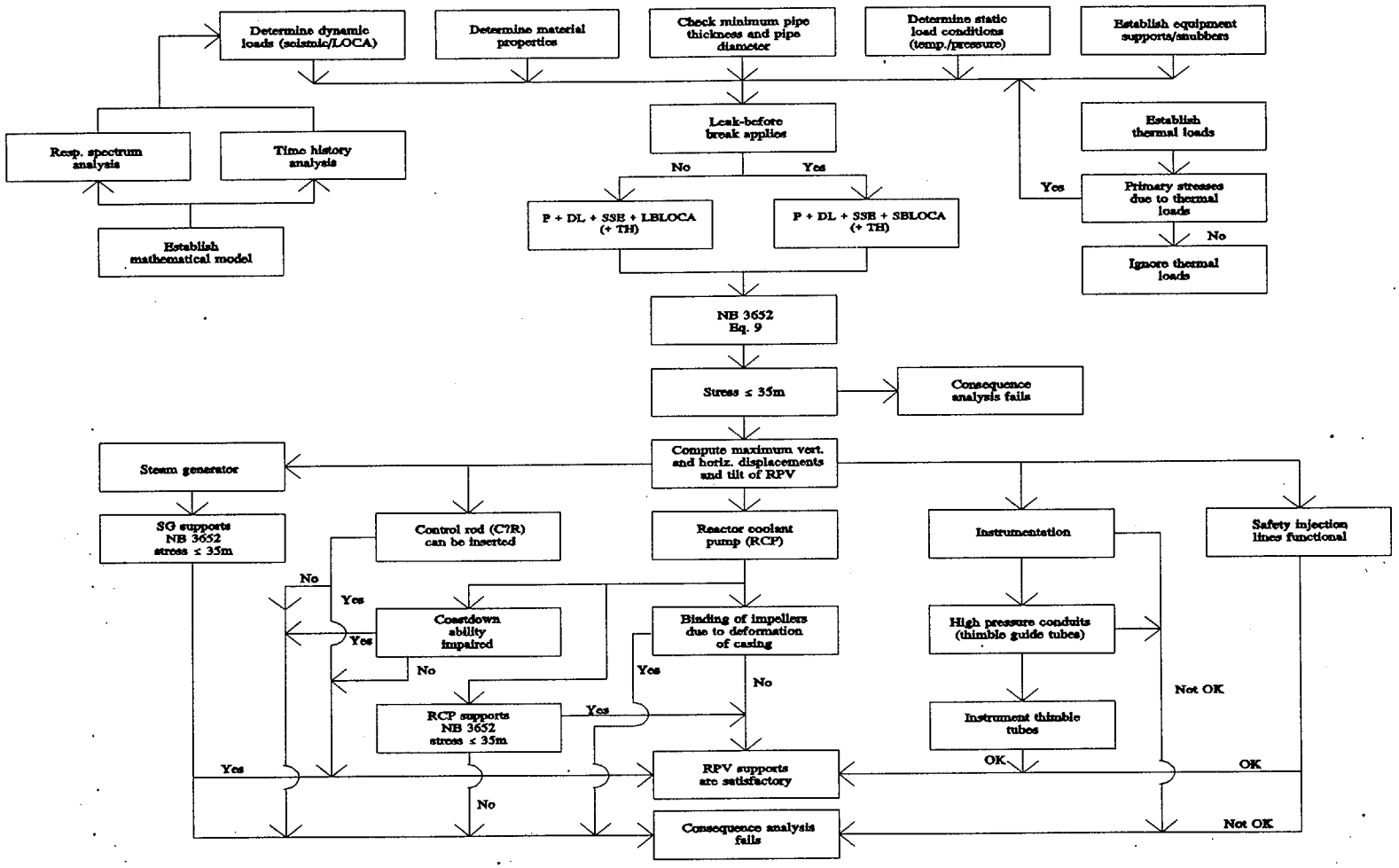

Figure 7-5 Structural Consequence Analysis

Table 1
Compilation of NDT Results

Material		NDT	σ	NDT + 1.3σ	NDT + 2σ
Cast Steels					
A-27, A-216	1"	- 6°F	12°F	10°F	18°F
(heat treated condition)	>1"	35	17	57	69
A-352				max. -20	
Wrought Steels					
all "mild" steels*		27	31	67	89
all "mild" steels except A-201		40	28	77	96
C-Mn*(as-hot rolled)		22	13	39	48
(normalized)		-28	18	- 5	8
HSLA* (as-hot rolled)		25**	12**	41**	49**
(normalized)		-50**	18**	-27**	-14**
Low Alloy, Non-Q&T					
A-302		8	28	45	64
A-353				max. -320	
A-387					65**
Quenched & Tempered					
A-508 C12				max. 40°F	
A-514				max. -10°F	
A-517				max. -20°F	
A-533B C11				max. 20°F	
A-537 C12				max. -60°F	
A-543				max. -60°F	

* See table 7-3 for ASTM specs included in this category

** HSLA steels, "high strength" means yield strength > 40 ksi. For further discussion on HSLA steels see Reference 3.

(From Table 4.4 of Reference 36)

Table 2

Minimum Fracture Toughness Data at 75°F

Plain Carbon	32	ksi	$in^{1/2}$
C/Mn	36	"	"
HSLA	36	"	"
Low Alloy (non Quenched and Tempered)			
A-302	30	"	"
A-353	150	"	"
A-387	65	"	"
Quenched and Tempered			
A-508	35	"	"
A-514/A-517	65	"	"
A-533	35	"	"
A-537	55	"	"
A-543	95	"	"
Other			
A-461, Gr. 630	100	"	"

(From Table 4.5 of Reference 36)

Table 7-3

Classification of Wrought Grades into Groups

Plain Carbon: A-7, A-53, A-106, A-201, A-212, A-283, A-284, A-285, A-306, A-307, A-501, A-515

Carbon-Manganese: A-36, A-105, A-516, A-537

High-strength low alloy: A-441, A-572, A-588, A-618

Low alloy (not quenched & tempered): A-302, A-322, A-353, A-387

Quenched & tempered: A-193, A-194, A-325, A-354, A-461, A-490 A-508, A-514, A-517, A-533, A-537, A-540 A-543, A-563, A-574.

(From Table 3.2 of Reference 36)

11. REFERENCES

1. ORNL/TM-10444, "Evaluation of HFIR Pressure Vessel Integrity Considering Radiation Embrittlement," Oak Ridge National Laboratory, 1988.

2. Memorandum from Warren Minners (NRC) to Eric S. Beckjorrd (NRC), dated January 16, 1990.

3. NUREG-0705, "Identification of New Unresolved Safety Issues Relating to Nuclear Power Plant Stations," U.S. Nuclear Regulatory Commission, June, 1981.

4. NUREG/CR-5320, "Impact of Irradiation Embrittlement on Integrity of Pressure Vessel Supports for Two PWR Plants," Oak Ridge National Laboratory, January 1989.

5. NUREG/CR-5556, "Review of Current Literature Related to Generic Safety Issue 15," Idaho National Engineering Laboratory, EG&G Idaho, Inc., July, 1990.

6. Craig A. Hrabal, "Modified Damage Parameters Applied to a Typical Light Water Reactor's Pressure Vessel Supports," Presented at the 7th ASTM-Euratom Symposium on Reactor Dosimetry, Strasbourg, France, August 27-29, 1990.

7. M. L. Hamilton and A. L. Heinesch, "Tensile Properties of Neutron Irradiated A 212-B Pressure Vessel Material," ASTM 14th International Symposium on Effects of Radiation on Materials, Andover, Mass., June 27-29, 1988.

8. NUREG/CR-5644, "Consequence Evaluation of Radiation Embrittlement of Trojan Reactor Pressure Vessel Supports," Lawrence Livermore National Laboratory, October, 1990.

9. NUREG-0800, "Standard Review Plan for the Review of Safety Analtsis Reports for Nuclear Power Plants," LWR Edition, U.S. Nuclear Regulatory Commission, June, 1987.

10. NUREG/CR-5748, "Radiation Embrittlement of the Neutron Shield Tank from the Shippingport Reactor," Argonne National Laboratory, October, 1991.

11. F. H. Ruddy, et al., "Reactor Cavity Neutron Dosimetry Results for the Trojan Nuclear Power Plant," STC Report 93-9TDO-TROJN-R1, Westinghouse Electric Corporation, Science & Technology Center, Pittsburgh, Pennsylvania, March 19, 1993.

12. L. R. Greenwood and R. K. Smither, "Specter: Neutron Damage Calculations for Material Irradiations," ANL/FPP/TM-197, 1979.

13. NUREG/CR-3320-Volume 5, "Simulated Void-Box-Capsule Charpy Impact Test Results," Fracture Control Corporation, for the U.S. Nuclear Regulatory Commission and the Electric Power Research Institute, Washington, D.C., August, 1986.

14 NUREG/CR-6117, "Neutron Spectra at Different High Flux Isotope Reactor (HFIR) Pressure Vessel Surveillance Locations," Oak Ridge National Laboratory, December, 1993.

15-a. S. Q. King and D. M. Gilliam, "Characterization of the Gamma Field in the B&W Owners Group Cavity Dosimetry Benchmark Experiment," Reactor Dosimetry, ASTM STP 1228, Harry Ferrar IV, E. Parvin Lippincott, and John G. Williams, Eds., American Society for Testing and Materials, Philadelphia, Pennsylvania, 1994.

-b. Letter, S. L. Anderson, Westinghouse Electric Corp., to R. E. Johnson, U. S. Nuclear Regulatory Commission, May 23, 1994.

16. ASME Boiler Pressure and Vessel Code, Section III, Division 1, American Society of Mechanical Engineers, New York, New York, 1989.

17. ASME Boiler and Pressure Vessel Code, Section XI, "Rules for Inservice Inspection of Nuclear Power Plant Components," American Society of Mechanical Engineers, New York, New York, 1989.

18 NUREG-0484, Rev. 1, "Methodology for Combining Dynamic Responses," U.S. Nuclear Regulatory Commission, May, 1980.

19. E. Rybicki and R. B. Stonesifer, "Computation of Residual Stresses Due to Multipass Welds in Piping Systems," Journal of Pressure Vessel Technology, Vol. 101, pp. 149-154, May, 1978.

20. ASTM E 208, "Standard Test Method for Conducting Drop-Weight Test to Determine Nil-Ductility Transition Temperature of Ferritic Steels," American Society for Testing and Materials, Philadelphia, PA 19103.

21. J. M. Barsom and S. T. Rolfe, "Fracture and Fatigue Control in Structures Application of Fracture Mechanics," Second Edition, Prentice-Hall, Inc., 1987.

22. R. J. McElroy, T. J. Williams, F. M. D. Boydon and B. Hamsworth, "Low Temperature Embrittlement of LWR RPV Support Structures," OECD/NEA Workshop on Safety Assessment of RPV's, Espoo, Finland, 8-9 October, 1990.

23. J. R. Hawthorne, "Temperature Dependence of Copper Influence on Radiation Embrittlement Sensitivity of Reactor Vessel Steels," American Nuclear Sosiety (ANS), Transactions, Vol. 15, No. 2, 1972.

24. American National Standard, ANSI/ANS 58.2, "An Acceptable Simplified Method for Calculation of Fluid Thrust Forces, Appendix B, 1988.

25. Regulatory Guide 1.60, "Design Response Spectra for Seismic Design of Nuclear Power Plants," Rev. 1, U.S. Nuclear Regulatory Commission, 1973.

26. Regulatory Guide 1.122, "Development of Floor Design Response Spectra for Seismic Design of Floor-Supported Equipment or Components," U.S. Nuclear Regulatory Commission, 1978.

27. Regulatory Guide 1.61, "Damping Values for Seismic Design of Nuclear Power Plants," U.S. Nuclear Regulatory Commission, 1973.

28. Buzzard, R. J. Gross and J. E. Srawley, "Mode II Fatigue Crack Growth Specimen Development," Fracture Mechanics: Seventeenth Volume, ASTM STP 905, p. 239-345, American Society of Testing and Materials, Philadelphia, PA, 1986.

29. Leslie Banks-Sills and Mircea Arcan, "A Compact Mode II Fracture Specimen,"

Fracture Mechanics: Seventeenth Volume, ASTM STP 905, American Society of Testing and Materials, Philadelphia, PA, 1986.

30. WASH-1400,"Reactor Safety Study," U.S. Nuclear Regulatory Commission, Washington, DC, 1975.

31. NUREG/CR-3568, "A Handbook for Value-Impact Assessment," Pacific Northwest Laboratory, PNL-4646, December, 1983.

32. NUREG/CR-4627, "Generic Cost Estimates," Revision 1, February, 1989.

33. B. Lopez and F. W. Sciacca, "FORECAST," 2.1 User Manual, Science and Engineering Associates, Inc., SEA Report No. 89-461-04-A:1, April, 1990.

34. NUREG/CR-2800, "Guideline for Nuclear Power Plant Safety Issue Prioritization Information Development," Pacific Northwest Laboratory, 1983.

35. NUREG/CR-4731, "Reactor Pressure Vessel Supports for Pressurized Water Reactors and Boiling Water Reactors, Residual Life Assessment of Major Light Water Reactor Components - Overview," Vol. 1, June, 1987.

36. NUREG/CR-3009, "Fracture Toughness of PWR Component Supports," Sandia National Laboratory, February, 1983.

APPENDICES:

A. R. E. Gregg, C. L. Smith, and R. W. Garner: "Cost/Benefit Analysis for GSI-15: Radiation Effects on Reactor Vessel Supports," Rev. 2, EGG-SSRE-9458, Idaho National Engineering Laboratory, August 1991.

B. C. A. Hrabal: "Shippingport Vessel/Shield-Tank Fluence Calculations," a summary of the program conducted by the Brookhaven National Laboratory for GSI-15.

C. Emmert D. McGarry: Synopsis of Work to Determine the Radiation Exposure to Vessel Support Structures in the Trojan Nuclear Reactor," National Institutes of Standards and Technology.

D. Reuter & Nagata: Summary of NUREG/CR-5846 on Thermal Embrittlement of Stainless Steel in the RCL

E. E. H. Ottewitte: "Potential Effects of Gamma Radiation," Idaho National Engineering Laboratory, October 1993.

APPENDIX A - GSI-15 Event Tree Uncertainty Analysis

The event tree uncertainty analysis was initiated by assigning an appropriate uncertainty to each event in both of the event tree sequences. Table A.1 lists each event with its mean value, standard deviation, and assumed underlying probability distribution type. The source listed in the table is the source of the event *mean* value. The standard deviation value for the two Poisson initiating events were calculated by the relationship of: standard deviation = $\sqrt{mean}$.[a] The standard deviation value for the log-normal distributions in the table were estimated based upon engineering judgement.

Table A.1. Sequence Event Uncertainty Parameters.

EVENT	MEAN	STANDARD DEVIATION	DISTRIBUTION TYPE	SOURCE
SSE	1.25×10^{-3}	3.5×10^{-2}	Poisson	Ref. 3
SBLOCA	5.0×10^{-4}	2.2×10^{-2}	Poisson	Ref. 4
RPVSF	5.0×10^{-1}	2.0×10^{-1}	Log-normal	EJ[b]
LBLOCA	5.0×10^{-1}	2.0×10^{-1}	Log-normal	EJ
RPSF	5.0×10^{-1}	2.0×10^{-1}	Log-normal	EJ
CSDSF	2.0×10^{-1}	1.0×10^{-1}	Log-normal	Ref. 4
ECCSF	1.0×10^{-1}	1.0×10^{-1}	Log-normal	EJ
RCF	1.0×10^{-3}	5.0×10^{-3}	Log-normal	Ref. 4
	1.0×10^{-2}	5.0×10^{-2}		EJ

[b] EJ = Engineering Judgement.

[a] This relationship is only valid on Poisson distributed events.

Normally probabilistic risk assessments assign log-normal distributions to the individual events contained in event trees. This arbitrary assignment of distributions stems from the fact that the log-normal distribution efficiently models events with low probabilities. But, for unlikely events (such as an earthquake) that occur at a constant rate and that change the system once the event does occur, a Poisson distribution is frequently used as the underlying distribution[a].

In Table A.1, event RCF is listed as having two parameters. The first parameter (1.0×10^{-3}) models the normal, independent failure of the containment, while the second parameter (1.0×10^{-2}) models the correlated failure mode of the emergency core cooling system and the reactor containment.

The event tree sequences were analyzed using a numerical Taylor series expansion routine to find the mean and standard deviation for each sequence outcome. The Taylor series expansion program was written by one of the authors (Smith) and was verified, both by hand calculations and textbook problems, before use on this project. Appendix C presents two samples of the program verification.

Table A.2 lists the sequence end states expected probability, 95th percentile probability, and standard deviation. The probability distribution for each sequence outcome is assumed to be log-normally distributed due to the multiplication of several events. The expected probability and standard deviation were obtained from the Taylor series expansion program. The 95th percentile valve was calculated using the obtained expected value and standard deviation and the assumption that the resulting distribution was log-normal.

---

[a] The PRA Procedures Guide, USNRC Report NUREG/CR-2300, Jan. 1983, illustrates calculating the occurrence of earthquakes by using the Poisson distribution. Other probability and statistics texts and seismic reports verify that events such as an earthquake may be modeled by the Poisson distribution.

Table A.2. Event Tree Sequence End State Results.

SEQUENCE END STATE	MEAN PROBABILITY	95th PERCENTILE	STANDARD DEVIATION
SPRA	8.8×10^{-4}	2.3×10^{-3}	2.1×10^{-2}
SF-PSD	3.9×10^{-4}	1.2×10^{-3}	6.6×10^{-3}
PWR 9	3.9×10^{-4}	1.0×10^{-3}	9.3×10^{-3}
PWR 8	3.9×10^{-7}	1.0×10^{-6}	9.4×10^{-6}
PWR 7	8.7×10^{-5}	2.6×10^{-4}	1.5×10^{-3}
PWR 3	4.4×10^{-8}	1.2×10^{-7}	1.0×10^{-6}
PWR 1	4.4×10^{-7}	1.2×10^{-6}	1.0×10^{-5}

Table A.2 lists the 95th percentile values for the sequence end state distribution. The different percentile values (5th, 50th, and 95th) and error factor (EF) for a log-normal distribution are calculated using the equations below. Traditionally, the 5th percentile is considered a lower bound while the 95th percentile is an upper bound.

$$EF = e^{1.645\left(\ln[1+(\sigma/\mu)^2]\right)^{1/2}}$$

$$median = 50th = \frac{\mu}{[1+(\sigma/\mu)^2]^{1/2}}$$

$$95th = median \cdot EF$$

$$5th = \frac{median}{EF}$$

where

σ = log-normal standard deviation

μ = log-normal mean

The risk is defined as the probability of an event multiplied by the release consequence of the event. The risk is then extrapolated over the estimated remaining lifetime of a typical reactor. Most of the embrittlement of the RPVSs occur early in the lifetime of a plant. For the purpose of illustration in this appendix, the analysis assumes that the plant has a 10 year remaining lifetime. The risk from each event sequence is then summed for the 10 years to get an upperbound total risk.

Table A.3 lists the whole body dose consequence associated with each end state category. The consequence data quantifies the WASH-1400 end states and is taken from NUREG/CR-2800. The consequence for the SPRA and SF-PSD end state are both assumed to be zero (no additional risk). The consequence dose values are not treated as uncertain variables. Rather, the values are handled as upper bound numbers, which requires the values to be treated as conservative point estimates.

Table A.3. End State Radioactive Release Consequences.

CATEGORY	Consequence Factor (person-rem)	
	Core Melt	Non Core Melt
PWR 1	5.4×10^6	
PWR 3	5.4×10^6	
PWR 7	2.3×10^3	
PWR 8		7.5×10^4
PWR 9		1.2×10^2

Table A.4 lists the results of the risk analysis. The end state release consequence is multiplied by the end state probability to get an end state risk. The risk is then summed and multiplied by the 10-year duration to get the total additional population risk associated with the possible RPV support failure due to a SSE or a SBLOCA.

Table A.4. Risk Analysis Uncertainty Results.

CATEGORY	EXPECTED RISK (person-rem)	STANDARD DEV. (person-rem)	95th PERCENTILE RISK (person-rem)
SPRA	0/year	0/year	0/year
SF-PSD	0/year	0/year	0/year
PWR 9	0.047/year	1.12/year	0.12 /year
PWR 8	0.029/year	0.71/year	0.077/year
PWR 7	0.20 /year	3.5/year	0.58 /year
PWR 3	0.24 /year	5.4/year	0.65 /year
PWR 1	2.4 /year	54.0 /year	6.4 /year
Σ =	2.9 /year	54 /year	8.2 /year
x 10 years	29	540	82

Table A.4 shows the expected risk is 29 person-rem for the entire ten year embrittlement duration. Accounting for the uncertainties in the event tree analysis gives a 95th percentile risk of 82 person-rem.

Figure A.1 shows the cumulative probability distribution curve for the base case risk. The base case median risk value can be found by taking 10 to the power of the 0.50-probability-risk-value (since the log scale is on a base 10). From the graph, the 0.50-probability-risk-value is approximately -0.8. Thus, the median risk is calculated to be:

$$Risk_{median} = 10^{-0.8} = 0.16 \ person\text{-}rem/year$$

or 1.6 person-rem for the ten year embrittlement duration. The difference between the median and the 95th values illustrates how the uncertainty can skew the calculated values. But even though the uncertainty may result in a wide range of values, the best estimate should be used in decisionmaking due to the conservative nature of the analysis.

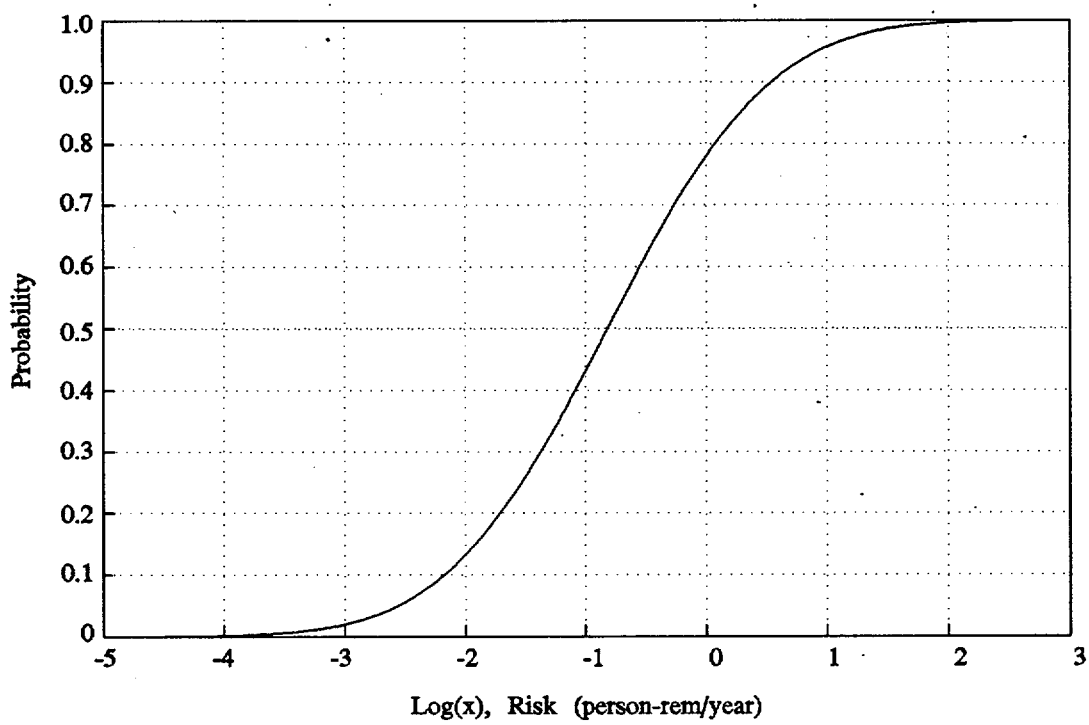

A.1 : Base Case Risk Cumulative Probability Curve.

DRAFT 2

APPENDIX B - GSI-15 Risk Sensitivity Analysis

To judge how sensitive the results of the GSI-15 risk calculations (benefit evaluation) were to the values used for event tree quantification, several supplemental cases were evaluated with even more conservative estimates of failure probabilities. Seven cases were evaluated as discussed below.

Case 1 Increase the frequency of an SSE by a factor of ten. For most plants, this will have the same effect as assuming that a 0.05g earthquake will have sufficient force to potentially result in RPVS failure.

Case 2 Increase offsite dose rates by a factor of 100. This will show the potential results for a plant located in an area of high population density.

Case 3 Increase the probabilities of RPVSF and LBLOCA to 1. This will show the maximum uncertainty in the RPVS failure mechanisms.

Case 4 Increase the probabilities of RPVSF and RPSF to 1 and decrease the probability of LBLOCA to 0. This will show the maximum uncertainty in the reactor protection system failure mechanisms.

Case 5 Increase the probability of ECCSF and CSDSF to 1. This will show the maximum uncertainty involved in initiating event-induced failure of these safety systems.

Case 6 Increase the probabilities of LBLOCA and ECCSF to 1. This will show the maximum uncertainty involving the dependence of a LBLOCA and ECCS

failure on RPVS failure. In other words, it simulates the pressure vessel falling sufficiently (following RPVS failure) to allow the ECCS injection lines to break or become inoperable.

Case 7 Set the probabilities of RPVSF, LBLOCA, RPSF, CSDSF, and ECCSF to 1. This allows for a worst case model of complete failure of the entire reactor protection system with the exception of the containment. This scenario should be considered to be a worst case scenario where the RPVSs and RPV supporting piping are embrittled. Following the initiating event, the subsequent shifting of the RPV results in failure of all core protection systems.

Table B.1. shows the risk results for each of the seven cases and the base case. The results for each case are given in terms of core melt frequency and expected offsite dose (person-rem) per year per plant. Also included in the table are the risks associated with ten, twenty, forty, and sixty years of cumulative operation in a condition where the RPVSs are susceptible to failure.

Table B.1. Sensitivity Analysis Results.

CASE	CORE MELT FREQUENCY (per year)	RISK (per year) [person-rem]	RISK (10 years) [person-rem]	RISK (20 years) [person-rem]	RISK (40 years) [person-rem]	RISK (60 years) [person-rem]
1	6.5×10^{-4}	21	210	420	840	1,300
2	8.8×10^{-5}	290	2,900	5,800	12,000	17,000
3	1.8×10^{-4}	10	100	200	400	600
4	3.5×10^{-4}	2.7	27	54	110	160
5	6.6×10^{-4}	26	260	520	1,000	1,600
6	8.8×10^{-4}	49	490	980	2,000	2,900
7	1.8×10^{-3}	98	980	2,000	3,900	5,900
Base	8.8×10^{-5}	2.9	29	58	120	170

Four extreme cases of cost/benefit were calculated from the results of Table B.1 and the costs from Table 7. The four extreme cases were:

$$I.\ \frac{\textit{maximum cost}}{\textit{minimum benefit}} \qquad II.\ \frac{\textit{maximum cost}}{\textit{maximum benefit}}$$

$$III.\ \frac{\textit{minimum cost}}{\textit{minimum benefit}} \qquad IV.\ \frac{\textit{minimum cost}}{\textit{maximum benefit}}$$

For the above case, the minimum benefit was assumed to be 27 person-rem (Table B.1, case 4, for 10 years), the maximum benefit was assumed to be 17,400 person-rem (Table B.1, case 2, for 60 years), the minimum cost was assumed to be $920,000 (Table 7, Option 2, with AOSC but without replacement power), and the maximum cost was assumed to be $89M (Table 7, Option 3, with AOSC and replacement power). The results of the four extreme cost/benefit cases are presented in Table B.2.

Table B.2. Extreme Cost/Benefit Results.

Case	Case Description	Cost/Benefit ($/person-rem)
I	maximum cost/minimum benefit	3,300,000
II	maximum cost/maximum benefit	5,100
III	minimum cost/minimum benefit	34,000
IV	minimum cost/maximum benefit	53

APPENDIX C - Taylor Series Expansion Program Verification

To assist with the analysis contained in this report, a computer program (TSE) was used to evaluate the Taylor series expansion expressions. As a check for the program, several sample problems were entered in the program to be verified. Also, portions of the analysis in this report were hand calculated to check the numerical results. The remainder of this appendix illustrates how the Taylor series calculations are made and two sample problems are given.

Two equations from the Taylor series expansion arise depending on whether the resulting variable is calculated by a product or a summation. For the case of the product $Z = X_1 \cdot X_2 \cdot X_3 \cdot \ldots \cdot X_n$, the mean and standard deviation are found by:

$$\textit{mean of } Z = \mu_Z = \mu_{X_1} \cdot \mu_{X_2} \cdot \mu_{X_3} \cdot \ldots \cdot \mu_{X_n}$$

$$\textit{standard deviation of } Z = \sigma_Z = \left[\sum_{i=1}^{n} \left[\frac{\partial Z}{\partial X_i} \right]^2 (\sigma_{X_i})^2 \right]^{1/2}$$

For the case of the summation, if $Z = X_1 + X_2 + X_3 + \ldots + X_n$, the mean and standard deviation are found by:

$$\textit{mean of } Z = \mu_Z = \mu_{X_1} + \mu_{X_2} + \mu_{X_3} + \ldots + \mu_{X_n}$$

$$\textit{standard deviation of } Z = \sigma_Z = \left[\sum_{i=1}^{n} (\sigma_{X_i})^2 \right]^{1/2}$$

The TSE program will calculate the mean and standard deviation for any function that can be entered into the program. The partial derivatives are numerically calculated within the program, thereby reducing the analysis time.

For the first sample problem to verify the TSE program, a problem from the statistics book Statistical Models in Engineering[a] by G. Hahn and S. Shapiro was evaluated. The problem asks to calculate the electron current for the circuit given in Figure C.1. The equation to calculate the current is:

$$I = V\left[\frac{1}{R_A} + \frac{1}{R_B} + \frac{1}{R_C}\right]$$

where I = current (amps)
V = voltage (volts)
R = resistance (ohms)

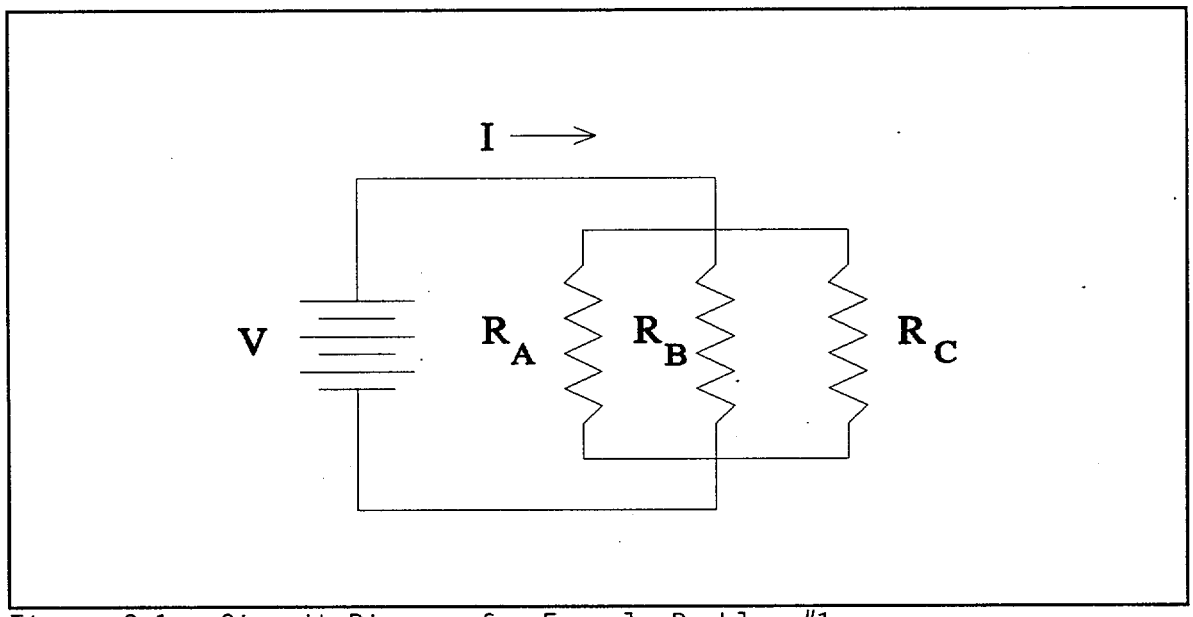

Figure C.1. Circuit Diagram for Example Problem #1.

[a] Hahn, G. J. and S. S. Shapiro, Statistical Models in Engineering, John Wiley & Sons, Inc., 1967, pp. 230-232.

Each of the parameters in the equation above are statistical variables. Table C.1 lists each variable with its mean and standard deviation. Hahn and Shapiro gave the answer for the current as a mean of 26.19 and a standard deviation of 1.616. The TSE program calculates the mean as 26.1 and the standard deviation as 1.61. Thus, very close agreement between the two answers is evident.

Table C.1. Variable Parameters for the Circuit Problem.

Variable	Mean	Standard Deviation
V	120	3.873
R_A	10	1
R_B	15	1
R_C	20	1.414

The second example problem is a hand calculation of the PWR 9 sequence for the analysis in this report. The PWR 9 sequence is contained within both the SSE event tree and the SBLOCA event tree (Figure 1 and Figure 2, respectively). For the SSE event tree, the PWR 9 sequence can be written as:

$$Z_1 = SSE \cdot RPVSF \cdot LBLOCA \cdot \overline{ECCSF} \cdot \overline{RCF}$$

where the bar over the event denotes the compliment of the event. Before evaluating this sequence, the event parameters must be known. From Appendix A, the parameters are shown in Table C.2. It should be pointed out that the numerically calculated results are shown in this Appendix with three significant digits for calculational purposes only.

Table C.2. Variable Parameters for PWR 9 Sequence.

Event	Mean	Standard Deviation
SSE	1.25×10^{-3}	3.5×10^{-2}
SBLOCA	5.0×10^{-4}	2.2×10^{-2}
RPVSF	5.0×10^{-1}	2.0×10^{-1}
LBLOCA	5.0×10^{-1}	2.0×10^{-1}
ECCSF	1.0×10^{-1}	1.0×10^{-1}
RCF	1.0×10^{-3}	5.0×10^{-3}

From page C-1, the mean and standard deviation for the equation Z_1 can be calculated as:

$$\mu_{Z_1} = \mu_{SSE} \cdot \mu_{RPVSF} \cdot \mu_{LBLOCA} \cdot \mu_{ECCSF} \cdot \mu_{RCF}$$

$$\sigma_{Z_1} = \left[\sum_{i=1}^{N} \left(\frac{\partial Z_1}{\partial X_i} \right)^2 (\sigma_{X_i})^2 \right]^{1/2}$$

Evaluating the mean results in:

$$\mu_{Z_1} = (1.25x10^{-3})\ (0.5)\ (0.5)\ (1 - 0.1)\ (1 - (1.0x10^{-3}))$$
$$= 2.81x10^{-4}$$

Taking the equation for the standard deviation, each term will be written out and evaluated separately. Thus, we find:

$$\sigma_{Z_1}^2 = \left[\frac{\partial Z_1}{\partial SSE} \right]^2 (\sigma_{SSE})^2 + \left[\frac{\partial Z_1}{\partial RPVSF} \right]^2 (\sigma_{RPVSF})^2 + \left[\frac{\partial Z_1}{\partial LBLOCA} \right]^2 (\sigma_{LBLOCA})^2$$
$$+ \left[\frac{\partial Z_1}{\partial ECCSF} \right]^2 (\sigma_{ECCSF})^2 + \left[\frac{\partial Z_1}{\partial RCF} \right]^2 (\sigma_{RCF})^2$$

Evaluating the first term in the equation above yields:

$$\left[\frac{\partial Z_1}{\partial SSE}\right]^2 (\sigma_{SSE})^2 = (\mu_{RPVSF} \cdot \mu_{LBLOCA} \cdot \mu_{ECCSF} \cdot \mu_{RCF})^2 (\sigma_{SSE})^2$$

Substituting the appropriate mean values results in:

$$\left[\frac{\partial Z_1}{\partial SSE}\right]^2 (\sigma_{SSE})^2 = \left[(0.5)\ (0.5)\ (1-0.1)\ (1-(1.0x10^{-3}))\right]^2 (3.5x10^{-2})^2$$
$$= 6.19x10^{-5}$$

The four remaining terms are:

$$\left[\frac{\partial Z_1}{\partial RPVSF}\right]^2 (\sigma_{RPVSF})^2 = (\mu_{SSE} \cdot \mu_{LBLOCA} \cdot \mu_{ECCSF} \cdot \mu_{RCF})^2 (\sigma_{RPVSF})^2$$
$$= \left[(1.25x10^{-3})\ (0.5)\ (1-0.1)\ (1-(1.0x10^{-3}))\right]^2 (0.2)^2$$
$$= 1.26x10^{-8}$$

$$\left[\frac{\partial Z_1}{\partial LBLOCA}\right]^2 (\sigma_{LBLOCA})^2 = (\mu_{SSE} \cdot \mu_{RPVSF} \cdot \mu_{ECCSF} \cdot \mu_{RCF})^2 (\sigma_{LBLOCA})^2$$
$$= \left[(1.25x10^{-3})\ (0.5)\ (1-0.1)\ (1-(1.0x10^{-3}))\right]^2 (0.2)^2$$
$$= 1.26x10^{-8}$$

$$\left[\frac{\partial Z_1}{\partial ECCSF}\right]^2 (\sigma_{ECCSF})^2 = \left(-(\mu_{SSE} \cdot \mu_{RPVSF} \cdot \mu_{LBLOCA} \cdot \mu_{RCF})\right)^2 (\sigma_{ECCSF})^2$$
$$= \left[-(1.25x10^{-3})\ (0.5)\ (0.5)\ (1-(1.0x10^{-3}))\right]^2 (0.1)^2$$
$$= 9.75x10^{-10}$$

$$\left[\frac{\partial Z_1}{\partial RCF}\right]^2 (\sigma_{\overline{RCF}})^2 = \left(-(\mu_{SSE} \cdot \mu_{RPVSF} \cdot \mu_{LBLOCA} \cdot \mu_{\overline{ECCSF}})\right)^2 (\sigma_{RCF})^2$$

$$= \left[-(1.25x10^{-3})\ (0.5)\ (0.5)\ (1-0.1)\right]^2 (5.0x10^{-3})^2$$

$$= 1.98x10^{-12}$$

From the five above terms, the standard deviation of Z_1 is found by:

$$\sigma_{Z_1} = \left(6.19x10^{-5} + 1.26x10^{-8} + 1.26x10^{-8} + 9.75x10^{-10} + 1.98x10^{-12}\right)^{1/2}$$

$$= 7.87x10^{-3}$$

Now, the PWR 9 sequence from the SBLOCA event tree will be analyzed in a similar manner. The PWR 9 sequence for the SBLOCA event tree can be written as:

$$Z_2 = SBLOCA \cdot RPVSF \cdot LBLOCA \cdot \overline{ECCSF} \cdot \overline{RCF}$$

The mean and standard deviation of the SBLOCA PWR 9 sequence are:

$$\mu_{Z_2} = \mu_{SBLOCA} \cdot \mu_{RPVSF} \cdot \mu_{LBLOCA} \cdot \mu_{\overline{ECCSF}} \cdot \mu_{\overline{RCF}}$$

$$\sigma_{Z_2}^2 = \left[\frac{\partial Z_2}{\partial SBLOCA}\right]^2 (\sigma_{SBLOCA})^2 + \left[\frac{\partial Z_2}{\partial RPVSF}\right]^2 (\sigma_{RPVSF})^2 + \left[\frac{\partial Z_2}{\partial LBLOCA}\right]^2 (\sigma_{LBLOCA})^2$$
$$+ \left[\frac{\partial Z_2}{\partial ECCSF}\right]^2 (\sigma_{\overline{ECCSF}})^2 + \left[\frac{\partial Z_2}{\partial RCF}\right]^2 (\sigma_{\overline{RCF}})^2$$

Calculating the mean value results in:

$$\mu_{Z_2} = (5.0x10^{-4})\ (0.5)\ (0.5)\ (1-0.1)\ (1-(1.0x10^{-3}))$$
$$= 1.12x10^{-4}$$

Calculating the five terms for use in the standard deviation equation results in:

$$\left[\frac{\partial Z_2}{\partial SBLOCA}\right]^2 (\sigma_{SBLOCA})^2 = 2.45x10^{-5}$$

$$\left[\frac{\partial Z_2}{\partial RPVSF}\right]^2 (\sigma_{RPVSF})^2 = 2.02x10^{-9}$$

$$\left[\frac{\partial Z_2}{\partial LBLOCA}\right]^2 (\sigma_{LBLOCA})^2 = 2.02x10^{-9}$$

$$\left[\frac{\partial Z_2}{\partial ECCSF}\right]^2 (\sigma_{ECCSF})^2 = 1.56x10^{-10}$$

$$\left[\frac{\partial Z_2}{\partial RCF}\right]^2 (\sigma_{RCF})^2 = 3.16x10^{-13}$$

Therefore, the standard deviation of Z_2 is found by:

$$\sigma_{Z_2} = \left(2.45x10^{-5} + 2.02x10^{-9} + 2.02x10^{-9} + 1.56x10^{-10} + 3.16x10^{-13}\right)^{1/2}$$
$$= 4.95x10^{-3}$$

Now, the total PWR 9 sequence probability is calculated by adding the SSE results to the SBLOCA results:

$$PWR\ 9_{TOTAL} = PWR\ 9_{SSE} + PWR\ 9_{SBLOCA}$$

From page C-1, when two variables are added, the mean and standard deviation can be calculated from:

$$\mu_{PWR\ 9_{TOTAL}} = \mu_{PWR\ 9_{SSE}} + \mu_{PWR\ 9_{SBLOCA}}$$
$$= 2.81x10^{-4} + 1.12x10^{-4} = 3.93x10^{-4}$$

$$\sigma_{PWR\ 9_{TOTAL}} = \left((\sigma_{PWR\ 9_{SSE}})^2 + (\sigma_{PWR\ 9_{SBLOCA}})^2\right)^{1/2}$$
$$= \left((7.87x10^{-3})^2 + (4.95x10^{-3})^2\right)^{1/2}$$
$$= 9.30x10^{-3}$$

Table A.2 lists the calculated sequence end states from the TSE program. For the total PWR 9 sequence, the calculated mean is $3.9x10^{-4}$ and the calculated standard deviation is $9.3x10^{-3}$. These calculated results confirm the above hand calculated values.

APPENDIX D - GSI-15 Cost/Benefit Ratio Graphs

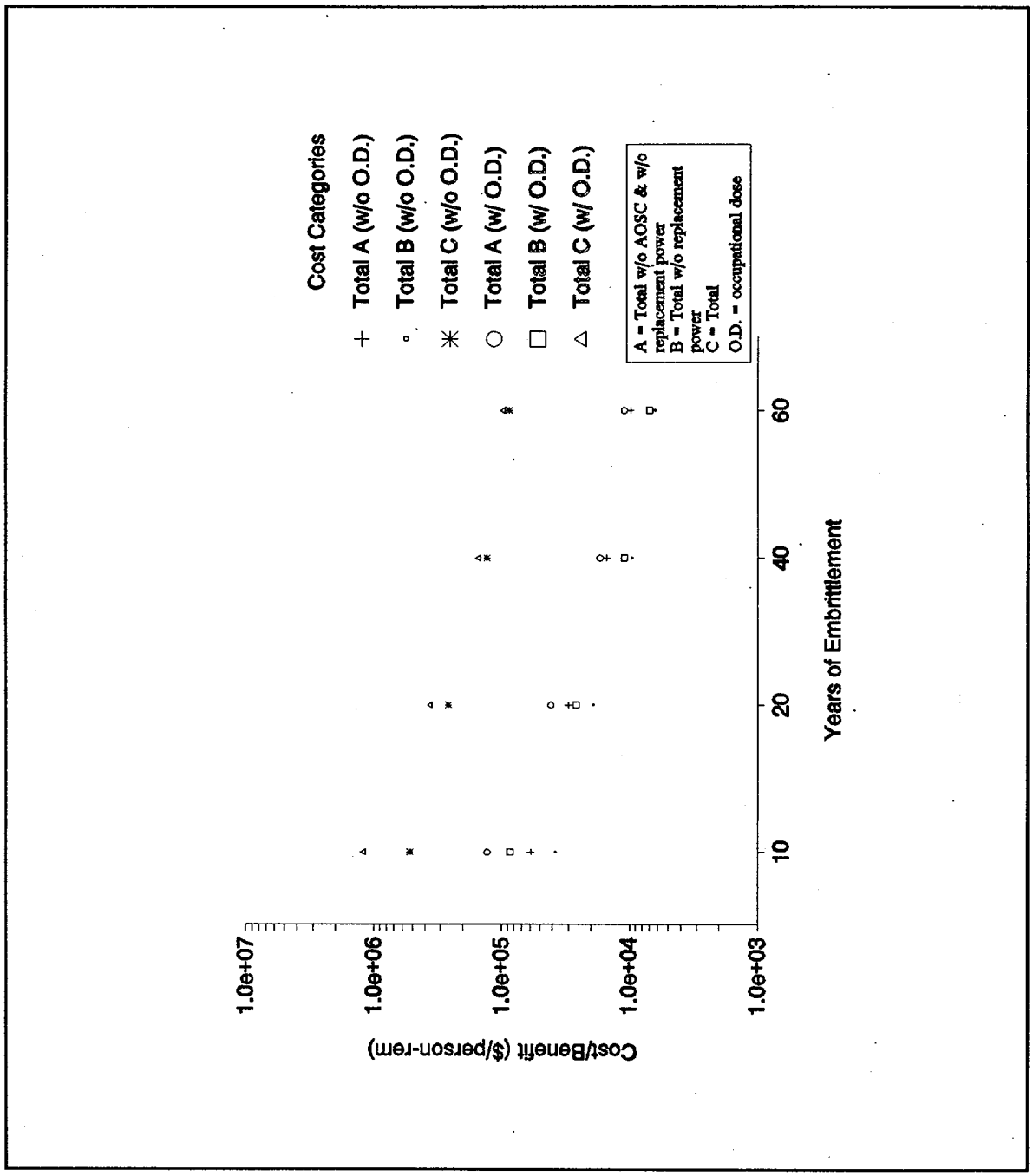

Figure D.1. Option 1 Cost/Benefit Ratios.

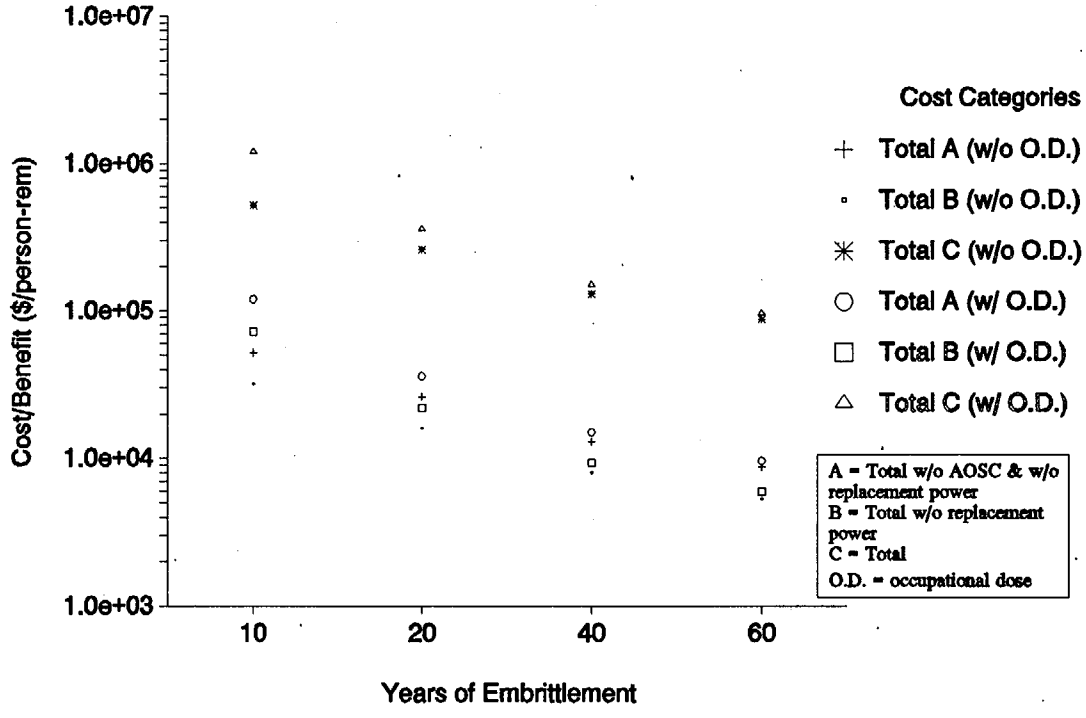

Figure D.2. Option 2 Cost/Benefit Ratios.

DRAFT 2

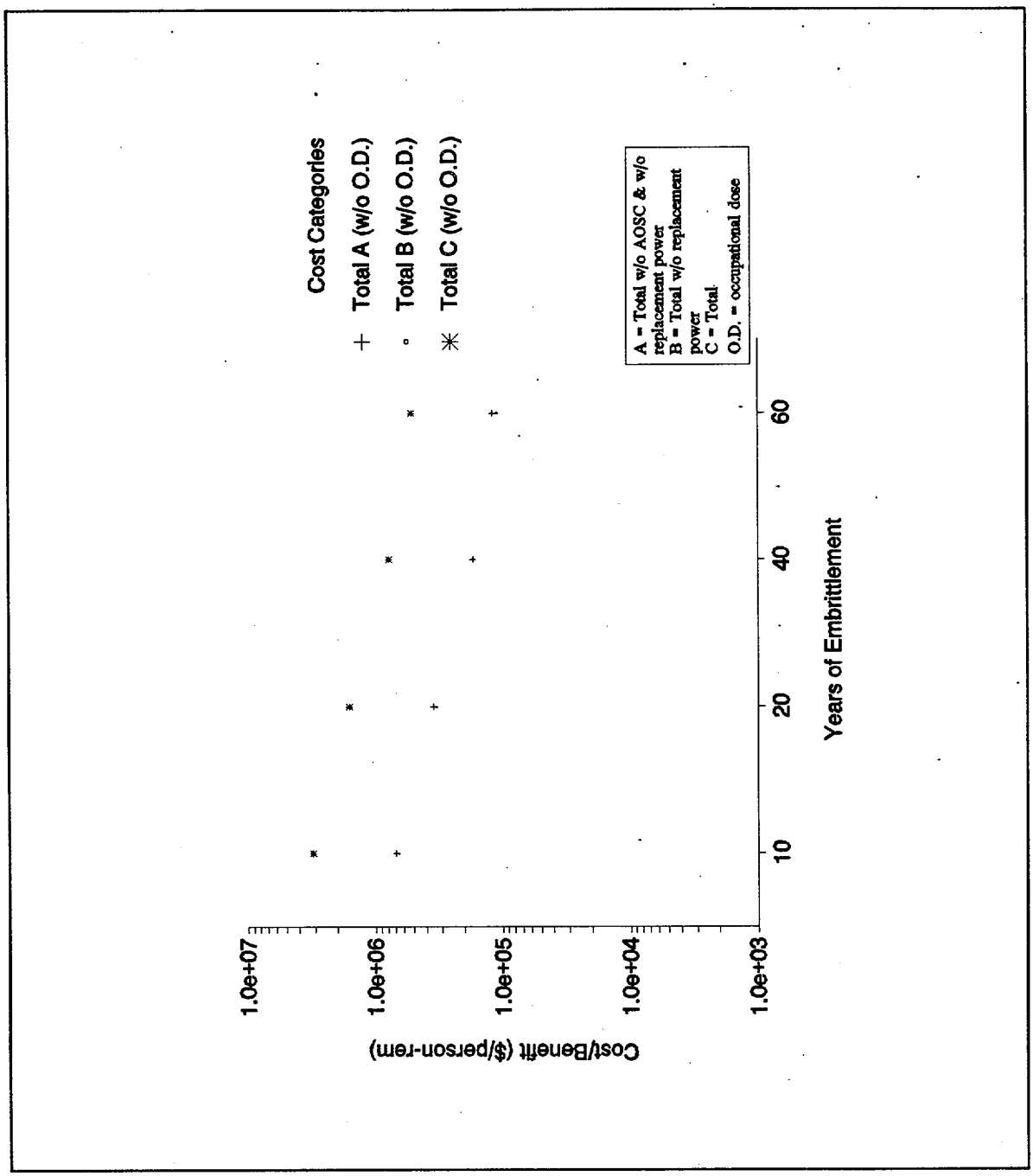

Figure D.3. Option 3 Cost/Benefit Ratios.

DRAFT 2

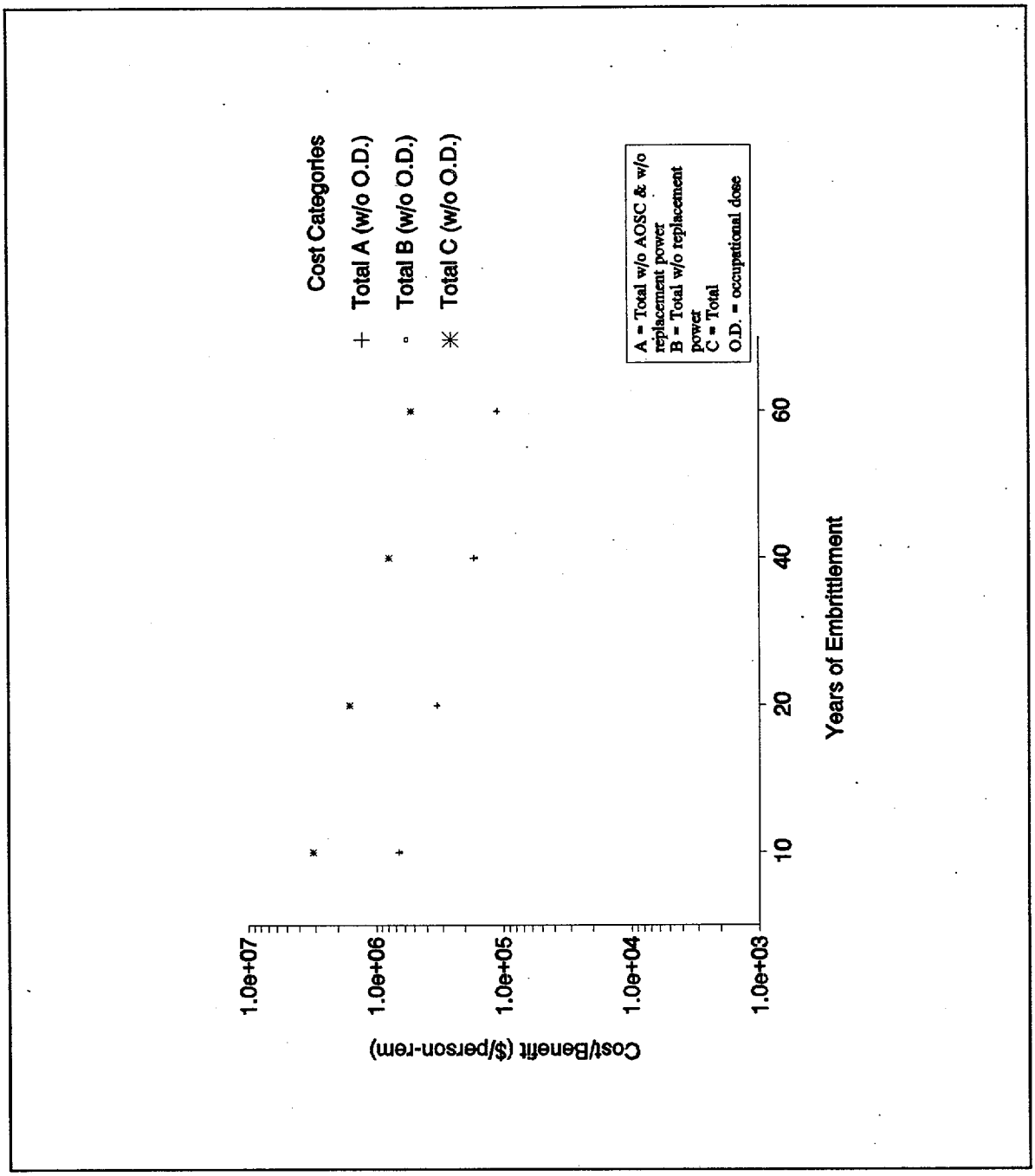

Figure D.4. Option 4A Cost/Benefit Ratios.

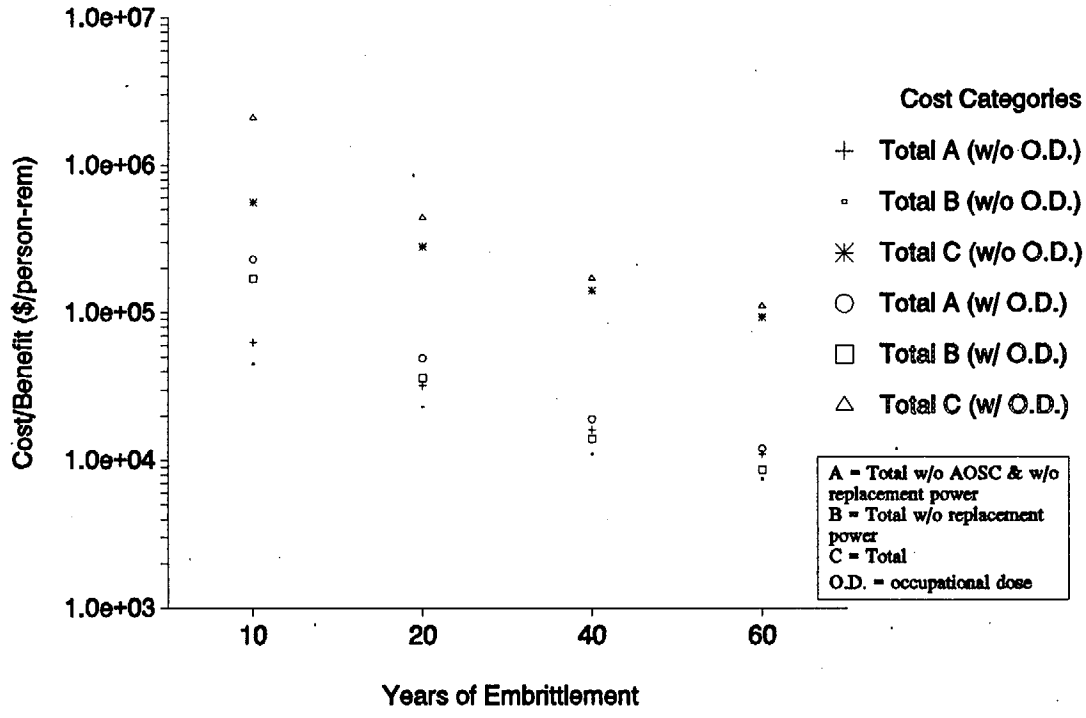

Figure D.5. Option 4B Cost/Benefit Ratios.

DRAFT 2

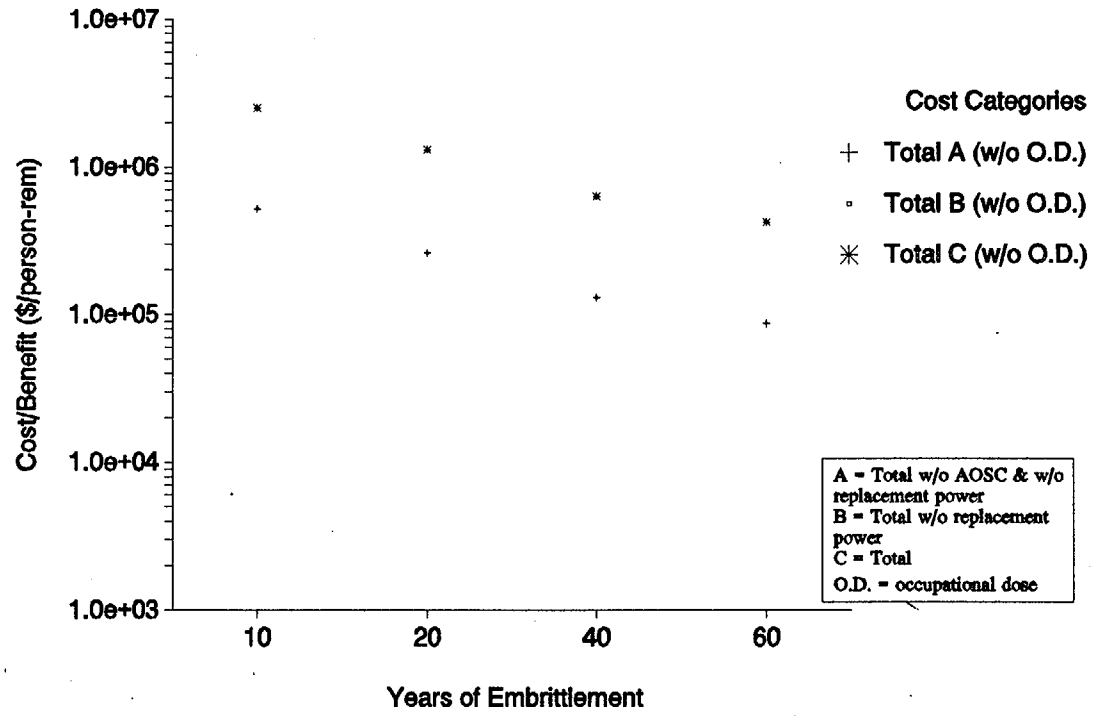

Figure D.6. Option 5 Cost/Benefit Ratios.

DRAFT 2

APPENDIX B

APPENDIX B

SHIPPINGPORT VESSEL/SHIELD-TANK FLUENCE CALCULATIONS

Craig A. Hrabal

1.0 INTRODUCTION

The Shippingport reactor vessel and neutron shield tank (NST) provided an independent source of measured data for evaluating ΔNDTT correlations and dependencies. The Shippingport NST was fabricated of ASTM A 212 carbon steel. The same steel specification was used in the HFIR pressure vessel. Both the Shippingport NST and the HFIR reactor vessel were exposed to a low neutron flux/high fluence radiation field. Despite this, the initial evaluation of the Shippingport materials suggested that the ΔNDT was much less than observed in the HFIR tests. Therefore, the principal objective of the study conducte by the Brookhaven National Laboratory (BNL) and reported here was to provide accurate estimates of the neutron fluence and spectra for the Shippingport vessel and NST to aid in the interpretation of materials property test data. This effort was further motivated by fairly large initial calculation-to-measurement differences for the fluence, the availability of newer codes, and improvements in methods relative to those used in the initial evaluations by the Bettis Laboratory.

The Shippingport reactor vessel and shield tank geometry are shown in elevation and plan views in Figures 1.1 through 1.4. Note that while the vessel and ex-vessel geometries remain unchanged, the details of the core geometry and layout of the internals varied for the three cores, PWR-1, PWR-2, and the LWBR (Refs. 1-3).

The approach used to analyze each of the core configurations (cf. Figures 1.2 - 1.4) will be described in Section 2; the resulting for energy spectra and fluence distributions at the vessel and selected shield tank locations will be given in Section 3.

2.0 CALCULATIONAL METHODOLOGY

The calculational methodology for determining the energy spectra and fluence distributions at the Shippingport reactor pressure vessel and neutron shield tank consisted of the six basic tasks summarized in Figure 2.1. These tasks were performed by BNL. Briefly, the initial task consisted of collecting the geometry, materials, and power distribution data that describe the three core-vessel-NST configurations and operating histories. Following that, one-dimensional multi-group discrete ordinates calculations were performed for each core to provide initial estimates of the fluence and energy spectra at locations of interest, as well as few-group, region-dependent cross sections for subsequent detailed two-dimensional analyses. Following the two-dimensional planar calculations for each core, the three-dimensional fluence at radial and azimuthal locations of interest was constructed based on axial factors, and operating power level and history data. The corresponding

detailed energy dependent spectra were then determined from an auxiliary series of calculations performed in one-dimensional geometry with a multi-group library designed for LWR slowing down calculations.

A summary of the above steps in flow-chart format is shown in Figure 2.2.

2.1 ONE-DIMENSIONAL CALCULATIONS

One dimensional calculations for the core-internals-vessel-NST geometry were performed with the ANISN discrete ordinates transport code (Ref. 4). An S-8 symmetric quadrature was assumed, and P-3 expansion cross sections from the BUGLE-80 (Ref. 5) library distributed by RSIC were employed. This library is based on ENDF/B-IV (Ref. 6), and contains cross section data in 47 neutron and 20 gamma groups. The BUGLE-80 library was selected for the baseline fluence determinations because it had been developed primarily for pressure vessel damage fluence calculations; consequently, while it has a relatively fine energy resolution above approximately 0.1 MeV, the remainder of the energy range is fairly sparsely covered, with only 2 groups below 0.414 eV. The primary purpose of the one-dimensional analyses was to generate few group cross sections for the subsequent two-dimensional calculations which cannot be performed, as a practical matter, with so many groups. The one-dimensional models served two other functions: 1) "sensitivity" type analyses to determine the optimal collapsed few group structure and the spatial mesh, and 2) determination of the full range energy spectra. As noted earlier, while the BUGLE-80 library is well suited to the evaluation of high energy neutron transport in LWR geometries, its treatment of lower energies (especially thermal) is crude. Consequently, since one of the primary objectives of the current analyses was to determine the full energy range spectra, a more appropriate cross section library was required. The MATXS-7, 69 neutron group library (Ref. 7), was selected for this purpose. This library contains 42 groups below 4.0 eV, is based on ENDF/B-V (Ref. 8), and was generated by LANL for EPRI for use in LWR slowing down spectrum codes. Therefore, it is well suited to the present application.

The ANISN models for the three Shippingport configurations were used to collapse the 47 group BUGLE-80 cross sections, by region, to few group macroscopic cross sections which preserved the essential characteristics of the greater than 0.1 MeV neutron flux spectra throughout the problem. It was found that the 18-group structure shown in Table 1 was sufficient for this purpose.

2.2 TWO-DIMENSIONAL CALCULATIONS

The two-dimensional calculations were performed with the DORT (Ref. 9) discrete ordinates transport code in (r,θ) geometry: an S-8 fully symmetric quadrature was employed with the 18-group region and core-configuration-specific cross sections generated by the one-dimensional analyses described above. As previously noted, an adequate radial mesh for the bulk of the problem (which is truly radial in character) was determined from the one-dimensional calculations. However, in order to determine an adequate (r,θ) spatial mesh to model the rectangular assemblies of the two PWR cores, or the pseudo-hexagonal LWBR core, the BNL developed MESH code (Ref. 10) was

employed. This program allocates (r,θ) geometry mesh blocks to the appropriate (x,y) or hexagonal assembly, and creates the spatial and energy-dependent source used in the fixed source DORT calculations.

2.3 SYNTHESIS OF 3-D FLUENCE

The three-dimensional fluence at specific locations was obtained by combining the few-group flux results from the three core-dependent DORT calculations with the appropriate power level, EFPH, and axial peaking factors. This task was performed by the FLUENCE program which also accounts for the individual symmetries of the PWR and LWBR configurations. The full energy range fluence spectra were obtained by scaling the one-dimensional MATXS7 results at the required radial location such that the flux greater than 1.0 MeV matched that obtained from the BUGLE-80 based calculation(s).

3.0 RESULTS

The results of the BNL calculations, presented in the following, consisted of neutron energy spectra, radial and azimuthal fast neutron (E > 1.0 MeV) fluxes at selected radial and angular sectors and radial zones, respectively, and core specific and total azimuthal fast neutron fluences at the pressure vessel and NST locations. The pressure vessel and NST fluxes were determined at the elevations where flux measurements had been carried out. As noted earlier, the two-dimensional (r,θ) discrete ordinate transport calculations were carried out using a collapsed 18-energy group cross section set derived from a 47-group BUGLE library. The adequacy of the 18-group set had been demonstrated by comparing neutron energy spectra in 18 groups and 47 groups in each of the 18 regions of each Shippingport configuration. Figures 3.1 and 3.2 show the 47- and 18-group spectra, respectively, in the inner blanket region of the PWR-2 core. The 47-group and 18-group spectra in the pressure vessel are shown in Figures 3.3 and 3.4, respectively. The (r,θ) mesh representation of one octant in the Shippingport DORT model for the PWR-2 configuration is shown in Figure 3.5. This model consists of 221 radial mesh intervals and 45 angular mesh intervals. Regions 1 through 5 represent the core octant. Region "E" represents the pressure vessel.

Eighteen-group radial and azimuthal neutron fluxes were obtained at each (r,θ) mesh point shown in Figure 3.5. Fast neutron (E > 1.0 MeV) fluxes at a desired (r,θ) mesh were obtained by summing over the energy groups above 1.0 MeV at that mesh. Radial flux distributions at 1° (flats), 24° and 45° are shown in Figures 3.6 through 3.8, respectively. Azimuthal fast neutron fluxes are shown at the core edge and at the inner and outer surfaces of the pressure vessel, in Figures 3.9, 3.10 and 3.11, respectively. The flattening of the azimuthal fluxes with increasing distance from the core was noted.

Based on Bettis and Duquesne Power accumulated exposure data, the fast neutron (E > 1.0 MeV) fluence from each individual Shippingport core has been determined. Using Bettis axial flux distributions, azimuthal fluences were determined at the six elevations at which measured materials data were available: 687.5 ft, 689.0 ft, 690.0 ft, 690.5 ft, 692.5 ft and 693.0 ft. Figure 3.12 shows schematically the 689.0, 690.0, and 692.5 ft elevations relative to the positions of the three Shippingport cores. Figures 3.13

through 3.15 show the individual azimuthal fluences of the PWR-1, PWR-2 and LWBR cores as well as the total fluence at the pressure vessel at 689.0 ft., 690.5 ft., and 692.5 ft., respectively. Similarly, at these elevations, plots of individual and total azimuthal fluences at the NST are given in Figures 3.16 through 3.18, for the inside surface, and in Figures 3.19 through 3.21, for the outside surface.

The results of the full energy (69-group) spectra calculations at the pressure vessel inner wall and at the NST inside and outside surfaces are presented in Table 3.1 and shown in Figures 3.22 through 3.24. The results of the neutron fluence calculations at the pressure vessel inner wall, at the inside and outside surface of the shield tank inner wall, and at the inside and outside surface of the shield tank outer wall are presented in Tables 3.2 through 3.6 for the locations where samples were taken. Also, the fluence values in Tables 3.2 through 3.6 are given in terms of the fast fluence (E>1.0MeV), the fast fluence (E>0.1MeV), the thermal fluence (E<0.4eV), and the total fluence.

4.0 REFERENCES

1. "The Shippingport Pressurized Water Reactor," Naval Reactors Branch, U.S.A.E.C., Westinghouse Electric Corporation and Duquesne, Addison-Wesley Publishing Co., Inc., 1958.

2. "Shippingport Operations During PWR Core 2 Depletion," (April 1965 to February 1974), WAPD-335, 1983.

3. "Shippingport Operations With the Light Water Breeder Reactor Core," WPAD-TM-1542, 1986.

4. W.W. Engle, Jr., "A Users Manual for Manual for ANISN," K-1693, Oak Ridge National Laboratory, 1967.

5. R.W. Roussin, "BUGLE-80, Coupled 47 Neutron, 20 Gamma-Ray, P_3, Cross Section Library for LWR Shielding Calculations" Oak Ridge National Laboratory, DLC-75, 1980.

6. ENDF-102 Data Formats and Procedures for the Evaluated Nuclear Data File, ENDF, BNL-NCS-50496, 1975.

7. R.E. MacFarlane, "TRANSX-CTR: A Code for Interfacing MATRIX Cross-Section Libraries to Nuclear Transport Codes for Fusion Systems Analysis," LA-9863 Los Alamos National Laboratory, 1984.

8. R. Kinsey, Ed., "ENDF-102, Data Formats and Procedures for the Evaluated Nuclear Data File, ENDF," Brookhaven National Laboratory, report BNL-NCS-50496 (ENDF-102) 2nd Edition (ENDF-102) 2nd Edition (ENDF/B-V), Revised, 1983.

9. "DORT, Two-Dimensional Discrete Ordinates Transport Code," RSIC Computer Code Collection, CCC-484, Oak Ridge National Laboratory, 1988.

10. M.D. Zentner, "MESH-A Code for Determining the DOT Fixed Neutron

Source," BNL memorandum, August 25, 1981.

APPENDIX C

SYNOPSIS OF WORK TO DETERMINE THE RADIATION EXPOSURE TO VESSEL SUPPORT STRUCTURES IN THE TROJAN NUCLEAR REACTOR

Prepared by Emmert D. McGarry
National Institute of Standards and Technology
Ionizing Radiation Division
Gaithersburg, Maryland 20899

Executive Summary:

To determine the neutron environment within the cavity region of the Trojan Nuclear Power Reactor, Portland, Oregon, during Cycle 13, neutron transport calculations and ex-vessel cavity dosimetry measurements were completed. The radiation embrittlement of a critical support structure that had a relative high degree of stress was of concern. Because the critical point on this beam was embedded in seven inches of concrete, the method of investigation was by discrete ordinates transport calculations, first calculated and checked against measurements at the locations of the neutron dosimetry in the ex-vessel cavity near the beam, then calculated for the concrete at the critical stress point of interest.

The Engineering Division/RES of the Nuclear Regulatory Commission contracted with the Oak Ridge National Laboratory (ORNL) and the National Institute of Science and Technology (NIST) to perform calculations and measurements, respectively, of the fast neutron exposure to critical pressure vessel support structures at the Trojan electrical power reactor. The measurements were made by the Westinghouse Science and Technology Center under contract to NIST.

Calculations using ENDF/B VI cross sections gave a fast fluence rate (E > 1 MeV) at the critical stress point equal to 6.9E+07 neutrons per cm^2 per second. The thermal-to-fast ratio at this point was computed to be 46. The DPA rate at the critical stress point was calculated to be 2.0E-13 displacements per atom per second. These conclusions are from a NUREG report (Ref. 1).

The calculations were done by Louisiana State University, Nuclear Science Center under contract to ORNL. All calculations are higher than the experimental results. It is believed that disagreements between measurements and calculations are due to incorrect, and now unattainable, power distribution information. The problem is identified in the second paragraph of page 3, Ref. 1. This synopsis will show that the calculated spectra agree fairly well with measured results but that there are flux magnitude disagreements, on the order of 40%, at all locations. Since the energy spectra appear to be correct and the calculational fluences are higher, it is considered conservative, and instructive, to use the calculated values for the computed DPA at the critical in-concrete position without attempting to normalize to the measured results.

Dosimetry Measurements:

Ref. 2, Page 3 provides a thorough description and figures of the Trojan Plant and experimental configuration. For the purpose of explaining Tables A.1 and A.2 in this synopsis, the following explanation of dosimetry locations is given.

The dosimeters were sealed (screwed shut) in patented aluminum holders nominally 1.5" x 4.5" x 0.75" thick. The four dosimetry sets were located in the cavity of the Trojan Reactor at two different radial locations: (1) 5 cm behind the thermal insulation that surrounds the pressure vessel at radius=257 cm and (2) two were attached within cut away sections of an ORNL designed and fabricated stainless steel pipe that was inserted into the ex-core neutron-detector instrumentation well. These two dosimetry packages were located vertically above and below the

midplane of the reactor near to the height of the critical support structure but not in direct line-of-sight with a polyethylene section that is a part of the reactor dosimetry instrumentation in that well at radius=321.6 cm. At both of these radial locations, the various activation foils, fission foils, and solid state track recorders (SSTR's) were at two heights: (1) 20.3 cm below and 121.9 cm above the core midplane. These dosimetry locations were named as follows:

Dosimetry Name	Location Radius	Azimuth	Height (relative to midplane)
A	257 cm	0°	+ 121.9 cm
B	257 cm	0°	- 20.3 cm
C	321.6 cm	0°	+ 121.9 cm
D	321.6 cm	0°	- 20.3 cm

Post-irradiation processing and analyses of the radiometric foils and gamma dosimeters was accomplished using the Waltz Mill (gamma counting) Laboratory of Westinghouse facilities. The calibrations of the gamma counting facility were checked against standard neutron field irradiations within one year of the processing of the radiometric foils. The calibration required that NIST-supplied radioactive foils be counted for each reaction. The results from the benchmark-irradiated dosimeters are summarized by observing that specific activities reported by the vendor were within ±5% of those certified by NIST, which were based upon irradiation fluences certified to ±2.5% multiplied by ^{235}U fission spectrum averaged cross sections.

Results:

Table A.1 summarizes the NIST analyses of radiometric and SSTR data measured by Westinghouse and reported to NIST in Ref. 2. Please note the sources of data because subsequent paragraphs present a NIST analysis, completed after Ref. 1 and 2 were published, that show the measurements and calculations give essentially the same energy spectrum but different flux magnitudes.

Table A.1, herein, is Table A.1 from Ref.1. The radiometric reaction rates and fission rates per nucleus listed in Section 1-A of Table A.2 are from Ref. 2. In particular, threshold radiometric reactions for capsule locations A, B, C, and D for $^{63}Cu(n,\alpha)$, ^{46}Ti, $^{54}Fe(n,p)$, and $^{58}Ni(n,p)$ are given in Table 6 of Ref. 2. The ^{238}U radiometric fission data, corrected for ^{235}U impurity response, was taken from Table 7 of Ref. 2. The ^{238}U and ^{237}Np SSTR data come from Table B-1 of Ref. 2.

Table A.1, herein, is in three sections:

1) Section 1-A is the above mentioned reaction and fission rates.

2) Section 1-B has normalized data for each location (e.g. A, B, C, and D) as well as their averages for each type of reaction. The data are normalized to that of the $^{58}Ni(n,p)$ reaction in the respective location. Note the similarity of the normalized data for all four locations. The standard deviation of the average is also given. Except for the 4.55 value for the $^{28}U(n,f)Ru$ result, which increases the associated standard deviation up to a noticeable 11.2%, all deviations are less than 5%, and most are considerably less. This shows that the

spectra in all four locations are very similar.

3) Section 1-C examines the average and standard deviation of the fast fluence rate magnitudes among the four locations. As seen, these range from 0.70 to 1.37. The relatively small standard deviations of the relative flux magnitudes suggest very good consistency among the measured dosimetry results.

Table A.2 is the same type of three-section table as A.1 but it deals with calculated results, using ENDF/B-VI cross sections. The page numbers in the column headings refer to data (from Ref.1) listed for the four locations. One significant difference between Tables A.1 and A.2 is that of the experimental (measured) and calculated averages and their ratios (E/C) for the data normalized to the ^{58}Ni(n,p) reaction, noted in Section 2-B of Table A.2. The E/C ratios show that both the measurements and calculations see essentially the same fast neutron spectrum for all four locations. This is a strong indication that the energy spectrum (at the dosimeters) has been determined and that the flux magnitude problems do stem from power distribution problems and, possibly, from local perturbation in the ex-core instrument well.

References:

1. M. Asgari, M. L. Williams (Louisiana State University), F. B. K. Kam (Oak Ridge National Laboratory), and E. D. McGarry (National Institute of Standards and Technology), "Transport Calculations of Radiation Exposure to Vessel Support Structures in the Trojan Reactor", NUREG/CR-XXXX, ORNL/TM-YYYY, February 1994.

2. F. H. Ruddy, J. G. Seidel, and J. L. Gonzalez (Westinghouse Track Recorder Laboratory) and A. H. Fero, S. L. Anderson, and M. R. Fawchak (Westinghouse Energy Systems Business Unit), "Reactor Cavity Neutron Dosimetry Results for the Trojan Nuclear Power Plant", Proprietary Class-2 WSTC Report 93-9TDO-TROJN-R1, March 19, 1993.

Table C.1 NIST analyses of radiometric and SSTR dosimetry data measured by Westinghouse during Trojan Cycle 13

Reaction	A	B	C	D	Avg.	Std(%)
1-A[d]						
Cu^{63}(n,a)	0.0242	0.032	0.0162	0.0211	0.0234	
Ti^{46}(n,p)	0.344	0.460	0.235	0.304	0.3358	
Fe^{54}(n,p)	1.560	2.070	1.060	1.350	1.5100	
Ni^{58}(n,p)	2.310	3.100	1.550	2.010	2.2425	
U^{28}(n,f)Ru	8.830	11.200	7.060	6.860	8.4875	
U^{28}(n,f)Zr	8.020	11.100	5.580	7.020	7.9300	
U^{28}(n,f)Cs	7.760	10.600	5.600	7.090	7.7625	
U^{28}SSTR	8.680	10.800	5.720	6.770	7.9925	
Np^{37}SSTR	124.00		162.00	81.20	110.00	119.30
1-B[b]						
Cu^{63}(n,a)		0.01048		0.01032		
0.01045	0.01050	0.0104	0.65			
Ti^{46}(n,p)	0.14892		0.14839			0.15161
0.15124	0.1500	0.94				
Fe^{54}(n,p)		0.67532		0.66774		
0.68387	0.67164	0.6746	0.88			
Ni^{58}(n,p)		1.0	1.0		1.0	1.0
U^{28}(n,f)Ru		3.82251		3.61290		
4.55484	3.41294	3.8508	11.21			
U^{28}(n,f)Zr		3.47186		3.58065		
3.60000	3.49254	3.5363	1.55			
U^{28}(n,f)Cs	3.35931		3.41935			3.61290
3.52736	3.4797	2.81				
U^{28} SSTR		3.75758		3.48387		
3.69032	3.36816	3.5750	4.37			
Np^{37} SSTR		53.6797		52.2581		52.3871
54.7264	53.263	1.90				
1-C[c]						
Cu^{63}(n,a)	1.03529	1.36898	0.69305	0.90267		
Ti^{46}(n,p)	1.02457	1.37007	0.69993	0.90544		
F^{54}(n,p)	1.03311	1.37086	0.70199	0.89404		
Ni^{58}(n,p)	1.0310	1.38239	0.69119	0.89632		
U^{28}(n,f)Ru						
U^{28}(n,f)Zr	1.01135	1.39975	0.70366	0.88525		
U^{28}(n,f)Cs	0.99968	1.36554	0.72142	0.91337		
U^{28}SSTR	1.08602	1.35127	0.71567	0.84704		
Np^{37}SSTR	1.03940	1.35792	0.68064	0.92205		
Avg.	1.0324	1.3708	0.7009	0.8958		
Std(%)	2.44	1.02	1.47	2.25		

Table C.1 Continued

[a]Radiometric reaction and fission rates per nucleus = > (where all values have an exponent of 10-17) < =.
[b]Ratios of above rates relative to Ni^{58}(n,p) reactions.
[c]Ratios of rates relative to their averages in part-A.

Table C.2 NIST analyses of calculated dosimetry data for TROJAN Cycle 13. Values in 2-A have exponents of 10-17 reactions per nucleus.

	On RPV	On RPV	Inst. Tube	Inst. Tube
	Z=121.90	Z= -20.3		Z=121.90
	Z= -20.3			
	A	B	C D	Avg.
	(Page 43)	(Page 37)	(Page	44)
	(Page 38)			
2-A				
Cu^{63}(n,a)	0.0336	0.0419	0.0249	0.0334
	0.0335			
Ti^{46}(n,p)	0.4470	0.5570	0.3340	0.4470
	0.4463			
Fe^{54}(n,p)	2.3400	2.9100	1.7800	2.3S00
	2.3525			
Ni^{58}(n,p)	3.2600	4.0600	2.4900	3.3300
	3.2850			
U^{238}(n,f)	11.5000	14.4000	8.9500	12.0000
	11.7125			
Np^{237}(n,f)	159.0000	201.0000	128.0000	171.0000
	164.7500			
Expt	E/C		Calc.	
	2-B		Avg.	
Avg.	Ratio			
Cu^{63}(n,a)	0.0103	0.0103	0.0100	
0.0100	0.0102	0.0104	1.023	
Ti^{46}(n,p)	0.1371	0.1372	0.1341	
0.1342	0.1357	0.1500	1. 1 0 6	
Fe^{54}(n,p)	0.7178	0.7167	0.7149	
0.7147	0.7160	0.6750	0.943	
Ni^{58}(n,p)	1.0000	1.0000	1.0000	
1.0000	1.0000	1.0000	1.000	
U^{238}(n,f)	3.5276	3.5468	3.5944	
3.6036	3.5681	3.5300	0.989	
Np^{237}(n,f)	48.7730	49.5074	51.4056	
51.3514	50.2593			
53.3000				
1.060				
2-C				
Cu^{63}(n,a)	.0045	.2526	0.7444	
0.9985				
Ti^{46}(n,p)	.0017	.2480	0.7485	
1.0017				
Fe^{54}(n,p)	0.9947	.2370	0.7566	
1.0117				
Ni^{58}(n,p)	0.9924			
1.2359	0.7580			
1.0137				
U^{238}(n,f)	0.9819	.2296	0.7641	
1.0245				
Np^{237}(n,f)	0.9651	.2200		
0.7769	.0379			
Calc. Avg	0.9900	.2372		
0.7581	.0147			
Expt. Avg	1.0320	.3710		
0.7010	.8960			
E/C of Avg	1.0424	1.1081		
0.9240	.8830			

Section 2-B: Ratios of radiometric and fission rates relative to Ni^{58}(n,p) reaction.

Section 3-B: Ratios of rates relative to their averages in Section 1-A.

APPENDIX D

R. E. Johnson: "Recommendations Regarding Evaluation of Cast Stainless Steel with Respect to Aging Embrittlement," based on reviews of ANL reports by P. K. Nagata and W. G. Reuter, INEL.

RECOMMENDATIONS REGARDING EVALUATION OF CAST STAINLESS STEEL WITH RESPECT TO AGING EMBRITTLEMENT

The results of the work done in support of the resolution of GSI-15 led to the conclusion that radiation embrittlement of RPV supports is not as serious a problem as the HFIR surveillance data first suggested. However, even the limited survey of supports in operating nuclear power plants showed that some steels of initial construction might exhibit limited resistance to brittle fracture. Therefore, as noted more fully in the text of this NUREG, there may be conditions which would lead licensees to conduct a structural reevaluation.

When work began on resolution of GSI-15, it was fully expected that some of the operating reactor RPV supports would require an engineering analysis to ensure the structural integrity. To that end, the staff and the Technical Assistance Contractor developed a method for doing such an analysis. The method can be found in Chapter 7. For those cases where insufficient data or other limitations prevent the analyst from completing the reevaluation on the basis of the fracture resistance, a structural consequence analysis is suggested. An evaluation was completed for the NRC by LLNL and those results could serve as guidance. As noted in Section 7e, a more realistic consequence analysis would consider the potential for degradation in components which are important to the safety of the plant in the event of RPV support failure.

Failure of the RPV supports would induce additional loads on the primary coolant piping. In fact, the LLNL report specifically included the piping as the conduit for the loads otherwise carried by the RPV supports. Therefore, the integrity of the vessel supports is an important part of the consequence analysis. For plants with ferritic steel piping in the primary coolant lines, evaluation methods recommended by the ASME Boiler and Pressure Vessel Code, Section XI, should be followed. For plants with Austenitic stainless steel primary coolant lines, the potential for degradation by the process of thermal aging must be considered. Because aging embrittlement of stainless steel may be unfamiliar to structural engineers, a brief overview of what it is, how it may play a role in the reassessment of RPV supports and how it may be analyzed is given in this Appendix.

AGING EMBRITTLEMENT

Although holding most common Austenitic stainless steels at a high temperature for a long time will induce a loss of ductility to some degree, experiments have shown that castings are more vulnerable. A rather thorough, recent, treatment dealing with the effect on tensile properties was published in Reference D.1. An earlier report (Reference D.2) presents a procedure and correlations for predicting Charpy impact energy, tensile flow stress, fracture resistance (in the form of J-R curves), tearing modulus (T) and the elastic-plastic toughness, J_{Ic}, of aged cast

stainless steel (specification: ASTM A 351) from given material parameters. Cast stainless steel made to ASTM A 351 is subject to embrittlement when exposed to low temperatures in the range 400 to 842°F. The thermal embrittlement is expressed as a decrease in the Charpy V-notch impact energy or decrease in the plane strain fracture toughness, K_{Ic}.

The chemical composition of cast stainless steel is adjusted to result in a duplex microstructure. That is, on solidification there will be a mixture of body-centered-cubic ferrite and face-centered-cubic Austenite. The ferrite will increase the strength and corrosion resistance and reduce the tendency toward hot cracking during solidification. Laboratory studies have led to the conclusion that the ferrite phase is responsible for the appearance of a transition behavior in Charpy impact data <u>and</u> for the aging embrittlement. Although the changes in properties resemble age-hardening phenomena, the kinetics of the aging reaction are very sluggish at pressure vessel operating temperatures (about 550°F). Metallurgical experiments (Reference D.3) have demonstrated that the physical change underlying the embrittlement is spinodal decomposition. Depending on the detailed chemical composition, precipitation of nickel- or silicon-rich "G" phase also may occur. Steels with relatively high volume fractions of ferrite may be more susceptible to embrittlement than run-of-the-mill steels. The microstructure of the steel is very important in determining the degree or extent of thermal embrittlement. For example, should the ferrite phase form a continuous network through the Austenite grains <u>or</u> should there be a continuous boundary between the two phases, there will be an easy path for crack propagation and the material will be prone to brittle fracture.

The grades of ASTM A 351 steel that are of importance to this study are CF-3, CF-8 and CF-8M. The first two also can be made to a restricted chemistry, within the bounds of the parent specification, to obtain a higher relative volume of the ferrite phase which confers a higher tensile yield and ultimate (those steels are denoted: CF-3A and CF-8A). The CF-3 steels are low-carbon and are least sensitive to thermal embrittlement; the CF-8M steels are high-carbon, contain Mo additions and are most prone to embrittlement. As noted below, evaluation of cast stainless steel as part of a consequence analysis will depend on the metallurgical details of the component.

<u>CONSEQUENCE ANALYSIS CONSIDERATIONS</u>

The potential for low-temperature embrittlement in cast stainless steel should be a sufficient motive to evaluate components constructed of those materials to ensure their continued ability to meet the design requirements independent of problems related to other components. The issues stemming from the use of cast stainless steels (embrittlement; limited inspectability) were addressed in a "Fitness-for-Service" format in Reference D.4. The importance of cast stainless steel primary piping in a

consequence evaluation was identified in Reference D.5 Using load combinations classified as Service Level D in accord with the ASME Boiler and Pressure Vessel Code, the analysts performed a structural evaluation of the consequences of RPV support failure. It was concluded that the primary coolant piping was capable of transferring the vessel loads to other support structures (of steam generators and main coolant pumps).

The evidence at hand, therefore, allows one to say that RPV support failure may be acceptable from the safety viewpoint of radioactive release providing that the piping does not fail. A consequence analysis done for the purpose of evaluating the risk associated with RPV support failure must include analyses of the cast stainless steel in the primary coolant lines. Because accidents, especially earthquakes, show no respect for structural conditions, the prudent approach is to evaluate the cast stainless under the worst conditions. From abundant experimental data, the behavior of embrittled cast stainless is not different in appearance from ferritic steels. That is, the shape of the curve of fracture resistance as a function of metal temperature is sigmoidal, being very low at low temperatures and rising to a upper shelf value at high temperatures. Thus many observers have noted that even after a long aging time (embrittling treatment), these alloys exhibit adequate fracture resistance at operating temperatures. Although that is essentially true, it is equally true that accidents may happen at any time. Therefore, the evaluation be for room temperature and end-of-life conditions.

EVALUATION

Detailed steps to be taken in evaluating the potential for low-temperature aging embrittlement of cast stainless steels can be obtained from Reference D.2. For completeness, the reviewer should familiarize himself with Reference D.6, an earlier report on procedures and correlations for predicting the aging embrittlement change in fracture toughness.

In Reference D.2, one can find a procedure for estimating the saturation Charpy V-notch impact energy (E_{C-V}) at room temperature. The E_{C-V} at saturation was defined as that value found in a given alloy after a very long time at temperature. Two different approaches were given to estimate the saturation E_{C-V} room temperature value. Both require knowledge of the steel chemistry. Either Certified Material Test Reports or chemical analysis of samples taken from the component (e.g.: prolongations, archival material, etc.) can be used.

In one approach (using the symbols given in Reference D.2), the following equation is solved:

$$\log_{10} C_{Vsat} = a + (b)\exp(-c\Phi),$$

where: Φ (a material parameter)
$= \delta_c(Cr + Si)(C + 0.4N)$ for CF-3 and CF-8,

$$= \delta_c(Ni + Si + Mn)^2(C + 0.4N)/5 \text{ for CF-8M;}$$

δ_c (ferrite content) $= 100.3(Cr_{eq}/Ni_{eq})^2 - 170.72(Cr_{eq}/Ni_{eq}) + 74.22$,

and:

$$Cr_{eq} = Cr + 1.21(Mo) + 0.48(Si) - 4.99,$$
$$Ni_{eq} = Ni + 0.11(Mn) - 0.0086(Mn)^2 + 18.4(N) + 24.5(C) + 2.77.$$

If the nitrogen content (N) is not known, a value of 0.04 wt.% can be used. The values of the constants a, b and c were given for the several grades of steel as:

Grade	Constants in the above equation		
	a	b	c
CF-3, CF-8	1.15	1.36	-0.035
CF8M (<10%Ni)	1.10	2.12	-0.041
CF8M (>10%Ni)	1.10	2.64	-0.064

In the second approach, the room temperature impact energy at saturation is calculated directly from the chemical analysis results. The relationship depends on the grade of steel.

For CF-3 AND CF-8:

$$\log_{10}C_{Vsat} = 5.64 - 0.006\delta_c - 0.185Cr + 0.273Mo - 0.204Si + 0.044Ni - 2.12(C + 0.4N),$$

and for CF-8M:

$$\log_{10}C_{Vsat} = 7.28 - 0.011\delta_c - 0.185Cr - 0.369Mo - 0.451Si + 0.044Ni - 4.71(C + 0.4N).$$

It was recommended (in Reference D.2) that for each evaluation, the saturation, room temperature, Charpy energy be calculated by both approaches and that the lower value be used.

Guidance can be found in Reference D.2 for the estimation of the fracture resistance of cast stainless steels in terms of J-R curves. One approach is to base the estimation on the room temperature, saturation, impact energy value. To do so, the power-law relation for the J-R curve is used:

$$J_d = C\Delta a^n,$$

where:

J_d is the deformation-theory J-integral.

From graphical correlations between the coefficient "C" and the room temperature saturation E_{C-V}, lower-bound curves were drawn for four material conditions: grades CF-3 or CF-8 as static or centrifugal castings and grade CF-8M in either of the same two

cast states. Thus four equations were given for the four combinations. The same thing was done using high temperature data but those results are of no concern here. The several lower-bound correlations were combined with the power-law equation as:

$$J_d = a[C_{Vsat}]^b[\Delta a]^n,$$

where:

$$n = c + d[\log_{10}C_{Vsat}].$$

Values for the constants a, b, c and d in the above two equations were given in tables in Reference D.2 for the three grades of ASTM A 351, as static- or centrifugally-cast at room or high temperature.

In the event that the chemical composition of the steel to be evaluated is not known, Reference D.2 provided values for the coefficient (C) and exponent (n) of the power-law equation for the J-R curve based on the ferrite content of the stainless steel. Values of the parameters were tabulated for the three grades of ASTM A 351 in the static- and centrifugally-cast conditions at room and elevated temperature at three ferrite content levels: <10, 10-to-15 and >15 %.

Enough information is available to evaluate the condition of cast stainless steel in a conservative way. After estimating a J-R curve, the methods of fracture mechanics can be employed to determine the margin for failure <u>for any known or assumed flaw size</u>. The less sophisticated approach is to determine the saturation Charpy V-notch energy at room temperature and decide if it is sufficient. To some extent, such an evaluation must rely on judgement. Inasmuch as the operating criterion of a minimum of 50 ft-lb has served well for ferritic reactor pressure vessels, it also should be adequate for cast stainless steel which behaves much like a ferritic steel when embrittled.

REFERENCES

D.1 NUREG/CR-6142, "Tensile-Property Characterization of Thermally Aged Cast Stainless Steels," Argonne National Laboratory, February, 1994.

D.2 NUREG/CR-4744, "Long-Term Embrittlement of Cast Duplex Stainless Steels in LWR Systems," Semiannual Report for April-September 1992, Argonne National Laboratory, July, 1992.

D.3 T. R. Leax, S. S. Brenner and J. A. Spitznagel, "Atom Probe Examination of Thermally Aged CF8M Cast Stainless Steel," AIME Metallurgical Transactions A, Vol. 23A, October, 1992, p. 2725.

D.4 "Cast Austenitic Stainless Steel Sourcebook," M. E. Lapides, ed., Electric Power Research Institute, Palo Alto, California, October, 1991.

D.5 NUREG/CR-5644, "Consequence Evaluation of Radiation Embrittlement of Trojan Reactor Pressure Vessel Supports," Lawrence Livermore National Laboratory, October, 1990.

D.6 NUREG/CR-4513, "Estimation of Fracture Toughness of Cast Stainless Steels During Thermal Aging in LWR Systems," Argonne National Laboratory, June, 1991.

APPENDIX E

Potential Effects of Gamma Radiation

Eric H. Ottewitte

October 1993

ABSTRACT

This present study investigates the role of gamma-induced radiation damage to reactor pressure vessels. It 1) evaluates the effects of gamma radiation based on a review of the literature and 2) specifically assesses the relative contribution of gamma radiation to atomic displacements in the reactor vessel wall. A review of the Sequoyah capsule data indicated that information on neutron to gamma ratios could not be obtained from the report. Consequently, a bounding calculation was performed.

Search of the literature indicates that, in addition to atomic displacement, photons can also

- cause changes in alloy morphology (grain structure)
- enhance diffusion, leading to decomposition of over-saturated austenite, and to strengthening and embrittlement of steel
- accelerate intergranular stress corrosion cracking of stainless steels and nickel-base alloys via its effects on material micro-chemistry (e.g, radiation-induced segregation), water chemistry (e.g., radiolysis), and stress (e.g., radiation induced creep and hardening).

First principal calculations suggest that γ-induced atomic displacement is $\ll 1\%$ of that from neutrons in the pressure vessel wall of power reactors. More detailed calculations, specific to the Sequoyah Reactor, would require extensive coupled neutron/photon transport calculations plus the computer programming of algorithms for calculation of energy-dependent, photon-induced, atomic displacement cross sections. The inclusion of TLDs in the capsule would be very useful.

In summary, this study indicates that although gamma radiation contributes little to atomic displacement or gas production, it may significantly affect grain structure, atomic diffusion and stress corrosion cracking. However, the isolation of the capsule specimens from water chemistry effects precludes their testing for stress corrosion cracking.

CONTENTS

ABSTRACT iii

INTRODUCTION 1

Literature Search on Gamma-Induced Radiation Damage 1
Neutron-Induced Damage to LWR Pressure Vessels 1
Gamma-Induced Damage Mechanisms 2

STATE-OF-THE-ART FOR GAMMA-RAY-INDUCED RADIATION DAMAGE 4

Literature Search 4

Summary of Book Sources 4
General Literature Search 4

Calculational Models for Gamma-Ray-Induced Radiation Damage 8

ANALYSIS OF GAMMA-RAY INTERACTION EFFECTS 10

Ionization Effects 10

Atomic Displacements by Energized Electrons 10

Estimation of the Gamma Spectrum-Averaged Dpa Cross Section $<\sigma_{\gamma,dpa}>$ for Iron 11
Estimation of the Neutron Dpa Cross Section $<\sigma_{n,dpa}>$ for Iron 14
Estimation of the Gamma-to-Neutron Flux and Dpa Ratios 14
Photon Dpa Production in a Fusion Reactor Environment 16

Effects of Heating 16

Synergistic Intergranular Stress-Assisted Corrosion Cracking 16

CONCLUSIONS AND RECOMMENDATIONS 18

REFERENCES 19

Appendix A--LLNL Communications A-1

Appendix B--Mini-Treatise on Gamma Irradiation Damage B-1

Potential Effects of Gamma Radiation

INTRODUCTION

This study investigates the role of gamma-induced radiation damage. It first examines the γ-induced phenomena found in the literature. It then estimates the number of atomic displacements per atom (dpa) induced by gamma rays relative to that by neutrons. Dpa constitutes the principal damage measure of concern in the Westinghouse surveillance program. A review of the Sequoyah capsule data indicated that information on neutron to gamma ratios could not be obtained from the report. Consequently, a bounding calculation was performed.

Literature Search on Gamma-Induced Radiation Damage

The literature was searched for measured and theoretical effects of gamma radiation on the mechanical properties of vessel steels and structural materials. This was accomplished by searching the conventional literature database of titles, abstracts and key words from reports, journal articles and conference proceedings for the broad combination of "gamma" and "radiation damage." That produced some 600 titles. Examination of these resulted in the selection of ten pertinent articles. Though many of those are either not in English or not readily available, we were able to obtain a few of the reports and abstracts from most.

Numerous books on radiation damage were assessed for subsection treatments of γ-induced radiation damage. Such sources are not always covered in the literature databases. Principal book sources are the series of annual reviews published by Annual Reviews Inc. of Palo Alto, the ASTM Conference Series on Radiation Damage and various textbooks. These book sources provided the basis for our assessment of γ-induced radiation damage by atomic displacement.

Neutron-Induced Damage to LWR Pressure Vessels[1]

The principal mechanisms in neutron-induced radiation damage are the number of atomic displacements and the quantity of helium and hydrogen gas produced. The helium gas lends itself as a nucleation site for accumulation of clustered vacancies and other gas atoms, leading to the formation of voids and subsequently to swelling and other macroscopic effects.

The ability of a steel pressure vessel, which contains the reactor core and its primary coolant, to resist fracture is an important factor in assessing the life and safety of nuclear power plants. The overall effects of fast neutron irradiation on the mechanical properties of low-alloy, ferritic pressure vessel steels such as SA508 Class 2 forging (base material of the Sequoyah Unit 2 reactor pressure vessel belt line) are well documented in the literature. Certain conditions of irradiation can cause low-alloy ferritic materials to increase in hardness and tensile properties, and to decrease in ductility and toughness.

Appendix G to Section III of the ASME Boiler and Pressure Vessel Code, "Protection Against Non-ductile Failure," presents a method for performing analyses to guard against fracture in reactor pressure vessels. The method uses fracture mechanics concepts and calculates the reference nil-ductility temperature (RT_{NDT}), adjusted for the effects of radiation.

To perform these adjustments requires knowledge of the neutron environment (energy spectrum, flux, fluence) to which the test specimens were exposed. These data are normally obtained from passive neutron flux monitors contained in each of the surveillance capsules.

To relate the changes observed in the test specimens to the present and future condition of the reactor vessel, a relationship must be established between the neutron environment at various positions within the reactor vessel and that experienced by the test specimens. The correlation of changes in measured materials properties with fast neutron fluence ($E > 1.0$ MeV) has traditionally been accepted for development of damage trend curves for assessing vessel condition. However, assessing the differences in neutron energy spectra at surveillance capsule locations on both sides of the pressure vessel wall should enable more accurate evaluation of damage gradients through the wall.

To obtain such an energy-dependent damage function for data correlation, ASTM Standard Practice E853, "Analysis and Interpretation of Light Water Reactor Surveillance Results," recommends reporting displacements per iron atom (dpa iron) along with fluence ($E > 1.0$ MeV) to provide a data base for future reference. ASTM Standard Practice E693, "Characterizing Neutron Exposures in Ferritic Steels in Terms of Displacements per Atom," specifies the energy-dependent dpa function to be used for this evaluation. Revision 2 to the Regulatory Guide 1.99, "Radiation Damage to Reactor Vessel Materials," promulgates the use of dpa to assess embrittlement gradients in the pressure vessel wall.

Ramirez et al.[1] evaluated the neutron dosimetry for the test specimens contained in surveillance Capsule X. They reported fast neutron exposure parameters in terms of fast neutron fluence ($E > 1.0$ MeV), fast neutron fluence ($E > 0.1$ Mev), and displacements per atom (dpa) of iron. The first two of these parameters simply represent integrals of the flux over a specific portion of the fast neutron energy spectrum. The dpa parameter provides a more sophisticated integral of the product of the energy-dependent flux and the energy-dependent cross section (probability) for neutrons to displace atoms from their present location; i.e., it incorporates the fact that the effectiveness of neutrons in displacing atoms varies with neutron energy. In addition to being more rigorous, the dpa parameter provides a basis for comparison to γ-induced atomic displacement damage which can also be expressed in terms of dpa.

Gamma-Induced Damage Mechanisms

Neutrons induce damage in structural materials principally through hadronic[a] interactions of neutron scattering with, and capture by, the nucleus. This results in atomic displacement and generation of hydrogen and helium gas.

Gamma rays cannot undergo such reactions: they interact by the weaker electromagnetic interaction[b] and effect little momentum transfer due to their zero rest mass. They cause very little direct displacement or gas production. However, they can energize electrons which in turn have sufficient mass to induce atomic displacement, though again by electromagnetic interaction.

To compare the effects of γ-induced damage to relative neutron-induced damage, one needs to use parameters or measures common to both phenomena: neutron flux is not equivalent to gamma ray

---

a. Hadrons such as neutrons, protons, and alphas interact with other nucleons (particles inside the nucleus) by means of the "strong" or "hadronic" interaction involving the exchange of virtual pions and other bosons.

b. Electromagnetic interactions consist of the exchange of massless photons only.

flux. The key neutron-induced damage parameters in structural materials are gas production rates and dpa. Gammas produce nil gas but do indirectly displace atoms. Cross sections for dpa production have been developed, allowing the direct comparison of neutrons and photons for atomic displacements.

Gamma rays are also able to directly deposit heat energy, subsequently inducing changes in the grain structure. They can also dissociate water molecules adjacent to structural materials, thereby enhancing stress-induced corrosion.

STATE-OF-THE-ART FOR GAMMA-RAY-INDUCED RADIATION DAMAGE

One principal objective of this study was to survey the current state-of-the-art for the effects of γ-irradiation on structural materials. Effects of γ-radiation upon molecular bonds (such as in glasses, bonding agents, and organic and inorganic compounds) were excluded. To do this survey a literature search was performed and discussions were held regarding radiation damage data with scientists at the National Nuclear Data Center at Brookhaven National Laboratory, Radiation Shielding Information Center at Oak Ridge National Laboratory and Nuclear Data Center at the Lawrence Livermore National Laboratory.

Literature Search

The literature search covered gamma-induced radiation damage in published books as well as in the general databases of reports, journal articles and conference proceedings. From past experience in radiation damage, principal book sources have been the series of annual reviews published by Annual Reviews Inc. of Palo Alto and the work of Kelly.[1] The following sections address these book and general literature sources in turn.

Summary of Book Sources

Table 1 contains the assessment of four major review articles on radiation damage. The 1953 review by Dienes[2] and the 1979 review by Stiegler and Mansur[3] do not specifically deal with γ radiation. A 1956 review by Brooks[4] mentions that the germanium atom displacement efficiency per photon is about 10^{-3} that of fast neutrons. The 1962 review by Goland[5] presents an empirical formulation for calculating γ-induced dpa. Kelly[2] further developed that work in 1966, discussed later in this report.

General Literature Search

Table 2 compiles the relevant articles found in some 600 titles obtained from a general literature search on gamma-induced radiation damage. Key results are the following:

- Fiore[6] concluded that γ-irradiation must affect the structure in some alloys since it causes property changes such as a decrease in toughness. In alloys which display a damping minimum in internal friction measurements, the precipitate morphology changes during irradiation, with coarsening and/or de-coarsening and re-nucleation being observed.

- Weidinger et al.[7] investigated irradiated molybdenum by the perturbed angular correlation technique using ^{111}In as the radioactive source. Their results show that defects become trapped at the probe atom in an annealing stage around 500 K. Three different defect configurations were identified.

- Kuribayashi et al.[8] found that γ-radiation increased intergranular stress corrosion cracking (IGSCC) susceptibility of sensitized type 304 stainless steel in boiling NaCl solution.

Table 1. Summary of review articles on radiation damage in the Annual Reviews of Materials Science (M) and Annual Reviews of Nuclear Science (N)

Volume	Year	First Author	Article Title	Substance of Article Pertinent to γ-Induced Damage in Structural Materials
M9	1979	Stiegler[4]	Radiation Effects in Structural Materials	Examines the microscopic mechanisms of radiation damage induced by energetic particles. Does not deal with specific effects of gammas.
N12	1962	Goland[6]	Atomic Displacements in Solids by Nuclear Radiation	Gamma rays are capable of producing displacements through a number of interactions. The three most prominent ones are the photoelectric effect, the Compton effect, and pair production. For the low gamma-ray energies found in fission reactors, the first and second effects are the most important ones to consider. In a solid both effects can produce secondary electrons having sufficient energy to displace atoms. Calculation of the atomic displacement cross section for gamma rays is difficult because it involves a triple integration over: (a) the differential cross section for energy transfer to electrons by the Compton or photo-electric process; (b) the range of the electrons, and (c) the differential displacement cross section for electrons, mentioned earlier. Dienes & Vineyard[9] discussed the problem and gave a few results for an assumed displacement threshold of 25 ev. Galavanov[10] treated it more thoroughly: he compared atomic-displacement cross sections for elastic scattering of gamma rays, for nuclear recoil during photoemission, and for elastic scattering of photoelectrons and Compton electrons. More recently Oen & Holmes[11] carried out extensive calculations for various values of gamma-ray energy, threshold energy, and atomic number. Their results have not yet been adequately correlated with experiments. In view of the accuracy of the computations, such comparisons should be of importance in relating property changes to the number of displaced atoms in a solid.
N6	1956	Brooks[5]	Nuclear Radiation Effects in Solids	Mentions that displacement efficiency per photon is about 10^{-3} that of fast neutrons in the case of Ge.
N2	1953	Dienes[3]	Radiation Effects in Solids	Focusses on fast massive particles.

Table 2. Synopsis of general near-term literature search on γ-induced radiation effects in reactor structural materials

Reference	Year	Article Title	Substance of Article Pertinent to γ-Induced Damage in Structural Materials
Fiore[7]	1974	Gamma-Irradiation Damage in Age Hardening Al Alloys	This report describes an experimental program directed toward an understanding of the mechanisms of γ-irradiation damage in precipitation-hardenable Al alloys. Pure Al and a series of age-hardenable Al alloys were γ-irradiated with a Co^{60} source at a dose of 6 x 10^3 rads/min. Internal friction measurements were made at 80 Khz by means of the Marx technique on samples in situ during irradiation. The results showed that toughness noticeably decreased with γ-irradiation. The authors concluded that γ-irradiation must influence structure since it influences properties. In Al and Al-3 w/o Cu, the damping decreased monotonically with irradiation as expected. The decrease is attributed to the immobilization of dislocations by the radiation-induced point defect pinners. In 2024-T6, 2017-T6 and Al-9.5 Mg, the damping passes through a minimum and begins an anomalous increase after 4 to 7 hours of irradiation. Electron micrographs show that in Al and Al-3 w/o Cu, irradiation does not influence structure. In the alloys which display the damping minimum however, precipitate morphology changes during irradiation, with coarsening and/or de-coarsening and re-nucleation being observed. The effect appears to depend upon the presence of Mg. Theory predicts that γ-irradiation can change the morphology by either Rutherford collision or Coulombic repulsion.
Weidinger[8]	1979	Defect Configurations in Irradiated Molybdenum	Irradiated molybdenum was investigated by the perturbed angular correlation technique using ^{111}In as the radioactive source. Results showed that defects become trapped at the probe atom in annealing stage III around 500 K. By quadrupole interaction three different defect configurations were identified.
Kuribayashi[9]	1983	Influence of Gamma Radiation on Intergranular Stress Corrosion Cracking of Austenitic Stainless Steel	In order to examine the environmental influence of gamma radiation on intergranular stress corrosion cracking (IGSCC) of sensitized austenitic stainless steel, tests were conducted with and without gamma radiation in boiling 12% NaCl solution, pH adjusted to 3 with HCl, and in high temperature oxygenated pure water (230°C). Results are as follows: 1) γ radiation increased IGSCC susceptibility of sensitized type 304 stainless steel in boiling 12% Nacl solution, Ph adjusted to 3 with Hcl. The ferric ions (Fe^{3+}) are radiolytically formed by γ radiation from the ferrous ions (Fe^{2+}) in acid solution, and this phenomenon is the widely known principal of Frick's Dosimeter. The ferric ions may act as strong oxidizing agent and may increase the susceptibility to IGSCC in the acid boiling chloride solution. 2) γ-radiation increased IGSCC susceptibility of sensitized type 304 stainless steel also in high temperature oxygenated pure water. The amount of total Fe in aqueous solution after SCC testing, increases by γ radiation, so the oxidization of metals is advanced by γ radiation in high temperature pure water.
Mural'[10]	1984	Gamma-Radiation Aging of Deformed Austenite	Effect of gamma-radiation treatment with an integral dose of 3.5×10^9 roentgen at normal temperature on aging of deformed austenite in the 10Kh18N13AM3 type steel has been studied. Stress-strain diagrams obtained for the specimens point to the fact that gamma-radiation treatment has analogy with aging at 200°C. It has been noted that decomposition of over-saturated austenite, strengthening, and embrittlement of steel are conditioned by radiation-enhanced diffusion but not by radiation defects.
Marsh[15]	1986	Influence of Radiation on the Corrosion of Stainless Steel	The effect of gamma radiation on the electrode corrosion of type 304L steel in 300 ppm Cl^- has been studied. In open systems with argon or Ar-20% oxygen gas blankets irradiation at a dose rate of 2000 Sv/h causes the steady rest potential of the metal to increase by 200-300 mV. This increase is partly due to cathodic depolarization by oxidizing radical and molecular radiolysis products, but may also involve adsorption of these species onto the metal surface. Radiolysis products also inhibit the initiation of pitting corrosion at low electrode potentials, but have no effect on the repassivation of established pits.

Table 2. Synopsis of general near-term literature search on γ-induced radiation effects in reactor structural materials (Continued)

Alexandrov[16]	1987	Effect of Gamma Radiation on Metal Corrosion Under Spent Fuel Storage Conditions	Authors found that γ-radiation accelerates corrosion of stainless steel and other metals in water and humid air under the conditions simulating spent nuclear fuel storage.
Gann[12]	1987	Simulation of Radiation Damage of the Reactor Cores Steel by Using High-Energy e^-/γ Beams	(In Russian; not yet translated according to National Translation Center. Title warrants interest and inclusion here. Suggest translation of at least the abstract.)
Neklyudov[17]	1988	Effects of High-Energy Electron and Gamma Radiation on Mechanical Properties of Steels Kh18N10T and 06Kh16N15M3B	Threshold dose for radiation hardening and radiation embrittlement occurs at 10^{-4} dpa for n, e^- or γ. Observable e^-/γ effects occur at <0.2 dpa.
Sudo[18]	1988	Effect of Gamma Irradiation on IGSCC Susceptibility of Type 304 Stainless Steel	Slow strain rate tests were conducted to evaluate the effect of gamma irradiation on IGSCC susceptibility of sensitized Type 304 stainless steel in high temperature water simulating two conditions at primary loop recirculation piping. Electrochemical potential (ECP) of Type 304 SS was measured to determine the environmental effect of gamma irradiation. Experiments showed that under gamma irradiation the ECP value and IGSCC susceptibility of Type 304 increased in one condition, while decreasing in the other condition.
Andresen[19]	1991	State of Knowledge of Radiation Effects on Environmental Cracking in Light Water Reactor Core Materials	Laboratory and field data show that long term neutron and gamma irradiation can accelerate intergranular stress corrosion cracking of stainless steels and nickel-base alloys. Radiation can exacerbate specific aspects of cracking susceptibility via its effects on material micro-chemistry (e.g, radiation induced segregation), water chemistry (e.g., radiolysis), and stress (e.g., radiation induced creep and hardening). Characterization of irradiation-assisted stress corrosion cracking (IASCC) as an *entirely unique* phenomenon is not consistent with the evidence that many of the same sensitivities, e.g., to water chemistry and stress, apply to cracking under both irradiated and unirradiated conditions. Development of models which integrate the effects of, e.g., the elevated corrosion potential and grain segregation induced by radiation are critical to the understanding and prediction of the effects of IASCC on core internals. Progress has been made in extending modeling of cracking under unirradiated conditions to account for radiation effects by evaluating long term, in-core data on fracture mechanics, crack growth rate specimens and corresponding water chemistry/corrosion potential data.

- Mural' and Shcherbedinskij[13] observed gamma-radiation effects analogous to those from aging at 200 °C. They noted that decomposition of over-saturated austenite, strengthening, and embrittlement of steel are conditioned by radiation-enhanced diffusion but not by radiation defects.

- Marsh et al.[14] observed that, in open systems with argon or Ar-20% oxygen gas blankets, irradiation causes the steady rest potential of the metal to increase. This increase is partly due to cathodic depolarization by oxidizing radical and molecular radiolysis products, but may also involve adsorption of these species onto the metal surface. Radiolysis products also inhibit the initiation of pitting corrosion at low electrode potentials, but have no effect on the repassivation of established pits.

- Alexandrov et al.[15] found that γ-radiation accelerates corrosion of stainless steel and other metals in water and humid air under the conditions simulating spent nuclear fuel storage.

- Neklyudov et al.[16] found that the threshold dose for radiation hardening and radiation embrittlement occurs at 10^{-4} dpa for n, e^- or γ. Observable e^-/γ effects occur at <0.2 dpa.

- Sudo et al.[17] concluded from slow strain rate tests that γ-radiation affects the electrochemical potential and IGSCC susceptibility of Type 304 in high temperature water. The direction of the changes depended upon the water chemistry.

- Laboratory and field data from Andresen et al.[18] show that long term neutron and gamma irradiation can accelerate intergranular stress corrosion cracking of stainless steels and nickel-base alloys. Radiation can exacerbate specific aspects of cracking susceptibility via its effects on material micro-chemistry (e.g, radiation induced segregation), water chemistry (e.g., radiolysis), and stress (e.g., radiation induced creep and hardening). Characterization of irradiation-assisted stress corrosion cracking (IASCC) as an entirely unique phenomenon is not consistent with the evidence that many of the same sensitivities, e.g., to water chemistry and stress, apply to cracking under both irradiated and unirradiated conditions.

These articles reveal a number of mechanisms, alternative to atomic displacement, whereby gamma radiation may affect the behavior of the pressure vessel wall. To quantify these phenomena for the Sequoyah pressure vessel and/or the surveillance capsule would be a major undertaking, far beyond the scope of the present study. The absence of articles on γ-induced atomic displacements in the general literature tends to confirm past and present experience that it plays a minor role relative to neutron-induced atomic displacement in a fission reactor environment.

Calculational Models for Gamma-Ray-Induced Radiation Damage

In 1982 γ-induced radiation damage to fusion first-walls was assessed at the Idaho National Engineering Laboratory (INEL). That work included the development of a formalism to calculate γ-induced dpa cross sections based on the work of Kelly.[2] Such data might be incorporated into the existing neutron/photon structure of the MACKLIB[19] radiation damage data base. This would then take advantage of, as well as enhance, existing coupled neutron/photon transport and damage analysis capability.[20]

An extensive library of neutron-induced dpa cross sections already exists. Consequently I contacted the sponsoring nuclear data community, namely the Cross Section Evaluation Working Group, coordinated through the National Nuclear Data Center (NNDC) to see if any work on γ-induced dpa had occurred since 1982. V. McLane[21] of NNDC directed me to Steven Warshaw at LLNL who is attempting to develop a fairly complete data base for γ-induced radiation damage, extending up to 40 MeV (Appendix A). That work, which is just begun, appears to center on photonuclear (γ,n) reactions, mostly at energies above those occurring in a fission reactor. Photonuclear cross sections contribute relatively little to radiation damage in a fission reactor: the cross sections are very low and the threshold gamma energy is generally >7 MeV.

I also checked with the Radiation Shielding Information Center at ORNL regarding the availability of codes and data. The only help there was that the codes TECALC[22] and HEITLER,[23] identified in 1982 for potential use as subroutines in writing a code, were still available.

ANALYSIS OF GAMMA-RAY INTERACTION EFFECTS

Gamma rays cause damage by three mechanisms: ionization, energized electrons and heating.[2] This section systematically evaluates how these mechanisms might individually and collectively affect the Sequoyah pressure vessel and its surveillance capsule. It uses the results of the literature search in the previous section and adds an evaluation of γ-induced atomic displacement damage. The role of the latter relative to neutron-induced damage is evaluated quantitatively. The other phenomena are only qualitatively analyzed.

Ionization Effects

The principal ionization effect will likely be in water radiolysis which in turn affects intergranular stress-assisted corrosion cracking, discussed in a later section. Neutrons can also contribute to radiolysis through atomic displacement reactions (via neutron scattering or capture). However, photons should dominate the breaking of atomic and molecular bonds by means of electromagnetic interactions with the atomic electrons: neutrons are incapable of such electromagnetic interactions. We note that the test specimens in the surveillance capsule will not experience the water chemistry effects that the vessel wall will.

Atomic Displacement by Energized Electrons

As discussed above, photons interact by electromagnetic interaction and are generally incapable of directly displacing atoms or generating helium and hydrogen gases. However, photons can set free energetic electrons which can transfer the 25-40 eV needed to displace atoms. We seek here to compare atomic displacements by photons to those by neutrons. Should the former be relatively insignificant from first principles, the extensive effort to calculate them specifically for the Sequoyah reactor pressure vessel would not be required.

The principal measure addressed here is one that is common to both neutrons and photons: the number of displacements per atom (dpa). Dpa is a product of the projectile flux and the projectile's cross section for producing displacements. The atomic displacement rate by either neutrons or photons can be calculated as follows:

$$(Dpa\ rate)_i = \int_{E_d}^{\infty} \sigma_{i,dpa}(E_i) \cdot \phi_i(E_i)\, dE_i \qquad (1)$$

where

i = neutron or photon

$\sigma_{i,dpa}$ = dpa cross section for particle i

ϕ_i = flux of particle i

E_i = energy of particle i

The ratio of γ-induced dpa to neutron-induced dpa will be the product of the photon to neutron ratio for the dpa cross section with the same ratio for the flux at the position of interest:

$$\frac{(Dpa\ rate)_\gamma}{(Dpa\ rate)_n} = \frac{\int_{E_d}^{\infty} \sigma_{\gamma,dpa}(E_\gamma) \cdot \phi_\gamma(E_\gamma)\ dE_\gamma}{\int_{E_d}^{\infty} \sigma_{n,dpa}(E_n) \cdot \phi_n(E_n)\ dE_n} = \frac{\langle \sigma_{\gamma,dpa} \rangle}{\langle \sigma_{n,dpa} \rangle} \cdot \frac{\int_{E_d}^{\infty} \phi_\gamma(E_\gamma)\ dE_\gamma}{\int_{E_d}^{\infty} \phi_n(E_n)\ dE_n} \tag{2}$$

where

$$\langle \sigma_{i,dpa} \rangle = \frac{\int_{E_d}^{\infty} \sigma_{i,dpa}(E_i) \cdot \phi_i(E_i) dE_i}{\int_{E_d}^{\infty} \phi_i(E_i) dE_i} \tag{3}$$

Estimation of the Gamma Spectrum-Averaged Dpa Cross Section $<\sigma_{\gamma,dpa}>$ for Iron

Kelly[2] shows in Appendix B that the dpa cross section $\sigma_{\gamma,dpa}$ is primarily due to Compton scattering. Figure 1 shows the variation of that cross section $\sigma^{C}_{\gamma,dpa}$ with gamma ray energy E_γ for select atomic numbers Z. Note that the cross sections vary smoothly with Z as well as with E_γ. That is because the electromagnetic interaction depends on Z and not on nuclear quantum numbers as the hadronic interactions do. Consistent with the ASTM standard and the report by Ramirez et al., we desire to evaluate the γ-induced dpa for iron (Z=26). However, for simplicity and because of the smooth behavior with Z, and considering that other uncertainties are much larger, we use the Z=29 curve in Figure 1 rather than interpolate or implement a computer program.

The reactor gamma flux spectrum $\phi_\gamma(E_\gamma)$, needed to evaluate $<\sigma_{\gamma,dpa}>$ in Equation (3), comprises four components: prompt fission gammas, delayed gammas from fission products, prompt gammas from neutron capture (n,γ) reactions, and delayed gammas from the decay of activation products other than fission products. The contribution of the latter component is generally negligible except perhaps locally to its source. The energy release per fission from the first three components totals approximately 20 MeV.[24,25,26]

Unruh and Tomlinson[27] (see also Soodak[28]) fit the reactor total gamma (prompt plus delayed) spectrum by the following expression:

$$\phi_\gamma(E_\gamma) \sim \exp(-1.11 E_\gamma) \tag{4}$$

where

ϕ_γ = gamma ray flux

E_γ = total energy of the gamma ray.

The average gamma energy from the spectrum in Equation (4) is 1/1.11 $\approx$ 0.9 MeV. (The average energy of prompt gamma rays is $\sim$ 1 MeV.[29] The energy of delayed and capture gamma rays should be lower because the total energy release is much lower in those reactions.)

Cross section for atomic displacement by Compton scattering,

$\sigma^{C}_{\gamma,dpa}$(b·dpa)

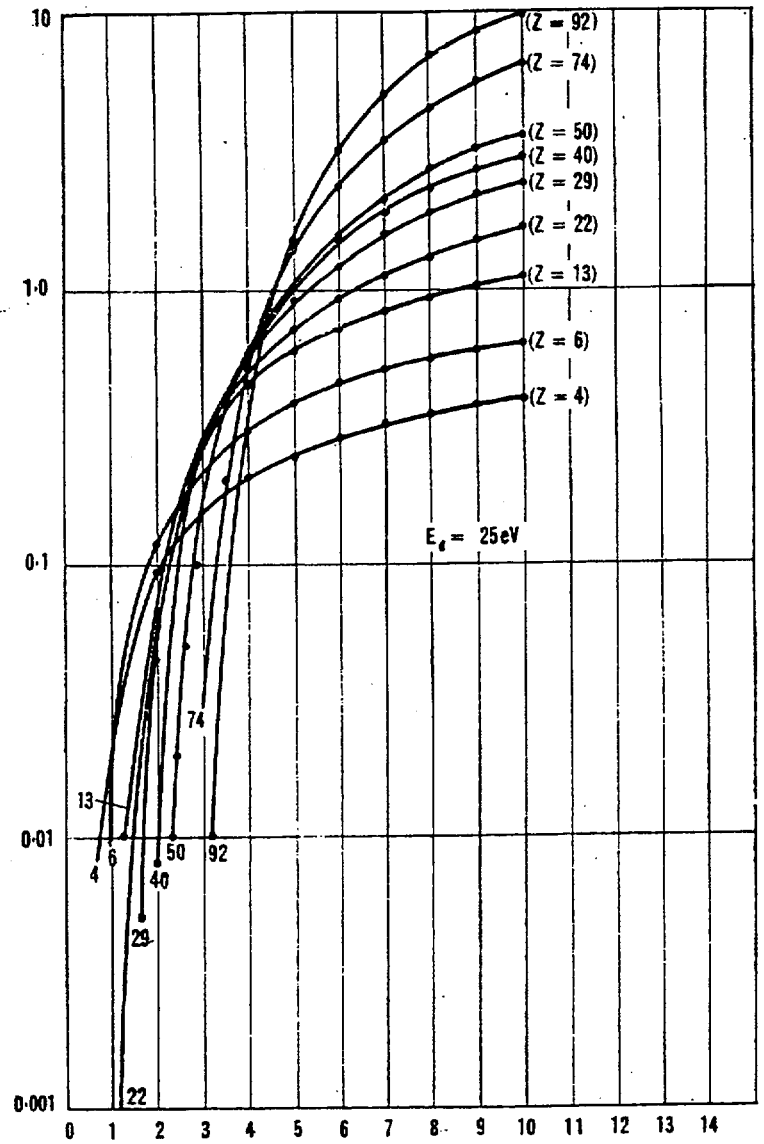

Gamma-ray energy (units of $m_e c^2$ = 0.511 MeV)

Figure 1. Cross sections for atomic displacement by Compton scattering[2]

Table 3 presents the spreadsheet evaluation of the gamma-spectrum-averaged cross section of Equation (3), using the cross sections from Figure 1 and the flux from Equation (4), and approximating the integrals by finite summations:

$$\langle \sigma_{\gamma,dpa} \rangle = \frac{\int_{E_d}^{\infty} \sigma_{\gamma,dpa}(E_\gamma) \cdot \phi_\gamma(E_\gamma) dE_\gamma}{\int_{E_d}^{\infty} \phi_\gamma(E_\gamma) dE_\gamma} \approx \frac{\sum_g \sigma_g \cdot \phi_g \cdot \Delta E_g}{\sum_g \phi_g \cdot \Delta E_g} \approx 31\ mb \qquad (5)$$

Table 3. Calculation of the spectrum-averaged cross section for gamma-induced dpa

Group No.	$E_{\gamma,lower}$ (MeV)	E_{avg} (MeV)	ΔE (MeV)	Flux, ϕ_γ (MeV)	$\phi_\gamma \cdot \Delta E$	$\sigma_{\gamma,dpa}(E_{avg})$ (barns)	$\sigma_{\gamma,dpa} \cdot \phi_\gamma \cdot \Delta E$
1	0	0.125	0.25	8.70E-01	2.18E-01		
2	0.25	0.375	0.25	6.60E-01	1.65E-01		
3	0.5	0.625	0.25	5.00E-01	1.25E-01		
4	0.75	0.875	0.25	3.79E-01	9.47E-02		
5	1	1.125	0.25	2.87E-01	7.17E-02	0	0.00
6	1.25	1.375	0.25	2.17E-01	5.43E-02	0.004	2.17E-04
7	1.5	1.625	0.25	1.65E-01	4.12E-02	0.02	8.23E-04
8	1.75	1.875	0.25	1.25E-01	3.12E-02	0.043	1.34E-03
9	2	2.125	0.25	9.45E-02	2.36E-02	0.08	1.89E-03
10	2.25	2.375	0.25	7.16E-02	1.79E-02	0.13	2.33E-03
11	2.5	2.625	0.25	5.43E-02	1.36E-02	0.2	2.71E-03
12	2.75	2.875	0.25	4.11E-02	1.03E-02	0.245	2.52E-03
13	3	3.125	0.25	3.12E-02	7.79E-03	0.3	2.34E-03
14	3.25	3.375	0.25	2.36E-02	5.90E-03	0.37	2.18E-03
15	3.5	3.625	0.25	1.79E-02	4.47E-03	0.45	2.01E-03
16	3.75	3.875	0.25	1.36E-02	3.39E-03	0.52	1.76E-03
17	4	4.125	0.25	1.03E-02	2.57E-03	0.6	1.54E-03
18	4.25	4.375	0.25	7.78E-03	1.94E-03	0.7	1.36E-03
19	4.5	4.625	0.25	5.89E-03	1.47E-03	0.75	1.11E-03
20	4.75	4.875	0.25	4.47E-03	1.12E-03	0.85	9.49E-04
21	5	5.125	0.25	3.38E-03	8.46E-04	0.92	7.78E-04
22	5.25	5.375	0.25	2.56E-03	6.41E-04	1.05	6.73E-04
23	5.5	5.625	0.25	1.94E-03	4.86E-04	1.1	5.34E-04
24	5.75	5.875	0.25	1.47E-03	3.68E-04	1.2	4.42E-04
25	6	6.125	0.25	1.12E-03	2.79E-04	1.25	3.48E-04
26	6.25	6.375	0.25	8.45E-04	2.11E-04	1.3	2.75E-04
27	6.5	6.625	0.25	6.40E-04	1.60E-04	1.4	2.24E-04
28	6.75	6.875	0.25	4.85E-04	1.21E-04	1.45	1.76E-04
29	7	7.125	0.25	3.68E-04	9.19E-05	1.6	1.47E-04
30	7.25	7.375	0.25	2.78E-04	6.96E-05	1.7	1.18E-04
31	7.5	7.625	0.25	2.11E-04	5.27E-05	1.75	9.23E-05
32	7.75	7.875	0.25	1.60E-04	4.00E-05	1.8	7.19E-05
33	8	8.125	0.25	1.21E-04	3.03E-05	1.95	5.90E-05
34	8.25	8.375	0.25	9.18E-05	2.29E-05	2	4.59E-05
35	8.5	8.625	0.25	6.95E-05	1.74E-05	2.05	3.56E-05
36	8.75	8.875	0.25	5.27E-05	1.32E-05	2.1	2.77E-05
37	9	9.125	0.25	3.99E-05	9.98E-06	2.15	2.15E-05
38	9.25	9.375	0.25	3.02E-05	7.56E-06	2.2	1.66E-05
39	9.5	9.625	0.25	2.29E-05	5.73E-06	2.3	1.32E-05
40	9.75	9.875	0.25	1.74E-05	4.34E-06	2.35	1.02E-05
	10						
SUM					8.97E-01		2.75E-02
0-10 MeV Average						0.030673	

Estimation of the Neutron Dpa Cross Section $<\sigma_{n,dpa}>$ for Iron

Ramirez et al.[1] calculated the neutron-induced dpa production rate (dpa/s) for iron in the Sequoyah pressure vessel. Dividing their reported dpa rates by their reported integral >0.1 MeV neutron flux one has

$$\langle\sigma_{n,dpa}\rangle = \frac{\int_{0.1\ MeV}^{\infty} \sigma_{n,dpa}(E_n)\cdot \phi(E_n)dE_n}{\int_{0.1\ MeV}^{\infty} \phi(E_n)dE_n} \approx 500\text{-}600\ barns \tag{6}$$

The choice of 0.1 MeV for the lower integral limit here is arbitrary but acceptable in as much as few displacements occur at lower neutron energies. It remains, however, to use the same limit in the flux ratio below. Flux monitors in the Sequoyah capsule indicate[1] the thermal flux to be about 1/4 of the total. On this basis, overall we expect an uncertainty less than a factor of 2 in $<\sigma_{\gamma,dpa}>$.

We calculate that the ratio of the efficiency (cross section) for displacing iron atoms by photons relative to that for fast neutrons is thus $31\text{x}10^{-3}/500 = \sim 0.06\ \text{x}10^{-3}$. This is considerably less than the 10^{-3} mentioned for germanium atoms by Brooks[5] in 1956, but not necessarily inconsistent for the following reasons:

1. atomic displacement by neutrons occurs predominantly at fast neutron energies. There different threshold nuclear reactions are opening up with increasing energy. Only for nuclei common to fission reactors have these cross sections been measured and/or evaluated with any significant accuracy. We expect a poor state of knowledge for fast neutron germanium cross sections in 1956 relative to the same for iron atoms presently.

2. neutron cross sections are totally dependent upon nuclear quantum numbers. Consequently cross sections fluctuate widely from nucleus to nucleus; proximity in atomic number Z will have little significance upon neutron cross sections.

Estimation of the Gamma-to-Neutron Flux and Dpa Ratios

Based on the release of 20 MeV gamma energy per fission and a mean gamma energy of 0.9 MeV as discussed above, we approximate the gamma population as 22 0.9-MeV gammas per fission. The mean number of fission neutrons per fission is ~2.5 for ^{235}U.[30] Thus we estimate that the gamma-to-neutron flux ratio in the core is of the order of 10^1.

Because gammas are more prone to absorption than neutrons and because reactors are designed to reflect neutrons back into the core, this ratio should decrease as one approaches and passes through the reactor vessel wall. Figures 2 and 3 confirm this trend: they show the calculated neutron flux and gamma dose distribution through a series of radial water and steel layers in a small (70 MW) pressurized water reactor. We then have from Equation (2):

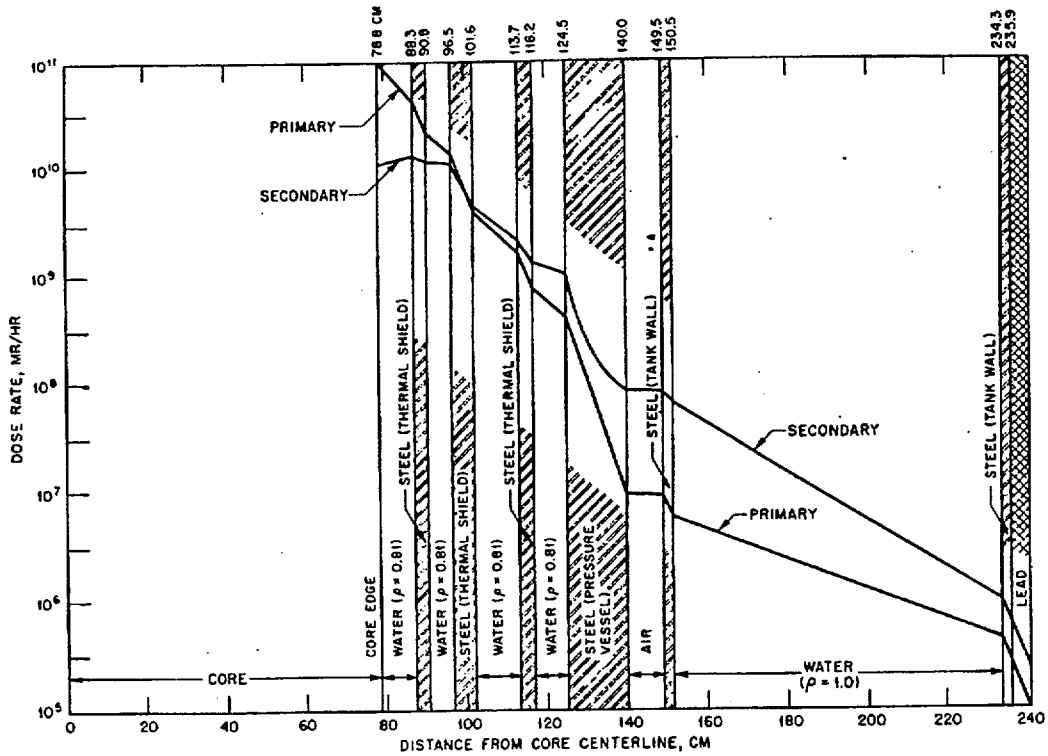

2. A figuration of primary and secondary γ-dose in a 70 MW reactor[31]

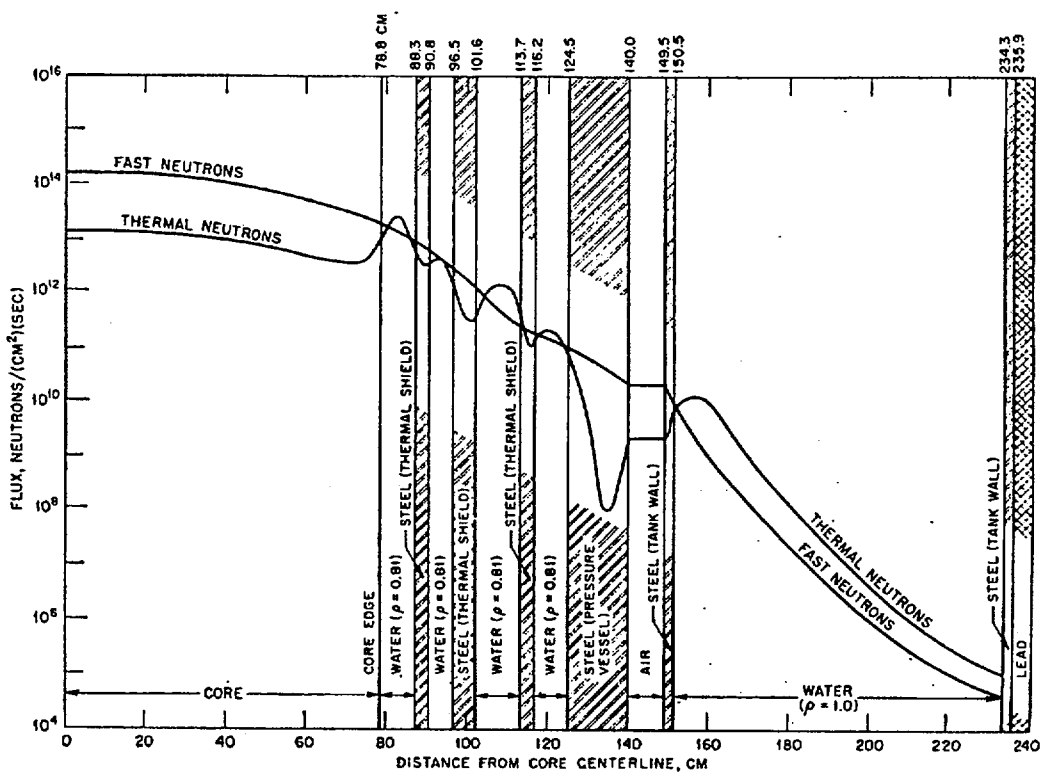

3. A figuration of fast and thermal neutron flux in a 70 MW reactor[32].

$$\frac{(Dpa\ rate)_\gamma}{(Dpa\ rate)_n} = \frac{\langle \sigma_{\gamma,dpa} \rangle}{\langle \sigma_{n,dpa} \rangle} \cdot \left\{ \frac{\int_{E_d}^{\infty} \phi_\gamma(E_\gamma)\ dE_\gamma}{\int_{E_d}^{\infty} \phi_n(E_n)\ dE_n} \right\} \leq \frac{31x10^{-3}}{500} \cdot 10 = 6x10^{-4} \tag{7}$$

Ramirez et al.[1] calculated that the neutron-induced dpa rate falls off by about a factor of 10 over the width of the Sequoyah pressure vessel wall. That reflects the decreasing fast neutron flux and the sharp decrease in the neutron-induced dpa cross section with neutron energy. However, from Figures 1-3 one expects the gamma flux and the gamma-induced dpa cross section to decrease even more sharply. As a result the gamma-to-neutron dpa ratio should further decrease through the pressure vessel wall by 1-2 orders of magnitude. However, we will conservatively not use that fact in our comparison: this further emphasizes our result to be an upper bound.

Together these arguments indicate that γ-induced atomic displacement is $\ll 1\%$ of that from neutrons in the pressure vessel wall of all fission power reactors including Sequoyah's. Note that the value of 1% allows for a factor of 16 uncertainty on our calculated estimate, not including the 1-2 orders of magnitude mentioned above.

Photon Dpa Production in a Fusion Reactor Environment

A 1982 unpublished INEL study concluded that the photon flux would have to be about 1000 times greater to equal the neutron induced atom displacement damage. Thus, even though the gamma flux was a factor of two higher it contributed only 0.2% of the neutron damage. That result supports the present work, being roughly at the same order of magnitude.

Effects of Heating

Photons also induce heating, leading to changes in alloy morphology (grain structure) and chemical diffusion. The importance of these phenomena was not addressed in this study. For the Sequoyah reactor, the effects of heating in the surveillance capsule specimens should represent the effects of heating in the actual pressure vessel wall.

Gamma heating likely exceeds neutron heating in the vessel wall and the surveillance capsule. This could be quantified by calculating photon and neutron heating rates ("kerma") once coupled neutron/photon fluxes were calculated. Neutron heating could be derived from the existing dosimetry measurements. Gamma heating could be deduced by adding thermoluminescent dosimeters (TLDs) into the surveillance capsule. For consistency and to minimize correction factors, neutron-sensitive TLDs could be added as well.

Synergistic Intergranular Stress-Assisted Corrosion Cracking

Intergranular stress-assisted corrosion cracking of stainless steels and nickel-base alloys occurs even under unirradiated conditions due to water chemistry and stress. Gamma-irradiation synergistically exacerbates cracking susceptibility via its combined effects on material micro-chemistry (e.g, radiation-induced segregation), water chemistry (e.g., radiolysis), and stress (e.g., radiation-induced creep and hardening).[16] We note that the test specimens in the Sequoyah surveillance capsule will not experience the water chemistry effects that the vessel wall will. Temperatures and

temperature gradients may also differ due to cooling differences. Thus the surveillance capsule may be non-representative for this synergistic phenomenon.

CONCLUSIONS AND RECOMMENDATIONS

1. Cursory evaluation indicates that γ-induced atomic displacement in the neighborhood of the Sequoyah Reactor pressure vessel wall is $\ll 1\%$ of that from neutrons. The surveillance capsule contained no detection devices capable of measuring the gamma fluence or energy deposition (such as TLDs). The atomic displacement damage encountered by the specimens in the surveillance capsule should be representative of that encountered in the pressure vessel wall.

2. Photons induce heating, leading to changes in alloy morphology (grain structure). They also enhance diffusion leading to decomposition of oversaturated austenite and to strengthening and embrittlement of steel. No specific analysis of these effects for Sequoyah was attempted. The impact of γ-heating upon the results from the surveillance capsule should be representative of those in the neighborhood of the pressure vessel wall.

3. Gamma-irradiation can accelerate intergranular stress corrosion cracking of stainless steels and nickel-base alloys. It exacerbates cracking susceptibility via its effects on material micro-chemistry (e.g, radiation-induced segregation), water chemistry (e.g., radiolysis), and stress (e.g., radiation induced creep and hardening). Many of these sensitivities, e.g., to water chemistry and stress, apply to cracking under unirradiated conditions as well. No specific analysis of these effects for Sequoyah was attempted. The results from the test specimens in the surveillance capsule may be non-representative of what the Sequoyah pressure vessel wall experiences in this regard due to their isolation from water chemistry effects.

A potential more-detailed evaluation of atomic displacement would include the following:

1. a coupled neutron/photon calculation of the Sequoyah Reactor, at least in one (radial) dimension, out through the pressure vessel. This would greatly increase the accuracy of both the total neutron to total photon flux ratio as well as provide the correct neutron and photon energy spectra for use in determining the dpa cross sections and reaction rates.

2. writing a Fortran program which will calculate the gamma-induced Dpa production cross section. EG&G Idaho Report RE-P-81-095 outlines the formalism. This report was authored in December 1981 and must first be brought up to date. We have checked and found that no one else has developed such a capability since 1981.

Conclusions 2 and 3 above are based on a qualitative assessment of the literature. A multi-discipline effort might further investigate these phenomena including an effort at quantification.

REFERENCES

1. B. T. Kelly, *Irradiation Damage to Solids,* Pergamon Press, 1966.

2. G. J. Dienes, "Radiation Effects in Solids," *Annual Reviews of Nuclear Science, 1953, 2,* pp.187ff.

3. J. O. Stiegler and L. K. Mansur, "Radiation Effects in Structural Materials," *Annual Reviews of Materials Science, 1979, 9,* pp.405-454.

4. H. Brooks, "Nuclear Radiation Effects in Solids," *Annual Reviews of Nuclear Science, 1956, 6,* pp. 215ff.

5. A. N. Goland, "Radiation Effects in Structural Materials," *Annual Reviews of Nuclear Science, 1962, 12,* pp.243 ff.

6. Nicholas P. Fiore, *Gamma-Irradiation Damage in Age Hardening Al Alloys*, No. 167, AD-786578, July 1974.

7. A. Weidinger et al., "Defect Configurations in Irradiated Molybdenum," *Physics Letters, Volume 72A,* No. 4, 5, 23 July 1979, p. 369.

8. Munetaka Kuribayashi et al., "Influence of γ-Radiation on Intergranular Stress Corrosion Cracking of Austenitic Stainless Steel," *Ishikawajima-Harima Giho (Japan) 23*, 6, November 1983, p. 521-526.

9. G. J. Dienes and G. H. Vineyard, *Radiation Effects in Solids*, New York: Interscience Publishers, 1957.

10. V. V. Galavanov, *Soviet Physics solid State 1*, 390 (1959)

11. O. S. Oen and D. K. Holmes, *J. Appl. Phys. 30*, No. 8, 1289 (1959).

12. V. V. Gann, et al., "Simulation of Radiation Damage of the Reactor Cores Steel by Using High-Energy e^-/γ Beams," *Physics of Radiation Defects and Radiation Materials Science. Scientific-Technical Collection,* INIS-SU-80, 1987, p. 70-72.

13. V. V. Mural' and G. V. Shcherbedinskij, "Gamma-Radiation Aging of Deformed Austenite," *Metalloved. Term. Obrab. Met. (USSR), v6*, 1984, p.47-48.

14. G. P. Marsh et al., "Influence of Radiation on the Corrosion of Stainless Steel," *Corros. Sci. (United Kingdom) 26*, 11, 1986, p. 971-982.

15. A. B. Alexandrov et al., "Effect of Gamma Radiation on Metal Corrosion Under Spent Fuel Storage Conditions," *Long Term Wet Spent Nuclear Fuel Storage. Proceedings of a Technical Committee Meeting on Behaviour of Used Fuel Assemblies and Storage Equipment at Long Term Wet Storage Conditions held in Leningrad, USSR, 26-30 May, 1986*, IAEA-TECDOC-418, CONF-8608147, April 1987, p. 181-190.

16. I. M. Neklyudov, et al., *Effects of High-Energy Electron and Gamma Radiation on Mechanical Properties of Steels Kh18N10T and 06Kh16N15M3B*, KFTI-88-53, 1988

17. A. Sudo et al., "Effect of Gamma Irradiation on IGSCC Susceptibility of Type 304 Stainless Steel," *Proceedings of 1988 JAIF International Conference on Water Chemistry in Nuclear Power Plants. Operational Experience and New Technologies for Management, Tokyo, Japan, 13 April 1988*, CONF-8804174, 1988, v.2.

18. P. L. Andersen et al., "State of Knowledge of Radiation Effects on Environmental Cracking in Light Water Reactor Core Materials," *1989 Workshop on LWR Radiation Water Chemistry and its Influence on In-core Structural Materials, Palo Alto, CA , 14-15 Nov 1989*, EPRI-NP-7033, Mar 1991, p.5.29-5.66.

19. Y. Gohar and M. A. Abdou, *MACKLIB-IV, a Library of Nuclear Response Functions Generated with the MACK-IV Computer Program from ENDF/B-IV*, ANL/FPP/TM-106.

20. E. H. Ottewitte, *FY 79-82 Overview of Radiation Effects Capability Development (Currently G3411812A)*, RE-P-81-019, February 1981.

21. V. McLane, National Nuclear Data Center, Brookhaven National Laboratory, private communication, 28 April 1993

23. P. S. Stansbury, *TECALC - A Program to Calculate Compton, Coherent, and Photoelectric Mass Attenuation Coefficients for Photons with Energies Less than 1 MeV and to Assist in the Evaluation and Formulation of Photon-Equivalent Materials*, ORNL-TM-4451, January 1974; RSIC Computer Code Collection, "Interactive Calculation of Compton Coherent and Photoelectric Mass Attenuation Coefficients for Photons (E < 1 MeV), and the Mass Absorption Coefficient for Known Materials." ORNL-PSR-74.

23. A. Foderaro, *Subroutine HEITLER*, AERE-M, 1956, (September 1967); RSIC Peripheral Shielding Routine Collection, "HEITLER Cross Section Generator," ORNL-PSR-4.

24. Harold Etherington (ed.), *Nuclear Engineering Handbook*, New York: McGraw-Hill Book Company, Inc., 1958.

25. Samuel Glasstone and Alexander Sesonske, *Nuclear Reactor Engineering*, Princeton, New Jersey: D. Van Nostrand Company, Inc., 1963.

26. Joel Weisman (ed.), *Elements of Nuclear Reactor Design*, New York: Elsevier Scientific Publishing Company, 1977.

27. W. G. Unruh and M. Tomlinson, "Mean Gamma-ray Energy Absorption Coefficients," *Nucl. Applications 3*, 1967, p. 548.

28. H. Soodak (ed.), *Reactor Handbook,* Second Edition, New York: Interscience Publishers, 1962, p.15-16.

29. Samuel Glasstone and Alexander Sesonske, *Nuclear Reactor Engineering*, Princeton, New Jersey: D. Van Nostrand Company, Inc., 1963, p. 93.

30. H. Soodak (ed.), *op.cit.*, p.9.

31. S. Glasstone and A. Sesonske, *op.cit.*, p.603

32. Ibid, p. 602

APPENDIX A

DRAFT 2

EGG-SSRE-9458
Revision 2

COST/BENEFIT ANALYSIS OF GSI-15: RADIATION EFFECTS ON REACTOR VESSEL SUPPORTS

Draft Report

R. E. Gregg
C. L. Smith
R. W. Garner

August 1991

EG&G Idaho, Inc.
Idaho Falls, Idaho 83415

Prepared for the
Office of Nuclear Regulatory Research
U.S. Nuclear Regulatory Commission
Washington, D.C. 20555
Under DOE Contract No. DE-AC07-76ID01570

DRAFT 2

FIN No. A1296

DRAFT 2

ABSTRACT

This report provides a cost/benefit (value/impact) analysis for Generic Safety Issue 15 (GSI-15). It assesses the core damage frequency and the risk associated with neutron embrittlement of the reactor pressure vessel supports (RPVSs). Five options for the resolution of GSI-15 are also evaluated. It then calculates the cost/benefit ratio that would result from implementation of any of the proposed options.

DRAFT 2

SUMMARY

Generic Safety Issue 15 (GSI-15) is concerned with neutron irradiation of the reactor pressure vessel supports (RPVSs). Neutron irradiation of structural materials causes embrittlement that may increase the probability of material failure due to a propagation of pre-existing flaws. The potential for neutron embrittlement of the RPVSs could be greater than was formerly anticipated. This report estimates the core damage frequency and the risk associated with RPVS failure, the cost involved in implementing any of five proposed resolutions, and the cost/benefit ratio that would be realized by implementation of each of the alternatives.

The five options proposed as resolutions for GSI-15 include: shielding the RPVSs from neutron irradiation, increasing the RPVS's operating temperature above the NDTT, replacing the RPVSs, heating the RPVSs sufficiently to anneal out any embrittlement, and strengthening or adding additional RPVSs.

The results indicate the estimated per plant costs range from a low value of $920,000 to increase the operating temperature of the supports to a high value of $89,000,000 to replace the existing supports. The low value takes into account averted onsite costs and assumes no replacement power would need to be purchased. The high value takes into account averted onsite costs, but assumes replacement power would have to be purchased for a 20-week period.

The results of the benefit analysis indicate a per-plant offsite dose risk of 2.9 person-rem/year of remaining reactor lifetime. This risk includes all the risk associated with support failure after embrittlement occurs. It was assumed that the implementation of any of the proposed options would remove 100% of the risk associated with failure of an embrittled support. The core damage frequency was found to be 8.8×10^{-5}/yr. This information provided cost/benefit ratios ranging from $5,300 per 77person-rem to $3,100,000 per person-rem.

DRAFT 2

CONTENTS

ABSTRACT ii
SUMMARY iii
ACRONYMS v

1. INTRODUCTION 1
2. BENEFIT EVALUATION 4
   2.1. Event Tree Analysis 4
   2.2. Safe Shutdown Earthquake Event Tree 6
   2.3. Small Break Loss-Of-Coolant Accident Event Tree 10
   2.4. Event Tree Results 12
   2.5. Sequence Risk Analysis 13
   2.6. Risk Analysis Results 15
3. COST EVALUATION 16
   3.1. Proposed Solution Options 17
   3.2. Discussion Of Options 17
   3.3. Cost Analysis Methodology 19
   3.4. Cost Estimate Categories 22
   3.5. Cost Evaluation Uncertainty 27
   3.6. Plant Modification Cost Estimate Results 29
   3.7. Radiation Exposure 31
4. COST/BENEFIT ASSESSMENT 32
   4.1. Dollar-to-Person-Rem Averted Ratio 32
   4.2. Cost/Benefit Results 32

5. SUMMARY OF COST/BENEFIT FINDINGS 37
6. REFERENCES 38

Appendix A - GSI-15 Event Tree Uncertainty Analysis
Appendix B - GSI-15 Risk Sensitivity Analysis
Appendix C - Taylor Series Expansion (TSE) Program Verification
Appendix D - GSI-15 Cost/Benefit Ratio Graphs

DRAFT 2

ACRONYMS

AOSC	--	Averted Onsite Costs
BWR	--	Boiling Water Reactor
COV	--	Coefficient of Variation
CSDSF	--	Chemical Shut Down System Failure
DPR	--	Dollar to Person-rem Averted Ratio
ECCSF	--	Emergency Core Cooling System Failure
EEDB	--	Energy Economic Data Base
EF	--	Error Factor
EFPY	--	Effective Full Power Years
GSI-15	--	Generic Safety Issue 15
LBLOCA	--	Large Break Loss-of-Coolant Accident
LOCA	--	Loss-of-Coolant Accident
LWR	--	Light Water Reactor
NDTT	--	Nil Ductility Transition Temperature
NNB	--	No net benefit
NRC	--	Nuclear Regulatory Commission
ORNL	--	Oak Ridge National Laboratory
PRA	--	Probabilistic Risk Assessment
PWR	--	Pressurized Water Reactor
QA/QC	--	Quality Assurance/Quality Control
RCF	--	Reactor Containment Failure
RCS	--	Reactor Cooling System
RP	--	Replacement Power
RPSF	--	Reactor Protection System Failure
RPV	--	Reactor Pressure Vessel
RPVS	--	Reactor Pressure Vessel Support
RPVSF	--	Reactor Pressure Vessel Support Failure
SBLOCA	--	Small Break Loss-of-Coolant Accident
SF-PSD	--	Safe Plant Shut Down
SPRA	--	Standard Probabilistic Risk Assessment
SSE	--	Safe Shutdown Earthquake

DRAFT 2

COST/BENEFIT ANALYSIS OF GSI-15: RADIATION EFFECTS ON REACTOR VESSEL SUPPORTS

1. INTRODUCTION

Neutron irradiation of structural materials causes embrittlement that may increase the probability of material failure due to a propagation of pre-existing flaws. In April 1988 data produced by Oak Ridge National Laboratory[1] (ORNL) suggested that the potential for neutron embrittlement of reactor pressure vessel supports (RPVS) could be greater than was formerly anticipated.

The first part of this report estimates the core damage frequency and risk associated with RPVS failure. The second part of this report presents the cost/benefit ratio for implementation of any of five solutions.

Normally the potential for brittle fracture in a material is quantified in terms of the material's nil ductility transition (NDT) temperature. The NDT temperature for a material is the temperature at which the material becomes prone to brittle failure. If the material is kept at a higher operating temperature than its NDT temperature, brittle fracture of the material will be prevented. The possible corrective measures to the damaged pressure vessel supports would fall in one of five categories:

- The supports can be shielded to reduce the neutron radiation exposure.
- The operating temperature of the supports can be increased above the NDTT of the support material.
- The embrittled supports can be replaced.
- The supports can be heated such that the embrittlement is annealed out.
- The embrittled supports can be left in place and additional supports can be added.

The RPVS designs for light water reactors (LWR) have been divided into five different categories (Reference 1). The support categories are skirt, long column, shield tank, short column, and suspension. The skirt type supports are located far enough away from the reactor core such that embrittlement induced failure of the support is not anticipated. All operating boiling water reactors (BWRs) except Big Rock Point have skirt type supports; therefore, they are not included in this study. Big Rock Point Nuclear Plant is the only operating plant with suspension type supports; it was not included in this study because of its small size (240 MWt) and low surrounding population density.

Table 1 lists the support type and the number of PWRs of each type in use. Since the skirt type supports are not likely to fail due to neutron embrittlement, they are removed from further consideration leaving 76 plants with susceptible supports.

Table 1. PWR Reactor Pressure Vessel Support Utilization.

Support Type	Number in Use
Skirt	7
Long Column	11
Short Column	57
Shield Tank	8
Total susceptible plants	76

The analysis first estimated the core damage frequency and the risk associated with operating the 76 PWRs with possible radiation damaged RPVSs. It is assumed that any one of the 76 PWRs could have suspect RPVSs. Therefore, the event tree analysis was very conservative to be able to bound the different failure modes for the four different support types. Also, it was assumed that modifying the supports would reduce the embrittlement risk.

The second part of the analysis estimated the costs associated with fixing the different support types. The reduction in risk is understood to be the benefit, while the expenditure in fixing the supports is the cost. The cost/benefit ratio is then used as a basis for recommending what action should be taken. Consideration is also given to the core damage frequency resulting from embrittled supports.

2. BENEFIT EVALUATION

The benefit is defined as the reduction in risk obtained by fixing the neutron embrittled RPVS. To estimate the risk, two different scenarios were considered that could fail the supports. Event trees for each scenario were developed to obtain the associated probability of RPVS failure. The probability of RPVS failure was then multiplied by the associated consequence of the failure, thus obtaining the failure risk.

2.1. Event Tree Analysis

The GSI-15 event tree evaluation involves two different scenarios. The first scenario is a safe shutdown earthquake (SSE) as an initiating event and the potential failure of the RPVSs. The second scenario involves a small break loss-of-coolant-accident (SBLOCA) as the initiating event. The discussion of the scenarios includes the associated event tree and a detailed explanation of each event contained in the event tree.

Typical event tree methodology is used in the generation of the scenario event trees. At each branch node, the downward path represents the failure event that is listed above that node, while the upward path symbolizes the complement of the failure event. Each failure event portrays a phase in the scenario development and represents the failure of a particular safety function. Human errors and procedural guideline flaws are not incorporated into the event tree model.

The sequence outcomes are grouped into one of seven different categories. Table 2 lists the different categories along with a description of each category. The offsite release categories are taken from the WASH-1400[2] reactor safety report and classify various degrees of radioactive releases from containment. Each sequence was assigned to the offsite release category that best modeled its outcome. When a sequence could fall into one or more release categories (i.e., PWR 1 or PWR2, PWR 3 or PWR 4, etc.), the most conservative release category was selected.

Table 2. Event Tree Sequence End State Categories.

CONSEQUENCE LABEL	EXPLANATION
SPRA	The sequence results in an event sequence whose risks are not associated with GSI-15. The sequence is not further developed on the event tree.
SF-PSD	The sequence results in an emergency plant shutdown. Thus, the plant is safe and in a shutdown mode.
PWR 1	The sequence results in core meltdown followed by a steam explosion. The containment sprays and heat removal systems are assumed to have failed. Radioactivity is released over a 10 minute period. The total release contains approximately 70% of the iodines and 40% of the alkali metals present in the core at the time of release.
PWR 3	The sequence results in containment failure prior to commencement of core melting. Core melting would cause radioactive materials to be released through a ruptured containment barrier. Approximately 20% of the iodines and 20% of the alkali metals present in the core at the time of release would be unleashed to the atmosphere. The release time would be approximately 1.5 hours.
PWR 7	The sequence results in core meltdown but is mitigated due to the fact that the containment barrier retains its integrity until the molten core melts through the containment. The release involves 0.002% of the iodines and 0.001% of the alkali metals present in the core at the time of release. The release time would be 10 hours.
PWR 8	The sequence results in large pipe break with failure of containment. The core would not melt. The release would involve 0.01% of the iodines and 0.05% of the alkali metals. Most of the release would occur in 0.5-hours.
PWR 9	The sequence results in a large pipe break. The core would not melt, and the containment would not fail. The release would contain 0.00001% of the iodines and 0.00006% of the alkali metals. The release would occur over a 0.5-hour time period.

2.2. Safe Shutdown Earthquake Event Tree

The first event tree is shown in Figure 1. The event tree models the occurrence of a SSE and the potential failure of the RPV supports. For this model, it is assumed that failure of the RPV supports may only cause a large break loss-of-coolant-accident (LBLOCA). Thus, a SBLOCA will not be considered as a contributor to the core-damage probability and will not be included in the event tree. This assumption is supported by the fact that the leak rate (less than 200 gpm) for a SBLOCA is easily replaced by various reactor makeup systems such as the high pressure safety injection system or the charging system.

The events for the SSE sequence event tree are defined below. The probability for each event is given as a mean value. The uncertainty analysis for the event trees is contained in Appendix A.

SSE. The event SSE models the initiating event of a safe shutdown earthquake. From NUREG-1211[3], it is assumed that frequency of occurrence is 2.5×10^{-4}/RY and the initiating event probability can be modeled as a Poisson distribution. Thus, the dimensionless parameter v for the Poisson distribution for one-year is 2.5×10^{-4}.

It is commonly accepted that earthquakes producing lower loads on structures occur more often than those resulting in higher loads, such as the SSE. Also, if plastic design methods are used, as described in Chapter N of the AISC Manual[4], the allowable stress in the load combinations including SSE is $0.9 \times F_y$[5], i.e., for A36 steel this would result in about 30 ksi. Taking 6 ksi as the minimum stress corresponding to the threshold of embrittlement, the ratio of the stresses (the stress at the SSE and the minimum stress which might be considered for brittle fracture) would be equal to five. Since force is proportional to acceleration, and stress is proportional to force, it may be inferred that the stresses induced by an earthquake will be in the same proportion as peak ground acceleration (PGA) for different earthquakes.

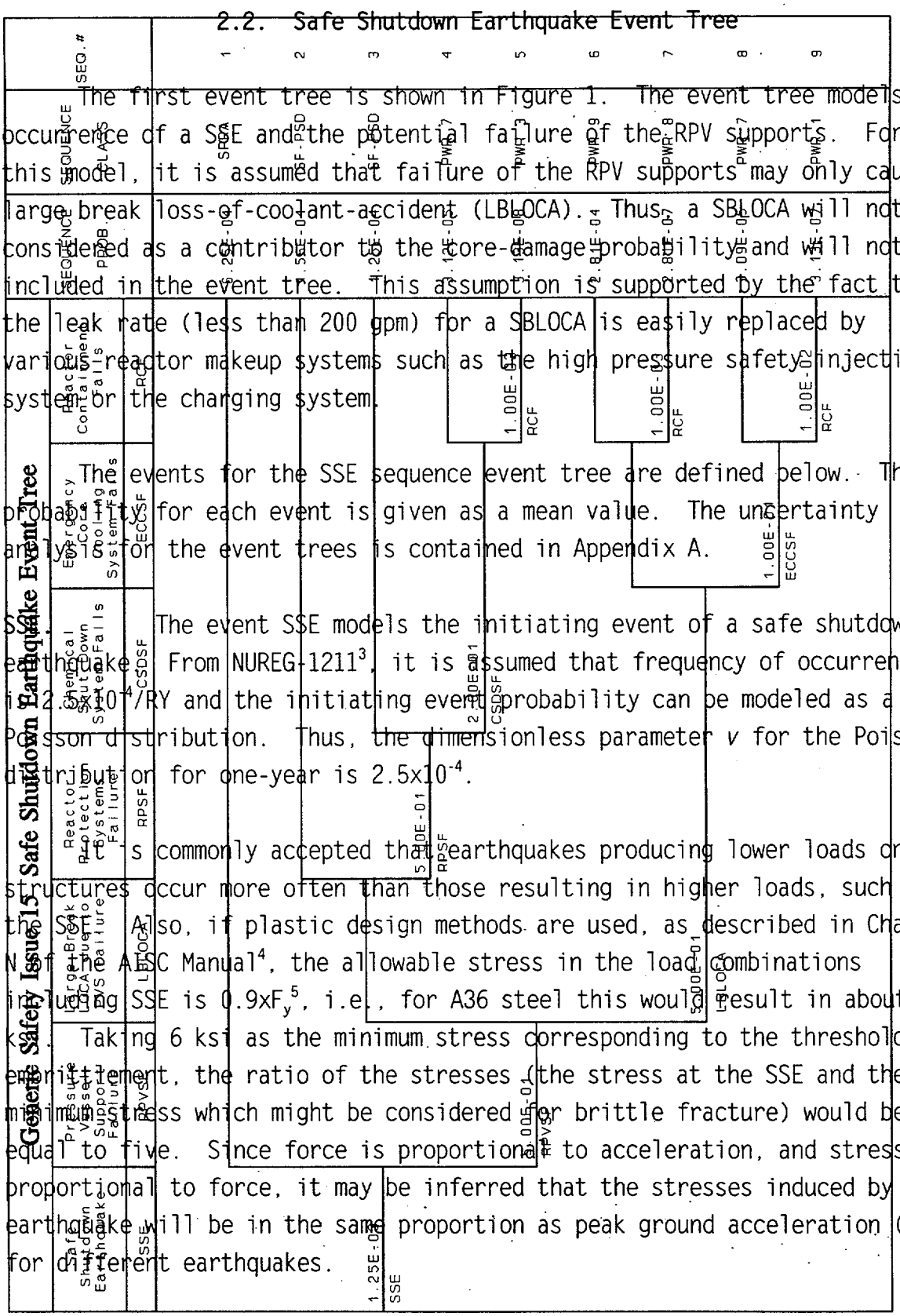

Figure 1 Safe Shutdown Earthquake Sequence Event Tree

Now, examination of the seismic hazard curves, relating annual frequency of exceedance of SSE and PGA[6], indicates that frequency of occurence of the earthquake corresponding to 6 ksi would be about five times that of the frequency of occurance of the PGA for the SSE. Reducing the stress threshold by a factor of five has the effect of increasing the frequency of the earthquake by about a factor of five. Consequently, it is justifiable to increase the dimensionless parameter v for the Poisson distribution for one year by a factor of five, to $v = 1.25\text{x}10^{-3}$. The probability of a damaging earthquake is then:

$$P(SSE) = 1 - P(x=0) = 1 - \frac{v^x e^{-v}}{x!} = 1 - e^{-1.25\text{x}10^{-3}} = 1.25\text{x}10^{-3}$$

RPVSF. Event RPVSF represents the failure of the RPV supports if a damaging earthquake occurs. The calculation for the probability of RPVSF should be site specific due to variables such as RPV support design and material composition, plant age and operating history, and RPV load before and after the earthquake. In order to keep the analysis generic, the conditional probability of RPVSF is conservatively estimated to equal 0.5. This assumption implies that if a damaging earthquake occurs, fifty percent of the time the RPV supports will fail. Also, it implies that below the damaging earthquake level the RPV supports will not fail. In the sensitivity analysis contained in Appendix B, the frequency of having a damaging earthquake was increased by a factor of 10 to account for the possibility of a lower peak-ground acceleration level earthquake which results in RPV support failure.

LBLOCA. The event LBLOCA models a large break LOCA if the RPV support system undergoes a failure. If the RPV support does fail, the resulting load on the reactor cooling system (RCS) piping may cause a rupture. A conservative estimate of the probability of a LBLOCA is assumed to be 0.5. The sensitivity analysis in Appendix B investigated the worst case of RPV support failure coupled with a LBLOCA by setting both probabilities to 1.

RPSF. The event RPSF models the failure of the reactor protection system. In the event of a SSE, the operator will attempt to manually scram the reactor. However, it is possible that the protection system will fail due to the tilting of the RPV, which causes the reactor control rods to become mechanically jammed. Thus, detailed analysis for this event should include both possible mechanical failures and human errors of commission.

Event RPSF is conditional on a LBLOCA not occurring. If a LBLOCA does occur, the moderator for the reactor will be removed and the reactor will shut down due to voiding of the core. Consequently, if a LBLOCA does not occur and the reactor protection system fails, the core will eventually melt even though the reactor coolant is still present. It is conservatively assumed that the probability of RPSF is 0.5. The sensitivity analysis in Appendix B investigated the worst case scenario by setting both RPVSF and RPSF to one. This would model coupled failure of both the RPV supports and the reactor protection system.

CSDSF. The event CSDSF models the failure of the chemical shutdown system. Typically, precise analysis of this event would include both the possible mechanical failures and human errors. For this analysis, the probability of CSDSF was found from the Sequoyah PRA[7] and is equal to 0.2. The sensitivity analysis in Appendix B investigated the worst case scenario by setting the probability of CSDSF failure to one.

ECCSF. Event ECCSF models the failure of the emergency core cooling system. If the emergency core cooling system works, it can prevent core melt even if a large break LOCA occurs. The probability of failure for this event is based upon typical PRA analysis. Based upon the Sequoyah PRA, the conditional probability of ECCSF is equal to 0.02. This mean conditional probability measures the failure probability of the systems (including human and mechanical) comprising the ECCS. Failure of ECCS following RPVS failure and the resulting RPV displacement and increased primary piping stresses would result in higher stresses on ECCS piping and components and would increase the conditional failure probability. Therefore, the event ECCSF probability was increased by a factor of five to

0.1. The sensitivity analysis in Appendix B investigated the worst case scenario (where the ECCS always fails given the appropriate initiating event) by setting the probability of CSDSF failure to one.

RCF. The event RCF represents the failure of the containment heat removal system along with the containment structure and containment isolation. Since the reactor containment and most of the systems in it have a median capacity of 1.5-2g peak ground acceleration, a SSE should not have a noticeable effect on the containment failure rate. Therefore, a typical PRA based failure rate is assumed for the reactor containment. Based upon the Sequoyah PRA, the probability of RCF is $1x10^{-3}$ in the mission time of one year. For those cases where ECCS has failed, the probability of RCF was assumed to be $1x10^{-2}$, which accounts for the possibility of a dependent ECCS/RCF failure mode.

Also, the Salem Nuclear Generating Station PRA[8] was used to compare the failure rates of the mechanical components for the analysis of both event trees.

2.3. Small Break Loss-Of-Coolant Accident Event Tree

The second event tree is shown in Figure 2. The event tree models the occurrence on a non-seismic induced SBLOCA and the resulting failure of the RPV supports. Given that a SBLOCA occurs, the resulting load normally carried by the fractured pipes will be transferred to the RPVSs thereby causing an additional load on the supports. If the supports have undergone neutron embrittlement, the addition of the SBLOCA induced load may cause the RPVSs to fail. If the RPVSs do fail, a large break LOCA may occur.

As can be seen in Figure 2, the SBLOCA event tree is similar to that from the SSE sequence discussed above. The basis for using a similar event tree with identical event probabilities is that if the RPVSs fail, the possible resulting LBLOCA, reactor protection system failure, chemical shutdown system failure, emergency core cooling system failure, and reactor containment failure events will most likely fall within the same realm

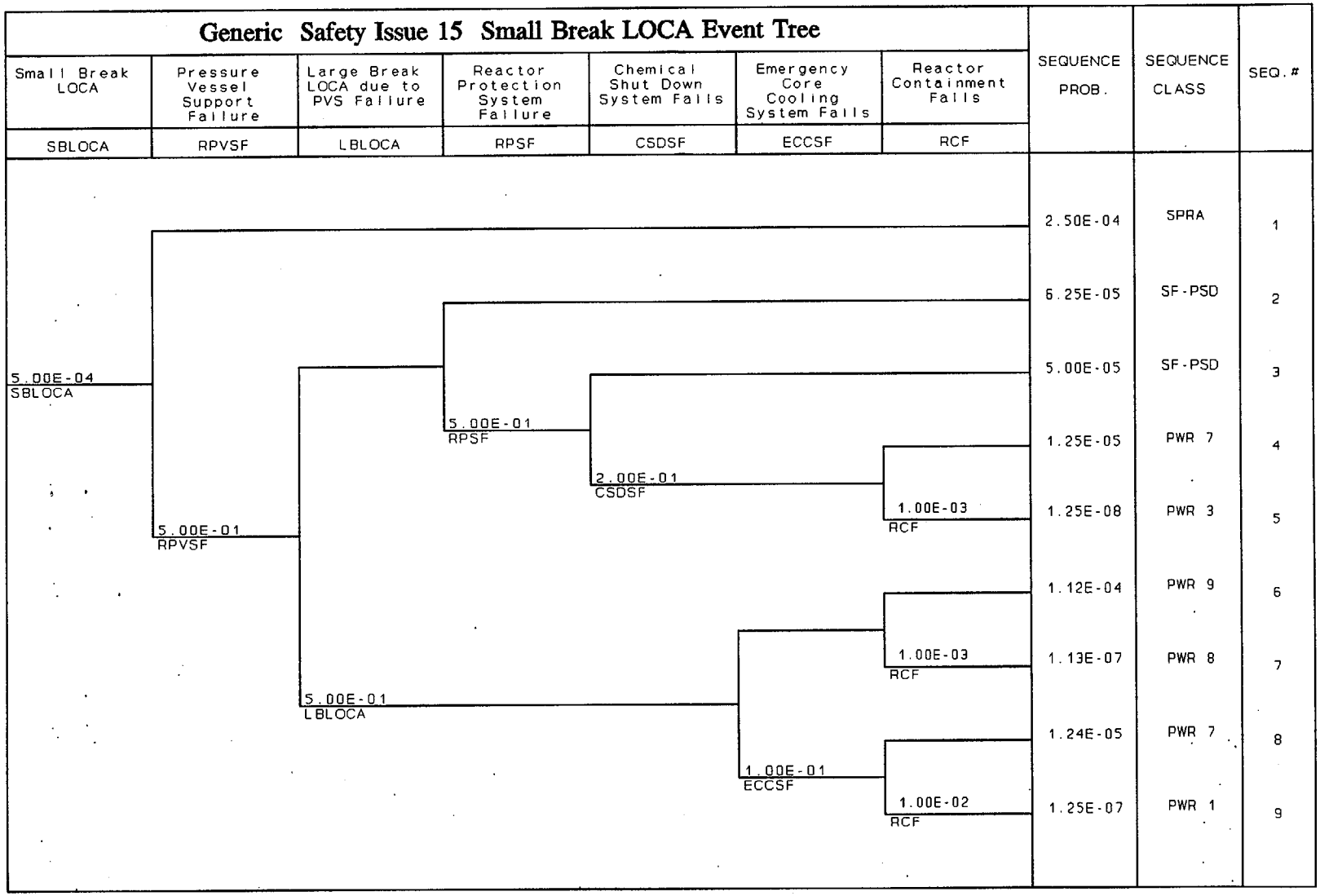

Figure 2. Small Break LOCA Event Tree.

DRAFT 2

regardless of the cause of the RPVSs failing. Thus, the only difference between the two event trees is the initiating event and its associated frequency.

SBLOCA. The initiating event for the second event tree is the occurrence of a small break LOCA. The frequency of occurrence was obtained from the Sequoyah PRA[7] source numbers. The nominal frequency for a small break LOCA is found to be $1x10^{-3}$. The assumption was made that only one-half of the possible small pipe breaks were close enough to the RPV to load the RPV supports such that failure of the supports may occur. Therefore, the frequency of occurrence for a SBLOCA is estimated to be equal to the nominal SBLOCA frequency multiplied by one-half, or $5x10^{-4}$/RY. Assuming the SBLOCA event can be modeled as a Poisson event, the probability of a SBLOCA in the mission time of one year is equal to $5x10^{-4}$.

The remaining events in the SBLOCA event tree have previously been defined and will not be reviewed. In both the SSE and SBLOCA sequences the following preexisting conditions must be met before the RPVSs can fail:

- The support must contain a critically sized flaw.
- The support must have been subjected to enough radiation for embrittlement to occur.
- Sufficient stresses must be present to cause brittle fracture.

Requirements for toughness were implemented after some plants were built. Therefore, some older plants may have been at or near the NDT temperature at the beginning of plant life. If this is the case, they may be susceptible to brittle failures without significant exposure to neutron radiation.

2.4. Event Tree Results

Since the two event trees lead to similar sequence outcomes, the identical outcomes from each tree can be combined to form a total probability of a particular end state. The end states can occur with

either the SSE or the SBLOCA as the initiator. Thus, the end state probability for the PWR 1 category is calculated by:

$$P(PWR1)_{total} = P\left((PWR1)_{SSE} \cup (PWR1)_{SBLOCA}\right)$$
$$\approx P(PWR1)_{SSE} + P(PWR1)_{SBLOCA} \quad (if\ P(PWR1) << 1).$$

Table 3 lists the sequence end states and the expected probability of occurrence for the mission time of one year. Since the expected probability is calculated by multiplying several random variables together, the probability distribution for the resultant product would tend to be log-normally distributed. As seen in Table 3, the total core damage frequency due to RPVS failure is 8.8×10^{-5}/yr.

Table 3. Event Tree End State Analysis Results.

SEQUENCE END STATE	EXPECTED PROBABILITY (per year)	CORE DAMAGE	TOTAL CORE DAMAGE FREQUENCY (per yr)
SPRA	8.8×10^{-4}	No	N/A
SF-PSD	3.9×10^{-4}	No	
PWR 9	3.9×10^{-4}	No	
PWR 8	3.9×10^{-7}	No	
PWR 7	8.7×10^{-5}	Yes	8.8×10^{-5}
PWR 3	4.4×10^{-8}	Yes	
PWR 1	4.4×10^{-7}	Yes	

2.5. Sequence Risk Analysis

The risk is defined as the probability of occurrence of an event multiplied by the radioactive release consequence associated with the event. The risk is then extrapolated over the estimated remaining lifetime of a typical reactor. The risk from each event sequence is then summed to

provide an upperbound total risk.

The fracture mechanics analysis reported in NUREG/CR-5320 described radiation embrittlement as a credible end-of-life failure mode, assuming 32 Effective Full Power Years (EFPY). Given the current "40-year license lifetime" and assuming an average plant is twenty years old, it is assumed that a remaining plant lifetime is 20 years, with the last 10 plant years encompassing the plausible radiation embrittlement failure mode.

Table 4 lists the consequence associated with each end state category. The consequence data quantify the WASH-1400 end states and are taken from NUREG/CR-2800[9]. The consequences for the SPRA and SF-PSD end states are both assumed to be zero (no additional risk).

Table 4. End State Radioactive Release Consequences (from NUREG/CR-2800).

CATEGORY	Whole Body Dose Consequence Factor (person-rem)	
	Core Melt	Non Core Melt
PWR 1	5.4×10^6	
PWR 3	5.4×10^6	
PWR 7	2.3×10^3	
PWR 8		7.5×10^4
PWR 9		1.2×10^2

The WASH-1400 release categories were assigned to those event tree sequences that resulted in a radioactive release not covered by the normal plant specific design PRA. The release category that best fit each sequence was used to obtain an offsite dose for that sequence. As discussed in NUREG-2800, the total offsite radioactive dose was calculated based on the following assumptions:

1. Calculations were based on a typical midwest site, adjusted to reflect the population density within a 50-mile radius of U.S. nuclear power plants.

2. Dose consequences represent whole-body population dose commitment (person-rem) received within 50 miles of the site.

3. A 1/2-mile exclusion area was assumed, with a uniform population density of 340 persons per square mile from the exclusion area to the 50-mile exposure radius.

4. Evacuation was not considered.

5. Meteorological data were taken from the U.S. Weather Service station at Moline, Illinois.

6. Core inventory at accident initiation time was assumed to be represented by a 3412 MWt (1120 MWe) plant.

7. All exposure pathways except ingestion were included.

2.6. Risk Analysis Results

Table 5 lists the results of the risk analysis. The end state release consequence (Table 4) is multiplied by the end state probability (Table 3) to get an end state risk. The risk is then summed and multiplied by the remaining reactor lifetime to get the total additional population risk associated with the possible RPVS failure due to a SSE or a SBLOCA.

As shown in Table 5, the expected risk is 2.9 person-rem/year for the remaining plant lifetime after embrittlement occurs. The 2.9 person-rem/year risk is based on the operation of one reactor and is estimated using very conservative event probabilities. To get a total industry-wide risk value, the 2.9 person-rem/year should be multiplied by the total

Table 5. Risk Analysis Results.

CATEGORY	EXPECTED RISK (person-rem)
SPRA	0/year
SF-PSD	0/year
PWR 9	0.047/year
PWR 8	0.029/year
PWR 7	0.20 /year
PWR 3	0.24 /year
PWR 1	2.4 /year
Σ =	2.9 /year
x 10 years	29
x 20 years	58
x 40 years	120
x 60 years	170

number of embrittlement susceptible plants and their respective remaining lifetimes. Assuming seventy-six susceptible plants, the total industry-wide risk value would be 2200 person-rem for a ten-year time period. If every embrittled support in the seventy-six plants were repaired, the expected total benefit from the reduction in risk would be 2200 person-rem.

3. COST EVALUATION

The proposed resolution modifications will have the effect of either preventing embrittlement from occurring, replacing or repairing potentially failed components, or changing the operating environment of embrittled components such that further embrittlement cannot occur. The risk reduction possible from the implementation of any of the proposed modifications is obtained from the event trees developed in Section 2.

3.1. Proposed Solution Options

Five possible options or alternatives were proposed as resolutions for GSI-15. It should be kept in mind that these are only potential solutions. A substantial engineering effort will be required before the feasibility of implementing any of these solutions at any given nuclear power plant is shown to be practical. The five options are:

1. Shielding the RPVSs from neutron radiation. This would prevent the RPVSs from becoming embrittled.

2. Increasing the operating temperature of the RPVSs above the new (embrittled) NDTT. This would remove the brittle fracture failure mode.

3. Replacing the existing RPVSs before embrittlement occurs.

4. Annealing the RPVSs to remove the effects of the embrittlement.

5. Strengthening the existing RPVSs or adding new supports.

3.2. Discussion Of Options

Before any proposed modification could be made to resolve this issue, an extensive engineering analysis would be required on a plant-by-plant basis. Included in this effort, the analysis would have to: assess the effects of neutron embrittlement on a plant-specific basis, calculate the risk associated with the possible embrittlement, insure that the implementation of any proposed modification is possible and that it will actually solve the problem, perform the design and engineering work for any proposed modification, pass the required engineering reviews, and obtain NRC design approval.

It should be noted that the RPVSs are located in an area of high radiation with extremely limited access. Even the act of visually

inspecting them would be a major undertaking, which would result in a considerable occupational exposure. Therefore, any proposed solution needs to be evaluated both on the merits of its cost-to-benefit ratio and in light of the additional occupational exposure that would result from its implementation.

Option 1 is to shield the RPVSs from neutron radiation. This would prevent the RPVSs from becoming embrittled. Because of the limited space available in the area of the RPVSs, adding shielding would not be practical unless a shielding with an extremely large neutron absorption cross-section is used. The procurement of suitable shielding would probably be expensive. Also, the shielding must not interfere with the normal, inherent heat transfer mechanisms of the RPVSs.

Option 2 is to increase the operating temperature of the RPVSs above the new (embrittled) NDTT. This would remove the brittle fracture failure mode. It is questionable if this option is applicable to the short column RPVSs. The short column supports have a small profile with a large temperature differential. In NUREG/CR-5320 it is estimated that for the Trojan plant, after 32 EFPY, there will be a 75°F shift in the NDTT in the area most likely to contain a critically-sized flaw. In order to elevate the RPVS's operating temperature sufficiently to accommodate this shift, it would probably require exceeding the temperature limit of the supporting concrete. This would have the effect of changing the failure mechanism from failure of the RPVS to failure of the supporting concrete structure.

Option 3 is to replace the existing RPVSs before embrittlement occurs. It is unlikely that this option could be completed during a scheduled shutdown. It would, therefore, involve the buying of replacement power. Because the RPVSs are keyed to the RPV nozzles, the replacement of the RPVSs would most likely involve either lifting or removing the RPV until the supports are replaced.

Option 4 is to anneal the RPVSs to remove the effects of neutron induced embrittlement. There are two methods by which the RPVSs could be

annealed. The possibilities are either in-place annealing of the supports or removing the supports and annealing at a remote location. In-place annealing would probably be the most cost effective; however, for those RPVSs that are attached to or imbedded in concrete (i.e. short column RPVSs) this may not be possible due to the temperature limit of the supporting concrete. Option 4 is calculated in two ways; the first way (Option 4A) takes into account removal of the RPVSs to an out-of-containment location for annealing, and the second way (Option 4B) calculates the cost of in-place annealing. Like Option 3, both options would most likely involve the buying of replacement power.

Option 5 is to strengthen the existing RPVSs or add new supports. It is questionable whether or not this option is possible. For most reactors, all the locations that can be used to support the RPV are currently in use, and any attempt to strengthen the existing supports would be akin to replacing the RPVSs, with all the implementation problems associated with Option 3. Like Options 3 and 4, this option would involve the buying of replacement power during the modification downtime.

3.3. Cost Analysis Methodology

The cost estimates of the five options were developed using the guidelines of NUREG/CR-3568[10], "A Handbook for Value-Impact Assessment," and NUREG/CR-4627[11], Revision 2, "Generic Cost Estimates," and the computer code FORECAST 2.1[12], which incorporates the cost evaluation information. FORECAST was developed under the auspices of the NRC. It has been used as the basis for estimating costs in several cost/benefit analyses prepared for the NRC. Cost estimation involved making an evaluation of each proposed modification, identifying equipment and materials necessary to make the proposed modifications, and assessing the work area in which the proposed modifications would be made. The following assumptions were included in the cost estimates:

1. If implemented, the solution would resolve the problem with 100% assurance.

2. Options 3, 4A, and 5 probably cannot be implemented without replacement power costs. Options 1, 2, and 4B may possibly be implemented without buying replacement power.

3. Socio-economic impacts will be considered minimal and will not be included as an increment of cost.

4. Costs were calculated using 1991 dollars.

5. Costs were calculated assuming that modifications would be required on the total support system.

6. For Option 1, shielding would have to be constructed from an alloy of cadmium. Based upon engineering judgement, material costs would be approximately $50,000 per support, for a total cost of $200,000 for four supports.

7. Option 4 has no equipment or materials costs.

8. Options 1, 2, and 5 have no removal labor costs associated with them. Option 4B removal costs would be the cost associated with removal of the annealing equipment and is estimated to be one-third of the installation cost.

9. Due to the high radiation dose present in the area containing the RPVSs, no modifications could be made without first defueling and draining the reactor vessel.

10. For Option 2, NUREG-0933[13] estimated that some plants would have material costs as low as $5200 and labor costs as low as $25,000. The numbers were calculated based on the assumption that the temperature of the RPVSs could be raised above the new NDTT by simply adjusting cooling flow to the RPVSs. We feel that even if this fix is possible, it would require the installation of additional temperature monitoring equipment,

such that the cost would be similar to the costs associated with the installation of heating systems discussed in NUREG-0933.

11. The cost of buying replacement power was made on the assumption that Options 1, 2, and 4B would require an additional 4 weeks of outage time, Options 3 and 4A would require an additional 20 weeks, and Option 5 would require an additional 16 weeks.

Expenses were calculated in accordance with FORECAST 2.1. The total cost of a modification is the sum of many different types of expenditures. The costs that were analyzed were limited to the following categories:

1. Equipment and material costs.

2. Labor costs associated with installation and/or removal.

3. Costs associated with engineering and quality control and quality assurance (QA/QC).

4. Radiation exposure.

5. Costs associated with health physics.

6. The costs to defuel, drain, and restore the reactor.

7. Replacement power costs.

8. Total NRC costs, both one-time and recurring costs.

9. Averted onsite costs (AOSC).

3.4. Cost Estimate Categories

Labor, Equipment, and Material Costs

The Energy Economic Data Base (EEDB), which is built into the FORECAST code, provided the basis for the equipment costs, material costs, and labor estimates. The EEDB incorporates "as-built" cost information (both the material unit cost and the installation or removal labor hours) for nuclear plant activities. Additionally, for operating nuclear power plants there are a number of workplace characteristics which significantly reduce the level of productivity and thus increase the number of labor hours required to accomplished a task. These characteristics, discussed in detail in FORECAST 2.1, include access, congestion and interference, radiation, task management, etc. Since the EEDB reflects only new (or "as-built") plant conditions, the installation labor hours were adjusted using FORECAST 2.1 to properly consider actual working conditions existing at operating nuclear plants. FORECAST 2.1 can modify the EEDB to take into account the factors that reduce worker productivity.

The total labor costs associated with the proposed modifications include overhead charges to account for contractor management, administrative support, rent, insurance, etc. Options 1, 2, and 4B installation labor hours were estimated based on 105 man-weeks obtained from Reference 13. The labor hours and material costs associated with Option 3 were obtained directly from the EEDB. Option 4A labor hours were assumed to be the same as Option 3, but its material costs were assumed to be zero. Option 5 material costs were assumed to be the same as Option 3, but the labor hours were adjusted to reflect that there would be no removal costs associated with Option 5.

Costs Associated with Engineering and QA/QC

These costs reflect the cost of engineering and design, as well as quality assurance and quality control (QA/QC) activities associated with implementing the requirements. For requirements affecting structures or

systems already in-place (operating plants), the guidelines of Abstract 6.4 of FORECAST recommend a 25% engineering and QA/QC factor be applied to the direct cost (i.e., the labor and materials cost without any overhead charges). All cost estimates developed in this study include this engineering and QA/QC cost component. In the case of Options 1, 2, and 4B, a large analytical effort would be required to insure that the implementation of any proposed modification is possible, that it will actually solve the problem, and that it can acquire NRC design approval. Therefore, for these two options a 40% engineering and QA/QC factor was applied.

Radiation Exposure Estimation

Worker radiation exposure estimates were derived based on guidelines presented in FORECAST. The collective radiation exposure associated with the implementation of a proposed plant modification is estimated by taking the product of the in-field labor hours necessary to perform the task and the work area dose rate associated with that particular task.

In this study, the work area in which the modifications would take place is considered to be high-dose contaminated area (inside the biological shield). Based on engineering judgement, radiation exposure level (with the reactor's fuel removed) is estimated to be 10 mrem/hour for the proposed modifications.

Costs Associated with Health Physics

Health physics requirements for the potential plant modifications were developed based on information and guidelines presented in Abstract 2.1.6 of Reference 12. Two factors were considered: the size of the work crew and the magnitude of the radiation field. The plant health physicist (HPs) monitor personnel radiation doses, perform radiological surveys throughout the modification duration, staff radiological checkpoints, set up anti-contamination clothing removal areas, as well as determine allowable stay times and badging requirements.

Cost to Defuel, Drain, and Restore the Reactor

If the nuclear reactor core is left in place, high radiation levels (2-3 REM/hr)[a] would be experienced in the area where the modifications would be made. Therefore, if any modification is to be made, the reactor must be defueled and drained and then refueled after the modifications are completed. In accordance with Abstract 2.1.3 of Reference 12, these defueling and restoring costs were developed for a typical PWR. Not included in these costs are the costs associated with fuel sipping and vessel surveillance and inspection.

Replacement Power Costs

Replacement power costs for the potential plant modifications were developed based on information and guidelines presented in Abstract 2.1.2 of Reference 12. A best estimate of $500,000/day was used, with high and low values of $900,000/day and $150,000/day, respectively.

Total NRC Costs

The total NRC costs include the one-time cost associated with supporting the implementation of any proposed modifications and the recurring costs associated with reviewing the operation and maintenance of a modification after it is implemented.

NUREG-2800 estimated it would take 16 man-weeks of staff effort to develop possible solutions. At a rate of $45.35 per hour, this amounts to $29,000. Supplementary contractor support was estimated to cost an additional $500,000, for a total cost of $529,000 for all 76 affected plants (or $6960/plant).

---

[a] As measured in the area of the reactor vessel nozzle's at the Trojan Nuclear Power Plant, per telephone conversation between R.W. Garner of the INEL and Arnie Fero of Westinghouse Electric on 5/16/90.

NRC efforts to support and review implementation of any modification was estimated by NUREG-2800 to be 15 man-weeks/plant. Also, it was estimated that for some modifications only 2 man-weeks would be required. However, due to the complicated issues involved in all of the proposed modifications, we feel the 15 week figure applies to all modifications. At a rate of $45.35 per hour, the 15 man-weeks/plant totals $27,000 per plant.

Recurring costs were estimated to be 1 man-week/RY per plant. Given ten years of remaining reactor life, at a cost of $45.35 per hour, this amounts to $18,100 per plant. Based on the above estimates, the total NRC cost per plant is given by:

$$\$(6960 + 27,000 + 18,100) = \$52,000$$

Averted Onsite Costs (AOSC)

In addition to the costs associated with the modification, the potential reduction of severe onsite consequences was evaluated. A Handbook for Value-Impact Assessment was used as the reference for this evaluation. The AOSC was calculated using the following equation:

$$V_{op} = NU(F_0 - F_N)$$

where

V_{op}	=	the cost of avoided onsite property damage
N	=	the number of affected facilities (on a per plant basis, N = 1)
U	=	the present value of onsite property damage given a release
F_0	=	the original core damage frequency (base case)
F_N	=	the core damage frequency after implementing an option (assumed to be zero)
F_0-F_N	=	8.8E-5 (from summation of core melt frequencies contained in Table 3)

and

$$U = \frac{C}{m}\left[\frac{e^{-rt_i}}{r^2}\right](1-e^{-r(t_f-t_i)})\,(1-e^{-rm})$$

where

C	=	cleanup, repair, and replacement power costs ($\$1.65\times10^9$, the data associated with scenario 3)
t_f	=	years remaining until end of plant life (10 years)
t_i	=	years before reactor begins operation (0 years)
m	=	period of time over which damage costs are paid out (10 years)
r	=	discount rate (for 10%, r= 0.10).

When uncertainty in the calculation of V_{op} is considered, it is appropriate to calculate a low, best, and high estimate for the value of U. These values can then be multiplied by the change in core damage frequency to yield a low, best, and high value for V_{op}. The cost handbook was used as a guide, and the best, high, and low estimate values for U were determined by:

1. The best estimate was calculated as discussed above.

2. The high estimate was assumed to be three times the best estimate.

3. The low estimate was calculated using data from scenario 2 ($103.5M over 7.5 years).

<u>A Handbook for Value-Impact Assessment</u> states that "the quantity, U, must be interpreted carefully to avoid misunderstandings. It does not represent the expected onsite property damage due to a single accident. Rather, it is the present value of a stream of <u>potential</u> losses extending over the remaining lifetime of the reactor. Thus, it reflects the expected

loss due to a single accident, the possibility that such an accident could occur with some small probability at any time over the remaining reactor life, and the effects of discounting these potential future losses to present value. When the quantity, U, is multiplied by the accident frequency, the result is the expected loss over the reactor life, discounted to present value."

The best, high, and low present onsite property damage costs (including cleanup cost, repair and refurbishment cost, and replacement energy cost) given a release were calculated as:

Low estimate of U = $\$4.6 \times 10^8$ /severe accident event
Best estimate of U = $\$6.6 \times 10^9$ /severe accident event
High estimate of U = $\$2.0 \times 10^{10}$/severe accident event

These values were then applied to the potential change in accident frequency to obtain dollar values for AOSC, as follows:

V_{op}(Low Estimate) = \$40,500[a]
V_{op}(Best Estimate) = \$581,000[a]
V_{op}(High Estimate) = \$1,760,000[a]

3.5 Cost Evaluation Uncertainty

The areas of uncertainty associated with the cost estimating model for this study included the following:

1. Labor rate variations due to plant site location,

---

[a] V_{op} is dependent on the remaining plant lifetime (t_f). These values were obtained using a 10-year t_f. If the remaining plant lifetime increases to 60 years, the best estimate of V_{op} increases to \$922,000. This will not have a significant impact on the cost/benefit results. Therefore, only the 10-year remaining lifetime AOSC value was used.

2. Variability of in-plant work environment conditions,

3. Variations in the cost of replacement power,

4. NRC procedural/administrative/analytical cost,

5. Equipment and material costs variations,

6. The degree of engineering effort required to obtain NRC approval of any proposed modification.

Each proposed option's cost estimate was evaluated to determine the areas of uncertainty. For the cost analysis uncertainty, the following assumptions were made:

1. Labor rate variations due to plant site location are considered when calculating labor costs. In accordance with FORECAST recommendation for labor cost variations, the assumed labor rate variation was as follows: best estimate is 100% of the labor cost, the high cost estimate is 112%, and the low cost estimate is 88%. These variations are applicable to installation and removal labor, health physics labor, NRC labor, and the costs associated with defueling the reactor.

2. Equipment and material costs were obtained from the FORECAST data base (or, in the case of Option 2, from NUREG-2800). The low estimate was assumed to be 75% of the best estimate and the high value was assumed to be 125% of the best estimate.

3. Best estimates for engineering QA-QC costs were obtained using FORECAST. However, due to the large

uncertainty in the degree of the engineering effort required to obtain NRC approval of any proposed modification, the low estimate was assumed to be 50% of the best estimate and the high estimate was assumed to be 150% of the best estimate.

4. Cost estimates for buying replacement power were found from the FORECAST data base. A best estimate of $500,000/day was used, with high and low estimates of $900,000/day and $150,000/day, respectively.

Table 6 shows the mean, the coefficient-of-variation (COV), and the standard deviation of each cost category for the five different proposed modifications. The COV is defined as the standard deviation divided by the mean and is a measure of the possible variation in the cost. For a detailed discussion of uncertainty calculations, see Appendix A.

3.6. Plant Modification Cost Estimate Results

A mean and standard deviation for the total cost of each option was calculated for each modification by using a numerical Taylor series expansion routine. Table 7 lists the cost results for the various modifications. Included in the table are the total cost estimate without AOSC or replacement power, the total cost including AOSC without replacement power, and the total cost with both AOSC and replacement power.

It should be noted that the normal costs are considered to be positive dollars. The AOSC cost is measured in negative dollars, thereby helping to lower the total costs.

Table 6. Cost Analysis Category Parameters.

COST CATEGORY	COV	OPTION[a] 1		OPTION 2		OPTION 3		OPTION 4A		OPTION 4B		OPTION 5	
		Mean ($)	Std.Dev.	Mean ($)	Std.Dev.	Mean ($)	Std.Dev.	Mean ($)	Std.Dev.	Mean ($)	Std.Dev.	Mean ($)	Std.Dev.
Equipment and Materials	25%	200K[b]	50K	52K	13K	1M	250K	n/a	n/a	n/a	n/a	1M	250K
Installation Labor	12%	770K	92K	770K	92K	10M	1.2M	10M	1.2M	770K	92K	10M	1.2M
Removal Labor	12%	n/a	n/a	n/a	n/a	3.4M	408K	3.4M	408K	250K	30K	n/a	n/a
Engineering QA/QC	50%	390K	195K	330K	165K	1.9M	950K	1.8M	900K	410KM	205K	1.5M	750K
Health Physics	12%	150K	18K	150K	18K	3.1M	372K	3.1M	372K	200K	24K	2.5M	300K
Defuel, Drain, and Recover	12%	165K	20K	165K	20K	165K	20K	165K	20K	165K	20K	165K	20K
Replacement Power	c	14M	3.5M	14M	3.5M	70M	18M	70M	18M	14M	3.5M	56M	14M
NRC Cost	12%	52K	6.2K	52K	6.2K	52K	6.2K	52K	6.2K	52K	6.2K	52K	6.2K
AOSC (-$)	c	581K	226K	581K	226K	581K	226K	581K	226K	581K	226K	581K	226K

[a] For a description of the different options refer to Section 3.1.

[b] K = thousand, M = million.

[c] Standard deviation is found by $3\sigma = ([High\ value - Best] + [Best - Low\ value])/2$, where σ = standard deviation.

Table 7. Cost Analysis Results.

COST TYPE	OPTION 1		OPTION 2		OPTION 3		OPTION 4A		OPTION 4B		OPTION 5	
	Mean ($)	Std. Dev.	Mean ($)	Std. Dev.	Mean ($)	Std. Dev.	Mean ($)	Std. Dev.	Mean ($)	Std. Dev.	Mean ($)	Std. Dev.
Total Cost w/o AOSC & w/o RP[a]	1.7M[b]	220K	1.5M	190K	20M	1.6M	19M	1.6M	1.8M	230K	15M	1.5M
Total Cost w/o RP	1.1M	320K	920K	300K	19M	1.6M	18M	1.6M	1.3M	320K	15M	1.5M
Total Cost	15M	3.5M	15M	3.5M	89M	18M	88M	18M	16M	3.5M	71M	14M

[a] RP = replacement power.

[b] M = million.

3.7. Radiation Exposure

The occupational radiation exposure results are presented in Table 8. These doses were calculated based on a 10 mrem/hour radiation field. This dose rate was applied only to those installation or removal labor hours that were estimated to be performed in the radiation area (37.5% of total installation or removal labor hours). Due to the congested nature of the area where the work would be performed, the installation of additional shielding to lower the exposure would not be possible.

Table 8. Total Occupational Radiation Exposure.

Exposure	OPTION 1	OPTION 2	OPTION 3	OPTION 4A	OPTION 4B	OPTION 5
Total labor hours	4,200[a]	4,200[a]	90,000[b]	90,000[b]	5,600[b]	71,000[b]
Labor hours in radiation zone	1,600	1,600	33,000	33,000	21,000	25,000
Total exposure (person rem)	16	16	330	330	21	250

[a] Estimated from Reference 13.

[b] Estimated from FORECAST data base.

The total exposures presented in Table 8 represent the total dose that would be received by the labor force. This total dose would be distributed throughout the work force performing the implementation of an option. The site as-low-as-reasonable-achievable (ALARA) program should ensure that none of the individual workers exceeds the maximum dose rates set by 10 CFR Part 20.

4. COST/BENEFIT ASSESSMENT

4.1. Dollar-to-Person-Rem Averted Ratio

One measure of the benefit achieved by modifying a plant, is the Dollar-to-Person-Rem Averted Ratio (DPR) as described in Reference 11. A value of $1000 per person-rem is generally used by the NRC as an upperbound guideline in deciding whether corrective measures may be appropriate. The DPR is calculated as cost of modification divided by the offsite person-rem averted if the modification is performed, or:

$$DPR = \frac{Modification\ Cost}{Averted\ Offsite\ Dose}$$

NRC policy recommends inclusion of the AOSC in the expression for the DPR. The inclusion of averted onsite costs reduces the cost of the modification, causing the cost benefit ratio to becomes more favorable. The DPR could then be calculated by:

$$DPR = \frac{Modification\ Cost - AOSC}{Averted\ Offsite\ Dose} = \frac{Total\ Costs}{Averted\ Offsite\ Dose}$$

4.2. Cost/Benefit Results

The results of the cost/benefit analysis were calculated using the formulas presented above, the modification costs developed in Section 3, and the offsite doses developed in Section 2. Tables 9 through 14 show the

cost/benefit results for the GSI-15 modifications (options 1-5), including the case where the occupational exposure is included in the calculation. Inclusion of the occupational dose is accomplished by subtracting the occupational exposure from the averted offsite dose, or:

$$DPR = \frac{Total\ Costs}{Averted\ Offsite\ Dose - Occupational\ Dose}$$

For those cases where the occupational exposure exceeds the averted offsite dose, no net benefit (NNB) is reported as the result. This is done because once the benefit becomes zero or less, the cost/benefit ratio indicates that performing the modification will result in a larger occupational dose than what would be expected for the populational dose if the modification is *not* implemented.

Tables 9 through 14 include the best estimates for a 10 year remaining lifespan, 20 year remaining lifespan, 40 year remaining lifespan, and 60 year remaining lifespan (see Appendix A and Appendix C for an example of the uncertainty calculations). The remaining lifespan is the time left to operate the plant *after* the supports have become brittle. The results in the tables are calculated for the three cost categories: without either AOSC or replacement power, with AOSC but without replacement power, and with both AOSC and replacement power. The calculated values are considered to be the "best" value and are presented as the results of the analysis. Graphical results of Tables 9 through 14 are presented in Appendix D. The graphs are given to assist in evaluating the relative cost/benefit magnitudes between the different options and the different cost categories.

Table 9. Cost/Benefit results for Option 1.

Years after embrittlement	Cost/Benefit (without occupational dose) [$/person-rem]			Cost/Benefit (with occupational dose) [$/person-rem]		
	Total w/o AOSC & w/o RP[a]	Total w/o RP	Total	Total w/o AOSC & w/o RP	Total w/o RP	Total
10	59K[b]	38K	520K	130K	86K	1.2M
20	30K	19K	260K	41K	26K	360K
40	15K	9.5K	130K	17K	11K	150K
60	9.8K	6.3K	87K	11K	7.0K	96K

[a] RP = Replacement Power
[b] K = thousand, M = million

Table 10. Cost/Benefit results for Option 2.

Years after embrittlement	Cost/Benefit (without occupational dose) [$/person-rem]			Cost/Benefit (with occupational dose) [$/person-rem]		
	Total w/o AOSC & w/o RP[a]	Total w/o RP	Total	Total w/o AOSC & w/o RP	Total w/o RP	Total
10	52K[b]	32K	520K	120K	72K	1.2M
20	26K	16K	260K	36K	22K	360K
40	13K	8K	130K	15K	9.3K	150K
60	8.7K	5.3K	87K	9.6K	5.9K	96K

[a] RP = Replacement Power
[b] K = thousand, M = million

Table 11. Cost/Benefit results for Option 3.

Years after embrittlement	Cost/Benefit (without occupational dose) [$/person-rem]			Cost/Benefit (with occupational dose) [$/person-rem]		
	Total w/o AOSC & w/o RP[a]	Total w/o RP	Total	Total w/o AOSC & w/o RP	Total w/o RP	Total
10	690K[b]	660K	3.1M	NNB[c]	NNB	NNB
20	350K	330K	1.6M	NNB	NNB	NNB
40	170K	170K	780K	NNB	NNB	NNB
60	120K	110K	520K	NNB	NNB	NNB

[a] RP = Replacement Power [b] K = thousand, M = million
[c] NNB = no net benefit

Table 12. Cost/Benefit results for Option 4A.

Years after embrittlement	Cost/Benefit (without occupational dose) [$/person-rem]			Cost/Benefit (with occupational dose) [$/person-rem]		
	Total w/o AOSC & w/o RP[a]	Total w/o RP	Total	Total w/o AOSC & w/o RP	Total w/o RP	Total
10	660K[b]	630K	3.1M	NNB[c]	NNB	NNB
20	330K	320K	1.6M	NNB	NNB	NNB
40	170K	160K	780K	NNB	NNB	NNB
60	110K	110K	520K	NNB	NNB	NNB

[a] RP = Replacement Power [b] K = thousand, M = million
[c] NNB = no net benefit

Table 13. Cost/Benefit results for Option 4B.

Years after embrittlement	Cost/Benefit (without occupational dose) [$/person-rem]			Cost/Benefit (with occupational dose) [$/person-rem]		
	Total w/o AOSC & w/o RP[a]	Total w/o RP	Total	Total w/o AOSC & w/o RP	Total w/o RP	Total
10	63K[b]	45K	560K	230K	170K	2.1M
20	32K	23K	280K	49K	36K	440K
40	16K	11K	140K	19K	14K	170K
60	11K	7.5K	93K	12K	8.6K	110K

[a] RP = Replacement Power
[b] K = thousand, M = million

Table 14. Cost/Benefit results for Option 5.

Years after embrittlement	Cost/Benefit (without occupational dose)			Cost/Benefit (with occupational dose)		
	Total w/o AOSC & w/o RP[a]	Total w/o RP	Total	Total w/o AOSC & w/o RP	Total w/o RP	Total
10	520K	520K	2.5M	NNB[c]	NNB	NNB
20	260K	260K	1.3M	NNB	NNB	NNB
40	130K	130K	630K	NNB	NNB	NNB
60	87K	87K	420K	NNB	NNB	NNB

[a] RP = Replacement Power
[b] K = thousand, M = million
[c] NNB = no net benefit

5. SUMMARY OF COST/BENEFIT FINDINGS

The cost results (see Table 7) indicate the estimated per plant costs range from a low value of $920,000 for Option 2 (increasing the operating temperature of the supports) to a high value of $89,000,000 for Option 3 (replacing the existing supports). The low value takes into account averted onsite costs and assumes no need to purchase replacement power. The high value also takes into account averted onsite costs, but assumes replacement power would have to be purchased for a 20-week period.

The results of the benefit analysis indicate a per plant offsite dose risk of 2.9 person-rem/year with a calculated core damage frequency of 8.8×10^{-5}/yr. The risk value includes all the risk associated with support failure after embrittlement occurs. It was assumed that the implementation of any of the proposed options would remove 100% of the risk associated with failure of an embrittled support.

The above information provided cost/benefit ratios ranging from $53 per person-rem (Option 2 with AOSC and without replacement power and occupational dose over a 60-year embrittlement period) to $3,100,000 per person-rem (Options 3 with AOSC and replacement power and without occupational dose over a ten year embrittlement period). When the occupational dose is considered, the cost benefit ratios increase. And in those cases where the occupational dose exceeds the averted offsite dose, no net benefit is obtained. Appendix B presents a number of sensitivity studies to show how the results can change given changes in the modeling data. Table B-2 gives four extreme cases of cost/benefit. In the case of minimum cost/maximum benefit, a potential cost/benefit ratio of $53 per person-rem is obtained. This represents the case where the minimum-cost option would correct the problem for a plant located in an area of high populational density (assuming no occupational dose and a 60-year embrittlement period).

DRAFT 2

6. REFERENCES

1. Cheverton, R. D., *et al.*, Impact of Radiation Embrittlement on Integrity of Pressure Vessel Supports for Two PWR Plants, Oak Ridge National Laboratory, NUREG/CR-5320, ORNL/Tm-10966, January 1989.

2. Reactor Safety Study, U.S. NRC, WASH-1400, 1975.

3. Chang, T. Y. and N. R. Anderson, Regulatory Analysis for Resolution of Unresolved Safety Issues A-46, Seismic Qualification of Equipment in Operating Plants, NUREG-1211, February 1987.

4. American Institute of Steel Construction, Manual of Steel Construction, Allowable Stress Design, 9th Ed.

5. NUREG-0800, Standard Review Plan, Section 3.8.3, Concrete and Steel Internal Structures of Steel or Concrete Containments, Rev. 1, U.S. Nuclear Regulatory Commission, July 1981.

6. NUREG/CR-4885, Seismic Characterization of the Eastern United States: Comparative Evaluation of the LLNL and EPRI Studies, U.S. Nuclear Regulatory Commission, May 1987.

7. Bertucio, R. C. and S. R. Brown, Analysis of Core Damage Frequency: Sequoyah, Unit 1, Internal Events, Sandia National Laboratory, NUREG/CR-4550, Revision 1, Volume 5, June 1989.

8. Public Service Electric and Gas Company, Salem Nuclear Generating Station Probabilistic Risk Assessment, EI International, Inc., October 1988.

9. Andrews, W., *et al.*, Guideline for Nuclear Power Plant Safety Issue Prioritization Information Development, Pacific Northwest Laboratory, NUREG/CR-2800, 1983.

10. Heaberlin, S. W., *et al.*, A Handbook for Value-Impact Assessment, Pacific Northwest Laboratory, NUREG/CR-3568, PNL-4646, December 1983.

11. Claiborne, E. *et al.*, Generic Cost Estimates, NUREG/CR-4627, Revision 1, February 1989.

12. Lopez, B. and F. W. Sciacca, "FORECAST", 2.1 User Manual, Science and Engineering Associates, Inc., SEA Report No. 89-461-04-A:1, April 1990.

13. Emrit, R. *et al.*, A Prioritization of Generic Safety Issues, NUREG-0933, Revision 2, December 1989.

[DRAFT] ENCLOSURE 1

REGULATORY ANALYSIS

Resolution of Generic Safety Issue No. 15, "Radiation Effects on Reactor Vessel Supports"

1. Statement of the Problem

Generic Safety Issue 15 (GSI-15) was established to evaluate the concern that low-temperature, low-flux neutron irradiation might embrittle reactor pressure vessel (RPV) supports more rapidly than predicted based on traditional trend bands. The concern arose when it was observed by the Oak Ridge National Laboratory that HFIR (steel) surveillance samples were embrittled considerably faster by radiation than expected (Ref. 1). At the time it was believed that the cavity environments of operating reactors were rather similar to that of the HFIR surveillance capsules; therefore, the potential for excessive embrittlement of RPV supports needed to be considered. The technical problem at the heart of GSI-15 was to determine how, and why, the fracture resistance of RPV supports in operating nuclear power plants will change with time and the degree to which the integrity of the supports may have been compromised.

Originally, prioritization of GSI-15 in November, 1983 resulted in a LOW priority ranking. In June, 1987, after reviewing the HFIR data presented in Ref.2, the ACRS requested the NRC to initiate further study of support steel embrittlement by exposure to low flux radiation at low temperature. GSI-15 was reprioritized, considering the impact of the new ORNL information on operating reactors (as interpreted in 1987), resulting in a HIGH ranking.

Experience has shown that the nil-ductility-transition should be well below the lowest operating temperature, or commonly observed flaws could serve as brittle fracture initiators. Traditionally, the NDT shift (increase) has served as an indicator of neutron radiation damage, displayed as a function of fast (energy > 1 MeV) neutron fluence. This method has been satisfactory for the RPV and reactor internals but it does not account for all of the low energy (< 1 MeV) neutron damage. Neutron-atom interactions will occur: an

Enc. 3

atom will absorb a neutron; atomic recoil on subsequent transmutation will result in damaging displacements. The environment in which RPV supports operate includes radiation by a neutron spectrum with an abundance of low-energy neutrons and a relatively low temperature, below about 150°F. At that temperature, the atomic diffusivity in steel is several orders of magnitude lower than in a vessel operating at about 550°F so the tenacity of the damage is comparably larger. Individual low-energy neutrons do not create much atomic damage but in abundance their resulting damage may be cumulatively significant. The net result is that different neutron spectra may induce different amounts of embrittlement for a given fluence.

Greater accuracy in neutron damage predictions can result by using displacements per atom (dpa); i.e., the calculated number of atomic displacements (vacancy-interstitial pairs) per atom resulting from irradiation. However, the dpa parameter only accounts for elastic collisions. Because some displaced atoms will recombine with vacancies, some of the point-defect damage is effectively annealed. To account for the presence of low energy neutrons and the resulting variety of atomic-level damage mechanisms, a modified dpa parameter (dpa mod.) was developed (Ref. 3). Before the staff could take steps to assess the intrinsic value of *dpa mod*, additional HFIR dosimetry experiments, designed in support of the GSI-15 Task Action Plan (TAP), Ref.4, resulted in high measured gamma radiation doses (Ref. 5). Analysis of the new experimental evidence led to a reassessment of the HFIR surveillance data and their relevance to RPV supports. First, the additional embrittlement beyond that predicted on the basis of neutron fluence can be accounted for by including the γ radiation in dpa calculations. Second, the finding that the HFIR γ flux is about 3,000 times greater than the peak γ measurement at the beltline in the cavity of an operating power reactor showed that the two environments were significantly different and that the HFIR surveillance data do not represent RPV support embrittlement.

2. Value/Impact Analysis

The GSI-15 cost-benefit analysis consisted of three steps. First, estimates were made of core damage frequency and risk associated with RPV support failures; second, detailed cost estimates were made of five alternative

corrective measures; third, cost/benefit (C/B) ratios were calculated for each of the five corrective measures. A detailed report of the (C/B) analysis can be found in Ref. 6.

Among the several scenarios used in past nuclear plant PRAs, two were judged to be potentially capable of failing the supports. The initiating event for the first scenario was a safe shutdown earthquake (SSE) and for the second scenario was a small break loss of coolant accident (SBLOCA). Benefit was defined as reduction in risk from implementing corrective action. Risk was estimated for the two (different) scenarios. The subsequent event in both was failure of the RPV supports. Typical event tree methodology was used to generate event trees. Initiating event frequencies were adjusted to fit the scenario of brittle failure of supports. In the SSE event tree, the earthquake probability was reduced to correspond to the peak ground acceleration and RPV support stress level at which brittle fracture could be expected to occur. In the SBLOCA event tree, the frequency used was taken from the Sequoyah 1 PRA, reduced by a factor of 2 under the assumption that not all break locations would produce significant loads on the RPV supports. Given the initiating event, it was assumed that the support failure probability would be 0.5. The event trees were quantified and the event sequences which led to core damage were grouped into one of seven different categories. Each sequence was assigned to the offsite release category which best modeled its outcome. The offsite release categories were taken from Ref. 7 in which various degrees of release from the reactor containment were classified. The best estimate base case considered in the analysis led to a total calculated contribution to core damage frequency from RPV support failure of 8.8×10^{-5}. The staff recognizes that the source terms in WASH-1400 (Ref. 7) are considered rather conservative. However, had newer information been used instead it would have served only to bolster our decision.

Five alternative corrective measures (options) were identified from the Contractor's engineering expertise, each of which would be capable of precluding RPV support failure in the event of an SSE or SBLOCA. They were:

1. shielding the RPV supports from neutron radiation;
2. increasing the RPVS operating temperature above the NDT temperature;
3. replacing the RPV supports;
4. heating the RPVSs sufficiently to anneal out any embrittlement;
5. strengthening or adding additional RPVS.

Discussions of the alternative actions can be found in Ref. 6.

Cost estimates were made for the five options with guidence from NUREG/CR-3568, NUREG CR-4627 (Rev. 2), and the computer code FORECAST 2.1 which incorporates cost evaluation information. Cost estimations included evaluation of each proposed option, identifying necessary equipment and materials, and assessing the work area in which the proposed modification would be made. Estimated costs varied widely from a maximum cost per plant of $89,000,000 (option 3, replacing existing supports), to a minimum of $920,000 (option 2, increasing the operating temperature of the supports).

C/B ratios were calculated using dollar-to-person-rem-averted ratios (DPR), which were calculated as modification costs divided by the offsite person-rem averted by implementation of a modification. In calculating costs, averted onsite costs (AOSC) were subtracted from modification costs. Occupational exposure, when considered, was subtracted from the averted offsite dose. When occupational exposure from implementation exceeded averted offsite dose, there was no net benefit. C/B ratios were calculated for 10, 20, 40, and 60 year remaining life spans (i.e., the remaining operational time left for the plant after embrittlement of the supports). C/B ratios were calculated for three cost categories: (1) without either AOSC or replacement power; (2) with AOSC but without replacement power; and (3) with both AOSC and replacement power.

The benefit analysis resulted in an offsite dose risk per plant of 2.9 person-rem/year with a calculated core damage frequency of 8.8×10^{-5}/yr. The risk value included all risks associated with support failure following embrittlement. Each of the proposed options was assumed capable of removing 100% of the risk from a support failure so that the risk from support failure following modification was assumed to be zero.

Sensitivity studies were conducted considering 10, 20, 40, and 60 years of operation with embrittled supports. C/B ratios were calculated both with and without consideration of occupational doses. Supplemental cases involving more conservative estimates of failure probability were evaluated for purposes of judging the sensitivity of the risk calculation results to the event tree input probabilities. Seven cases were evaluated:

Case 1 Increase the SSE frequency by a factor of ten; for most plants, this is equivalent to a 0.5g (earthquake) peak ground acceleration and may result in RPV support failure.

Case 2 Increase offsite dose rates by a factor of 100 to simulate a plant at a high population density site.

Case 3 Increase the probabilities of reactor pressure vessel support failure and LBLOCA to 1 to expose the maximum uncertainty in the RPVS failure mechanisms.

Case 4 Increase the failure probabilities of the RPV supports and the reactor protection system to 1 and decrease the LBLOCA probability to 0.

Case 5 Increase the failure probabilities of ECCS and CSDS to 1 to simulate failure of these safety systems.

Case 6 Increase the LBLOCA occurrence and ECCS failure probabilities to 1, simulating sufficient pressure vessel displacement (from RPV support failure) to rupture the ECCS injection lines or render them inoperable.

Case 7 Set the failure probabilities of the RPV supports, RPS, CSDS, ECCS and the LBLOCA occurrence to 1 as a worst case scenario wherein the RPV supports and reactor coolant piping are embrittled leading to complete failure of the entire reactor protection system (with the exception of the containment). Following the initiating event, RPV shifting results in failure of all core protection systems.

The sensitivity analysis results were tabulated in Ref. 6. for each of the above cases on a per year basis as well as for ten, twenty, forty and sixty years. Core melt frequencies per year were obtained by modifying the appropriate events in the sequence event trees for the two initiating events: SSE and SBLOCA. A "Base Case" set of results was for the original analysis without modification by the sensitivity analysis parameters. For other cases, the risk per year in person-rem was obtained by multiplying the

probabilities for each sequence (PWR 7, PWR 3, and PWR 1) by the corresponding Consequence Factors taken from NUREG/CR-2800. The risks for 10, 20, 40, and 60 years were the product of risk per year times the given number of years. The sensitivity analysis provided extreme values of the C/B ratio.

The minimum benefit was obtained from Case 4 with a risk reduction of 27 person-rem for a period of ten years. The maximum benefit was obtained from Case 2, with 17,400 person-rem for a period of 60 years. Costs varied from a minimum of $920,000 to a maximum of $89M. Those minima and maxima in costs and benefits yielded four extremes of the C/B ratio. They were:

$\frac{\text{max cost}}{\text{min benefit}}$ = $3,300,000/person-rem	$\frac{\text{max cost}}{\text{max benefit}}$ = $5,115/person-rem
$\frac{\text{min cost}}{\text{min benefit}}$ = $34,074/person-rem	$\frac{\text{min cost}}{\text{max benefit}}$ = $53/person-rem

The most significant, of course, were the max/min and min/max ratios which resulted in 3,300,000 and 53 dollars per person-rem, respectively. The calculations revealed the following. First, the uncertainty in the GSI-15 C/B analysis was very large. Second, the combination of highest cost and least benefit would make the implementation of mitigating action <u>not</u> cost effective (much greater than $1000/person-rem). Third, implementation for a lowest cost-to-greatest benefit ratio case <u>would</u> make mitigating action cost-effective. Additional C/B ratios for the full range of parameters considered were reported in Tables 9 to 14, inclusive, Ref. 6.

The C/B analysis results exhibited such wide variability that the staff found them inconclusive and could not use them to support a regulatory requirement for GSI-15. Historically, the NRC has taken the nominal value of 1,000 dollars per person-rem as a support level to justify taking regulatory action. Although the lowest C/B ratio (53 $/person-rem) was well within the target, it was clear from the sensitivity study results that the bias in the C/B ratio was far above the level justifying actions to mitigate against accident exacerbation. Moreover, the estimated Base Case reduction in core damage

frequency of 8.8×10^{-5} per reactor year (Ref. 6), although sufficient to warrant further evaluation, was not large enough to serve as justification for taking regulatory action. "Further evaluation" meant turning to the C/B ratio, thus it was clear that value/impact considerations did not support regulatory requirements. The staff concluded that the licensees could decide if the integrity of the RPV supports was suspect and, for the few plants in which there might be such a question, reevaluation could follow the technical findings from the proposed resolution of GSI-15.

3. Elements of the Proposed Resolution

The elements of the proposed resolution of GSI-15 include the following.

1. Close out GSI-15 based on experimental evidence indicating that the HFIR surveillance data do not apply to operating plant RPV supports.
2. Issue documents to publish the technical findings obtained in the course of work on GSI-15.
3. Issue an NRC Information Notice to inform licensees of the resolution of GSI-15 and the bases for it.

NUREG-XXXX, to be published, describes the findings from the work done under the program set forth in the GSI-15 TAP (Ref. 4), including details of an engineering approach and criteria for RPV support evaluation. At the outset of GSI-15 it was expected that such work would be required; thus, screening and evaluation criteria were developed to ensure the uniformity and acceptability of the evaluations. The ACRS will be given the option of reviewing the proposed resolution of GSI-15. The CRGR may not have to review the resolution because no new or revised requirements will be imposed. Assuming favorable responses from those organizations, the NRC Office of Nuclear Regulatory Research would issue the documents setting forth the proposed resolution. The Office of Nuclear Reactor Regulation will issue an information notice to all licensees to inform them of the resolution of GSI-15 and the bases for it. With the issuance of the above documents, GSI-15 activities will be complete since there will be no required implementation.

4. Summary and Conclusions

Based on the evidence at hand, it has been concluded that:

1. the γ flux at the HFIR surveillance specimen capsules was about the same as that at an operating RPV inner surface but was several factors of 10 greater than the (HFIR) companion neutron flux;
2. the fast neutron flux at the HFIR surveillance specimen capsules was very low having been moderated by the foot or two of intervening water;
3. consequently, a long time (about 20 years) was required to accumulate a significant fluence of neutrons with energies greater than 1 MeV;
4. because the surveillance specimen temperature was kept low (< 200°F), the atomic-level damage inflicted on the steel specimens by low energy neutrons and γ radiation was retained and added to the elastic collision spikes expected from neutrons of E > 1 MeV;
5. as a result, the shift in the ductile-to-brittle fracture mode transition temperature as measured with Charpy impact specimens was significantly greater than expected from test reactor experiments at the same fluence;
6. the γ flux in HFIR was much greater (by about 3000 times) than the γ flux measured in the cavity of an operating reactor;
7. therefore, additional embrittlement from γ radiation observed in the HFIR surveillance specimens should not occur in RPV supports, in which the effect of radiation should be predictable based on relevant dpa values (calculated from the cavity neutron flux and energy spectrum, and operating time);
8. cost/benefit ratios from an analysis of the GSI-15 issue were inconclusive because of the wide-ranging variability of the results, although only the most favorable set of conditions would justify taking any regulatory action;
9. although the processes of degradation affecting the RPV supports and the components that can be associated with the integrity (or lack thereof) of the supports will continue, the resolution proposed for GSI-15 remains unchanged for plants which may operate for 60 years.

The staff proposes that GSI-15 be resolved by taking the following two actions: (1) an internal close-out memorandum should be issued based on the above conclusions; (2) a NUREG should be issued to present the GSI-15

findings. Upon approval of the proposed resolution, an information notice should be issued to all holders of licenses and construction permits to present the technical basis for resolution of GSI-15 and to note that addressees may choose to avail themselves of the information in the notice and take action as deemed appropriate.

Some licensees may find it appropriate to reevaluate the RPV supports, verifying that the strength and fracture resistance are adequate for all anticipated transients and accident loadings. The idea of reevaluation is supported by findings made during the course of GSI-15 that the initial (as-built) transition temperature of some steels used in RPV support construction may have been so high as to leave essentially no margin for increase by neutron radiation. It would be prudent to ensure that the RPV supports have adequate fracture resistance, especially for those plants contemplating future license renewal.

5. Alternatives

The following alternatives for the resolution of GSI-15 were considered by the staff.

a. Close-out the issue with an internal memorandum but take no other action.

b. Issue a generic letter (GL) requesting reevaluation of RPV supports in accord with the provided recommended methodology.

c. Terminate GSI-15 as an issue resolved on a technical basis but open a new Generic Issue under either compliance or back-fit requirements.

d. Close GSI-15 and issue an information notice to inform licensees of the resolution of GSI-15 and the bases for it.

6. Evaluation of Alternatives and Decision Rationale

a. Assessments of Alternatives

Alternative 4.a, issue a close-out memorandum but take no other action, was rejected because the technical findings achieved by the work on GSI-15 are important enough that they should be called to the attention of the nuclear

industry. Moreover, as discussed more fully below in the Alternative 4.c analysis, the safety aspects of the issue may have to be addressed in the future within the Plant Life Extension Program.

Alternative 4.b, to request reevaluation of RPV supports by issuing a GL, was rejected as not cost-effective. The basis for that decision was the detailed C/B analysis (Ref. 6), previously discussed. Although a requirement to reevaluate RPV supports and take indicated corrective actions could be justified at one extreme value of the range of C/B ratios reported, the basic problem with such a position is that information available to the staff was insufficient to categorize the 110 operating nuclear power plants into those that are and are not potentially vulnerable to RPV support failure. Such information would be disclosed in licensees' responses to the GL. However, the bias in the cost-benefit uncertainty generally was in the non-beneficial range and by removing the concern derived from the HFIR surveillance data, a GL requiring licensee action could not be justified.

Alternative 4.c, resolve and terminate GSI-15 but open a new Generic Issue, also was rejected because the same C/B figures cited in the Alternative 4.b analysis apply to this case and would not support action to go forward with a new Generic Issue dealing with the basic question of integrity. However, arguments favoring the alternative should be noted. The findings accumulated during the work on GSI-15 led to the concern that the integrity of RPV supports could be called into question even in the absence of radiation effects. That was based on the fact that some of the construction steels could exhibit initial (as-built) transition temperatures high enough to be of concern (Ref. 8). Also, there are other potential problems of material deterioration in associated components which may further exacerbate the effects of an accident should the RPV supports fail. Specific problems include: aging embrittlement of stainless steel primary coolant loop piping (especially centrifugally cast pipes); degradation of large hydraulic snubbers in the RCL supports (refer to the resolution of GI-113 where backfitting for improved snubber reliability was not cost-beneficial); relatively low toughness (fracture resistance) in steam generator (SG) and main coolant pump supports in PWRs (Ref. 9), also dismissed because back-fitting was not cost-

effective; and service-induced flaws in SG tubing which might fail if accident loads were increased as a result of RPV support failure. Cumulatively, these findings provided an argument in favor of the alternative. Therefore, it is prudent to ensure that the RPV supports exhibit adequate fracture resistance, both for the current licensing period and for those plants contemplating future license renewal. However, the finding that the HFIR surveillance data were unique to that reactor and not relevant to operating plants eliminated a major concern regarding RPV support integrity leaving insufficient support for Alternative 4.c.

The staff recommends Alternative 4.d. The approach includes issuing an information notice (IN) to all licensees requiring no action on their part. The reasons for selecting Alternative 4.d are given in the following.

b. Basis for Selection of Alternative 4.d

The proposed resolution of GSI-15 is contained in a close-out memorandum and NUREG-XXXX, to be published. Alternative 4.d includes the issuance of an IN to inform licensees of the resolution of GSI-15 and the technical bases for it. The IN would be accompanied by NUREG-XXXX which sets forth the technical findings resulting from work on GSI-15, including a detailed reevaluation procedure.

The concern for safety embodied in GSI-15 rested in large measure on the excessive radiation embrittlement observed by the Oak Ridge National Laboratory in HFIR surveillance samples (Ref. 1) and the presumed similarity in environment between the cavity at an operating reactor and the ID wall at the HFIR vessel. The technical problem addressed by the GSI-15 TAP (Ref. 4) was to determine the influence of initial construction and service environment (primarily radiation effects) on the fracture resistance of RPV supports in operating nuclear power plants. In the early stages of the work on GSI-15 it became evident from some of the technical findings that not all plants will be equally vulnerable because of the great variety of RPV support designs and fuel loadings. Later work by ORNL in support of GSI-15 included experiments designed to provide details on the HFIR radiation environment. They showed that the gamma flux was several orders of magnitude higher than the neutron

flux (Ref. 5). That led to a reassessment of the HFIR surveillance data and their relevance to RPV supports. First, the excess NDT shift beyond that predicted on the basis of neutron fluence can be accounted for by including the γ radiation in dpa calculations. Second, noting that the HFIR γ flux is about 3,000 times greater than the peak value measured in the cavity of an operating power reactor, the HFIR environment was significantly different from the radiation at RPV supports. Thus the HFIR surveillance data are not relevant and a major factor in the concern for RPV support integrity has been eliminated. The staff concludes that the effect of radiation on RPV supports should be predictable from trend curves of NDT shift as a function of dpa.

In view of the conclusion derived from the GSI-15 findings regarding the decreased relevance of the HFIR data and lessened safety importance of the issue, an information notice should be issued to all holders of licenses and construction permits to inform them of the technical findings and resolution of GSI-15. It may be appropriate for some to reevaluate their RPV supports and verify that the strength and fracture resistance are adequate for all anticipated transients and accident loadings but the information in Ref. 6 showed that it would not be cost-effective to make the reevaluation of RPV supports and follow-up corrective action a regulatory requirement. The appropriateness stems from findings made during the course of GSI-15 that the as-built transition temperature of some steels used to construct RPV supports may have been so high as to leave essentially no margin for increase by neutron radiation. It would be prudent to ensure that there is adequate fracture resistance in the RPV supports, especially if license renewal is being contemplated. An engineering approach to RPV support reevaluation was given in Ref. 8 including steps for screening, using criteria provided, and on the basis of the calculated radiation exposure and the peak tensile stress, determining the potential for brittle failure of the supports. Given a possibility of failure, there are several options (such as those in Ref. 8) for demonstrating that the plant can operate without undue risk to the public.

c. Costs and Benefits

Because the proposed resolution of GSI-15 does not include any new or revised regulatory requirements, there will be no cost to the industry. The RPV

support reevaluation procedure set forth in Ref. 8 would be followed on a voluntary basis and any related costs would be in the category of ordinary preventive maintenance. With no requirements to oversee, there will be no implementation costs to the NRC. Likewise, there can be no claim for benefits from this Generic Issue since nothing will be required by way of increased safety.

d. Decision Rationale

The C/B analysis results (Ref. 6) exhibited such wide variability that the staff found them inconclusive and could not use them to support a regulatory requirement for GSI-15. Although the lowest C/B ratio (53 dollars per person-rem) was far below the cost-effective cut-off of 1,000 dollars per person-rem, the staff had no assurance that that ratio would apply to any operating plant. Also, the estimated reduction in core damage frequency of 8.8×10^{-5} per reactor year was just a bit too small to be considered "substantial" (Ref. 10). Since the dosimetry experiments virtually eliminated the potential for radiation embrittlement, the staff had no basis for requiring consideration of action(s) to mitigate against accident exacerbation. The one factor that remains as a threat to RPV support integrity is an initial construction NDT so high (or fracture toughness so low) that even a modest amount of radiation embrittlement could jeopardize the structural integrity. Evaluation of such a possibility is best left to the licensee.

Another consideration in support of the idea that licensees may want to reassess their RPV supports is the potential for degradation in other components which would have to carry much higher loads than their design basis in the event of RPV support failure. The other critical components are: (1) primary coolant piping; (2) large snubbers supporting primary coolant lines; (3) steam generator and primary coolant pump supports (in PWRs); and (4) PWR steam generator tubing. The modes of degradation differ in each of the above four categories but each, in its own way, may be vulnerable to failure in a severe accident. These considerations also support reevaluation of the RPV supports by licensees to ensure adequate resistance to accident loads and to avoid conditions wherein failure of RPV supports would result in challenges to any of the related components.

The staff concludes that GSI-15 should be resolved by issuing an information notice and a NUREG to provide technical findings and guidance, as proposed in Alternative 4.d.

References

1. ORNL/TM-10444, "Evaluation of HFIR Pressure Vessel Integrity Considering Radiation Embrittlement," Oak Ridge National Laboratory, 1988.

2. R. D. Cheverton, et al., "Impact of Radiation Embrittlement on Integrity of Pressure Vessel Supports for Two PWR Plants," NUREG/CR-5320, Oak Ridge National Laboratory, January, 1989.

3. Craig A. Hrabal "Modified Damage Parameters Applied to a Typical Light Water Reactor's Pressure Vessel Supports," Presented at the 7th ASTM-Euratom Symposium on Reactor Dosimetry, Strasbourg, France, August 27-31, 1990. To be published.

4. Warren Minners, "Transmittal of Approved Task Action Plan (TAP), Revision 2, for Generic Safety Issue 15, 'Radiation Effects on Reactor Vessel Supports,'" Memorandum to Eric S. Beckjord, March 5, 1993.

5. I. Remec and F. B. Kam, "Neutron Spectra at Different High Flux Isotope Reactor (HFIR) Pressure Vessel Surveillance Locations," NUREG/CR-6117, Oak Ridge National Laboratory, December, 1993.

6. R. E. Gregg, C. L. Smith, R. W. Garner, "Cost/Benefit Analysis of GSI-15: Radiation Effects on Nuclear Vessel Supports," EG&G-SSRE-9458, EG&G Idaho, Inc., June 1991, Appendix A in NUREG-XXXX.

7. WASH-1400, "Reactor Safety Study," U. S. Nuclear Regulatory Commission, Washington, D. C., 1975.

8. R. E. Johnson and R. E. Lipinski, NUREG-xxxx, to be published.

9. NUREG-0577, "Potential for Low Fracture Toughness and Lamellar Tearing in PWR Steam Generator and Reactor Coolant Pump Supports," U. S. Nuclear Regulatory Commission, Washington. D.C., October, 1983.

10. NUREG/BR-0058, "Regulatory Analysis Guidelines of the U. S. Nuclear Regulatory Commission" [Draft Report for Comment], U. S. Nuclear Regulatory Commission, Washington, D. C., August, 1993.

UNITED STATES
NUCLEAR REGULATORY COMMISSION
OFFICE OF NUCLEAR REACTOR REGULATION
WASHINGTON, D.C. 20555

April XX, 1994

NRC INFORMATION NOTICE 94-XX: GENERIC SAFETY ISSUE 15 RESOLUTION - RADIATION EFFECTS ON REACTOR VESSEL SUPPORTS

Addressees

All holders of operating licenses or construction permits for nuclear power reactors.

Purpose

The U. S. Nuclear Regulatory Commission (NRC) is issuing this information notice to advise addressees that Generic Safety Issue No. 15 (GSI-15) has been resolved technically and a NUREG was prepared for the purpose of publishing the technical findings which were the bases for the resolution. Licensees may wish to avail themselves of the information transmitted by this information notice regarding assessment of reactor pressure vessel (RPV) support structures and take any action they deem appropriate. However, suggestions contained in this information notice are not NRC requirements; therefore, no specific action or written response is required.

Description of Circumstances

GSI-15 was established to evaluate a concern that low-temperature, low-flux neutron irradiation might embrittle reactor pressure vessel (RPV) supports more rapidly than predicted based on traditional trend bands. The concern arose after it was observed by the Oak Ridge National Laboratory (ORNL) that steel surveillance samples in the High Flux Isotope Reactor (HFIR) were embrittled by irradiation considerably faster than expected. The NRC staff, believing the environment in the cavity of operating reactors was similar to that in the HFIR, concluded that the potential for excessive embrittlement of RPV supports should be considered. The technical problem at the heart of GSI-15 was to determine the influence of initial construction and service conditions on the fracture resistance of RPV supports in operating nuclear power plants, and the degree to which the structural integrity of the supports might be compromised.

Experience has shown that the nil-ductility-transition (NDT) should be well below the lowest operating temperature or commonly observed flaws could serve as brittle fracture initiators. Traditionally, the NDT shift (increase) has served as an indicator of neutron radiation damage, displayed as a function of fast (energy > 1 MeV) neutron fluence. This method has been satisfactory for the RPV and reactor internals but it does not account for all of the low energy (< 1 MeV) neutron damage. Neutron-atom interactions will occur: an atom will absorb a neutron; atomic recoil on subsequent transmutation will result in damaging displacements. The environment in which RPV supports

Enc. 4

operate includes radiation by a neutron spectrum with an abundance of low-energy neutrons and a relatively low (< 150°F) temperature. At that temperature, the atomic diffusivity in steel is several orders of magnitude lower than in a vessel operating at about 550°F so the damage is retained much longer. Individual low-energy neutrons do not create much atomic damage but in abundance their resulting damage may be cumulatively significant. The net result is that different neutron spectra may induce different amounts of embrittlement for a given fluence.

More accurate neutron damage predictions can be made by using the exposure parameter displacements per atom (dpa). However, dpa only accounts for elastic collisions and some of the point-defect damage will be effectively annealed through recombination of displaced atoms with vacancies. Such events and the effect of low energy neutrons can be accounted for by using a modified dpa parameter (dpa mod), developed in the course of work on GSI-15. More importantly, experiments done in support of the issue provided measured gamma radiation doses in HFIR which led to a reassessment of the HFIR surveillance data and their relevance to RPV supports. First, the additional embrittlement beyond that predicted on the basis of neutron fluence can be accounted for by including the γ radiation in dpa calculations. Second, the finding that the HFIR γ flux is about 3,000 times greater than that in the cavity of an operating power reactor showed that the two environments were significantly different; thus, the surveillance data were not representative.

Discussion

GSI-15 has been resolved and the following actions taken. This information notice is being sent to all holders of operating licenses or construction permits. NUREG-XXXX was prepared and placed in the NRC Public Document Room to present the findings from the work done in the program described in the GSI-15 Task Action Plan. This notice announces that NUREG-XXXX and some of the documents referenced therein constituted the basis for resolution of GSI-15. Licensees may wish to avail themselves of the information in this notice and take action as they deem appropriate.

Reevaluation of RPV supports may be appropriate for some licensees since findings made during the course of GSI-15 indicated that some steels used in the construction of RPV supports may have had initial (as-built) transition temperatures high enough to leave essentially no margin for increase by neutron radiation. Reevaluation could verify that the RPV supports have adequate fracture resistance, especially for those plants contemplating future license renewal. One acceptable reevaluation approach could be based on the screening process and criteria detailed in NUREG-XXXX. From accurate calculated radiation exposures and peak tensile stresses, analysts can determine the potential for brittle failure in supports. Given a possibility of failure, several options for demonstrating that the plant can operate without undue risk to the public were noted in NUREG-XXXX. Among the technical findings noted during work on GSI-15 was the fact that plants will not be equally vulnerable because of the great variety of RPV support designs and fuel mnagement procedures.

This information notice requires no specific action or written response. If you have any questions about the information in this notice, please contact one of the technical contacts listed below or the appropriate Office of Nuclear Reactor Regulation (NRR) project manager.

Brian K. Grimes, Director
Division of Operating Reactor Support
Office of Nuclear Reactor Regulation

Technical contacts: Keith R. Wichman, NRR
(301) 504-2757

Barry J. Elliot, NRR
(301) 504-2709

Richard E. Johnson, RES
(301) 415-6758

Attachment:
List of Recently Issued NRC Information Notices

NUREG/CR-6117
ORNL/TM-12484

Neutron Spectra at Different High Flux Isotope Reactor (HFIR) Pressure Vessel Surveillance Locations

Prepared by
I. Remec, F. B. Kam

Oak Ridge National Laboratory

Prepared for
U.S. Nuclear Regulatory Commission

9401140025 137pp.

NUREG/CR-6117
ORNL/TM-12484
RF, R5, 9L

Neutron Spectra at Different High Flux Isotope Reactor (HFIR) Pressure Vessel Surveillance Locations

Manuscript Completed: November 1993
Date Published: December 1993

Prepared by
I. Remec,* F. B. Kam

Oak Ridge National Laboratory
Managed by Martin Marietta Energy Systems, Inc.

Oak Ridge National Laboratory
Oak Ridge, TN 37831-6285

Prepared for
Division of Safety Issue Resolution
Office of Nuclear Regulatory Research
U.S. Nuclear Regulatory Commission
Washington, DC 20555-0001
NRC FIN L2552
Under Contract No. DE-AC05-84OR21400

*Josef Sefan Institute, Ljubljana, Slovenia

ABSTRACT

This project addresses the potential problem of radiation embrittlement of reactor pressure vessel (RPV) supports. Surveillance specimens irradiated at the High Flux Isotope Reactor (HFIR) at relatively low neutron flux levels (about 1.5E+8 $cm^{-2}. s^{-1}$) and low temperature (about 50°C) showed embrittlement more rapidly than expected[1]. Commercial power reactors have similar flux levels and temperatures at the vessel support structures. The purposes of this work are to provide the neutron fluence spectra data that are needed to evaluate previously measured mechanical property changes in the HFIR, to explain the discrepancies in neutron flux levels between the nickel dosimeters and two other dosimeters, neptunium and beryllium, and to address any questions or peculiarities of the HFIR reactor environment.

The current work consists of neutron and gamma transport calculations, dosimetry measurements, and least-squares logarithmic adjustment to obtain the best estimates for the neutron spectra and the related neutron exposure parameters. The results indicate that the fission rates in neptunium-237 (Np-237) and uranium-238 (U-238) and the helium production rates in beryllium-9 (Be-9) are dominated by photo-induced reactions. The displacements per atom rate for iron (dpa/s) from gamma rays is five times higher than the dpa/s from neutrons. The neutron fluxes in key 7, position 5 do not show any significant gradient in the surveillance capsule, but key 4 and key 2 showed differences in magnitude as well as in the shape of the spectrum. The stainless steel monitor in the V-notch of the Charpy specimens of the surveillance capsules is adequate to determine the neutron flux above 1.0 MeV at the desired V-notch location. Simultaneous adjustment of neutron and gamma fluxes with the measurements has been demonstrated and should avoid future problems with photo-induced reactions.

CONTENTS

	Page
ABSTRACT	iii
LIST OF FIGURES	vii
LIST OF TABLES	viii
EXECUTIVE SUMMARY	ix
ACKNOWLEDGMENTS	xi
ABBREVIATIONS	xiii
1. INTRODUCTION	1
2. EXPERIMENTAL PROGRAM	2
2.1 Experimental Locations	2
2.2 Dosimetry Capsules	2
2.3 Radiometric Measurements	2
3. METHODOLOGY	4
3.1 Background	4
3.2 Gamma-Induced Reactions	6
3.3 Photon-Induced Reaction-Rate Correction Factor	10
3.4 Adjustment Options	12
3.5 Adjustment Procedure	12
4. RESULTS AND DISCUSSION	16
5. CONCLUSIONS AND RECOMMENDATIONS	28
6. REFERENCES	29
APPENDIX A. LETTER REPORT ON NIST SUPPORT	31
APPENDIX B. HELIUM ANALYSES OF BERYLLIUM HAFMs FROM HFIR: DOS-2/3	41
APPENDIX C. RESULTS FOR SOLID STATE TRACK RECORDERS	49
APPENDIX D. NEUTRON TRANSPORT CALCULATIONS FOR HFIR	69
APPENDIX E. RESULTS FOR KEY 7, POSITION 5	77
APPENDIX F. RESULTS FOR KEY 2, POSITION 9	87

CONTENTS
(continued)

APPENDIX G. RESULTS FOR KEY 4, POSITION 2 97

APPENDIX H. RESULTS FOR KEY 4, POSITION 10 107

APPENDIX I. SCHEMATIC OF DOSIMETRY CAPSULE WITH SLOT LOCATIONS 117

LIST OF FIGURES

Page

1. Horizontal cross section through the HFIR at the core midplane, showing locations of the surveillance keys and the DOS 1 experiment 3
2. Calculated (1D) distribution of Np(n,f) and Np(gamma,f) reaction rates 7
3. Calculated (1D) distribution of fast (E > 1 MeV) neutron flux 8
4. Calculated (1D) distribution of absorbed gamma dose rate in Si 9
5. Calculated and adjusted neutron spectrum, key 7, position 5, J 23
6. Calculated and adjusted neutron spectrum, key 2, position 9, J 24
7. Calculated and adjusted neutron spectrum, key 4, position 2, J 25
8. Calculated and adjusted neutron spectrum, key 4, position 10, J 26

E.1 Calculated and adjusted neutron spectrum, key 7, position 5, D 85

E.2 Calculated and adjusted neutron spectrum, key 7, position 5, A 86

F.1 Calculated and adjusted neutron spectrum, Key 2, position 9, D 94

F.2 Calculated and adjusted neutron spectrum, key 2, position 9, A 95

G.1 Calculated and adjusted neutron spectrum, key 4, position 2, D 104

G.2 Calculated and adjusted neutron spectrum, key 4, position 2, A 105

H.1 Calculated and adjusted neutron spectrum, key 4, position 10, D 114

H.2 Calculated and adjusted neutron spectrum, key 4, position 10, A 115

I.1 Schematic of dosimetry capsule with slot locations 119

LIST OF TABLES

		Page
1.	Comparison of measured and calculated reaction rates for fission and Be monitors	5
2.	Comparison of measured and corrected reaction rates of fission and Be monitors with calculations	11
3.	Comparison of different adjustment runs, key 7, position 5	17
4.	Comparison of simultaneous neutron and gamma adjustment to neutron adjustment run, key 7, position 5	19
5.	Irradiation parameters at the centers of capsules	21
6.	Adjusted neutron fluxes at the centers of the examined capsules	22
E.1	Calculated and adjusted irradiation parameters, key 7, position 5	80
E.2	Measured reaction rates, C/M, and A/M ratios, key 7, position 5	82
E.3	Calculated and adjusted neutron group fluxes, key 7, position 5, slot J	84
F.1	Calculated and adjusted irradiation parameters, key 2, position 9	89
F.2	Measured reaction rates, C/M, and A/M ratios, key 2, position 9	91
F.3	Calculated and adjusted neutron group fluxes, key 2, position 9	93
G.1	Calculated and adjusted irradiation parameters, key 4, position 2	99
G.2	Measured reaction rates, C/M, and A/M ratios, key 4, position 2	101
G.3	Calculated and adjusted neutron group fluxes, key 4, position 2, slot J	103
H.1	Calculated and adjusted irradiation parameters, key 4, position 10	109
H.2	Measured reaction rates, C/M, and A/M ratios, key 4, position 10	111
H.3	Calculated and adjusted neutron group fluxes, key 4, position 10, slot J	113

EXECUTIVE SUMMARY

This project addresses the potential problem of radiation embrittlement of reactor pressure vessel (RPV) supports. Surveillance specimens irradiated at the High Flux Isotope Reactor (HFIR) at relatively low neutron flux levels (about 1.5E+8 $cm^{-2}. s^{-1}$) and low temperature (about 50°C) showed embrittlement more rapidly than expected.[1] Commercial power reactors have similar flux levels and temperatures at the vessel support structures. The purposes of this work are to provide the neutron fluence spectra data that are needed to evaluate previously measured mechanical property changes in the HFIR, to explain the discrepancies in neutron flux levels between the nickel dosimeters and two other dosimeters, neptunium and beryllium, and to address any questions or peculiarities of the HFIR reactor environment.

The scope of this project consists of neutron and gamma transport calculations, dosimetry measurements, and least-squares logarithmic adjustment of the transport calculations and dosimetry measurements to obtain the best estimates for the neutron spectra. The neutron calculations were performed using the three-dimensional (3-D) transport code, TORT[2], and a one-dimensional (1-D) transport code, XSDRN[3], to obtain coupled neutron and gamma calculations. The neutron spectral adjustments were performed using the code LSL-M2[4]. The dosimetry measurements followed ASTM standards[5]. The measurements are traceable to fluence standards provided by NIST [Appendix A]. The gamma dosimeters, which were irradiated in the HFIR, were furnished and counted by NIST. The gamma measurements were performed to verify that the gamma field as obtained from 1-D neutron and gamma transport calculations, was adequate to determine the gamma contribution to the fast fission and the beryllium radiometric monitors.

This report will show the following major findings:

1. the discrepancies for the fast flux for energies above 1.0 MeV in key 7, position 5 of HFIR Dosimetry Experiment 1 (DOS1) are the results of photofission and photoneutron reactions in the neptunium and beryllium monitors respectively;

2. the photo-induced reactions dominate the value for the total reaction rates in the beryllium and fast threshold fission dosimeters in the HFIR capsule environment. This finding makes the use of these dosimeters good candidates as gamma dosimeters in certain radiation fields;

3. the fluxes at key 7, position 5 do not show any significant gradient in the surveillance capsule. However, key 4 and key 2 show large fast and thermal flux gradients in the capsule;

4. the stainless steel monitor located in the V-notch of the Charpy specimens of the surveillance capsule is adequate to determine the neutron flux above 1.0 MeV at the V-notch;

5. the total gamma dpa is about five times higher than the dpa from neutrons in key 7, position 5; and

6. the feasibility of the application of simultaneous adjustment of neutron and gamma fluxes performed in the analysis has been demonstrated. Even though this finding does not affect the current results, the methodology would be extremely useful in future work.

If gamma displacements can be shown to cause mechanical property changes, the HFIR specimens should be re-evaluated using the total dpa from neutron and gammas as the exposure parameter. Additional gamma measurements to verify the gamma contribution may be necessary at the surveillance keys. It is also recommended that a more sophisticated coupled neutron-gamma calculation should be performed (preferably 3-D) that takes into account neutrons arriving at the Charpy specimens from the photoneutron reaction in the beryllium reflector. These neutrons from the beryllium reflector may account for the approximately 30% scale factor in the adjustment runs.

ACKNOWLEDGMENTS

The authors wish to express their appreciation to the following consultants for their contribution to the planning, design, and review of the various tasks on this program: L. R. Greenwood of Battelle Pacific Northwest Laboratories, J. G. Williams of the University of Arizona, E. D. McGarry and Jim Grundl of the National Institute of Standards and Technology (NIST). L. R. Greenwood, Frank Ruddy of Westinghouse, and Brian Oliver of Rockwell International were very cooperative in providing dosimeters for the irradiations on relatively short notice. The solid state track recorders and helium accumulation fluence monitors were analyzed by Frank Ruddy and Brian Oliver respectively. E. D. McGarry provided the neutron fluence standards, and Bill McLaughlin provided the gamma dosimeters to provide a check of the gamma calculations. The comments of L. R. Greenwood, E. D. McGarry, and J. G. Williams are appreciated.

The valuable contributions from Ken Farrell, Greg Hirtz, Randy Hobbs, and Dennis Heatherly of the Oak Ridge National Laboratory (ORNL) have been responsible for keeping the fabrication, assembly, disassembly, and irradiations of the experiments on schedule. Thanks to Frank Dyer and David Glasgow of the Analytical Chemistry Division for counting all the radiometric dosimeters, and J. V. Pace of the Engineering Physics and Mathematics Division for performing all the transport calculations. The authors wish to give special thanks to Pat Hileman for the efficient preparation of this report and for making the numerous revisions that were requested. Thanks also to Cathy Shappert for providing the editorial review.

Finally, the authors gratefully acknowledge the programmatic support and encouragement of R. E. Johnson of the Nuclear Regulatory Commission (NRC). Comments and advice from Al Taboada, T. J. Walker, and Craig Hrabal, consultants from NRC, are appreciated.

ABBREVIATIONS

HAFM	Helium Accumulation Fluence Monitor
SSTR	Solid State Track Recorders
RM	Radiometric Monitors
ASTM	American Society for Testing and Materials
HFIR	High Flux Isotope Reactor
NIST	National Institute of Standards and Technology
BPNL	Battelle Pacific Northwest Laboratory
ORNL	Oak Ridge National Laboratory
DOS1-75	First HFIR dosimetry experiment in key 7, position 5
DOS2-75	Second HFIR dosimetry experiment in key 7, position 5
DOS2-29	Second HFIR dosimetry experiment in key 2, position 9
DOS2-42	Second HFIR dosimetry experiment in key 4, position 2
DOS2-410	Second HFIR dosimetry experiment in key 4, position 10
DOS3-75	Third HFIR dosimetry experiment in key 7, position 5
DOS3-29	Third HFIR dosimetry experiment in key 2, position 9
DOS3-42	Third HFIR dosimetry experiment in key 4, position 2
DOS3-410	Third HFIR dosimetry experiment in key 4, position 10
DOS4-75	Fourth HFIR dosimetry experiment in key 7, position 5
DOS4-G	Gamma measurements in the fourth HFIR dosimetry experiment in key 7, position 5
F>1.0 MeV	Neutron flux with energies greater than 1.0 MeV
F>0.1 MeV	Neutron flux with energies greater than 0.1 MeV
F<0.4 eV	Neutron flux with energies less than 0.4 eV
dpa	Displacements per atom for iron
dpa/s	Displacements per atom per second for iron
dpa (ASTM)	Displacements per atom, calculated with ASTM displacement cross section for iron
G-dpa	Displacements per atom induced by gamma rays, calculated using Baumann's[12] cross sections
G-flux	Total gamma rays flux
Be-9	Beryllium with atomic weight of 9
Be (n,x) He	The sum of the three reactions: Be-9 (n,a) He-6 --> Li-6; Be-9 (n,2n) Be-8 (2a); and Be-9 (n,d) Li-8 --> Be-8 (2a)
Slot ET*	Slot E, gradient wire at the top of the capsule
Slot EM*	Slot E, gradient wire at the middle of the capsule
Slot EB*	Slot E, gradient wire at the bottom of the capsule
M	Measured reaction rate in reactions per second per atom
C/M	Calculated-to-measured reaction rate ratios
A/M	The ratio of adjusted-to-measured reaction rates
M/C	Measured-to-calculated reaction rate ratios

*The location of all slots are shown in Fig. L1 and T, M, B refers to top, middle, and bottom respectively.

1 INTRODUCTION

Surveillance specimens irradiated at the HFIR at relatively low neutron flux levels and low temperatures exhibited embrittlement more rapidly than expected. Commercial nuclear power reactors have similar neutron flux levels and temperatures at the vessel support structures. This study at the HFIR:

1. finds the cause(s) for the discrepancies which were found in DOS1* neutron flux levels inferred from the nickel dosimeter and from two other dosimeters, neptunium and beryllium; and

2. determines the neutron flux spectra data to evaluate the previously measured mechanical property changes in HFIR surveillance specimens.

The results of the proposed work are needed for the resolution of Generic Safety Issue 15 (GSI-15) which addresses the potential problem of radiation embrittlement of commercial reactor vessel supports.

This report discusses a three-step fluence spectrum determination analysis procedure[6] that addresses:

1. transport calculations to compute the flux spectra at Charpy specimens,

2. dosimetry measurements to determine reaction rates at the specimens, and

3. consolidation of measurements and calculations to reduce the uncertainties of the neutron exposure parameters using a spectrum adjustment technique.

---

*K. Farrell et al., "The DOS1 Neutron Dosimetry Experiment at the HB-4-A Key 7 Surveillance Site on the HFIR Pressure Vessel," ORNL/TM-12511, (to be published).

2 EXPERIMENTAL PROGRAM

2.1 Experimental Locations

The surveillance locations chosen for the DOS2, DOS3, and DOS4 experiments were key 7, position 5, key 2, position 9, and key 4, positions 2 and 10 (Fig. 1). All locations were chosen so that the ongoing HFIR surveillance program would not be compromised.

2.2 Dosimetry Capsules

The dosimetry capsules are intended to reproduce the physical conditions of the standard surveillance capsules. Hence, the flux dosimeters were placed in standard cans furnished from the inventory of the surveillance program. Further details of this container are available in its quality assurance documents recorded in File JOB 5-1-143 in the Research Reactors Division (RRD) Document Control Center. These dosimetry cans were notched and engraved with characters to distinguish them from the surveillance packages. All fabrication, assembly and disassembly procedures are maintained in the RRD Document Control Center.

The three ferritic steel Charpy specimens in each surveillance capsules are simulated by carbon steel blocks to hold the dosimeters. A complete description of DOS2, DOS3, and DOS4 experiments and measured results were sent to the NRC project manager and to all consultants in the program.

2.3 Radiometric Measurements

Except for the HAFMs and the SSTRs, the neutron radiometric dosimeters were analyzed at ORNL. Prior to the counting, neutron fluence standards for the iron and nickel sensors were used so that the results would be traceable back to NIST. Two neptunium monitors were also verified with NIST. Several spectrometers were utilized for the counting. Periodic quality control checks are made (daily, when making measurements) to verify that the efficiencies of the particular counting geometry are correct and that all components of the spectrometry system are functioning properly. Calibrations are performed with weighted portions of a solution of mixed radionuclides, designated QCY.48, which is produced and sold every six months by Amersham International, plc. The daily control checks are made with a Co-60 source that was purchased from Amersham and is traceable to NIST. The measured activity of this source is allowed to differ from the specified value by no more than 5%. If the observed difference exceeds this value, measurements must cease until the error is corrected. Calibrations of the energy scale of the spectrometer systems are made with a sample of U-232 that emits gamma rays with energies in the range 238 and 2614 keV. A presentation and passouts of the counting methods were presented to NRC staff and independent consultants on the project at the March 4, 1993 meeting.

The HAFMs were analyzed by B. Oliver of Rockwell International [Appendix B] and the SSTRs by F. Ruddy of Westinghouse Electric Company [Appendix C]. The results from the SSTR fission monitors were in agreement with the radiometric fission monitors except for the U-235 SSTR at key 7, position 5. Several adjustment runs were performed to investigate the influence of the radiometric U-235 monitor and the SSTR U-235 monitor. The runs indicated that the radiometric dosimeter gave results that agreed with the middle segment of the gradient cobalt dosimeters.

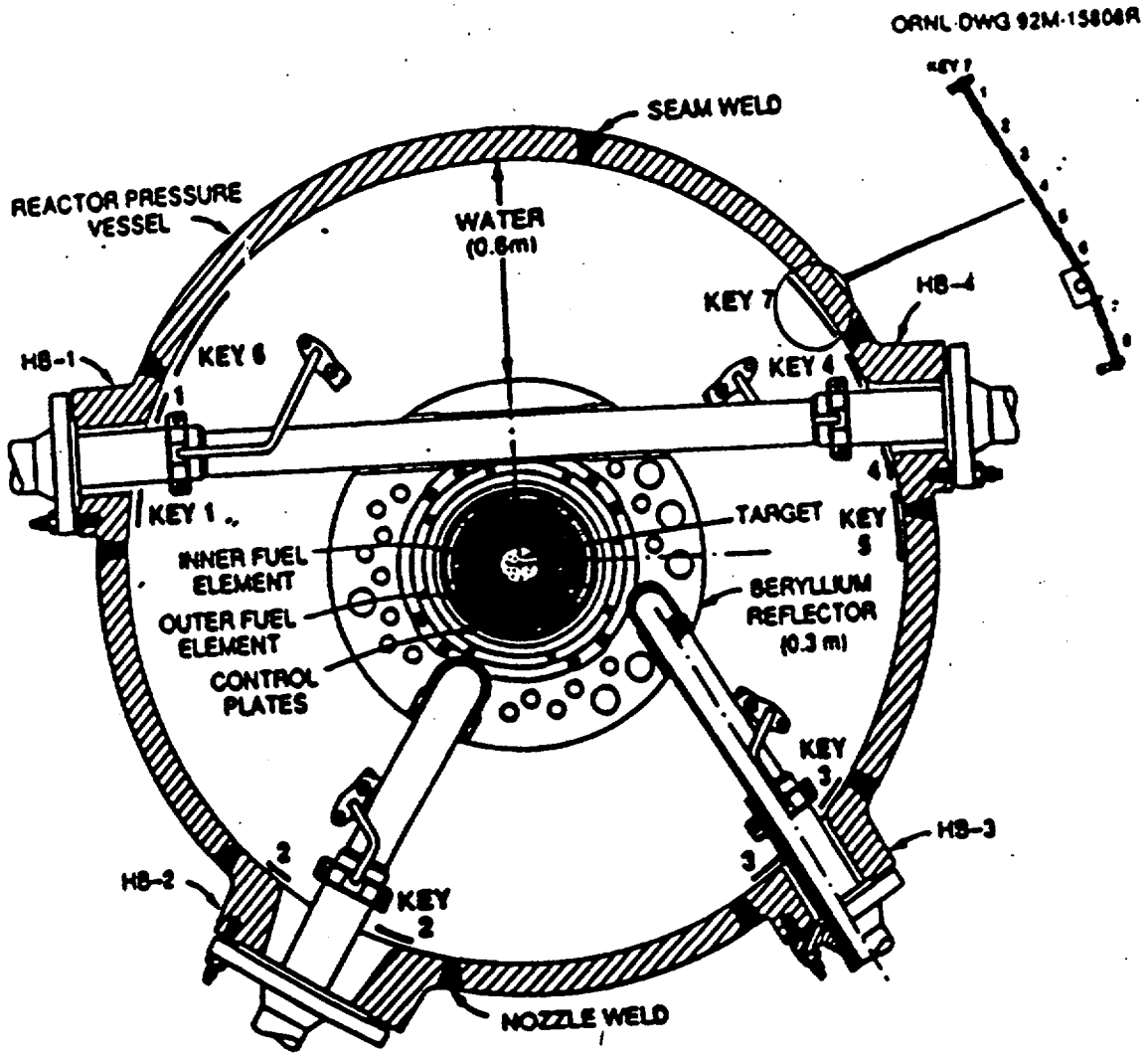

Fig. 1 Horizontal cross section through the HFIR at the core midplane, showing locations of the surveillance keys

3 METHODOLOGY

3.1 Background

To determine the neutron spectra at the HFIR surveillance positions, the three-step analysis procedure that combines transport calculations of the neutron and gamma field and measurements using radiometric monitors is used to obtain the best estimates for the neutron spectra and the related irradiation parameter rates. The experimental program is described in Section 2, and the transport calculations are presented in Appendix D.

This methodology is typically applied whenever accurate and reliable neutron irradiation parameters are needed (e.g., in the experiments that study changes in material properties caused by the neutron irradiation or in power reactor surveillance capsule analysis).

Applying this procedure to the HFIR surveillance capsules created a temporarily unexplained outcome: the DOS1 experiment showed that the fast-neutron flux (E >1 MeV) values as derived from the measured activity of Np and Be monitors were respectively approximately 17 times and 15 times higher than the flux value derived from the Ni monitors. Careful checking of the measurements ruled out experimental error. In order to help find the solution to this situation additional dosimetry experiments were initiated.

The DOS2 and DOS3 experiments provided comprehensive dosimetry results for key 7 position 5, key 2 position 9, and key 4 positions 2 and 10. In addition to the Ni, threshold activation monitors Al, Ti, Cu, and Fe and thermal monitors Sc, Co and Au were used. In the DOS2 experiment the dosimeters were used "bare," while in the DOS3 experiment, a 4-mil gadolinium cover was used in order to attenuate the thermal neutron flux and to prevent interference with the monitors responses. In the DOS3 experiment the fission monitors U-235, U-238 and Np-237 were used as radiometric monitors and independently verified with solid-state track recorders of the same fission isotopes. Also, the beryllium HAFMs were used in the DOS2 experiment, and in one location of DOS3.

The analysis of the DOS2 and DOS3 measurements showed again that the measured reaction rates for the Np-237 and Be monitors, as well as for the U-238 monitors were inconsistent with the reaction rates observed for other fast neutron monitors. The ratios of measured-to-calculated neutron reaction rates for these monitors were much larger than for the other monitors used as shown in Table 1. The measurements at key 7 position 5 were particularly suitable for analyzing these discrepancies because measured activities showed no significant gradients inside the capsule. For this reason it was decided to analyze data from that position first.

It is well known that fission monitors are sensitive not only to the neutrons but also to photofission reactions. Measured specific activities contain the contributions from both gamma- and neutron-induced fissions. A similar outcome appears for the Be monitor. The helium generated in Be occurs from both neutron-induced reactions and photon-induced reactions.

Since the measured responses for U-238, Np-237 and Be-9 monitors were much larger than the reaction rates obtained by folding the calculated neutron spectrum with neutron cross sections, the attention was focused on the possible contributions from the photon-induced reactions for these detectors.

Table 1 Comparison of measured and calculated reaction rates for fission and Be monitors

	Measured*	Calculated**	M/C***	M/C for Ni monitor
KEY 7.5				
Be (n,x) He				
DOS1	1.46E-15	7.60E-17	19.2	1.35 TOP
DOS2	1.44E-15	7.60E-17	18.9	1.42 BOT.
DOS2	1.42E-15	7.60E-17	18.7	
DOS3	1.46E-15	7.60E-17	19.3	
U-238 (n,f)	1.60E-15	6.24E-17	25.6	
Np-237 (n,f)	4.59E-15	2.25E-16	20.4	
U-238 (n,f) SSTR	1.36E-15	6.24E-17	21.8	
Np-237 (n,f) SSTR	4.75E-15	2.25E-16	21.1	
U-235 (n,f)	7.75E-15	8.13E-15	1.0	
U-235 (n,f) SSTR	1.50E-14	8.13E-15	1.8	
KEY 2.9				
Be (n,x) He	1.82E-15	2.84E-16	6.4	1.47 TOP
Be (n,x) He	2.19E-15	2.84E-16	7.7	2.90 BOT.
U-238 (n,f)	2.74E-15	2.69E-16	10.2	
Np-237 (n,f)	9.57E-15	1.15E-15	8.4	
U-238 (n,f) SSTR	2.01E-15	2.69E-16	7.5	
Np-237 (n,f) SSTR	8.62E-15	1.15E-15	7.5	
U-235 (n,f)	2.85E-13	2.05E-13	1.4	
KEY 4.2				
Be (n,x) He	1.38E-15	1.12E-16	12.3	0.91 TOP
U-238 (n,f)	1.48E-15	1.11E-16	13.3	1.60 BOT.
N-237 (n,f)	6.84E-15	5.41E-16	12.6	
U-238 (n,f) SSTR	1.65E-15	1.11E-16	14.9	
Np-237 (n,f) SSTR	6.08E-15	5.41E-16	11.2	
U-235 (n,f)	5.46E-13	3.48E-13	1.6	
U-235 (n,f) STR	5.97E-13	3.48E-13	1.7	
KEY 4.10				
Be (n,x) He	7.96E-16	2.08E-16	3.8	0.69 TOP
U-238 (n,f)	1.62E-15	1.90E-16	8.5	1.37 BOT.
Np-237 (n,f)	6.52E-15	8.51E-16	7.7	
U-238 (n,f) SSTR	1.29E-15	1.90E-16	6.8	
Np-237 (n,f) SSTR	5.66E-15	8.51E-16	6.7	
U-235 (n,f)	5.45E-13	3.89E-13	1.4	
U-235 (n,f) SSTR	6.98E-13	3.89E-13	1.8	

*Reaction rate per atom per second, including neutron and gamma reactions
**Reaction rate per atom per second, for neutron reactions only
***Measured-to-calculated reaction rate ratio

3.2 Gamma-Induced Reactions

An estimation of the gamma field was obtained from a 1-D coupled neutron-gamma calculation using the computer code XSDRN.

In the 1-D cylindrical, axially symmetric geometry many simplifications were made to model the actual geometry of the HFIR reactor. In particular the experimental beam tubes and other structures between cylindrical beryllium reflector and the reactor vessel were omitted. Therefore, one does not expect that the absolute values for neutron and gamma fluxes obtained from 1-D calculation will agree well with 3-D calculations or the measurements.

Variation of neutron-and gamma-induced reaction rates as a function of the distance from the core vertical axis, as obtained from the 1-D calculation, is illustrated on Fig. 2 for the Np monitor. The neutron-induced fissions dominate strongly inside the core and beryllium reflector. However, in the water, neutron flux attenuates much faster than gamma flux, so that at about 20 cm from the beryllium reflector the gamma-induced and neutron-induced fission rates are equal. After 20 cm, the fissions from gammas become increasingly dominant over fissions from neutrons. Similar behavior was found for the U-238 and Be monitors also.

At the position of the capsule, the gamma-induced reaction rates for Np-237, U-238 and Be from the 1-D calculations were larger by factors of 51, 52 and 61 than the corresponding neutron-induced reaction rates. However, at the location of the capsule, the fast-neutron flux from 1-D calculation was almost an order of magnitude lower than the fast flux from 3-D calculation, for key 7, position 5. A possible explanation, accounting for part of this discrepancy, is that in the 1-D calculation there was just water between the beryllium reflector and the capsule location, while in the HFIR, there is a tangential experimental beam tube between the reflector and key 7, position 5. This beam tube was modeled in the 3-D calculations, and is filled with air so that the resulting neutron flux attenuation is significantly lower than in the 1-D water geometry. This necessitated evaluating the 1-D results at a location closer to the core. A new location (radius) was selected so that the fast neutron flux from 1-D calculation at this radius is equal to the fast flux from 3-D calculation at the capsule location. The fast flux from the 3-D calculations at the capsule location was, for key 7 position 5, 1.17E+8 neutrons $cm^{-2}. s^{-1}$, while in 1-D calculation the fast flux of 1.16E+8 neutrons $cm^{-2}. s^{-1}$ was found at 100.06 cm from the core vertical axis (Fig. 3).

This selection was supported at a later date by the DOS4-G experiment, which provided the measurement of the absorbed gamma dose rate in silicon. The measured value was 36.4 Gy/s. The dose rate, obtained from calculated gamma fluxes at the above described location gave the value of 36.6 Gy/s (Fig. 4).

Also, the comparison of 1-D calculated neutron spectra showed only minor differences between the capsule location and the new location. The same result holds for the gamma spectrum. Therefore, it seems reasonable to calculate the gamma-to-neutron reaction rate ratios at the above mentioned location and use the corrections for the Np-237, U-238, U-235 and Be monitors in the capsule.

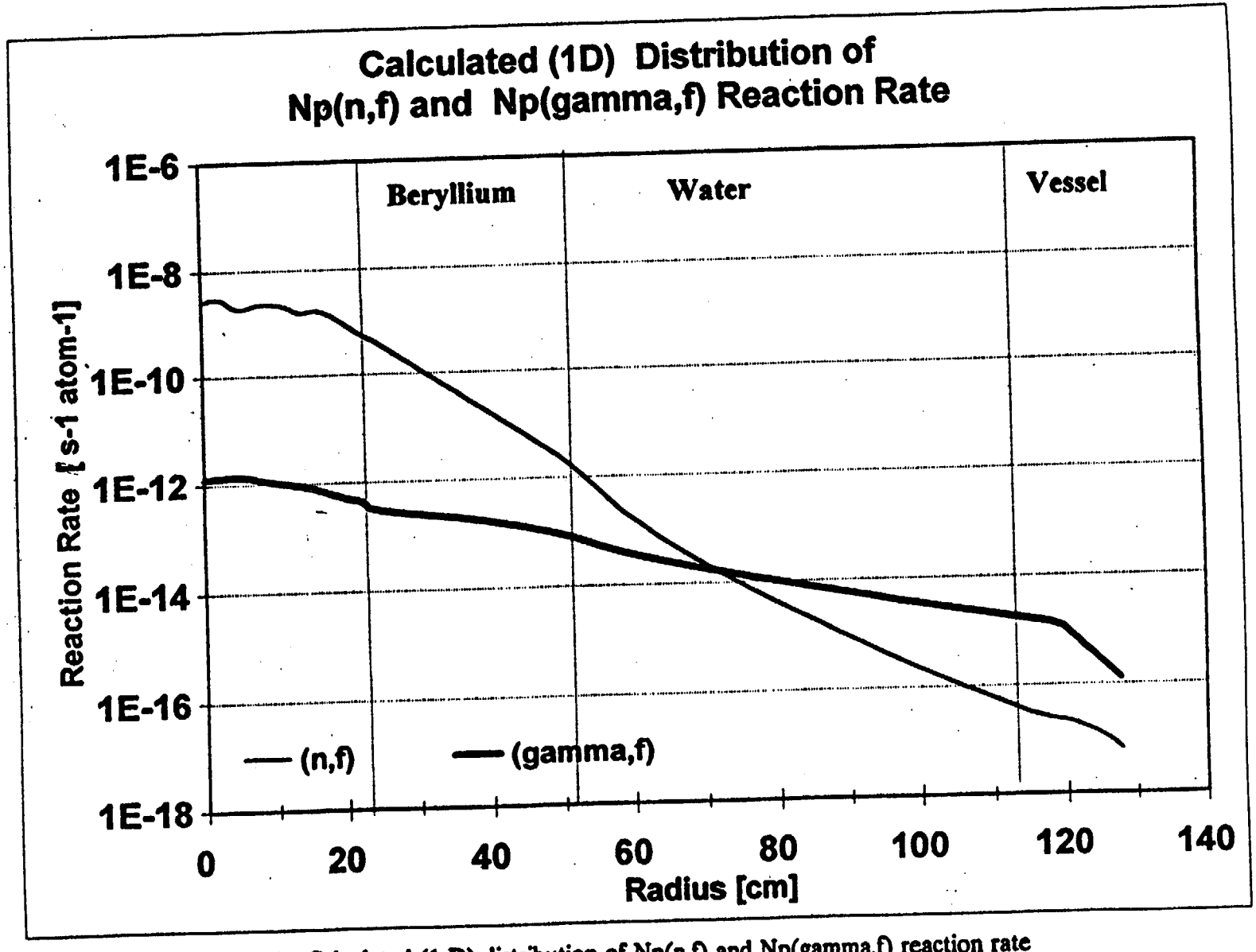

Fig. 2 Calculated (1-D) distribution of Np(n,f) and Np(gamma,f) reaction rate

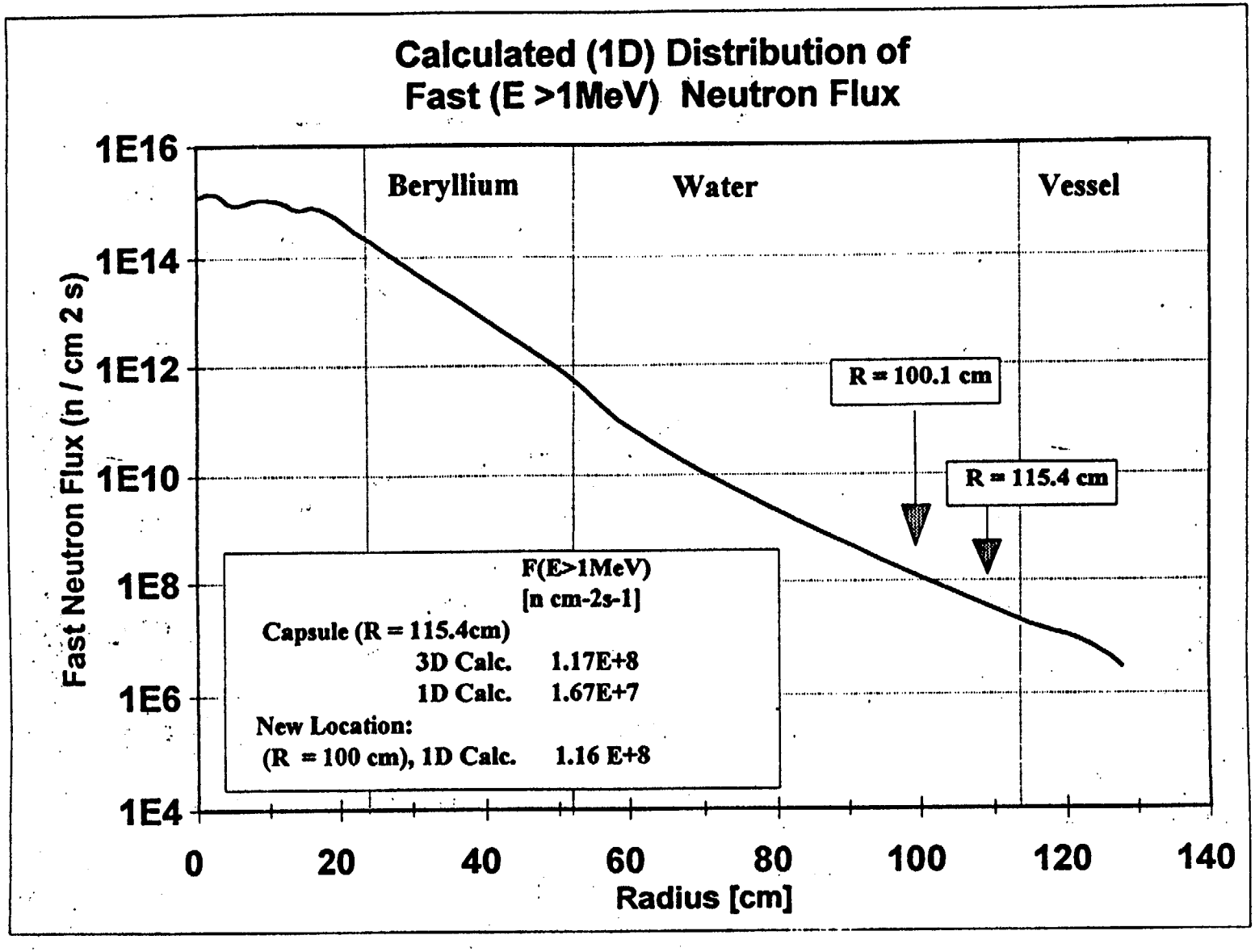

Fig. 3 Calculated (1-D) distribution of fast (E > 1 MeV) neutron flux

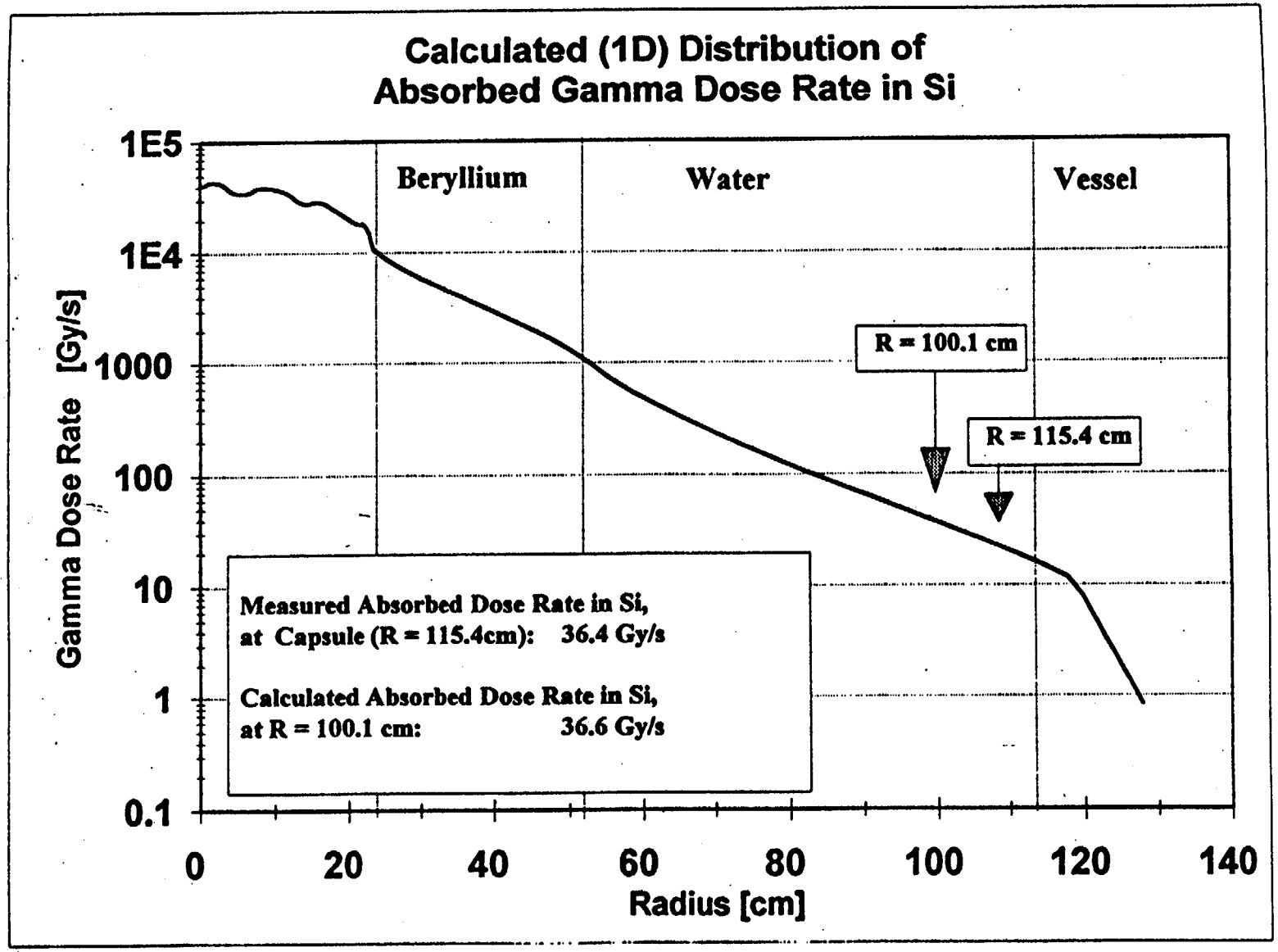

Fig. 4 Calculated (1-D) distribution of absorbed gamma dose rate in Si

3.3 Photon-Induced Reaction Rate Correction Factor

The correction factor CF, is defined as follows:

$$CF = \frac{R^n}{R^n + R^\gamma}$$

where

R^γ = calculated reaction rate induced by gamma flux:

$$R^\gamma = \sum_{g=1}^{NOGG} \sigma_g^\gamma \phi_g^\gamma$$

R^n = calculated reaction rate induced by neutron flux:

$$R^n = \sum_{g=1}^{NONG} \sigma_g^n \phi_g^n$$

ϕ_g^n = calculated (1-D) neutron flux in group g,

ϕ_g^γ = calculated (1-D) gamma flux in group g,

σ_g^n = neutron cross section in group g,

σ_g^γ = gamma cross sections in group g,

NONG = number of neutron groups in 1-D calculation,

NOGG = number of gamma groups in 1-D calculation.

These correction factors for Np-237, U-238, Be-9, and U-235 are listed in Table 2. The neutron-induced reaction rates represent only 4.5%, 5.5%, 6.1% of the total reaction rate for the Be-9, U-238, and Np-237 monitors respectively. For these three monitors, one concludes that the gamma-induced reactions account for most of their responses. The "corrected" measurements bring the values for the U-238 and the Np-237 in agreement with the other dosimeters, while the Be-9 monitor appears to be over corrected. The U-235 monitor is much less affected because the neutron fission cross section is much larger than the photo fission cross section.

Table 2 Comparison of measured and corrected reaction rates of fission and Be monitors with calculations

(Corrections are for the contribution of gammas induced reactions.)

	Measured*	Calculated*	M/C**	Correction Factor	Corrected M/C**	M/C for Ni monitor
KEY 7.5						
Be (n,x) He						
DOS1	1.46E-15	7.60E-17	19.2	4.535E-02	0.9	1.35 TOP
DOS2	1.44E-15	7.60E-17	18.9	4.535E-02	0.9	1.42 BOT.
DOS2	1.42E-15	7.60E-17	18.7	4.535E-02	0.8	
DOS3	1.46E-15	7.60E-17	19.3	4.535E-02	0.9	
U-238 (n,f)	1.60E-15	6.24E-17	25.6	5.512E-02	1.4	
Np-237 (n,f)	4.59E-15	2.25E-16	20.4	6.141E-02	1.3	
U-238 (n,f) SSTR	1.36E-15	6.24E-17	21.8	5.512E-02	1.2	
Np-237 (n,f) SSTR	4.75E-15	2.25E-16	21.1	6.141E-02	1.3	
U-235 (n,f)	7.75E-15	8.13E-15	1.0	8.222E-01	0.8	
U-235 (n,f) SSTR	1.50E-14	8.13E-15	1.8	8.222E-01	1.5	

*Reactions per second per atom
**Measured-to-calculated reaction rate ratio

3.4 Adjustment Options

With the knowledge that the U-238, Np-237, and Be-9 monitors detect mostly gammas in the HFIR surveillance locations investigated, the three possible paths for the adjustment of the calculated neutron spectrum are

A. to perform the adjustment with all dosimeters including those that require corrections;
B. to perform the adjustment with all dosimeters except the dosimeters that require gamma corrections; and
C. to perform the simultaneous adjustment of the neutron and gamma spectra using all detectors.

Approach A has the disadvantage that large corrections are applied to the Np-237, U-238, and the Be-9 monitors. Such large corrections to a few monitors may distort the results, but the consistency of the corrected reaction rates with the other dosimeters can be shown through the adjustment procedure.

Approach B applies the adjustment procedure to all the measurements and rejects any measurement that is inconsistent. In this study, the adjustment procedure rejected the uncorrected Np-237, U-238, and the Be-9 measurements. The disadvantage of this approach is that the cause for the rejection is not explained.

Approach C represents major modification and improvement to the current adjustment methodology. The equation used to calculate the neutron-induced reaction rates is exactly the same as the equation to calculate the photo-induced reaction rates. By adding the gamma spectrum and cross sections to the neutron set, the two can be adjusted simultaneously. This approach has several advantages; no corrections for gamma contribution to the measured reaction rates are necessary, gamma measurements can be added to the other neutron measurements, and gamma and neutron irradiation parameters are determined (e.g., neutron and gamma dpa/s). The disadvantages are more input data, namely calculated gamma spectrum and cross sections for gamma reactions. Also, some assumptions need to be made regarding the gamma spectrum covariance matrix.

3.5 Adjustment Procedure

The adjustment code LSL-M2 was used for all of the adjustment runs. In runs where only the neutron spectra were adjusted, ten different locations inside a capsule were considered. Four of these locations correspond to the slot D, slot J, slot B, and slot A. The Ni and Co gradient wires on the same side of the capsule (i.e., E and G on one side, and F and H on the other side) were grouped together. A schematic of the dosimetry capsule with slot locations is shown in Appendix I, Fig. I.1. On each side three locations were considered: the top, middle and bottom portions of the wires. This makes additional six locations, treated in the adjustment procedure.

Three-dimensional transport calculations provided multigroup neutron fluxes at 1 point per capsule; thus the same calculated spectrum was input in the adjustment code for all ten locations in each capsule. Measurements in all the capsules except the key 7, position 5 showed big variations in reaction rates from top to bottom of the capsules, indicating severe neutron

gradients. For this reason and to avoid large adjustments of the neutron spectra at certain locations, the adjustment runs employed the scaling option which splits the total spectrum adjustment in two parts: one is scaling of the magnitude of the calculated spectrum and the other is the "true" adjustment, or in other words actual modification of the calculated spectrum through the adjustment procedure. Accordingly, in the tables of the calculated and adjusted values given in Appendices E-H, the scale factors and adjustment factors are listed. Their products give the total adjustment factors, which equal the ratios of adjusted to calculated values of the exposure parameters.

The spectrum correlation coefficient matrix, as calculated for the simulated surveillance capsule position for the ORR PSF Metallurgical Experiment, was used.[7,8] The original calculation of the fluence variance-covariances covers only the range from 18 MeV to 0.1 MeV. Therefore two energy groups from 1 E-4 eV to 0.1 eV and from 0.1 eV to 0.1 MeV were added with large variances of 150% and 75%, respectively and small correlations of 0.2 and 0.1. Also, the variances of energy groups above 0.1 MeV were increased from the original values to 40% and the high-energy boundary was extended to 20 MeV. The spectrum covariance matrix was converted in the group structure used in the adjustment with the computer code FLXPRO from the LSL-M2 code package. Obviously the assumed spectrum variance-covariance information is only approximate; however, it does not appear to be critical for the analysis since comprehensive dosimetry measurements are available, and in such cases the adjustment results are in general not very sensitive to the details in the spectrum covariance matrix. The cross correlation factors for the spectra at different locations were assumed to be 0.8.

The activation cross-section library in 640-energy groups was created from the IRDF 90 and ENDF V dosimetry files. To account for the 4 mils gadolinium cover in the DOS3 experiment the set of cross sections was generated, where the 640-group cross sections were multiplied by the attenuation factors, defined as:

$$AF = \exp(-(D*AV/AT) * TH * CS),$$

where

AF = attenuation factor,
D = density of cover material (7.9004 g/cm^3 for Gd),
AV = Avogadros number,
AT = atomic weight (157.25 for Gd),
TH = thickness of the cover (4 mils),
CS = total absorption cross section of Gd (taken from the IRDF90 file).

The above formula is, of course, only a crude approximation and does not consider the geometry of the covers and the dosimeters. However, it appears to be reasonably accurate for the current application with the possible exception of gold dosimeters.

Resulting cross sections were then converted in 40 energy groups in the same way as the bare cross sections. Computer code FLXPRO from the LSL-M2 code package was used for this purpose.

Data for the photofission cross sections were taken from Verbinski.[9] The photoneutron cross section for beryllium, which leads to the formation of helium through the reaction $Be^9 + \gamma \rightarrow n + \alpha + \alpha$, was generated first from the plot in the "Reactor Handbook"[10] and later from the Warshaw[11] evaluation. No significant differences in the calculated reaction rates were observed. The gamma displacement cross section in iron was taken from Baumann.[12]

Measured activities were converted to reaction rates, taking into account the reactor power history for the cycle of the irradiation. Computer code ACT from the LSL-M2 code package was used for this purpose. Reaction rates so obtained were mostly used without any further correction, except in the following cases:

1. For the key 7, position 5, U-238, Np-237, and Be reaction rates were corrected for the gamma contribution as discussed in details above,

2. The Au and Co dosimeters were corrected for the self-shielding, since pure metal wires of 20 mils (Co) and 8 mils (Au) outer diameter were used in both DOS2 and DOS3 experiments. The correction factors were obtained from the ratios of measured activities of diluted and pure Au and Co wires, which were used in DOS4 experiment. The correction factors were 1.13 and 1.96 for bare and Gd shielded Co, respectively, and 1.68 and 5.10 for the bare and Gd-shielded Au, respectively.

3. The activities for Co gradient wires for DOS2 and DOS3 and Ni gradient wires for DOS3 for the top, middle, and bottom segments (Fig. I.1) were determined as follows:

   a. the bent section of the gradient wire was cut off at the top of the capsule (Fig. I.1);

   b. 1-cm sections, starting at the top, were cut off from the remainder of the wire;

   c. the bottom segment was slightly longer than 1 cm and was left that way; and

   d. the activities of the top, middle, and bottom segments were plotted against the wire length starting from the bottom (X=0). The coordinates along the X-axis of the latter segments were plotted at their respective midpoints.

   The activities of the Ni gradient wires for DOS2 were determined using the following procedure:

   a. the bend in the wires were straightened and 1-cm segments, starting at the top, were cut off the full length of the wire;

   b. the bottom segment was slightly longer than 1 cm and was left that way;

   c. the activities of all the 1-cm segments were counted and plotted on a curve starting from the bottom segment;

   d. the activities were plotted at the coordinates corresponding to the midpoints of each segment;

   e. the activities corresponding to the coordinates for the top, middle, and bottom segments were then obtained by interpolation.

The variances of the measured reaction rates were estimated from the observed spread of experimental data and were treated as uncorrelated.

For the adjustment the neutron spectrum was collapsed from the 64 groups in which the transport (3-D) calculation was done to the 40 energy groups.

4 RESULTS AND DISCUSSION

All three approaches described in Section 3.4 were used for key 7, position 5. This key is the only location where gamma measurements were made so that approaches A and C are supported by experimental data.

Four different adjustment runs are presented in Table 3. Run R4 is taken as the standard (best run). This run uses a total of 69 measured reaction rates from DOS1, DOS2, DOS3 and DOS4 experiments. Gamma corrections were made to the U-235, U-238, Np-237, and the Be-9 dosimeters. Six dosimeters were not used since their reaction rates required large adjustments and were, therefore, rejected as not consistent with the others. The adjusted values of the exposure parameters are listed together with their standard deviation in percent. The ratios of adjusted values for each of the other runs (R1, R2, and R3) to the values from run R4 are listed along with the fractional standard deviation.

The effect of rejecting the six dosimeters in run R4 is seen from the column labeled R1/R4. The six dosimeters not used in run R4 were added to run R1. The adjusted exposure parameters from the two runs agree within 1% and their standard deviations are also in agreement. However, the chi square per degree of freedom is 1.2 in run R1 and 0.81 in run R4, which clearly indicates that the rejected dosimeters were inconsistent with the others. Nevertheless, including some of the slightly inconsistent measurements in run R1 has practically no effect on the adjusted irradiation parameters since the adjustment is directed by the large body of 69 consistent measurements.

In the run R3 all the dosimeters that needed gamma corrections were not used so that adjustment is performed according to Approach B. The results are in good agreement with the run R4. The largest difference in the adjusted values from the two runs is observed for the thermal flux in the slot J and is 12%, which is still smaller that the quoted standard deviation of 19%. One can conclude therefore that Approach B is acceptable in determining the adjusted neutron exposure parameters.

The monitors in run R2 were not corrected for gamma-induced reactions, but were corrected in run R4. As expected, this change has a dramatic effect on the results as shown in Table 3. The chi square per degree of freedom rose to the value of 23, clearly indicating that major inconsistencies exist in the input data. The conclusion is drawn that one must not use the Np-237, U-238 and Be monitors in the neutron adjustment procedure without correcting the measured reaction rates for the gamma contributions.

Finally, Table 4 gives the comparison of the adjusted irradiation parameters from run R4 (neutron column) and the simultaneous neutron and gamma (N + gamma column) spectrum adjustment run. In the coupled neutron-gamma adjustment run, spectra at only the four locations were adjusted simultaneously because of the current limitations in the adjustment computer code LSL-M2. At these locations the same dosimetry measurements as in run 4 were used, and the measured absorbed gamma dose rate in silicon was added in the position of slot B. In the simultaneous neutron and gamma adjustment the reaction rates, as measured, of the fission and Be monitors are used as input.

Table 3 Comparison of different adjustment runs, key 7, position 5

	R1/R4		R2/R4		R3/R4		R4	
							VALUE	STD.
Slot D								
F > 1MeV*	1.01 ±	0.06	6.41 ±	0.06	0.99 ±	0.08	1.547E+08 ±	6
F > 0.1MeV*	1.01 ±	0.09	7.44 ±	0.09	0.99 ±	0.11	2.289E+08 ±	9
F < 0.4 eV*	0.99 ±	0.05	1.00 ±	0.05	1.00 ±	0.05	2.835E+08 ±	5
dpa/s**	1.01 ±	0.05	4.93 ±	0.05	1.00 ±	0.06	2.421E-13 ±	5
Slot A								
F > 1MeV	1.01 ±	0.07	5.34 ±	0.07	1.00 ±	0.08	1.580E+08 ±	7
F > 0.1MeV	1.01 ±	0.10	6.08 ±	0.10	1.00 ±	0.11	2.361E+08 ±	10
F < 0.4 eV	1.00 ±	0.04	1.00 ±	0.04	1.00 ±	0.04	2.879E+08 ±	4
dpa/s	1.01 ±	0.06	4.14 ±	0.06	1.00 ±	0.06	2.474E-13 ±	6
Slot B								
F > 1MeV	1.01 ±	0.05	25.04 ±	0.06	1.01 ±	0.68	1.504E+08 ±	6
F > 0.1MeV	1.00 ±	0.08	27.53 ±	0.08	1.00 ±	0.68	2.249E+08 ±	8
F < 0.4 eV	0.99 ±	0.07	1.01 ±	0.07	1.00 ±	0.08	2.742E+08 ±	7
dpa/s	1.01 ±	0.05	19.31 ±	0.05	1.01 ±	0.66	2.346E-13 ±	5
Slot J								
F > 1MeV	1.01 ±	0.06	13.47 ±	0.06	1.06 ±	0.08	1.491E+08 ±	6
F > 0.1MeV	1.01 ±	0.09	15.15 ±	0.09	1.04 ±	0.11	2.241E+08 ±	9
F < 0.4 eV	1.01 ±	0.18	1.03 ±	0.19	0.88 ±	0.19	3.086E+08 ±	19
dpa/s	1.01 ±	0.05	10.07 ±	0.05	1.05 ±	0.07	2.360E-13 ±	5
Slot ET								
F > 1MeV	1.01 ±	0.07	5.35 ±	0.07	1.00 ±	0.08	1.538E+08 ±	7
F > 0.1MeV	1.00 ±	0.10	6.10 ±	0.10	1.00 ±	0.11	2.295E+08 ±	10
F < 0.4 eV	1.00 ±	0.06	1.00 ±	0.06	1.00 ±	0.06	2.987E+08 ±	6
dpa/s	1.00 ±	0.06	4.15 ±	0.06	1.00 ±	0.07	2.408E-13 ±	6
Slot EM								
F > 1MeV	1.01 ±	0.07	5.35 ±	0.07	1.00 ±	0.08	1.562E+08 ±	7
F > 0.1MeV	1.00 ±	0.10	6.10 ±	0.10	1.00 ±	0.11	2.332E+08 ±	10
F < 0.4 eV	1.00 ±	0.06	1.00 ±	0.06	1.00 ±	0.06	2.731E+08 ±	6
dpa/s	1.00 ±	0.06	4.15 ±	0.06	1.00 ±	0.07	2.444E-13 ±	6
Slot EB								
F > 1MeV	1.01 ±	0.07	5.36 ±	0.07	1.00 ±	0.08	1.569E+08 ±	7
F > 0.1MeV	1.00 ±	0.10	6.10 ±	0.10	1.00 ±	0.11	2.345E+08 ±	10
F < 0.4 eV	1.00 ±	0.06	1.00 ±	0.06	1.00 ±	0.06	2.707E+08 ±	6
dpa/s	1.00 ±	0.06	4.16 ±	0.06	1.00 ±	0.07	2.456E-13 ±	6
Slot FT								
F > 1MeV	1.01 ±	0.07	5.35 ±	0.07	1.00 ±	0.08	1.507E+08 ±	7
F > 0.1MeV	1.00 ±	0.10	6.10 ±	0.10	1.00 ±	0.11	2.249E+08 ±	10
F < 0.4 eV	1.00 ±	0.06	1.00 ±	0.06	1.00 ±	0.06	2.859E+08 ±	6
dpa/s	1.00 ±	0.06	4.15 ±	0.06	1.00 ±	0.07	2.359E-13 ±	6

Table 3 (continued)

	R1/R4		R2/R4		R3/R4		R4	
Slot FM							VALUE	STD.
F > 1MeV	1.01 ±	0.07	5.35 ±	0.07	1.00 ±	0.08	1.583E+08 ±	7
F > 0.1MeV	1.00 ±	0.10	6.09 ±	0.10	1.00 ±	0.11	2.360E+08 ±	10
F < 0.4 eV	1.00 ±	0.06	1.00 ±	0.06	1.00 ±	0.06	2.630E+08 ±	6
dpa/s	1.00 ±	0.06	4.16 ±	0.06	1.00 ±	0.07	2.473E-13 ±	6
Slot FB								
F > 1MeV	1.01 ±	0.07	5.35 ±	0.07	1.00 ±	0.08	1.608E+08 ±	7
F > 0.1MeV	1.00 ±	0.10	6.10 ±	0.10	1.00 ±	0.11	2.400E+08 ±	10
F < 0.4 eV	1.00 ±	0.06	1.00 ±	0.06	1.00 ±	0.06	2.836E+08 ±	6
dpa/s	1.00 ±	0.06	4.16 ±	0.06	1.00 ±	0.07	2.515E-13 ±	6
	Chi^2 = 1.21 #R = 65 DOSIMETERS FROM DOS1,2,3,4 SLOT J: ADDED NI (EM+FM)/2		Chi^2= 22.92 #R = 59 Same as R4, but: NO GAMMA CORRECTIONS		Chi^2 = 0.52 #R = 45 Same as R4, but: all dosimeters that need gamma correction NOT USED		Chi^2 = 0.81 #R = 59 Not used: D: Au (DOS 4) A: Au (DOS3) B: U-235--Ru U-238--Zr Np-237--Ru J: Co (in Gd)	

* Units are $cm^{-2} . s^{-1}$
** Units are s^{-1}

NOTE: Chi^2 is chi square per degree of freedom. #R is number of residuals. Scaling option is used, therefore, the number of residuals is equal to the number of measured reaction rates used minus the number of locations at which the spectrum is adjusted (10 in these runs).

Table 4 Comparison of simultaneous neutron and gamma adjustment to neutron adjustment run, key 7, position 5

	Neutron		N + Gamma		
	Value	Std. %	Value	Std. %	
	A1		A2		A2/A1
Slot D					
F > 1 MeV*	1.55E+08	± 6	1.54E+08	± 8	0.99
F > 0.1 MeV*	2.29E+08	± 9	2.26E+08	± 11	0.99
F < 0.4 eV*	2.84E+08	± 5	2.84E+08	± 5	1.00
dpa (ASTM)**	2.42E-13	± 5	2.41E-13	± 6	0.99
G-dpa**			1.34E-12	± 15	
G-flux***			1.39E+13	± 27	
Dose rate in Si****			3.66E+01	± 22	
Slot J					
F > 1 MeV*	1.49E+08	± 6	1.58E+08	± 8	1.06
F > 0.1 MeV*	2.24E+08	± 9	2.37E+08	± 11	1.06
F < 0.4 eV*	3.09E+08	± 19	3.11E+08	± 19	1.01
dpa (ASTM)**	2.36E-13	± 5	2.50E-13	± 7	1.06
G-dpa**			1.22E-12	± 7	
G-flux***			1.27E+13	± 20	
Dose rate in Si****			3.31E+01	± 13	
Slot B					
F > 1 MeV*	1.50E+08	± 6	1.41E+08	± 27	0.94
F > 0.1 MeV*	2.25E+08	± 8	2.09E+08	± 27	0.93
F < 0.4 eV*	2.74E+08	± 7	2.72E+08	± 7	0.99
dpa (ASTM)**	2.35E-13	± 5	2.21E-13	± 26	0.94
G-dpa**			1.31E-12	± 8	
G-flux***			1.39E+13	± 9	
Dose rate in Si****			3.62E+01	± 5	
Slot A					
F > 1 MeV*	1.58E+08	± 7	1.59E+08	± 8	1.00
F > 0.1 MeV*	2.36E+08	± 10	2.36E+08	± 11	1.00
F < 0.4 eV*	2.88E+08	± 4	2.88E+08	± 4	1.00
dpa (ASTM)**	2.47E-13	± 6	2.49E-13	± 6	1.00
G-dpa**			1.38E-12	± 32	
G-flux***			1.45E+13	± 35	
Dose rate in Si****			3.81E+01	± 33	

*Units are neutrons $cm^{-2}.\ s^{-1}$
**Units are s^{-1}
***Units are gammas $cm^{-2}.\ s^{-1}$
****Units are $Gy.s^{-1}$

As seen from Table 4, the adjusted neutron exposure parameters from the two runs agree very well. The largest difference observed is 7% for F > 0.1 MeV at slot B. The adjusted absorbed dose rate in Silicon is 36.2 Gy/s, which compares well to the measured value of 36.4 Gy/s. The measured responses of fission dosimeters and Be monitors are consistent with the responses of other monitors not affected by the gamma field, and with the measured absorbed gamma dose rate in the Silicon. These agreements support the conclusion that the measured reaction rates of Np-237, U-238 and Be monitors are larger than the reaction rates of other threshold monitors due to the significant contributions from the gamma-induced reactions. The chi-square per degree of freedom for the neutron-gamma run was 0.77 and the number of residuals was 42.

Table 4 also shows that at key 7, position 5, the displacements per atom rate induced by gamma rays is about 5 times higher than the neutron-induced dpa rate. Therefore, it may be of interest to re-evaluate the mechanical property changes of the HFIR specimens based on the total dpa from the neutrons and the gamma rays.

The analysis of key 7 position 5 showed that the neutron adjustment parameters, obtained by rejecting all the dosimeters that needed substantial corrections for gamma contributions, gave results that are in excellent agreement with the adjustments where the affected dosimeters were corrected for gamma contributions and taken into account in the adjustment procedure. Also, results from both of these adjustment runs are in good agreement with the results obtained from the simultaneous adjustment of the neutron and gamma field. This latter approach appears to be the most consistent technique to analyze dosimetry measurements when considerable contribution from the gamma field is suspected. The comparisons of different adjustment runs, described above, show also that reliable fast-flux irradiation parameters can be derived from the calculated spectra and measured activities of the stainless steel wires, located in the V-notch of the Charpy specimens.

Based on the results for key 7, position 5 and because no independent gamma field measurements were available at the other locations, the neutron spectrum adjustment runs were done without the Np-237, U-238, and Be dosimeters. Detailed results of the adjustment runs are listed in Appendices E, F, G, and H.

Adjusted irradiation parameters for the four surveillance locations considered are summarized in Table 5. For each of the capsules, slot J is located at the center of the capsule. Irradiation parameters for that location, therefore, correspond to the position of the V-notch of the Charpy specimens irradiated in the HFIR surveillance capsules. The calculated (3-D transport calculation) and adjusted neutron spectra for the Slot J, are illustrated in the Figs. 5-8. Adjusted group fluxes for these locations are also tabulated in Table 6.

From Table 5 it can be seen that the neutron field is considerably different at the surveillance positions analyzed. Differences are in the magnitude as well as in the neutron spectrum. Even though details can be seen from Table 5, let us mention here for example that the fast (E > 1 MeV) neutron flux is 8 times greater at key 2, position 9 than at key 7, position 5. Thermal flux at key 4, position 10 is even 90 times higher than at the key 7, position 5. The thermal-to-fast-flux ratio is approximately 2, 13, 75, and 67 for the key 7, position 5, key 2, position 9, key 4, position 2, and key 4, position 10 respectively. Therefore, while neutron flux with energies below 0.1 MeV do not contribute significantly to the dpa rate at the key 7, position 5, it is much more important for the other locations where neutron spectrum is considerably

Table 5 Irradiation parameters at the centers of capsules

	Key 7 Position 5		Key 2 Position 9		Key 4 Position 2		Key 4 Position 10	
	Value	Std. %	Value	Std. %	Value	Std. %	Value	Std. %
F > 1 MeV*	1.49E+08	± 6	1.21E+09	± 9	3.10E+08	± 10	4.09E+08	± 10
F > 0.1MeV*	2.24E+08	± 9	2.11E+09	± 12	6.43E+08	± 13	8.05E+08	± 13
F < 0.4 eV*	3.09E+08	± 19	1.61E+10	± 6	2.33E+10	± 6	2.75E+10	± 6
dpa/s**	2.36E-13	± 5	1.89E-12	± 7	6.66E-13	± 6	8.62E-13	± 6

*Units are neutrons . cm^{-2}. s^{-1}
**Units are s^{-1}

Table 6 Adjusted neutron fluxes at the centers of the examined capsules

Group Upper Energy Boundary [eV]	Key 7 Position 5 [$cm^{-2}.s^{-1}$]	Key 2 Position 9 [$cm^{-2}.s^{-1}$]	Key 4 Position 2 [$cm^{-2}.s^{-1}$]	Key 4 Position 10 [$cm^{-2}.s^{-1}$]
2.000E+07	1.087E+06	2.356E+06	8.033E+05	8.997E+05
1.271E+07	3.399E+06	9.059E+06	2.659E+06	3.575E+06
1.013E+07	8.408E+06	2.698E+07	7.235E+06	1.102E+07
8.072E+06	1.398E+07	5.743E+07	1.310E+07	2.316E+07
6.434E+06	1.150E+07	5.791E+07	1.212E+07	2.105E+07
5.523E+06	1.301E+07	7.595E+07	1.549E+07	2.533E+07
4.742E+06	1.193E+07	8.075E+07	1.665E+07	2.518E+07
4.071E+06	8.687E+06	7.089E+07	1.547E+07	2.164E+07
3.495E+06	9.697E+06	8.778E+07	1.897E+07	2.473E+07
3.000E+06	7.005E+06	6.626E+07	1.523E+07	1.904E+07
2.724E+06	2.126E+07	2.229E+08	5.409E+07	6.589E+07
2.038E+06	5.608E+06	6.294E+07	1.700E+07	2.083E+07
1.850E+06	6.937E+06	8.044E+07	2.260E+07	2.763E+07
1.655E+06	6.343E+06	7.464E+07	2.198E+07	2.656E+07
1.480E+06	7.801E+06	9.213E+07	2.867E+07	3.438E+07
1.282E+06	1.248E+07	1.457E+08	4.778E+07	5.790E+07
1.000E+06	1.302E+07	1.520E+08	5.179E+07	6.111E+07
7.653E+05	2.169E+07	2.543E+08	9.141E+07	1.106E+08
4.704E+05	2.162E+07	2.591E+08	9.586E+07	1.149E+08
2.297E+05	1.866E+07	2.269E+08	9.390E+07	1.097E+08
1.000E+05	4.016E+07	3.658E+08	3.275E+08	3.942E+08
1.202E+04	1.092E+07	1.050E+08	9.783E+07	1.149E+08
6.004E+03	1.076E+07	1.041E+08	9.995E+07	1.193E+08
3.000E+03	3.086E+07	3.105E+08	3.173E+08	3.768E+08
3.911E+02	1.025E+07	1.070E+08	1.168E+08	1.389E+08
1.978E+02	1.027E+07	1.089E+08	1.235E+08	1.478E+08
1.000E+02	1.452E+07	1.573E+08	1.863E+08	2.232E+08
3.817E+01	2.019E+07	2.259E+08	2.853E+08	3.419E+08
1.000E+01	7.279E+06	8.386E+07	1.113E+08	1.332E+08
6.178E+00	1.084E+07	1.276E+08	1.750E+08	2.090E+08
3.000E+00	8.293E+06	1.002E+08	1.420E+08	1.684E+08
1.770E+00	2.546E+07	3.351E+08	5.000E+08	5.591E+08
3.970E-01	3.824E+06	5.546E+07	9.632E+07	1.142E+08
3.300E-01	4.939E+06	9.798E+07	2.028E+08	2.212E+08
2.700E-01	8.708E+06	2.627E+08	6.280E+08	6.451E+08
2.150E-01	2.178E+07	8.834E+08	2.238E+09	2.195E+09
1.620E-01	4.626E+07	2.309E+09	4.003E+09	4.492E+09
1.040E-01	9.470E+07	5.228E+09	6.757E+09	8.447E+09
5.000E-02	1.170E+08	6.594E+09	8.503E+09	1.034E+10
1.000E-02	1.145E+07	6.501E+08	8.364E+08	9.958E+08
1.000E-05*				

*Lower energy boundary of the 40th group.

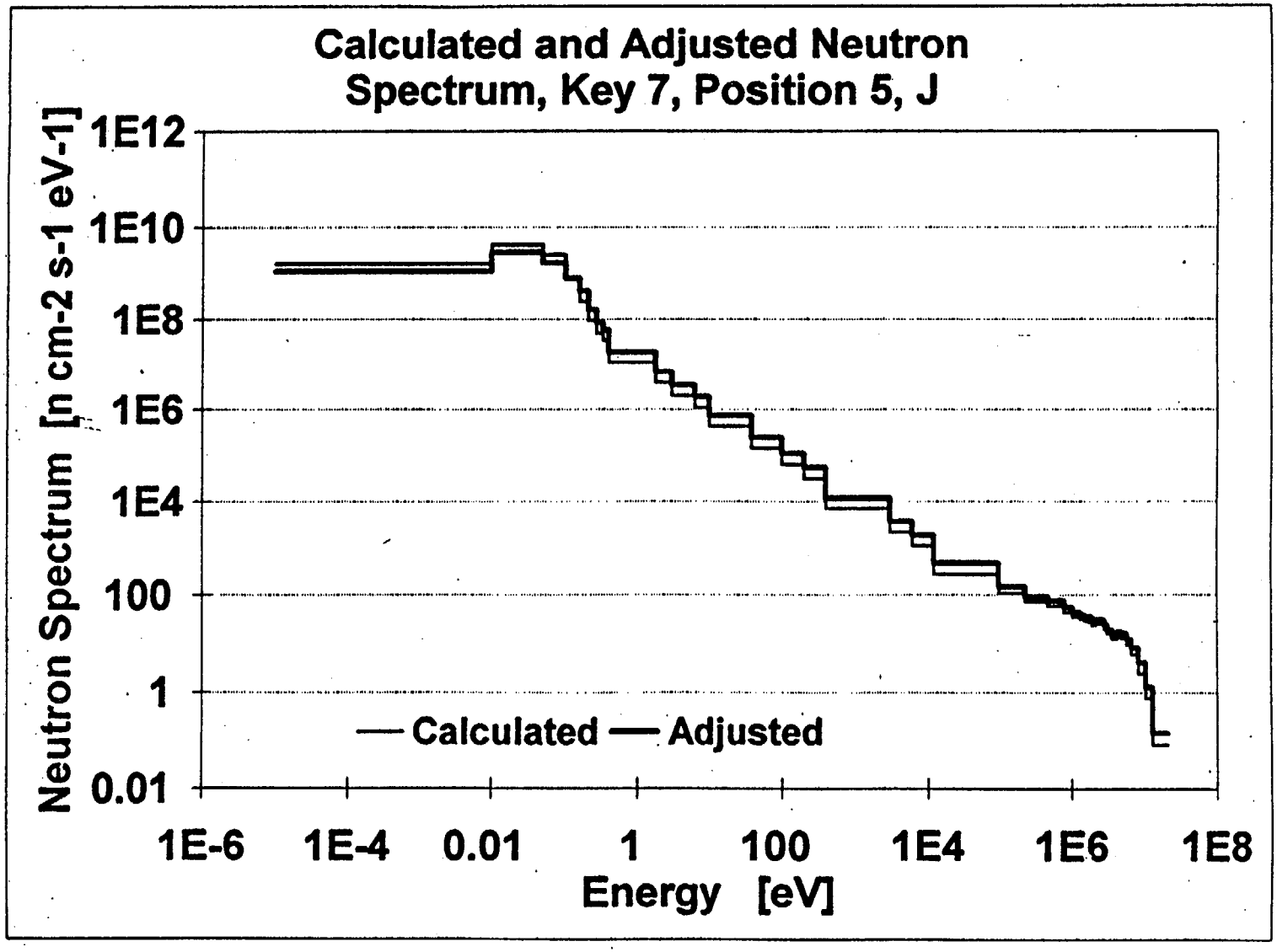

Fig. 5 Calculated and adjusted neutron spectrum, key 7, position 5, J

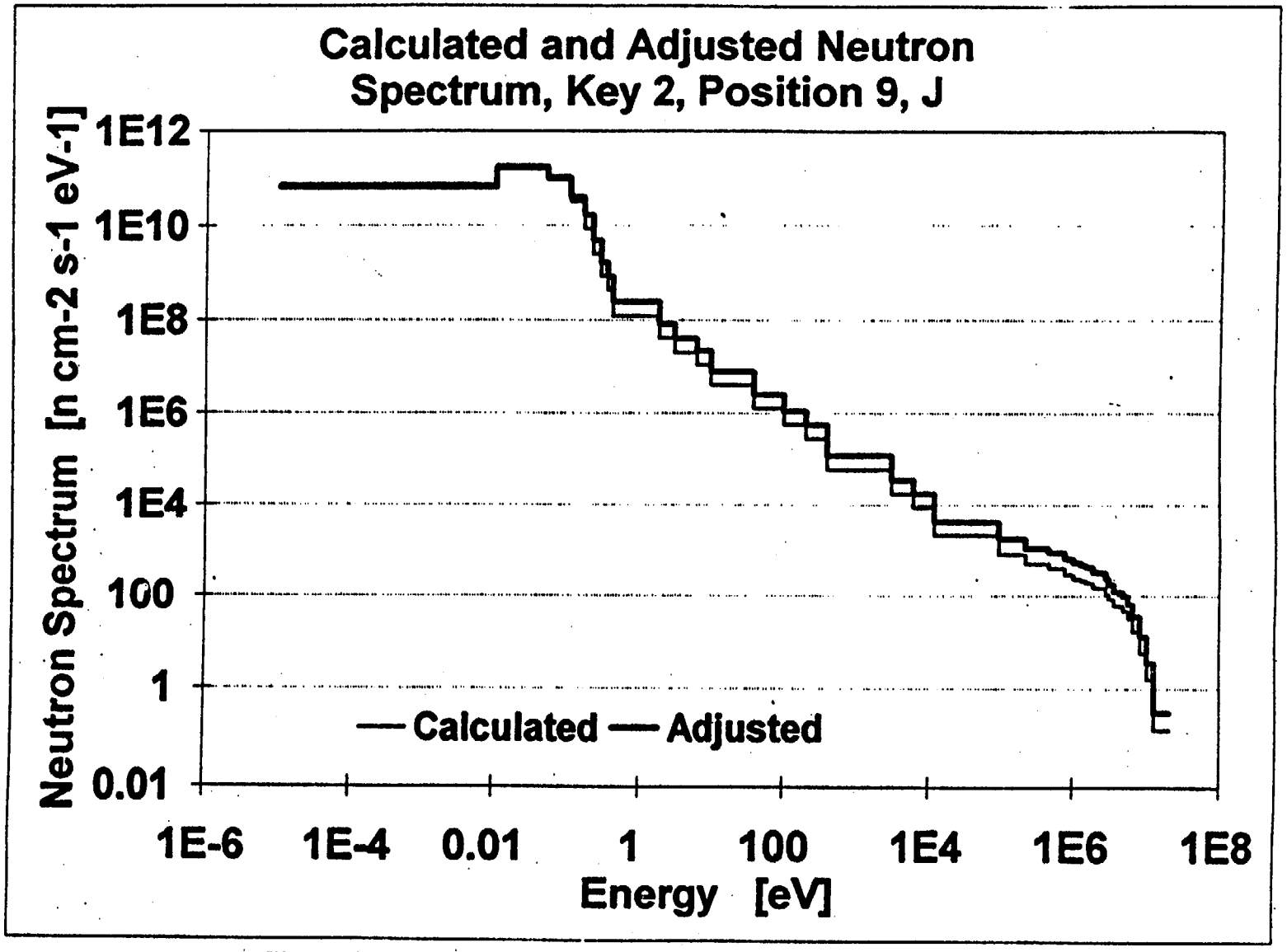

Fig. 6 Calculated and adjusted neutron spectrum, key 2, position 9, J

Fig. 6 Calculated and adjusted neutron spectrum, key 2, position 9, J

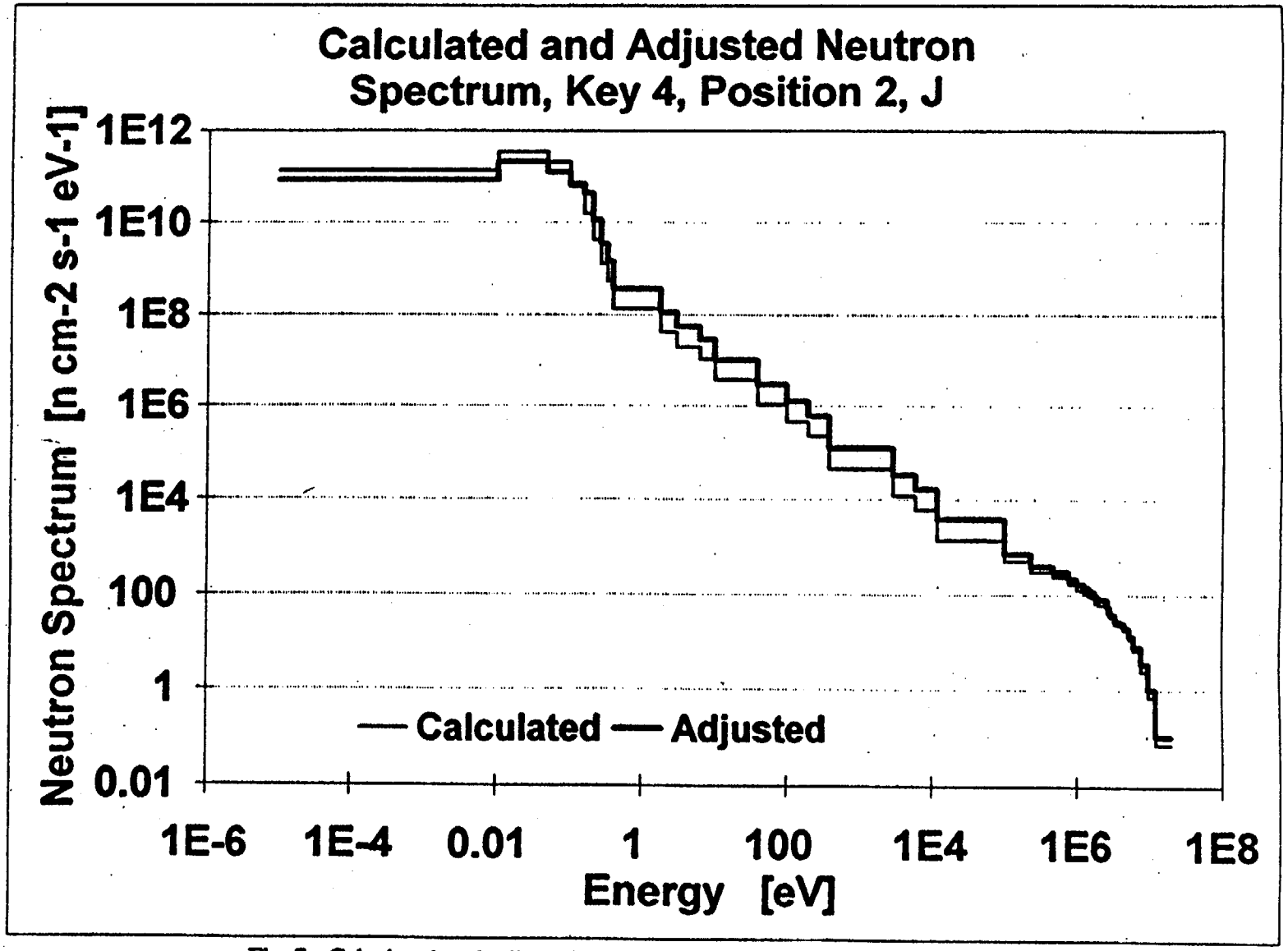

Fig. 7 Calculated and adjusted neutron spectrum, key 4, position 2, J

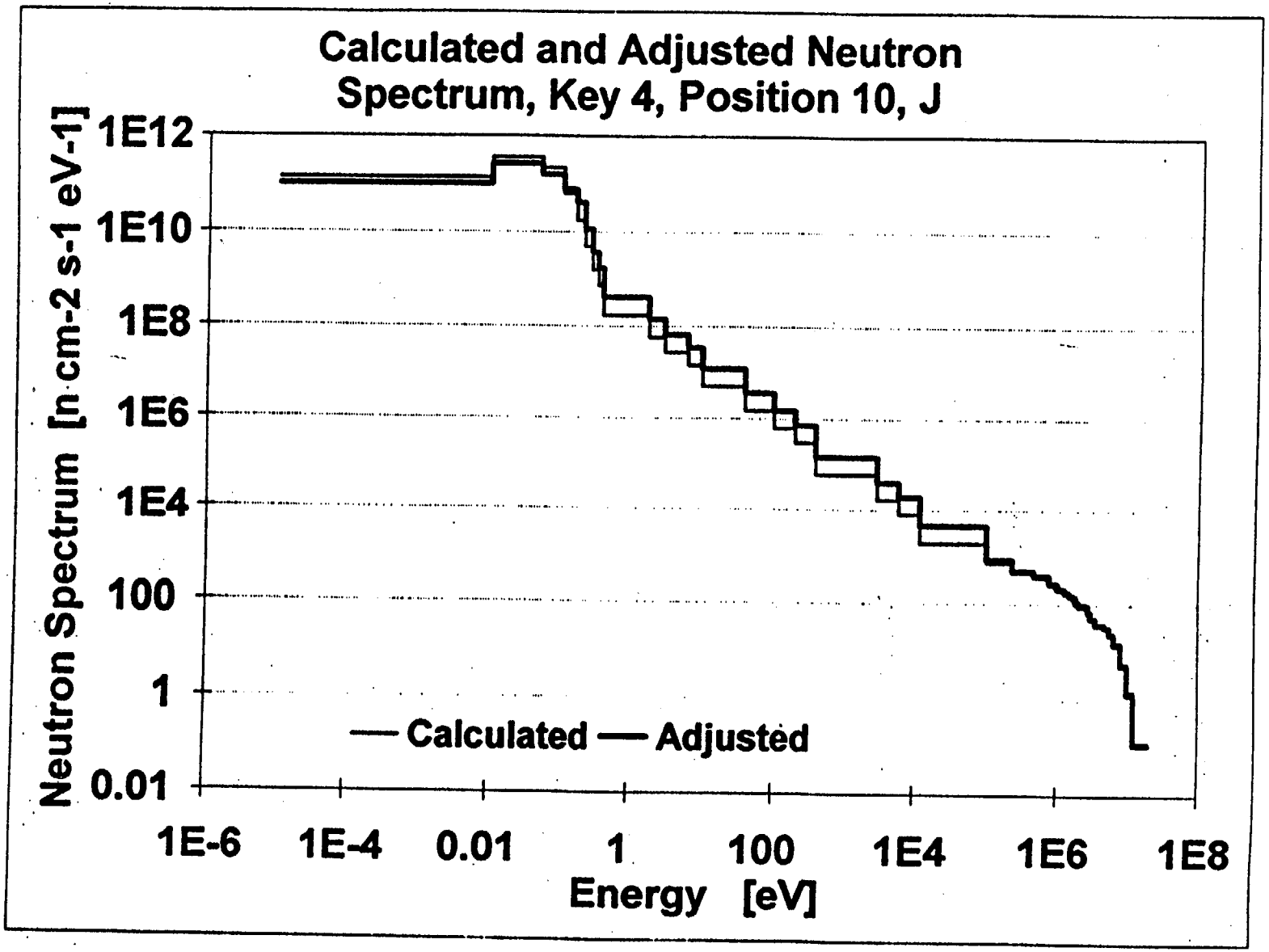

Fig. 8 Calculated and adjusted neutron spectrum, key 4, position 10, J

softer. Neutrons with energies below 0.1 MeV contribute 3%, 9%, 33%, and 30% to the dpa rate for key 7, position 5; key 2, postiion 9; key 4, position 2; and key 4, position 10, respectively. The dpa rate-to-fast-flux ratio is 1.58E-21 cm^2, 1.56E-21 cm^2, 2.15E-21 cm^2, and 2.11E-21 cm^2 for the key 7, position 5, key 2, position 9, key 4, position 2, and key 4, position 10 respectively. Variations in these ratios from one position to the other, which are of about 35%, reflect the considerable differences in the neutron spectrum at different surveillance locations and indicate that besides fast neutrons, lower energy neutrons also contribute significantly to the dpa rate. Therefore, they are included in the calculation of the neutron-induced dpa rate. Besides the above-mentioned differences between surveillance positions analyzed within this work, it needs to be mentioned that for all the locations except at the key 7, position 5, significant variations in the neutron field inside the surveillance capsules were found. In all of the capsules located around the experimental beam tubes, the neutron flux was considerably higher at the capsule end which was closer to the beam tube. This end of the capsule is called bottom, and the opposite end is called top. This notation is used in all of the tables given in the Appendices E, F, G, and H, where the measured activities as well as adjusted irradiation parameters for the locations of gradient wires are given. As mentioned before the gradients inside the key 7, position 5 are insignificant. For the other locations, however, the bottom-to-top ratios are 2.0, 1.8, and 2.0 for the fast flux (E > 1 MeV) and flux over 0.1 MeV, and 3.1, 5.8, and 5.7 for the thermal flux for the key 2, position 9, key 4, position 2, and key 4, position 10 respectively. These variations in the neutron field are very probably caused by the neutrons that leak or are scattered out of the experimental beam tubes. There is no significant gradient in the transverse direction in any of the capsuled analyzed.

These gradients complicate the analysis of the dosimetry experiments, since the calculated spectrum was provided in just one point for each capsule. However, they are not important for the determination of the irradiation parameters based on the activities from the steel monitor wires located in the V-notches of the Charpy specimens in the HFIR surveillance capsules.

5 CONCLUSIONS AND RECOMMENDATIONS

A comprehensive dosimetry experiment was performed at the following HFIR surveillance sites; key 7, position 5, key 4, positions 2 and 10, and key 2, position 9. The results are

1. The best estimates for the fast-neutron flux (E > 1.0 MeV), fast-neutron flux (E > 0.1 MeV), thermal neutron flux (E < 0.4 eV), and displacement rates per atom at the Charpy V-notch in the four capsules analyzed are shown in Table 5.

2. Photo-induced reactions accounted for the discrepancies between the nickel dosimeters and the beryllium and fast-fission threshold dosimeters in the DOS1 experiment. The wide water region between the beryllium reflector and the pressure vessel of the HFIR resulted in the extremely high gamma-to-neutron flux ratios at the surveillance capsules.

3. Insignificant flux gradients were present in key 7, position 5, but the keys adjacent to the beam tubes, key 2 and 4, show substantial fast and thermal neutron flux gradients. The thermal-to-fast ratios at the keys 2 and 4 are significant.*

4. In key 7, position 5, where gamma measurements were made, the dpa rate from gammas is approximately five times higher than the dpa rate from neutrons.

5. Based on the current study, the adjustment procedure using the stainless steel dosimeter in the Charpy V-notch and neutron transport calculations should give reliable fast neutron exposure parameters.**

6. The feasibility of adjusting gamma and neutron fluxes simultaneously was also demonstrated, probably for the first time. This simultaneous adjustment of gamma and neutron spectra adds very important gamma information to the three-step procedure for fluence determination of reactor pressure vessels.

Although it has not been shown that the rapid embrittlement of the HFIR specimens can be attributed to gammas or to neutrons, re-evaluation of mechanical property changes of the specimens in key 7, using the total dpa from gammas and neutrons, may show some interesting results. We believe that the HFIR's special environment, involving extremely high gamma-to-neutron ratios, is probably significantly different from the environment at the support structures of a pressurized water reactor so that any application of the embrittlement data from HFIR should be treated very carefully.

---

*L. K. Mansur and K. Farrell, "On Mechanisms by which a Soft Neutron Spectrum May Induce Accelerated Embrittlement," Journal of Nuclear Materials 170 (1990) 236-245.

**The current experiment showed that reaction rates of Ni-58 and Fe-54 are in agreement with the other dosimeters. In ORNL/TM-10444, page 193, Table E-1 it was shown that the reaction rates from iron and nickel in the 304 stainless steel dosimeter used in the HFIR surveillance capsules were in agreement with the pure iron and nickel dosimeters.

6 REFERENCES

1. R. D. Cheverton, J. G. Merkle, and R. K. Nanstad, eds., "Evaluation of HFIR Pressure-Vessel Integrity Considering Radiation Embrittlement," ORNL/TM-10444, April 1988.

2. W. A. Rhoades and R. L. Childs, "The TORT Three-dimensional Discrete Ordinates Neutron/Photon Transport Code," ORNL-6268, November 1987.

3. N. M. Greene and C. W. Craven, Jr., "XSDRN: A Discrete Ordinate Spectral Averaging Code," ORNL/TM-2500, July 1969.

4. F. W. Stallmann, "LSL-M2: A Computer Program for Least Squares Logarithmic Adjustment of Neutron Spectra," NUREG/CR-4349, ORNL/TM-9933, March 1986.

5. 1992 Annual Book of ASTM Standards, Vol. 12.02, Nuclear, Solar, and Geothermal Energy.

6. F. B. K. Kam et al., "Pressure Vessel Fluence Analysis and Neutron Dosimetry," NUREG/CR-5049, December 1987.

7. R. E. Maerker, M. L. Williams, B. L. Broadhead , J. J. Wagschall, and C. V. Fu, "Revision and Extension of the Data Base in the LEPRICON Dosimetry Methodology," EPRI NP-3841, Electric Power Research Institute, Palo Alto, Calif., January 1985.

8. F. W. Stallmann, "Determination of the Damage Exposure Parameter Values in the PSF Metallurgical Irradiation Experiment," NUREG/CR-3841, ORNL/TM-9166, U.S. Nuclear Regulatory Commission, Washington, D.C., October 1984.

9. V. V. Verbinski et al., "Photointerference Corrections in Neutron Dosimetry for Reactor Pressure Vessel Lifetime Studies," *Nucl. Sci. and Eng.*: 75, pp. 159-166 (1980).

10. E. P. Blizard et al., "Reactor Handbook," Volume III, Part B, Shielding, p. 23.

11. S. I. Warshaw, "4 π Photoneutron Cross-Section for ^{9}Be from Threshold to 16 MeV: Initial Evaluations," Physical Data Note, 14 August 1989.

12. N. P. Baumann, "Gamma-Ray Induced Displacement in D20 Reactors," Proc. Seventh ASTM-Euratom Symposium on Reactor Dosimetry, pp. 689-697, 1992.

APPENDIX A

LETTER REPORT ON NIST SUPPORT

NIST
UNITED STATES DEPARTMENT OF COMMERCE
National Institute of Standards and Technology
Gaithersburg, Maryland 20899

LETTER REPORT ON NIST SUPPORT FOR MEASUREMENT OF NEUTRON AND GAMMA FIELDS AT HIFR SURVEILLANCE CAPSULE LOCATIONS.

E.D. McGarry & J.A. GRUNDL
Neutron Interactions and Dosimetry Group
National Institute for Standards and Technology

Neutron Dosimetry Fluence Standards

NIST has developed and maintains both U-235 and Cf-252 neutron-fission-spectrum fields for irradiations calibration work. The most direct output from these fields is a certified fluence to which a dosimeter was exposed. A natural validation of a dosimeter-response measuring system is to derive a fluence from its evaluation of dosimeter response and compare with the certified value.

Iron and Nickel Neutron Fluence Standards for HFIR

A central issue related to measurement of the radiation fields at the HFIR pressure vessel surveillance capsule locations was that 1992-dosimetry results from fission foils or Helium Accumulation Fluence Monitors did not agree with fluences predicted by threshold (n,p) reactions.

In January 1993 NIST supplied ORNL radioactive disks from U-235 fission spectrum irradiations of the Ni58(n,p)Co58 and Fe54(n,p)Mn54 threshold reactions. In February NIST supplied test reports for these irradiations (see attached reports). Table I compares ORNL and NIST results, which agree within the NIST stated uncertainties.

Np237 Fluence Standard for HFIR

Prior to the DOS-2,-3, and -4 HFIR dosimetry measurements, NIST had received and gamma counted the DOS-1 Np-273 dosimeter. The fission product results agreed within 5 to 7% with those found by ORNL. Along with DOS-1, NIST also received a second Np-237 foil that was unirradiated. It was identified as NIST-1, given a certified U-235 fluence exposure, and supplied to ORNL for additional dosimeter measurement verification, if necessary.

Gamma Dosimetry for HFIR

Gamma dosimetry was accomplished to confirm the unusually large gamma dose predicted by transport calculations at the locations of the Np237 dosimeters, which in turn explains the larger-than-expected response of the Np237(n,f) reaction in HIFR because of photofission in neptunium.

The dosimetry method, suggested and implemented by Dr. William McLaughlin at NIST, was to measure the change in optical absorption in polychlorostyrene film after its exposure to gamma radiation. This gamma dosimeter, developed by Far West Technology Inc., is 25 w/o chlorine, 69 w/o carbon, and 5.8 w/o hydrogen, with a sensitivity range of 2 to 50 kiloGrays. the hydrogen concentration is low to minimize sensitivity to neutrons, which produce knock on protons. Several sets of aluminum wrapped dosimeters, each 1 cm X 1 cm X 0.05 mm, were supplied to ORNL for HIFR irradiation and then returned to NIST. The optical densities were recorded by a spectrophotometer, before and after exposure, and large exposures of 26.0 and 26.4 kiloGray (silicon dose) were reported. See the attached NIST Report of Special Measurements.

Neutron Response of the Gamma Dosimeters

The gamma dosimeters are supposed to have a small neutron sensitivity, However, the data to substantiate this is not readily available; perhaps because of previous security classification (?). Therefore, an additional test of this sensitivity was accomplished at NIST by irradiating the dosimeters in the neutron plus gamma radiation fields near a Cf-252 source.

The neutron-to-gamma fluence-in-air ratio for the source is 4 (in units of neutrons > 1 MeV / gamma > 2 MeV). A pair of dosimeters were mounted on opposite side of the source with a separation distance of 3.8 ±0.15 cm, which represents an average source-to-dosimeter distance of 1.9 cm with an uncertainty of about 15% for the pair response. The dosimeters were exposed to a certified neutron fluence of 3.3E+013 n/cm^2 (E > 1 MeV). This corresponds to a total neutron fluence of 4.8E+013 n/cm^2 ± 20%. The length of the irradiation was 311.2 hours. This total neutron dose corresponds to a total gamma dose of 1.6 kGy in silicon, (which divided by 0.9 is approximately the dose in tissue). The total dose is for no absorber around the gamma dosimeters which were, however, in aluminum. It is known from previous dose measurements with the NIST Cf252 sources that about 0.6 of the total neutron dose is received when the source is enclosed in two millimeters of iron. Assuming that the thicker aluminum around the gamma dosimeters is equivalent, the shielded total gamma dose would be (1.6 x 0.6) = 0.96 kGy Si. The dose measured with the polychlorostyrene gamma dosimeters was 0.90 kGy Si.

Conclusions: The estimated gamma dose from the Californium irradiation conservatively accounts for all of the measured response. For the HFIR exposure, the estimated dose (if it were assumed that all the response were from the Cf252 neutrons) would be 0.003 kGy Si, as compared to the reported 26 kGy Si HFIR dose. However, because of a temperature dependence of polychlorostyrene, shown in Fig. 1, the reported NIST results appear to require an adjustment of about 20% to account for temperature response at a HFIR irradiation temperature of nominally 50 degrees centigrade.

TEST REPORT OF FLUENCE STANDARD MADE IN U235 FISSION SPECTRUM

Fluence Standard # Ni-AK for Ni58(n,p)Co58 Reaction

The subject fluence standard was made in a U235 fission spectrum irradiation that ended 5/24/1991. The irradiation was continuous at steady reactor power. The fluence was monitored by activation of a separate nickel foil that was subsequently counted on a GeLi gamma detector previously calibrated against a known fluence exposure in a Cf252 neutron field.

Irradiation Details:

SOI: 16:15 EST 21 May 1991
EOI: 15:25 EST 24 May 1991
LOI: 2.5620E+05 seconds

	QUANTITY	VALUE	+%
1.	Cf252 Cal of Co-58 [cps/g(Sat)/Cf neut]	1.893E+05	2.8%
2.	1/2" Diam. Nickel Monitor [cps/g @ EOI]	3924.0	0.32%
3.	This Irradiation's Saturation Factor	0.0286	0.15%
4.	Free Field Fluence Rate @ Center of U235 Field [1.893E+05 * (3924/.0286)]	2.597E+10	2.9%
5.	Free Field Fluence @ Dosimeter Nickel AK [2.597E+10 * 1.15 * 2.562E+05]	7.65E+15	3.1%
6.	Mass Nickel AK (grams)	0.2814	0.2%
7.	U235 Cross section of N58(n,p)Co58 (mb)	105.0	2.6%
8.	Ni58(n,p)Co58 Reaction Rate (@ Satuaration) [2.59E+10 * 1.15 * 0.105E-24]	3.14E-15	4.2%*

Note the significant part of the uncertainty in the cross section, which does not come into play until the final conversion to reaction rate.

TEST REPORT OF FLUENCE STANDARD MADE IN U235 FISSION SPECTRUM

Fluence Standard # Fe-B1 for Fe54(n,p)Mn54 Reaction

The subject fluence standard was made in a U235 fission spectrum irradiation that ended 1/13/1991. Except for 23 minutes near the middle of the irradiation when there was a big decrease in power, the irradiation was continuous at steady reactor power. The fluence was monitored by activation of a separate nickel foil that was subsequently counted on a GeLi gamma detector previously calibrated against a known fluence exposure in a Cf252 neutron field.

Irradiation Details:

SOI: 15:38 EST 10 January 1991
EOI: 14:03 EST 13 January 1991
Time at Power: 2.521E+05 seconds

	QUANTITY	VALUE	+%
1.	Cf252 Cal of Co-58 [cps/g(Sat)/Cf neut]	1.893E+05	2.8%
2.	1/2" Diam. Nickel Monitor [cps/g @ EOI]	5275	1.8%
3.	This Irradiation's Saturation Factor	0.02857	0.3%
4.	Free Field Fluence Rate @ Center of U235 Field [1.893E+05 * (5275/1.015)/.02857]	3.43E+10	3.3%
5.	Free Field Fluence @ Dosimeter Iron Fe-B1 [3.43E+10 * 1.056 * 2.521+05]	9.13E+15	3.6%
6.	Mass Iron Fe-B1 (grams)	0.5088	0.15%
7.	U235 Cross section of Fe54(n,p)Mn54 (mb)	81.0	3.0%
8.	Fe54(n,p)Mn54 Reaction Rate (@ Satuaration) [3.43E+10 * 1.056 * 0.081E-24]	2.93E-15	4.7%*

Note the significant part of the uncertainty in the cross section, which does not come into play until the final conversion to reaction rate.

NIST IRON AND NICKEL NEUTRON FLUENCE STANDARDS

MONITOR NUMBER	COUNTING DATE	COUNTING TIME	DET. NUMBER	COUNTING GEOMETRY (mm)	SAMPLE WEIGHT (g)	EOI DATE	EOI TIME	SPECIFIC ACTIVITY at EOI (Bq/g)	1-SIGMA COUNTING ERROR (%)	REACTION RATE	
										ORNL	NIST
NICKEL AK	25-Jan-93	16:27	1	80	0.2814	24-May-91	16:25	6.50E+05	0.4	3.24E-15	3.14E-15
IRON FE-B1	27-Jul-93	18:43	3	102	0.5104	13-Jan-91	14:03	1.17E+04	0.3	2.90E-15	2.93E-15

United States Department of Commerce
National Institute of Standards and Technology
Gaithersburg, MD 20899 USA

REPORT OF SPECIAL MEASUREMENT

OF: HFIR Pressure Vessel
by use of NIST
FWT-67-20 Chlorostyrene Dosimeters

FOR: Oak Ridge National Lab (ORNL)
through
Jim Grundl, Neutron Interactions and Dosimetry Group Leader

ATTN: F. B. Kam
Reference:

DESCRIPTION: Chlorostyrene film packets were sent to ORNL for irradiation in their irradiator. Each packet consisted of three calibrated FWT-67-20 film dosimeters, held inside a 0.015mm layer of aluminum foil. Upon their return to NIST, the dosimeters were analyzed using a Cary 3 spectrophotometer(S/N 1101115, 4.0 nm S.B.W.). Absorbed dose interpretations were made from a calibration of the radiochromic dosimeters performed in June 1993. The results are summarized in the following table.

Dosimeter ID	NIST Interpolated Dose, kGy(D_{si})
31-33	26.0
40-42	26.4

Fig. 1

Temperature Dependence of Solid Phase Chemical Dosimeters.
Curve #5 Refers to Polychlorostyrene with 25 w/o Chlorine.

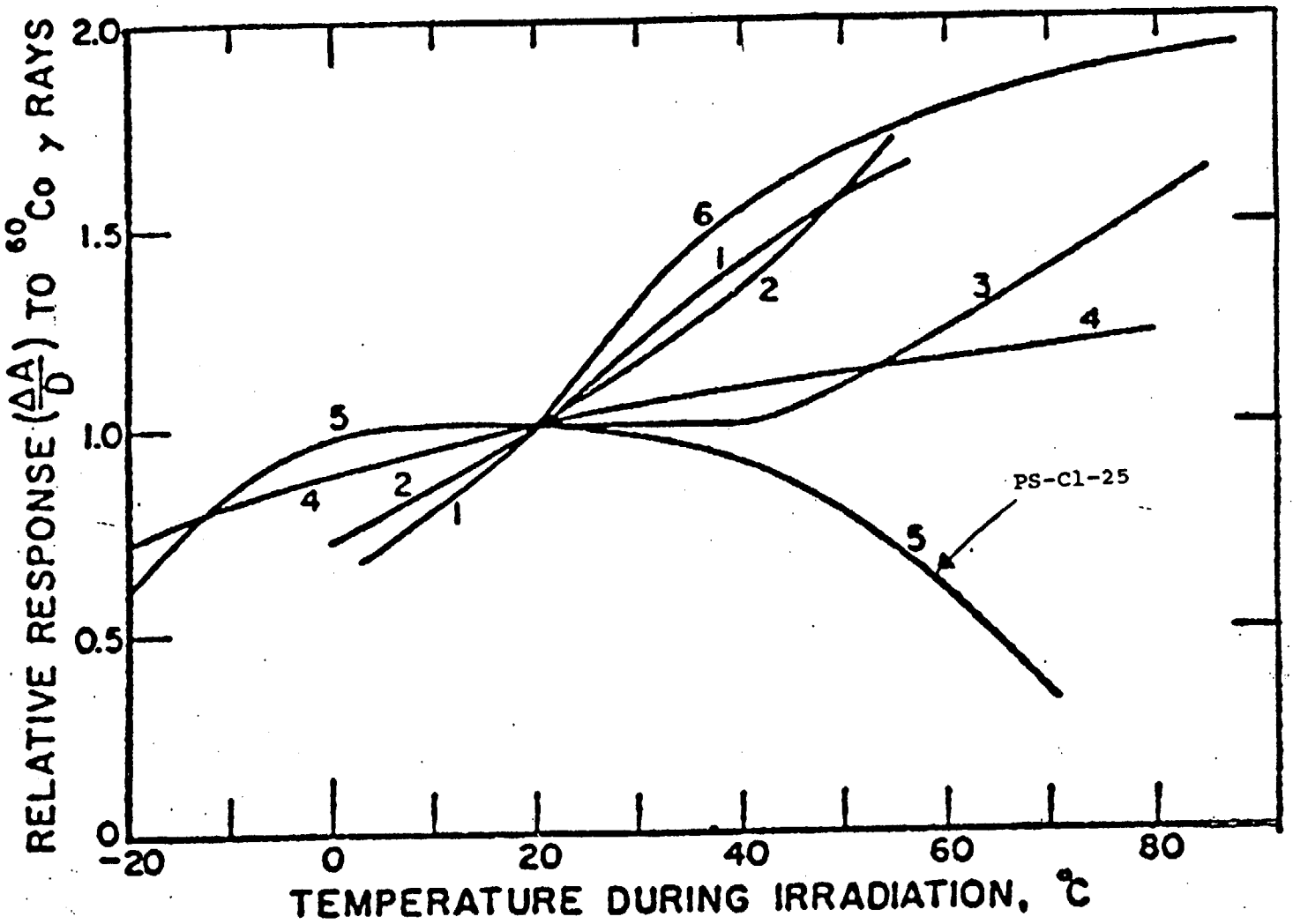

APPENDIX B

HELIUM ANALYSES OF BERYLLIUM HAFMs FROM HFIR: DOS-2/3

Enclosure
92RC00784
April 29, 1993

HELIUM ANALYSES OF BERYLLIUM HAFMs FROM HFIR: DOS-2/3

B. M. Oliver

April 29, 1993

Rockwell International
Rocketdyne Division
6633 Canoga Avenue
Canoga Park, California 91309

Work performed under ORNL Contract 36B-99979V

HELIUM ANALYSES OF BERYLLIUM HAFMs FROM HFIR: DOS-2/3

B. M. Oliver

Rockwell International
Canoga Park, California 91309

A. SUMMARY

Helium concentrations measured in six beryllium metal helium accumulation fluence monitors (HAFMs) irradiated in the High Flux Isotope Reactor (HFIR) at Oak Ridge National Laboratory (ORNL) are reported. The samples were irradiated as part of tests DOS-2 and -3 in the HFIR. The purpose of the tests were to check earlier measured helium generation and activation measurements conducted as part of the DOS-1 dosimetry experiment.

Mean helium concentration values measured in the beryllium HAFMs ranged from 1.51 appb at the Key 4,10 location, to 4.16 appb at the Key 2,9 location. The average measured helium concentration for the three beryllium HAFM sets at the DOS-2/3, Key 7,5 location is 2.73±0.04 appb, which is in excellent agreement with a value of 2.78±0.03 appb measured earlier at the Key 7,5 location in the DOS-1 experiment. Reproducibility between the duplicate analyses averaged 0.8%, very close to the inherent reproducibility of the analysis system.

No difference is observed in the measured helium concentrations for the bare and shielded beryllium HAFMs at the Key 7,5 location, indicating that the correction for small residual boron impurities in the beryllium is small at this location. Additionally, no difference is observed in the measured helium concentrations for the Lot 6 and Lot 7 beryllium material at the Key 7,5 location.

B. HELIUM ANALYSIS SAMPLES

Six sets of helium accumulation fluence monitors irradiated in the HFIR DOS-2 and -3 experiments were received from ORNL for helium analysis. The samples were received in two separate plastic bottles, one containing a single aluminum capsule labeled H56 and the other containing five aluminum capsules labeled H52, H53, H54, H55, and H57. The H56 capsule had been irradiated in a gadolinium cover. The remaining five capsules were irradiated bare.

Each capsule contained two sets of beryllium pieces from Rockwell Lot No. 6 and No. 7. The Lot 7 material had been used in the earlier DOS-1 experiment. Each set had been prepared previously at Rockwell and contained three individual pieces of beryllium metal weighing from 3 to 4 mg each wrapped in aluminum foil. The Lot 7 material was obtained from Electronics Space Products International (ESPI). The material has a stated purity of 99.99%. Previous measurements at Rockwell have indicated a residual helium content in the beryllium material of 0.050±0.030 appb (10^{-9} atom fraction), and a residual boron impurity of 8.9±2.0 wt. ppm (7.4±1.7 appm). The Lot 6 beryllium was obtained from Kawecki Berylco Industries, Inc. The stated beryllium purity is 99.78%. Residual boron content in the material, determined by Rockwell, is 5.6±0.7 wt ppm (4.7± 0.6 appm). No residual helium has been detected in the Lot 6 beryllium.

Five of the six capsules also contained separate lengths of Al-Li and Al-B dosimetry wire. The Al-Li alloy came from Rockwell Lot 5(I) material, originally fabricated by the Central Bureau for Nuclear Measurements (CBNM) at Geel, Belgium.[1] The composition of the Al-Li is Al-0.73±0.01 wt.% Li, with a ^{6}Li content of 95.7±0.1 at.%. The Al-B alloy [Rockwell Lot 6(I)] was also fabricated by CBNM, and has a composition of Al-0.484±0.01 wt.% B, with a ^{10}B content of 19.8 atom %. Capsule H57 did not contain any Al-Li or Al-B material.

Table 1 summarizes the HAFM samples included in each irradiation capsule. The mass values in Table 1 are those measured at ORNL during capsule assembly.

TABLE 1

HELIUM ACCUMULATION FLUENCE MONITORS IN HFIR: DOS-2/3

Capsule	Al-Li Alloy	Al-B Alloy	Be-Lot 6	Be-Lot 7
H52	7.78	8.73	14.85	17.89
H53	7.65	8.69	13.46	15.51
H54	7.38	8.90	17.70	16.90
H55	7.64	8.80	19.81	17.76
H56	7.64	8.76	19.08	18.28
H57	none	none	17.20	19.91

C. SAMPLE PREPARATION

Following identification by package number, each irradiation capsule was opened by cutting off the welded end using a small wire blade saw. The contents of each capsule were removed, and the individual samples identified and placed in separate coin envelopes. The present analysis effort was limited to the Be-Lot 7 samples located in each capsule, and the Be-Lot 6 sample located in Capsule H55.

Each of the analyzed beryllium samples were prepared in the same way. First, the package was carefully unwrapped and the individual beryllium pieces removed. Each piece was then examined under a low-power optical microscope to verify sample integrity, and weighed. The two highest mass pieces were then taken for duplicate helium analysis. Duplicate helium analyses are performed routinely to give an indication of the analysis reproducibility and also to give an indication of the gross helium homogeneity within each sample.

After selection, each beryllium piece was etched to remove ~0.05 mm off the surface. The purpose of the etching step was to remove surface material which could have been affected by α-recoil either into or out of the sample during irradiation. Etching was done in dilute hydrochloric acid (HCl), followed by rinsing in deionized water and then acetone. At intervals during the etching process, the sample was approximately weighted to verify the amount of material removed. Prior to helium analysis, the mass of each beryllium piece was accurately determined using a substitution weighing scheme and mass standards traceable to the National Institute for Standards and Technology (NIST).

D. HELIUM ANALYSIS PROCEDURE

The helium content of each specimen was determined by gas mass spectrometry following vaporization in a resistance-heated tungsten-wire crucible in one of the mass spectrometer system's high-temperature vacuum furnaces.(2) The absolute amount of ^{4}He released was measured relative to a known quantity of added ^{3}He "spike." The ^{3}He spikes were obtained by expanding and partitioning a known quantity of gas through a succession of calibrated volumes.(3) The mass spectrometer was calibrated for mass sensitivity during each series of runs by analyzing known mixtures of ^{3}He and ^{4}He.

E. HELIUM ANALYSIS RESULTS

The results of the helium measurements are given in Table 2, where they are listed as total atoms of helium released and as helium concentrations in atomic parts per billion (10^{-9} atom fraction). Conversion from total helium to helium concentration was based on a calculated value of 6.682 x 10^{22} atoms of beryllium per gram of material.

Two corrections have been applied to the helium data in Table 2. The first correction is to account for the small residual helium content of 0.05±0.03 appb in the Lot 7 material. This value had been determined at Rockwell through previous analysis of numerous unirradiated specimens of the Lot 7 material. During the present analysis series, an additional unirradiated piece of the beryllium was also analyzed and gave a value of 0.053, which is consistent with the previously determined 0.050± 0.030 appb value. Analysis of a single piece of unirradiated Lot 6 beryllium, showed no detectable residual helium (<0.006 appb). For the Lot 7 beryllium, the residual helium correction ranged from ~1.2 to 2.9% of the total helium generation.

The second correction was to account for helium generation from the known small boron impurities in the two beryllium lots (5.6 and 8.9 wt. ppm for Lots 6 and 7 respectively). The correction was calculated using a helium generation value for ^{10}B of 1628 appb, as measured earlier in the Key 7,5 location of the DOS-1 experiment, normalized for the thermal neutron flux at the present HFIR locations. Flux values used in the normalizations were from Pace et al.[4]. The boron impurity corrections ranged from 0.002 appb (~0.1 %) at Key 7,5, to 0.191 appb (~11%) at Key 4,10. No boron correction was applied to Sample H56-Be7, since the H56 irradiation capsule was shielded with gadolinium.

Absolute uncertainty (1σ) in the individual helium analysis results in Table 2, based on the cumulative uncertainties in the sample mass, isotope ratio measurement, and spike size, is estimated to be ~1%. Additional uncertainty from the two corrections applied to the data were discussed above.

F. DISCUSSION OF RESULTS

Mean helium concentration values measured in the DOS-2/3 beryllium HAFMs ranged from 1.51 appb at the Key 4,10 location in HFIR, to 4.16 appb at the Key 2,9 location. Reproducibility between the duplicate analyses averaged 0.8%. This is very close to the inherent reproducibility of the mass spectrometer system (from ~0.4 to 0.5%), and therefore indicates excellent homogeneity and reproducibility in the helium contents.

In addition to the observations noted above, several important additional observations can also be made:

1) The average measured helium concentration for the three beryllium HAFM sets at the DOS-2/3, Key 7,5 location is 2.73±0.04 appb, which is in excellent agreement with a value of 2.78±0.03 appb measured earlier at the Key 7,5 location in the DOS-1 experiment.

2) No significant difference is observed in the measured helium concentrations for the bare and shielded beryllium HAFMs at the Key 7,5 location. This verifies that the correction for small residual boron impurities in the beryllium is small at this location, and further, is introducing negligible additional uncertainty. Boron impurity corrections are somewhat larger at the other irradiation locations due to significantly higher thermal neutron flux levels.

3) No significant difference is observed in the measured helium concentrations for the Lot 6 and Lot 7 beryllium material at the Key 7,5 location. This verifies that there is no systematic effect on the helium generation from any differences which may exist between the two

TABLE 1

HELIUM CONCENTRATIONS IN DOS-2/3 BERYLLIUM SAMPLES

Specimen	HFIR Location	Specimen Mass[a] (mg)	Measured ^{4}He (10^{11} atoms)	Helium Concentration (appm) Measured[b]	Corrected[c]	Average[d]
H52-Be7-A	Key 2,9	2.560	6.154	3.598	3.450	3.45
-B	bare	2.718	6.541	3.602	3.454	±0.00
H53-Be7-A	Key 4,2	2.109	4.054	2.877	2.644	2.61
-B	bare	2.586	4.864	2.815	2.582	±0.04
H54-Be7-A	Key 4,10	2.396	2.833	1.770	1.529	1.51
-B	bare	2.643	3.050	1.727	1.486	±0.03
H55-Be7-A	Key 7,5	2.588	4.773	2.760	2.708	2.69
-B	bare	2.658	4.856	2.734	2.682	±0.02
H55-Be6-A	Key 7,5	2.903	5.289	2.727	2.725	2.73
-B	bare	2.430	4.455	2.744	2.742	±0.01
H56-Be7-A	Key 7,5	2.014	3.789	2.816	2.766	2.77
-B	shielded	2.396	4.522	2.824	2.774	±0.01
H57-Be7-A	Key 2,9	3.985	11.56	4.341	4.193	4.16
-B	bare	3.747	10.72	4.282	4.134	±0.04

[a]Mass uncertainty is ±1 μg.
[b]Helium concentration in atomic parts per million (10^{-6} atom fraction) with respect to the total number of beryllium atoms in the specimen.
[c]Measured helium concentrations corrected for residual helium in the material and for helium generation from small amounts of boron impurity (see text).
[d]Mean and standard deviation (1σ) of Column 6 data.

material lots. This strongly suggests that no unknown impurities are contributing to the observed helium generation.

REFERENCES

1. J. Van Audenhove, Central Bureau for Nuclear Measurements, Geel, Belgium, CBNM Lots SP 3335(I) and SP 3336(I), July, 1979.

2. Harry Farrar IV and B. M. Oliver, "A Mass Spectrometer System to Determine Very Low Levels of Helium in Small Solid and Liquid Samples," J. Vac. Sci. Technol. A4, 1740 (1986).

3. B. M. Oliver, J. G. Bradley, and Harry Farrar IV, "Helium Concentration in the Earth's Lower Atmosphere," Geochim. Cosmochim. Acta 48, 1759 (1984).

4. J. V. Pace III, C. O. Slater, and M. S. Smith, "Letter Report on Beginning-Of-Cycle HFIR Flux/Response Calculations at Keys 2, 4, 5, and 7", July 30, 1992.

APPENDIX C

RESULTS FOR SOLID STATE TRACK RECORDERS

STC REPORT 93-9TD1-ORNLA-R1

NEUTRON DOSIMETRY RESULTS FOR SOLID STATE TRACK RECORDERS IRRADIATED IN THE HIGH FLUX ISOTOPE REACTOR AT OAK RIDGE NATIONAL LABORATORY

F. H. Ruddy, J. G. Seidel, and J. L. Gonzalez
Track Recorder Laboratory

May 24, 1993

Westinghouse STC
1310 Beulah Road
Pittsburgh, Pennsylvania 15235-5098

Westinghouse

Westinghouse

NEUTRON DOSIMETRY RESULTS FOR SOLID STATE TRACK RECORDERS IRRADIATED IN THE HIGH FLUX ISOTOPE REACTOR AT OAK RIDGE NATIONAL LABORATORY

F. H. Ruddy, J. G. Seidel, and J. L. Gonzalez
Track Recorder Laboratory

ABSTRACT

Solid State Track Recorder (SSTR) neutron dosimetry sets exposed in the High Flux Isotope Reactor at Oak Ridge National Laboratory have been analyzed.

Absolute fission rates have been obtained for each of the 12 SSTR neutron dosimeters that were exposed, with 11 out of 12 having uncertainties less than 5%.

Results of physical examination, uniformity analyses, and calibration data review of the ultra low-mass fissionable deposits indicate that all 12 of the deposits are reusable in subsequent dosimetry measurements.

93-9TD1-ORNLA-R1

Westinghouse

Westinghouse

1. INTRODUCTION

Solid State Track Recorder (SSTR) neutron dosimeters were prepared at Westinghouse Science & Technology Center (W STC) under contract to Martin Marietta Energy Systems for exposures at Oak Ridge National Laboratory in the High Flux Isotope Reactor (HFIR). A total of twenty-one ultra low-mass fissionable deposits of ^{235}U, ^{237}Np, and ^{238}U with mica SSTRs were assembled into ten dosimetry packets during November, 1992. The as-built information for these dosimeters is contained in Table 1. Following irradiation of four of these dosimetry packets in the reactor, the dosimeters were retrieved and shipped to W STC for analysis. The SSTR neutron dosimeters were received and disassembled for analyses in March, 1993. Analyses of these SSTR neutron dosimeters have been completed, and the calculated fission reaction rates and associated experimental uncertainties are contained in this report.

Westinghouse

Table 1 SSTR Neutron Dosimetry As-Built Information for HFIR

Location*	Packet Label**	Cover	Deposit Label/SSTR Label ^{235}U	^{237}Np	^{238}U
Key 7, P5	HFIR-1B	Al	W-459/W32-1	---	---
Key 7, P5	HFIR-1C	Gd	W-482/W32-2	W-534/W32-3	W-211/W32-4
Key 4, P2	HFIR-2B	Al	W-433/W32-5	---	---
Key 4, P2	HFIR-2C	Gd	W-462/W32-6	W-535/W32-7	W-201/W32-8
Key 2, P9	HFIR-3B	Al	W-451/W32-9	---	---
Key 2, P9	HFIR-3C	Gd	W-456/W32-10	W-565/W32-11	W-198/W32-12
Key4, P8	HFIR-4B	Al	W-83/W32-13	---	---
Key4, P8	HFIR-4C	Gd	W-75/W32-14	W-564/W32-15	W-200/W32-16
spare	HFIR-5B	Al	W-449/W32-17 W-454/W32-20	---	---
spare	HFIR-5C	Gd	W-500/W32-21	W-554/W32-22	W-217/W32-23

*The SSTR neutron dosimetry packets were designed for irradiations in these locations. However, the actual deployment was different (see text and Table 6).

**Packets labeled B are for bare or Al covered irradiation positions. Packets labeled C are for Gd or Cd covered irradiation positions.

Westinghouse

2. DOSIMETRY SET DESIGN

Isotopic reaction rates for the dosimetry locations were estimated by L. Greenwood[1] using his SCOPER computer code and F. Kam's calculated neutron spectra and ENDF/B-V cross sections (see Appendix A).

These neutron fluences were used to calculate the fissionable deposit masses that would give optimum track densities as a result of exposure to fluences equal to those calculated. Deposit masses were sized to give approximately 20,000 tracks for each location. In addition, a fifth dosimetry set was assembled containing two ^{235}U deposits and ^{238}U and ^{237}Np deposits sized to give useful results if exposed in any of the four locations.

All SSTR dosimetry sets were fabricated and assembled in a dust-free laboratory. Each set was double-wrapped in 0.5 mil Al foil to protect the dosimeters from dust while outside of the laboratory. Even small amounts of dust can lead to fissionable background due to the ubiquitous presence of natural uranium as an impurity at the ppm level. The SSTR dosimetry sets were not designed to be sealed against the incursion of water or other solvents.

Westinghouse

Westi

3. DOSIMETRY SET RECOVERY AND DISASSEMBLY

Four of the SSTR neutron dosimetry packets described in Table 1 were loaded in dosimetry capsules and the capsules were deployed in HFIR. At the end of the irradiation, the dosimeters were removed and the SSTR dosimetry packets were separated and sent to W STC for analysis.

During disassembly of the SSTR neutron dosimetry sets, the initial as-built locations of the mica SSTRs and fissionable deposits listed in Table 1 were verified. No exceptions to the as-built data were noted. However, it was noted during disassembly that the packets had apparently been washed with a solvent, rewrapped, and relabelled. It was determined[2] that, because of HFIR operating rules, the ink from the marker pen used to label the packets had to be removed prior to irradiation. During the course of the washing and relabling, some solvent penetrated into the interior of the packets. Although the packets were dry when received, some smearing of the ink markings on the backs of deposits was noted, particularly in the case of capsule HFIR-1C. Therefore, particular attention was directed to the appearance of the tracks in the SSTRs. The presence of solvent within the SSTR packet during the irradiation would attenuate the ranges of the fission tracks in the SSTRs leading to smaller tracks. Also, damage to the deposits in the form of partial dissolution or contamination by the solvent could result. In all cases, the track sizes appeared normal and the track densities dropped abruptly at the edges of the deposits, indicating that no observable deposit damage or contamination had occurred.

No other evidence of physical damage to any of the SSTR packets was observed, and the overall as-received condition of the sets was good. After disassembly each mica SSTR and fissionable deposit was closely inspected under a microscope for physical damage which may have occurred during exposure or shipment. All deposits and all SSTRs appeared free from detectable physical damage.

Westinghouse

4. SSTR PROCESSING AND ANALYSIS

All 12 SSTRs were etched in 49% HF at 22.0°C for a minimum of one hour. Deposit uniformities were consistent with previous experience in most cases and presented no difficulties for track scanning.

All SSTRs but one were scanned with the W STC Automated Track Scanner[3]; SSTR W32-2 could not be scanned with the automated scanner because of its large track density (greater than 10^6 tracks per cm^2.). This SSTR was subjected to a manual estimating procedure.[4] Although replicate agreement of the two manual scans was within 25%, because of the very high track density the number counted is probably low. Therefore, the fission rate derived from SSTR W32-2 should be regarded as a lower limit. The number of fissions obtained for each SSTR is contained in Table 2. In all cases, at least two independent scans were performed and replicate agreement between the two scans was required. The minimum and maximum track counts obtained were 22,957 and 1,458,815 respectively.

All of the automated track scanning data and scanner operating parameters have been stored on computer disks on a microscope field-of-view by field-of-view basis. A listing of the computer file names corresponding to each SSTR scan is contained in Table 3.

In addition to the data files, in all cases the SSTR itself is being stored as a permanent record of the SSTR neutron dosimetry exposure.

Westinghouse

Table 2. High Flux Isotope Reactor SSTR Scanning Data

SSTR Label	Manual JGS	Manual JLG	Automated Scan 1	Automated Scan 2	Avg*
W32-2	894,006	1,458,815			1.18×10^6 (±24%)
W32-3			329,134	324,793	326,963 (±0.66%)
W32-4			279,720	261,401	270,561 (±3.39%)
W32-6			103,001	99,548	101,274 (±1.70%)
W32-7			96,639	97,404	97,021 (±0.39%)
W32-8			208,906	208,810	208,857 (±0.02%)
W32-10			84,028	83,174	83,601 (±0.51%)
W32-11			75,728	77,114	76,421 (±0.91%)
W32-12			92,338	90,802	91,569 (±0.84%)
W32-14			23,482	22,958	23,220 (±1.13%)
W32-15			67,127	66,782	66,954 (±0.26%)
W32-16			164,865	166,909	165,887 (±0.62%)

* The number in parentheses represents the standard deviation of the average of the results of independent scans of each SSTR.

Westinghouse

Table 3. Permanent Computer Files for the High Flux Isotope Reactor SSTR Scans

SSTR Label	File Name Scan 1	File Name Scan 2
W32-3	HF32-3A	HF32-3D
W32-4	HF32-4A	HF32-4B
W32-6	HF32-6A	HF32-6B
W32-7	HF32-7A	HF32-7B
W32-8	HF32-8A	HF32-8B
W32-10	HF32-10C	HF32-10D
W32-11	HF32-11A	HF32-11B
W32-12	HF32-12A	HF32-12B
W32-14	HF32-14B	HF32-14C
W32-15	HF32-15A	HF32-15B
W32-16	HF32-16A	HF32-16B

Westinghouse

5. SSTR NEUTRON-INDUCED FISSION RATES

The SSTR track counts and the fissionable deposit mass calibration data were used to calculate fission rates in fissions per atom for each of the SSTRs scanned. In all cases, the fissionable deposit mass scales have been renormalized to the results of benchmark irradiations of representative deposits at the National Institute for Standards and Technology (NIST).[7-12]

The measured fission rates are listed in Table 4.

The overall uncertainties were calculated from a quadrature summation of the individual sources of uncertainty listed in Table 5.

After the irradiation it was reported[2] that the intended locations for the SSTR packets that are listed in Table 1 were not used. The SSTR fission reaction rates are listed with the locations actually used in Table 6. The relocation of the SSTR packet HFIR-1C is primarily responsible for the generally high track densities for this packet and the track density exceeding the scannable limit in SSTR W32-2.

In general, the reaction rates measured are higher than calculational estimates[1] prior to the exposures. The track densities obtained were therefore generally higher than anticipated, but still well within the scannable range.

Table 4 High Flux Isotope Reactor SSTR Fission Rates

Packet Label	Isotope	Deposit Label	Mass(ng)	SSTR Label	Number of Fissions*	Fissions/Atom
HFIR-1C	^{235}U	W-482	0.8981(±0.73%)	W32-2	1.18×10^{6}(±24%)**	$>5.1\times10^{-7}$**
	^{237}Np	W-534	7.897(±1.95%)	W32-3	326,963(±0.66%)	1.63×10^{-8}(±2.4%)
	^{238}U	W-211	28.04(±0.64%)	W32-4	270,561(±3.39%)	3.81×10^{-9}(±4.1%)
HFIR-2C	^{235}U	W-462	3.490×10^{-2}(±2.40%)	W32-6	101,274(±1.70%)	1.13×10^{-6}(±3.2%)
	^{237}Np	W-535	3.316(±1.98%)	W32-7	97,021(±0.39%)	1.15×10^{-8}(±2.4%)
	^{238}U	W-201	26.36(±1.77%)	W32-8	208,857(±0.02%)	3.13×10^{-9}(±2.4%)
HFIR-3C	^{235}U	W-456	2.475×10^{-2}(±1.80%)	W32-10	83,601(±0.51%)	1.32×10^{-6}(±2.4%)
	^{237}Np	W-565	2.809(±1.71%)	W32-11	76,421(±0.91%)	1.07×10^{-8}(±2.5%)
	^{238}U	W-198	14.86(±0.40%)	W32-12	91,569(±0.84%)	2.44×10^{-9}(±2.5%)
HFIR-4C	^{235}U	W-75	0.319(±1.00%)	W32-14	23,220(±1.13%)	2.84×10^{-8}(±2.7%)
	^{237}Np	W-564	2.937(±2.08%)	W32-15	66,954(±0.26%)	8.98×10^{-9}(±2.5%)
	^{238}U	W-200	25.43(±0.91%)	W32-16	165,887(±0.62%)	2.58×10^{-9}(±2.4%)

*The number in parentheses is the standard deviation of the average of at least two replicate scans of the same SSTR.

**The track density for this SSTR exceeds the upper limit for accurate track counting. Although a relative standard deviation of 24% was obtained, the track count may be low by as much as a factor of two. Therefore, the derived fission rate should be regarded as a lower limit.

Westinghouse

Table 5. Sources Of Uncertainty In SSTR Neutron-Induced Fission Rate Measurements

Source of Uncertainty	Magnitude (1σ)
1. Track Identification	
Manual Estimate - agreement between independent scanners	25%[4]
Automated	1.0-1.8%[3]
2. Optical Efficiency*	
Manual	0.86%[5]
Automated	1.19%[6]
3. Statistics on number of tracks observed.	$10^2(1/N)^{1/2}$ where N is the number of tracks observed.
4. Deposit Mass Uncertainty (includes uncertainties due to radiometric counting statistics, decay constants, spike ratios, and counter efficiencies).	$\leq$ 4%

* The optical efficiency is the ratio of tracks/cm^2 in an SSTR to fissions/cm^2 in a neighboring thin deposit held in firm contact with the SSTR.

Table 6. SSTR NEUTRON DOSIMETRY RESULTS FOR HFIR

SSTR ID	LOCATION	ISOTOPE	FISSIONS/ATOM
W32-2	K2,P9	^{235}U	$>5.1\times10^{-7}$
W32-3	K2,P9	^{237}Np	1.63×10^{-8} (±2.4%)
W32-4	K2,P9	^{238}U	3.81×10^{-9} (±4.11)
W32-6	K4,P2	^{235}U	1.13×10^{-6} (±3.2%)
W32-7	K4,P2	^{237}Np	1.15×10^{-8} (±2.4%)
W32-8	K4,P2	^{238}U	3.13×10^{-9} (±2.4%)
W32-10	K4,P10	^{235}U	1.32×10^{-6} (±2.4%)
W32-11	K4,P10	^{237}Np	1.07×10^{-8} (±2.5%)
W32-12	K4,P10	^{238}U	2.44×10^{-9} (±2.5%)
W32-14	K7,P5	^{235}U	2.84×10^{-8} (±2.7%)
W32-15	K7,P5	^{237}Np	8.98×10^{-9} (±2.5%)
W32-16	K7,P5	^{238}U	2.58×10^{-9} (±2.4%)

6. SUMMARY

12 SSTR neutron dosimeters were exposed in the High Flux Isotope Reactor and fission rates have been obtained from each SSTR.

Absolute uncertainties on the fission rates are less than 4% in ten out of twelve cases. All 12 deposits were found to be in excellent condition and can be used for subsequent cavity dosimetry measurements.

The relevant analyses data for the High Flux Isotope Reactor SSTR neutron dosimeters will be kept in archival storage. The SSTRs themselves will be stored as permanent records of the dosimetry exposure.

7. REFERENCES

1. L. R. Greenwood, Private Communication (November, 1992).

2. F. B. K. Kam, Private Communication (May, 1993).

3. F. H. Ruddy, A. E. Manhardt, and J. G. Seidel, "Analysis of Solid State Track Recorders with the Westinghouse Research and Development Center Automated Track Counter", Sixth ASTM - Euratom Symposium on Reactor Dosimetry, Jackson, WY, June 1987 ASTM STP-1001, p. 676 1989).

4. F. H. Ruddy and J. H. Roberts, "Solid State Track Recorder Measurements at High Neutron Fluence and High Temperature", Nuclear Tracks and Radiation Measurements 11, 193 (1986).

5. J. H. Roberts, F. H. Ruddy and R. Gold, "Optical Efficiencies for Fission Fragment Track Counting in Muscovite Solid State Track Recorders", Nuclear Tracks and Radiation Measurements", 8, 365 (1984).

6. F. H. Ruddy, "Advances in High Fluence Solid State Track Recorder Neutron Dosimetry", Nuclear Tracks and Radiation Measurements 19, 521 (1991).

7. F. H. Ruddy, "Benchmark Referencing of Babcock & Wilcox Solid State Track Recorder Fissionable Deposits in Standard Neutron Fields", Westinghouse R&D Report 88-2S31-SSTRB-R2, August 5, 1988.

8. F. H. Ruddy and J. G. Seidel, "Solid State Track Recorder Pressure Vessel Surveillance Neutron Dosimetry at Commercial Light Water Reactors," Sixth ASTM-Euratom Symposium on Reactor Dosimetry, Jackson, WY, June 1987 ASTM STP-1001 p. 175 (1989).

9. F. H. Ruddy and E. D. McGarry, "Benchmark Referencing of Ultra Low-Mass Solid State Track Recorder Neutron Dosimetry in NBS Standard Neutron Fields" in Proceedings of IAEA Advisory Group Meeting on Status and Requirements of Nuclear Data for Radiation Damage and Related Safety Aspects, IAEA Press, Vienna (in press) Westinghouse Science & Technology Center Report 89-1S31-RAPRO-P4, August 31, 1989.

10. F. H. Ruddy and E. D. McGarry, "Benchmark Referencing of Solid State Track Recorder Neutron Dosimeters in Standard Neutron Fields" in Proceedings of the Seventh ASTM-Euratom Symposium on Reactor Dosimetry, Strasbourg, France, August 29, 1990, Kluwer Academic Publishers, London, 1992, p 825.

11. F. H. Ruddy and E. D. McGarry, "Solid State Track Recorder Neutron Dosimetry and Its Applications", OECD Nuclear Energy Agency Specialists Meeting on In-Core Instrumentation and Reactor Core Assessment, October 1, 1991 (Proceedings in press), Westinghouse Science & Technology Center Report 91-5TD1-SCANS-P1, September 16, 1991.

12. F. H. Ruddy, "Neutron Dosimetry in High Intensity Fields: A Review", Nuclear Tracks and Radiation Measurements 11, 197 (1986).

APPENDIX A

Reaction Rate Estimates Used for SSTR Neutron Dosimeter Design

Westinghouse

11/09/92 11:40 ☎509 376 1297 ACL 001

Battelle

Pacific Northwest Laboratories
Battelle Boulevard
P.O. Box 999
Richland, WA 99352

FACSIMILE TRANSMITTAL

DATE: November 6, 1992

To: Frank Ruddy
Company: Westinghouse
City/State: Pittsburgh, PA
Facsimile #: 412-256-1007
Telephone #: 412-256-1064

From: Larry Greenwood
Analytical Chemistry Laboratory
Facsimile #: 509-376-1297
Telephone #: 509-376-6918

Transmittal Consists of [2] Page(s) including cover page.

11/09/92 11:41 ☎509 376 1297 ACL 002

Calculated Reaction Rates for HFIR Surveillance Positions

	Key 7, P5	Key 4, P2	Key 2, P1	Key 4, P8
U-235(n,f)	1.76E-13	1.34E-11	7.25E-12	3.97E-12
+Gd	2.40E-15	2.55E-14	2.49E-14	2.33E-14
U-238(n,f)	6.29E-17	1.13E-16	2.72E-16	1.64E-16
Np-237(n,f)	2.37E-16	9.27E-16	1.38E-15	9.43E-16

93-9TD1-ORNLA-R1

APPENDIX D

NEUTRON TRANSPORT CALCULATIONS FOR HFIR

Joseph V. Pace III,[1] Charles O. Slater,[1] Mark S. Smith[1]

THREE-DIMENSIONAL DISCRETE ORDINATES RADIATION TRANSPORT CALCULATIONS OF NEUTRON FLUXES FOR BEGINNING-OF-CYCLE AT SEVERAL PRESSURE VESSEL SURVEILLANCE POSITIONS IN THE HIGH FLUX ISOTOPE REACTOR

REFERENCE: Pace III, J. V., Slater, C. O., Smith, M. S., "Three-Dimensional Discrete Ordinates Radiation Transport Calculations of Neutron Fluxes for Beginning-of-Cycle At Several Pressure Vessel Surveillance Positions in the High Flux Isotope Reactor," Reactor Dosimetry ASTM STP 1228, Harry Farrar IV, E. Parvin Lippincott, and John G. Williams, Eds., American Society for Testing and Materials, Philadelphia, 1994.

ABSTRACT: The objective of this research was to determine improved thermal, epithermal, and fast fluxes and several responses at mechanical test surveillance location keys 2, 4, 5, and 7 of the pressure vessel of the Oak Ridge National Laboratory High Flux Isotope Reactor (HFIR) for the beginning of the fuel cycle. The purpose of the research was to provide essential flux data in support of radiation embrittlement studies of the pressure vessel shell and beam tubes at some of the important locations.

KEYWORDS: radiation damage, radiation transport, reactor pressure vessel, neutron fluxes, damage surveillance, dosimetry

---

The High Flux Isotope Reactor (HFIR) (Fig. 1) at the Oak Ridge National Laboratory began full-power operation in 1966 at 100 MW. As indicated by its name, it has a primary purpose of producing transuranium isotopes for research, industrial and medical applications. Because it has the highest steady-state neutron flux available in any of the world's reactors [1], it can provide for a myriad of other test and experiments in various irradiation facilities throughout the reflector.

The reflector core assembly is located in 2.44-m diameter pressure vessel (Fig. 2), which itself is located in a pool of water. It has a target in the center, inner and outer fuel regions, a reflector composed of removable and permanent beryllium, water, and finally the pressure vessel.

For the first 20 years of HFIR operation, radiation damage was monitored with a vessel-material surveillance program. In November 1986, these tests indicated that the reactor vessel was being embrittled by neutron irradiation faster than previously predicted. After the HFIR was shut down for approximately two years, it was allowed to restart, but with a power of 85 MW.

---

[1]Research staff, Oak Ridge National Laboratory, P.O. Box 2008, Oak Ridge, TN 37831-6363.

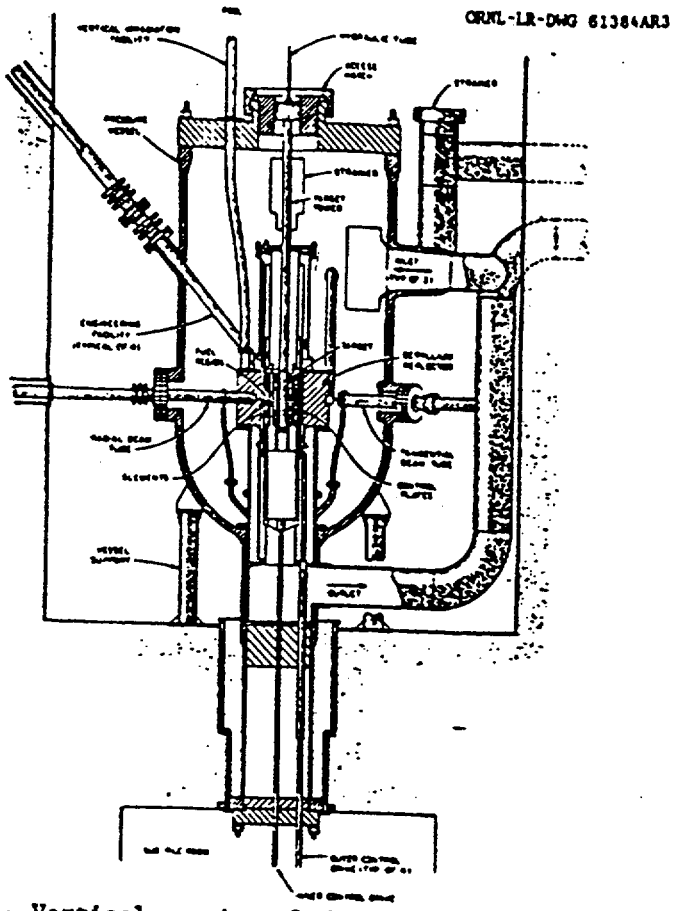

Fig. 1--Vertical section of the HFIR pressure vessel and core.

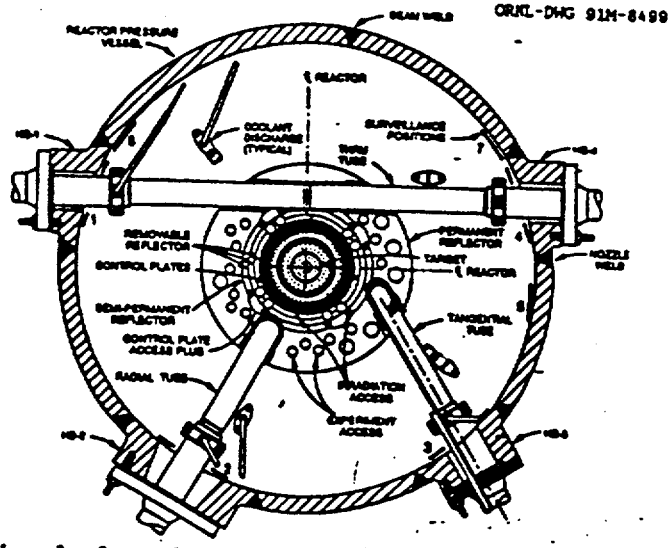

Fig. 2--Sectional plan view of the HFIR target, reactor core, beryllium reflector, coolant, and pressure vessel.

During the two-year shutdown period, extensive studies were undertaken to determine the radiation damage. As part of this effort, reactor fluxes were required to be determined independent of those derived from experiments. Therefore, this study was initiated to determine the thermal, epithermal, and fast beginning-of-cycle (BOC) neutron flux at keys (surveillance positions) 2, 4, 5, and 7 (shown as numbered line segments in Fig. 2) on the pressure vessel of the HFIR. The purpose of the calculations was to aid in determining the reduction in fracture toughness of the HFIR vessel.

CALCULATIONAL PROCEDURE

The procedure to calculate the flux at keys 2, 4, 5, and 7 was to produce a broad-group cross-section set, run a two-dimensional discrete-ordinates calculation to produce directional fluxes throughout the model, produce three-dimensional models which included the keys of interest, and make the three-dimensional calculations. The initial set of calculations was to be made for key 7.

Neutron cross sections required for the calculations were chosen from the 99 neutron group ANSL-V[2] library. One- [3] and two-dimensional [4] HFIR geometry models had been previously constructed for the updated HFIR safety analysis. The one-dimensional model for BOC and the cross-section library were used in the AMPX [5] modules BONAMI, NITAWL, and XSDRNPM to self-shield the cross sections and reduce them to a 64-neutron group structure, which was more economically manageable. This group structure contained 23 energy groups from 20 MeV to 1.07 MeV, 12 groups from 1.07 MeV to 0.1 MeV, 19 groups from 0.1 MeV to 0.397 eV, and 10 groups from 0.397 to 1.0×10^{-5} eV. There were a total of 12 upscatter groups, which covered the energy range 3 to 1.0×10^{-5} eV. The criteria for this broader group cross-section set was that the group fluxes in the water between the permanent beryllium and the pressure vessel could not deviate from the 99-group fluxes by more than five percent at each one-dimensional space mesh.

The 64-group cross sections and the two-dimensional model were input to the DORT code [6] to produce directional fluxes at locations near Key 7. Then the VISTA code [7] reformatted the DORT directional fluxes for input to the DOTTOR code [8]; this code transformed the VISTA flux into a surface boundary source for the three-dimensional discrete-ordinates transport code TORT [9].

A three-dimensional model of the HFIR which contained Beam Tube 4, and thus Keys 4 and 7, had been developed previously [10]. This configuration consisted of a 32x33x6 mesh with X values between 0.0 and 128.52 cm, Y values between -15.24 and 88.96 cm, and Z values between 0.0 and 15.24 cm. The transformed directional fluxes from the two-dimensional calculation were input to the three-dimensional radiation transport code. The boundary sources for TORT using these geometry models were calculated using an S_{10} angular quadrature and a P_3 Legendre expansion cross-section set of the 64 neutron-group library. Calculated three-dimensional flux results at Key 7 indicated that previous calculations in the late 1980's [10] had produced thermal fluxes that were an order of magnitude larger.

At this point, two additional efforts were made to help resolve this anomaly. First, several one-dimensional calculations were made to determine if the present transport or cross sections or both were in error. Second, a dosimetry specimen containing thermal activation material was inserted at Key 7 in the HFIR, since there were no experimental values to compare to the results of the transport calculations.

For the first effort, several one-dimensional calculations were made with the present set of cross sections, with those used previously in the late 1980's [11], and with another set which contained many thermal groups which contained upscatter [12]. The results indicated that the late 1980's set contained thermal cross sections which were not correct. Results from the second effort of the irradiation in the HFIR indicated that the thermal fluxes from the current set of calculations were in much better agreement.

The second model contained beam tube 2 with key 2, which consisted of a 53x16x16 mesh with X values between 27.66 and 127.0 cm, Y values between 0.0 and 20.24 cm, and Z values between 0 and 20.24. The TORT calculations were also performed with the same angular quadrature and cross-section expansion as those for key 7.

The three-dimensional XYZ geometry representation for Key 5 was modeled last. Previous calculations [10] indicated a concern that neutron streaming in beam tube 4 might influence the response at Key 5. Therefore, beam tube 4 was included in the calculational model.

Since the model had to include Key 5, Ionization Chamber 3, and beam tube 4, it was necessary to reduce the amount of data being handled to manageable sizes. Therefore, while the calculation was performed with the 64 neutron-group cross sections, the angular quadrature and the cross-section Legendre expansion were reduced to S_6 and P_1, respectively. The effects which lowering those parameters have on the fluxes at Keys 4 and 5 were studied for the top 52 groups using two-dimensional DORT calculations (thermal neutron fluxes were not calculated due to the additional computational time required for iterating over those groups). The DORT calculations were performed with an angular quadrature and a cross-section Legendre expansion of $S_{10}P_3$, $S_{10}P_1$, and S_6P_1, respectively. The results showed that the largest effect was due to the reduction of the scattering order (fluxes lowered by factors of 1.65 to 1.75 between the $S_{10}P_3$ and $S_{10}P_1$ cases). The overall effect of changing the calculation from $S_{10}P_3$ to S_6P_1 was a nearly uniform factor of 2.0 decrease in the flux at the specimen positions for all 52 groups. It is not certain whether this factor holds for Key 4 locations, where results are influenced greatly by neutron streaming in the beam tube. Nor is it certain that the factor is applicable to the thermal-neutron fluxes. Nevertheless, a factor of 2.0 was applied to the calculated fluxes and responses for the Key 5 positions.

RESULTS

As reported above, a dosimetry experiment was performed in 1992 at a HFIR surveillance location on the vessel wall at the mid-plane of the core. Position 5 (8 total positions) of key 7 (Fig. 2) was chosen as the exposure location for the experiment and corresponds to the fourth position nearest horizontal beam tube 4 which exits the reactor pressure vessel. The dosimetry capsule contained gold, silver, cobalt, nickel, and neptunium activation monitors; additionally, helium accumulation monitors of lithium/aluminum, boron/aluminum, and beryllium were included.

At this location, the measured thermal flux was 2.4×10^{12} neutrons.$m^{-2}.s^{-1}$ versus 3.7×10^{12} neutrons .$m^{-2}.s^{-1}$ from the calculations. The measured fast flux (> 1 MeV) from nickel monitors was 1.5×10^{12} neutrons .$m^{-2}.s^{-1}$ versus 1.2×10^{12} neutrons .$m^{-2}.s^{-1}$ for the calculations. Some of these discrepancies may be due to the calculation being made at the beginning of cycle; future work to reduce the variances will include calculations at the middle-of-cycle and end-of-cycle.

There were very large discrepancies in the measurements of the fast flux from the neptunium and beryllium monitors (2.6×10^{13} neutrons $.m^{-2}.s^{-1}$), a factor of 15 higher than from the nickel monitor. Initially, the problem was investigated by concentrating the effort on neutron contributions to the beryllium monitors from neutrons produced in the beryllium reflectors by gamma rays. Since gamma-ray cross sections were required, a coupled 39-neutron group (subset of the 99-neutron group) and 44-gamma group library was used. Several HFIR one-dimensional coupled neutron-gamma radiation transport calculations were made using the model developed for the cross-section production. This model contained the target area, inner and outer core, removable and permanent beryllium reflectors, water, and pressure vessel. No beam tubes were included since the model was one-dimensional. However, this time a beryllium gamma-neutron (g,n) cross section was included to account for the neutrons produced in the reflectors from gamma rays. The results of these calculations indicated that the neutron flux at the pressure vessel could increase only by about 30 percent, which was insufficient to cause the experimental discrepancy.

From the one-dimensional neutron-gamma calculations, it was noticed that the gamma-ray flux at the pressure vessel was three to four orders of magnitude larger than the neutron flux, with most of the gamma flux coming from the core[13]. The HFIR was constructed such that once gamma-rays had left the core region, the only materials they encountered before the pressure vessel were the beryllium reflectors and the water, all of which were low-Z materials, and thus would not reduce the gamma flux very much. Therefore, the beryllium (g-n) and neptunium-237 gamma-fission (g,f) cross sections were folded with the gamma fluxes, and compared to the beryllium neutron and neptunium-237 neutron-fission (n,f) responses obtained from the neutron fluxes at the pressure vessel. The ratio of the helium production from the beryllium gamma-produced neutron flux to that from the core-produced neutron flux was 80; and the ratio of the neptunium-237 (g,f) response to the neptunium-237 (n,f) at the pressure vessel was 50. Thus, it appeared very possible that the increase in the helium production in beryllium and the increase in the neptunium-237 fission response in the monitors at the pressure vessel was due to the high gamma flux at that location, and thus the experimental flux values could not be compared with the calculated values. Additional experimental verification of this would be undertaken separately.

CONCLUSION

Neutron fluxes have been calculated using the three-dimensional discrete-ordinates code TORT for HFIR keys 2, 4, 5, and 7. For the only position where measurements were made, the three-dimensional neutron transport calculations have yielded results that are about 50 percent high in the thermal range and 20 percent low in the fast range. While some activation measurements yielded inconsistent flux values, the inconsistencies have partially been explained by gamma-ray interactions in the foil or neutron production by gamma-ray interactions near the vessel.

REFERENCES

[1] Pamphlet titled "High Flux Isotope Reactor", Oak Ridge National Laboratory, P.O. Box 2008, Oak Ridge, TN 37831-6387, July 1991.

[2] W.E. Ford, et al, "ANSL-V: ENDF/B-V Based Multigroup Cross-Section Libraries for Advanced Neutron Source (ANS) Reactor Studies,"Oak Ridge National Lab, ORNL-6618, 1990.

[3] R.T. Primm III, "Reactor Physics Input to the Safety Analysis Report for the High Flux Isotope Reactor", Oak Ridge National Lab, ORNL/TM-11956, October 1991.

[4] W.W. Engle, RZ Base Case, Shielding Input to the HFIR SAR, EPM.HFIR.91.001, Jun 1991.

[5] N.M. Greene, et al, "AMPX-77: A Modular Code System for Generating Coupled Multigroup Neutron-Gamma Cross-Section Libraries form ENDF/B-IV and/or ENDF/B-V", Oak Ridge National Lab, ORNL/CSD/TM-283, October 1992.

[6] W.A. Rhoades and R.L. Childs, "The DORT Two-Dimensional Discrete Ordinates Transport Code, "Nucl. Sci. & Engr. 99, 1, 88-89, May 1988.

[7] W.A. Rhoades, et al, "Vehicle Code System (VCS) User's Manual", Oak Ridge National Lab, ORNL-TM-4648, Aug 1974.

[8] J.L. Thompson, et al, "Development and Evaluation of DOTTOR, a Computer Code to Couple Two-Dimensional to Three-Dimensional Discrete Ordinates Calculations", Oak Ridge National Lab, ORNL/TM-9919, 1986.

[9] W.A. Rhoades and R.L. Childs, "The TORT Three-Dimensional Discrete Ordinates Neutron/Photon Transport Code", Oak Ridge National Lab, ORNL-6268, Nov 1987.

[10] R.L. Childs, W. A. Rhoades, and L.R. Williams, "Three-Dimensional Calculations of Neutron Streaming in the Beam Tubes of the ORNL HFIR Reactor", Proceedings, 7th International Conference on Radiation Shielding, VOL II, Sept. 1988.

[11] "The ELXSIR Cross-Section Library for LWR Pressure Vessel Irradiation Studies: Part of the LEPRICON Computer Code System", Oak Ridge National Lab, EPRI NP-3654, 1984.

[12] "SCALE: A Modular Code System for Performing Standardized Computer Analyses for Licensing Evaluation," NUREG/CR-0200 Rev. 4 (ORNL/NUREG/CSD-2/R4) Excerpts from Vols. I, II, and III, (Draft March 1992).

[13] I. Remec, F. Kam, "HFIR Neutron Spectra Determination," DRAFT NUREG/CR to be published.

APPENDIX E

RESULTS FOR KEY 7, POSITION 5

EXPLANATION OF THE TABLES AND FIGURES IN THE APPENDICES E-H

Table E.1 Lists the irradiation parameters for the 10 locations considered in the adjustment.

The tabulated quantities are:

Calculated	- quantities obtained from 3-D transport calculation
Value	- value of the parameter
STD	- standard deviation in percent
Adjusted	- quantities obtained after adjustment
Value	- value of the parameter
STD	- standard deviation in percent
Scale Fact.	- factor by which the calculated spectrum is scaled at the particular location
Adj. Fact.	- factor by which the parameter is changed due to "true" adjustment of the spectrum
Adj/Calc.	- ratio of adjusted to calculated value of the parameter. Also equal to the product of the scale and adjustment factor as defined above.

Table E.2 First column at the left gives the reaction identifier.

M measured reaction rate in reaction per second per atom, as were used in the adjustment runs. All necessary corrections are already included in the values listed. For key 7, position 5 listed values of fission and Be dosimeters contain correction for the contributions from gamma induced reactions. Self-shielding corrections for Co and Au monitors are also included.

C/M indicates calculated-to-measured reaction rate ratios. Calculated means as obtained by folding activation cross sections with the neutron fluxes form the 3-D calculation.

A/M is the ratio of adjusted-to-measured reaction rates. Adjusted reaction rates are obtained by folding the adjusted neutron fluxes with the activation cross sections.

Table E.3 Lists the group structure and neutron group fluxes as calculated, that is as obtained from 3-D transport calculation (column labeled "Calculated") and as obtained from adjustment (column labeled "Adjusted"). The spectrum is given for the position of slot J, which corresponds to the middle of the capsule, that is to the position of V-notch tips of the Charpy specimens in the surveillance capsules.

Fig. E.1 and E.2 give the neutron multigroup spectra as obtained from 3-D calculations "Calculated" and from the adjustment run "Adjusted," for the slot D and slot A in the dosimetry capsule.

NOTE: The equivalent set of Tables and Figures is presented in Appendices F, G, and H for the other three surveillance locations considered in the analysis.

Table E.1 Calculated and adjusted irradiation parameters, key 7, position 5

	Calculated Value*	Calculated Std.%	Adjusted Value	Adjusted Std. %	Scale Fact.	Adj. Fact.	Adj./ Calc.
Slot D							
F > 1MeV	1.17E+08	± 38	1.55E+08	± 6	1.290	1.03	1.33
F > 0.1MeV	1.75E+08	± 38	2.29E+08	± 9	1.290	1.01	1.31
F < 0.4 eV	3.97E+08	± 137	2.84E+08	± 5	1.290	0.55	0.71
dpa/s	1.82E-13	± 37	2.42E-13	± 5	1.290	1.03	1.33
Slot J							
F > 1MeV	1.17E+08	± 38	1.49E+08	± 6	1.421	0.90	1.28
F > 0.1MeV	1.75E+08	± 38	2.24E+08	± 9	1.421	0.90	1.28
F < 0.4 eV	3.97E+08	± 137	3.09E+08	± 19	1.421	0.55	0.78
dpa/s	1.82E-13	± 37	2.36E-13	± 5	1.421	0.91	1.30
Slot B							
F > 1MeV	1.17E+08	± 38	1.50E+08	± 6	1.305	0.99	1.29
F > 0.1MeV	1.75E+08	± 38	2.25E+08	± 8	1.305	0.98	1.28
F < 0.4 eV	3.97E+08	± 137	2.74E+08	± 7	1.305	0.53	0.69
dpa/s	1.82E-13	± 37	2.35E-13	± 5	1.305	0.99	1.29
Slot A							
F > 1MeV	1.17E+08	± 38	1.58E+08	± 7	1.395	0.97	1.36
F > 0.1MeV	1.75E+08	± 38	2.36E+08	± 10	1.395	0.97	1.35
F < 0.4 eV	3.97E+08	± 137	2.88E+08	± 4	1.395	0.52	0.73
dpa/s	1.82E-13	± 37	2.47E-13	± 6	1.395	0.97	1.36
Slot ET							
F > 1 MeV	1.17E+08	± 38	1.54E+08	± 7	1.351	0.98	1.32
F > 0.1 MeV	1.75E+08	± 38	2.30E+08	± 10	1.351	0.97	1.31
F < 0.4eV	3.97E+08	± 137	2.99E+08	± 6	1.351	0.56	0.75
dpa/s	1.82E-13	± 37	2.41E-13	± 6	1.351	0.98	1.32
Slot EM							
F > 1 MeV	1.17E+08	± 38	1.56E+08	± 7	1.370	0.98	1.34
F > 0.1 MeV	1.75E+08	± 38	2.33E+08	± 10	1.370	0.97	1.33
F < 0.4eV	3.97E+08	± 137	2.73E+08	± 6	1.370	0.50	0.69
dpa/s	1.82E-13	± 37	2.44E-13	± 6	1.370	0.98	1.34

Table E.1 (continued)

	Calculated Value*	Std.%	Adjusted Value	Std. %	Scale Fact.	Adj. Fact.	Adj./ Calc.
Slot EB							
F > 1 MeV	1.17E+08	± 38	1.57E+08	± 7	1.387	0.97	1.35
F > 0.1 MeV	1.75E+08	± 38	2.35E+08	± 10	1.387	0.96	1.34
F < 0.4eV	3.97E+08	± 137	2.71E+08	± 6	1.387	0.49	0.68
dpa/s	1.82E-13	± 37	2.46E-13	± 6	1.387	0.97	1.35
Slot FT							
F > 1 MeV	1.17E+08	± 38	1.51E+08	± 7	1.319	0.98	1.29
F > 0.1 MeV	1.75E+08	± 38	2.25E+08	± 10	1.319	0.97	1.28
F < 0.4eV	3.97E+08	± 137	2.86E+08	± 6	1.319	0.55	0.72
dpa/s	1.82E-13	± 37	2.36E-13	± 6	1.319	0.98	1.30
Slot FM							
F > 1 MeV	1.17E+08	± 38	1.58E+08	± 7	1.375	0.99	1.36
F > 0.1 MeV	1.75E+08	± 38	2.36E+08	± 10	1.375	0.98	1.35
F < 0.4eV	3.97E+08	± 137	2.63E+08	± 6	1.375	0.48	0.66
dpa/s	1.82E-13	± 37	2.47E-13	± 6	1.375	0.99	1.36
Slot FB							
F > 1 MeV	1.17E+08	± 38	1.61E+08	± 7	1.405	0.98	1.38
F > 0.1 MeV	1.75E+08	± 38	2.40E+08	± 10	1.405	0.97	1.37
F < 0.4eV	3.97E+08	± 137	2.84E+08	± 6	1.405	0.51	0.71
dpa/s	1.82E-13	± 37	2.52E-13	± 6	1.405	0.98	1.38

* Units are neutrons . cm^2. s^{-1} for F>1 MeV, F>0.1 MeV, F<0.4 eV, and s^{-1} for dpa rate (dpa/s).

Table E.2 Measured reaction rates, C/M, and A/M ratios, key 7, position 5

Reaction	M*	C/M	A/M
Slot D			
Al-27 (n,a) Na-24 [Bare]	1.304E-18	0.63	1.05
Al-27 (n,a) Na-24	1.305E-18	0.63	1.05
Ti-48 (n,p) Sc-48 [Bare]	5.854E-19	0.52	0.85
Ti-48 (n,p) Sc-48	4.948E-19	0.61	1.01
Cu-63 (n,a) Co-60 [Bare]	6.548E-19	0.66	1.04
Cu-63 (n,a) Co-60	6.255E-19	0.69	1.08
Ti-46 (n,p) Sc-46 [Bare]	9.759E-18	0.59	0.88
Ti-46 (n,p) Sc-46	8.817E-18	0.65	0.97
Fe-54 (n,p) Mn-54 [Bare]	3.290E-17	0.76	1.06
Fe-54 (n,p) Mn-54	3.406E-17	0.73	1.02
Ti-47 (n,p) Sc-47 [Bare]	7.638E-18	0.67	0.95
Ti-47 (n,p) Sc-47	6.890E-18	0.75	1.05
Fe-58 (n,g) Fe-59 [Bare]	2.904E-16	1.45	1.04
Fe-58 (n,g) Fe-59	1.734E-17	1.61	0.99
Sc-45 (n,g) Sc-46 [Bare]	6.328E-15	1.38	0.99
Sc-45 (n,g) Sc-46	2.367E-16	1.69	1.04
Ni-58 (n,p) Co-58	4.413E-17	0.72	1.00
Co-59 (n,g) Co-60	6.608E-16	1.62	0.97
Np-237 (n,f)	3.061E-16	0.74	0.98
Slot J			
U-235 (n,f)	1.233E-14	0.66	0.96
U-238 (n,f)	7.496E-17	0.83	1.09
Np-237 (n,f)	2.917E-16	0.77	1.00
Be (n,x) He	6.639E-17	1.14	1.50
Be (n,x) He	6.526E-17	1.16	1.53
Be (n,x) He	6.431E-17	1.18	1.55
Co-59 (n,g) Co-60 [Bare]	8.441E-15	1.48	1.16
Ni-58 (n,p) Co-58 [Bare]	4.485E-17	0.71	0.94
Ni-58 (n,p) Co-58	4.465E-17	0.71	0.95
Slot B			
U-235 (n,f) Ba-140	6.576E-15	1.24	1.03
U-235 (n,f) Zr-95	6.828E-15	1.19	0.99
U-238 (n,f) Ba-140	8.852E-17	0.71	0.93
U-238 (n,f) Ru-103	8.075E-17	0.77	1.02
Np-237 (n,f) Ba-140	2.919E-16	0.77	1.00
Np-237 (n,f) Zr-95	3.090E-16	0.73	0.94
Li-6 (n,a) H-3 [Bare]	2.035E-13	1.48	1.01
B-10 (n,a) Li-7 [Bare]	8.540E-13	1.44	0.99
Be (n,x) He	6.612E-17	1.15	1.50

Table E.2 (continued)

Reaction	M*	C/M	A/M
Slot A			
Ni-58 (n,p) Co-58 [Bare]	4.296E-17	0.74	1.04
Ni-58 (n,p) Co-58	4.632E-17	0.68	0.96
Co-59 (n,g) Co-60 [Bare]	8.946E-15	1.40	1.01
Co-59 (n,g) Co-60	1.045E-15	1.02	1.02
Au-197 (n,g) Au-198 [Bare]	3.998E-14	1.14	0.92
Au-197 (n,g) Au-198 [Bare]	3.886E-14	1.17	0.95
Co-59 (n,g) Co-60 [Bare]	8.880E-15	1.41	1.02
Ni-58 (n,p) Co-58 [Bare]	4.483E-17	0.71	0.99
Slot ET			
Ni-58 (n,p) Co-58 [Bare]	4.422E-17	0.72	0.98
Ni-58 (n,p) Co-58	4.332E-17	0.73	1.00
Co-59 (n,g) Co-60 [Bare]	9.376E-15	1.33	1.00
Co-59 (n,g) Co-60	9.980E-16	1.07	1.00
Slot EM			
Ni-58 (n,p) Co-58 [Bare]	4.444E-17	0.71	0.99
Ni-58 (n,p) Co-58	4.439E-17	0.71	0.99
Co-59 (n,g) Co-60 [Bare]	8.535E-15	1.46	1.01
Co-59 (n,g) Co-60	9.967E-16	1.07	1.00
Slot EB			
Ni-58 (n,p) Co-58 [Bare]	4.547E-17	0.70	0.97
Ni-58 (n,p) Co-58	4.393E-17	0.72	1.01
Co-59 (n,g) Co-60 [Bare]	8.422E-15	1.48	1.01
Co-59 (n,g) Co-60	1.065E-15	1.00	1.00
Slot FT			
Ni-58 (n,p) Co-58 [Bare]	4.355E-17	0.73	0.98
Ni-58 (n,p) Co-58	4.236E-17	0.75	1.00
Co-59 (n,g) Co-60 [Bare]	8.978E-15	1.39	1.00
Co-59 (n,g) Co-60	9.481E-16	1.13	1.01
Slot FM			
Ni-58 (n,p) Co-58 [Bare]	4.525E-17	0.70	0.99
Ni-58 (n,p) Co-58	4.491E-17	0.71	0.99
Co-59 (n,g) Co-60 [Bare]	8.228E-15	1.52	1.01
Co-59 (n,g) Co-60	9.420E-16	1.13	1.01
Slot FB			
Ni-58 (n,p) Co-58 [Bare]	4.591E-17	0.69	0.99
Ni-58 (n,p) Co-58	4.562E-17	0.69	0.99
Co-59 (n,g) Co-60 [Bare]	8.880E-15	1.41	1.01
Co-59 (n,g) Co-60	9.986E-16	1.07	1.01

*Reactions per second per atom

Table E.3 Calculated and adjusted neutron group fluxes, key 7, position 5, slot J

Group	Group Upper Energy Boundary* [eV]	Neutron Group Fluence Rate Calculated**	Adjusted**
1	2.000E+07	6.263E+05	1.087E+06
2	1.271E+07	2.016E+06	3.399E+06
3	1.013E+07	5.119E+06	8.408E+06
4	8.072E+06	1.016E+07	1.398E+07
5	6.434E+06	8.829E+06	1.150E+07
6	5.523E+06	1.037E+07	1.301E+07
7	4.742E+06	9.503E+06	1.193E+07
8	4.071E+06	7.303E+06	8.687E+06
9	3.495E+06	8.207E+06	9.697E+06
10	3.000E+06	5.729E+06	7.005E+06
11	2.724E+06	1.719E+07	2.126E+07
12	2.038E+06	4.511E+06	5.608E+06
13	1.850E+06	5.583E+06	6.937E+06
14	1.655E+06	5.104E+06	6.343E+06
15	1.480E+06	6.272E+06	7.801E+06
16	1.282E+06	9.993E+06	1.248E+07
17	1.000E+06	1.031E+07	1.302E+07
18	7.653E+05	1.709E+07	2.169E+07
19	4.704E+05	1.711E+07	2.162E+07
20	2.297E+05	1.425E+07	1.866E+07
21	1.000E+05	2.366E+07	4.016E+07
22	1.202E+04	6.436E+06	1.092E+07
23	6.004E+03	6.340E+06	1.076E+07
24	3.000E+03	1.818E+07	3.086E+07
25	3.911E+02	6.037E+06	1.025E+07
26	1.978E+02	6.053E+06	1.027E+07
27	1.000E+02	8.554E+06	1.452E+07
28	3.817E+01	1.189E+07	2.019E+07
29	1.000E+01	4.289E+06	7.279E+06
30	6.178E+00	6.385E+06	1.084E+07
31	3.000E+00	4.887E+06	8.293E+06
32	1.770E+00	1.500E+07	2.546E+07
33	3.970E-01	2.253E+06	3.824E+06
34	3.300E-01	2.910E+06	4.939E+06
35	2.700E-01	5.131E+06	8.708E+06
36	2.150E-01	1.283E+07	2.178E+07
37	1.620E-01	4.591E+07	4.626E+07
38	1.040E-01	1.392E+08	9.470E+07
39	5.000E-02	1.719E+08	1.170E+08
40	1.000E-02	1.682E+07	1.145E+07
	1.000E-05***		

*Energy in eV
**Group fluxes in neutrons cm^{-2}. s^{-1}
***Lower energy boundary of 40th group

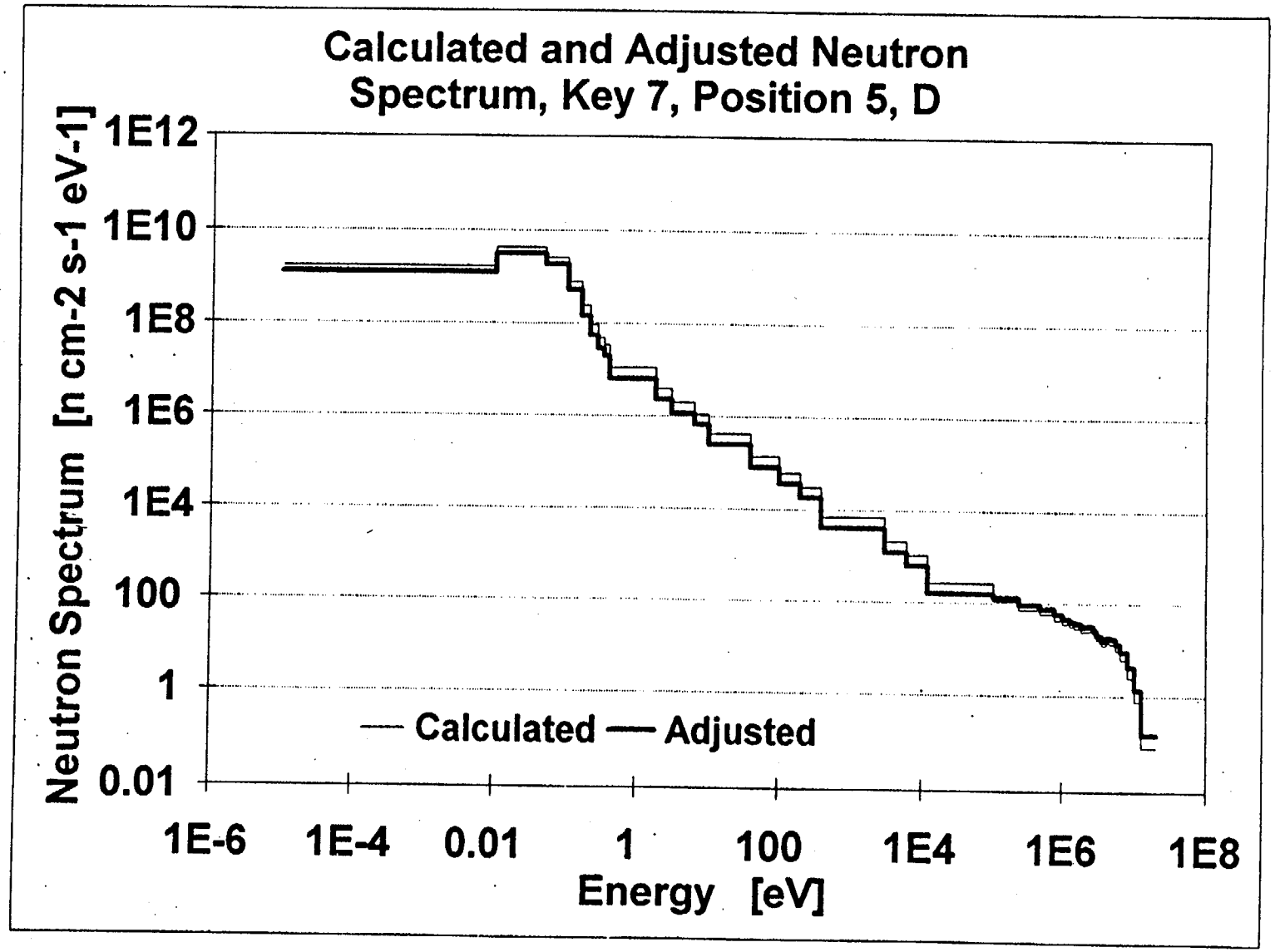

Fig. E.1 Calculated and adjusted neutron spectrum, key 7, position 5, D

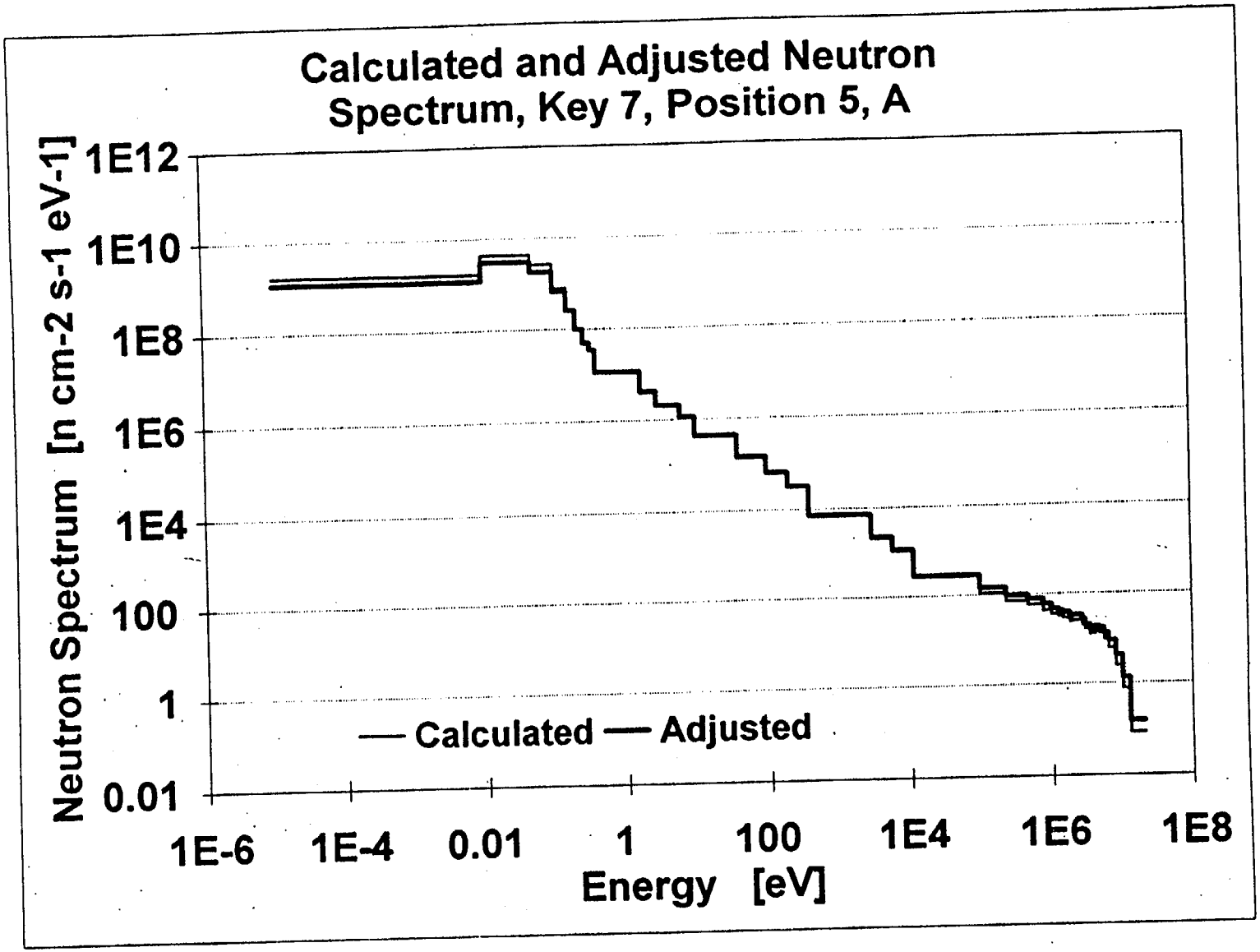

Fig. E.2 Calculated and adjusted neutron spectrum, key 7, position 5, A

APPENDIX F

RESULTS FOR KEY 2, POSITION 9

Table F.1 Calculated and adjusted irradiation parameters, key 2, position 9

	Calculated Value*	Calculated Std.%	Adjusted Value	Adjusted Std. %	Scale Fact.	Adj. Fact.	Adj./ Calc.
Slot D							
F > 1MeV	5.67E+08	± 38	8.81E+08	± 8	1.357	1.15	1.55
F > 0.1MeV	9.79E+08	± 38	1.51E+09	± 12	1.357	1.13	1.54
F < 0.4 eV	1.67E+10	± 139	9.38E+09	± 5	1.357	0.41	0.56
dpa/s	9.72E-13	± 41	1.34E-12	± 6	1.357	1.01	1.38
Slot J							
F > 1MeV	5.67E+08	± 38	1.21E+09	± 9	2.123	1.01	2.14
F > 0.1MeV	9.79E+08	± 38	2.11E+09	± 12	2.123	1.01	2.15
F < 0.4 eV	1.67E+10	± 139	1.61E+10	± 6	2.123	0.45	0.96
dpa/s	9.72E-13	± 41	1.89E-12	± 7	2.123	0.92	1.95
Slot B							
F > 1MeV	5.67E+08	± 38	1.12E+09	± 39	1.950	1.01	1.98
F > 0.1MeV	9.79E+08	± 38	1.94E+09	± 40	1.950	1.02	1.98
F < 0.4 eV	1.67E+10	± 139	1.55E+10	± 41	1.950	0.47	0.92
dpa/s	9.72E-13	± 41	1.75E-12	± 31	1.950	0.92	1.80
Slot A							
F > 1MeV	5.67E+08	± 38	1.74E+09	± 9	3.223	0.95	3.07
F > 0.1MeV	9.79E+08	± 38	3.05E+09	± 12	3.223	0.97	3.11
F < 0.4 eV	1.67E+10	± 139	3.24E+10	± 6	3.223	0.60	1.94
dpa/s	9.72E-13	± 41	2.82E-12	± 7	3.223	0.90	2.90
Slot ET							
F > 1 MeV	5.67E+08	± 38	8.70E+08	± 9	1.492	1.03	1.53
F > 0.1 MeV	9.79E+08	± 38	1.51E+09	± 12	1.492	1.03	1.54
F < 0.4eV	1.67E+10	± 139	9.57E+09	± 6	1.492	0.38	0.57
dpa/s	9.72E-13	± 41	1.34E-12	± 7	1.492	0.92	1.37
Slot EM							
F > 1 MeV	5.67E+08	± 38	1.22E+09	± 9	2.119	1.02	2.16
F > 0.1 MeV	9.79E+08	± 38	2.12E+09	± 12	2.119	1.02	2.16
F < 0.4eV	1.67E+10	± 139	1.61E+10	± 6	2.119	0.45	0.96
dpa/s	9.72E-13	± 41	1.90E-12	± 7	2.119	0.92	1.96

Table F.1 (continued)

	Calculated Value*	Calculated Std.%	Adjusted Value	Adjusted Std. %	Scale Fact.	Adj. Fact.	Adj./ Calc.
Slot EB							
F > 1 MeV	5.67E+08	± 38	1.70E+09	± 9	3.042	0.98	2.99
F > 0.1 MeV	9.79E+08	± 38	2.95E+09	± 12	3.042	0.99	3.02
F < 0.4eV	1.67E+10	± 139	2.83E+10	± 6	3.042	0.56	1.69
dpa/s	9.72E-13	± 41	2.70E-12	± 7	3.042	0.91	2.78
Slot FT							
F > 1 MeV	5.67E+08	± 38	8.65E+08	± 9	1.493	1.02	1.53
F > 0.1 MeV	9.79E+08	± 38	1.50E+09	± 12	1.493	1.03	1.53
F < 0.4eV	1.67E+10	± 139	9.27E+09	± 6	1.493	0.37	0.55
dpa/s	9.72E-13	± 41	1.33E-12	± 7	1.493	0.91	1.36
Slot FM							
F > 1 MeV	5.67E+08	± 38	1.21E+09	± 9	2.132	1.00	2.14
F > 0.1 MeV	9.79E+08	± 38	2.10E+09	± 12	2.132	1.01	2.15
F < 0.4eV	1.67E+10	± 139	1.61E+10	± 6	2.132	0.45	0.96
dpa/s	9.72E-13	± 41	1.89E-12	± 7	2.132	0.91	1.94
Slot FB							
F > 1 MeV	5.67E+08	± 38	1.77E+09	± 9	3.206	0.97	3.11
F > 0.1 MeV	9.79E+08	± 38	3.08E+09	± 12	3.206	0.98	3.15
F < 0.4eV	1.67E+10	± 139	3.01E+10	± 6	3.206	0.56	1.80
dpa/s	9.72E-13	± 41	2.82E-12	± 7	3.206	0.91	2.91

* Units are neutrons . cm^{-2}. s^{-1} for F>1 MeV, F>0.1 MeV, F<0.4 eV, and s^{-1} for dpa rate (dpa/s).

Table F.2 Measured reaction rates, C/M, and A/M ratios, [illegible] 2, position 9

Reaction	M*	C/M	A/M
Slot D			
Al-27 (n,a) Na-24 [Bare]	3.177E-18	0.60	0.95
Ti-48 (n,p) Sc-48 [Bare]	1.154E-18	0.61	0.96
Ti-48 (n,p) Sc-48	1.055E-18	0.67	1.04
Cu-63 (n,a) Co-60 [Bare]	1.569E-18	0.70	1.08
Cu-63 (n,a) Co-60	1.618E-18	0.68	1.05
Ti-46 (n,p) Sc-46 [Bare]	2.845E-17	0.58	0.90
Ti-46 (n,p) Sc-46	2.599E-17	0.64	0.98
Fe-54 (n,p) Mn-54 [Bare]	1.268E-16	0.70	1.07
Fe-54 (n,p) Mn-54	1.305E-16	0.68	1.03
Ti-47 (n,p) Sc-47 [Bare]	3.270E-17	0.58	0.89
Ti-47 (n,p) Sc-47	2.924E-17	0.65	0.99
Fe-58 (n,g) Fe-59 [Bare]	9.140E-15	1.92	1.08
Sc-45 (n,g) Sc-46 [Bare]	2.114E-13	1.75	0.98
Sc-45 (n,g) Sc-46	5.599E-15	1.91	1.04
Slot J			
Ni-58 (n,p) Co-58 [Bare]	2.473E-16	0.46	0.97
Ni-58 (n,p) Co-58	2.348E-16	0.49	1.02
Co-59 (n,g) Co-60 [Bare]	4.706E-13	1.09	1.02
Co-59 (n,g) Co-60	3.144E-14	0.62	1.03
Slot B			
U-235 (n,f) Ba-140	2.922E-13	0.70	1.00
U-235 (n,f) Zr-95	2.769E-13	0.74	1.06
U-235 (n,f) Ru-103	2.847E-13	0.72	1.03
Slot A			
Ni-58 (n,p) Co-58 [Bare]	3.455E-16	0.33	1.00
Ni-58 (n,p) Co-58	3.364E-16	0.34	1.02
Co-59 (n,g) Co-60 [Bare]	9.410E-13	0.55	1.02
Co-59 (n,g) Co-60	6.766E-14	0.29	1.01

Table F.2 (continued)

Reaction	M*	C/M	A/M
Slot ET			
Ni-58 (n,p) Co-58 [Bare]	1.763E-16	0.65	0.98
Ni-58 (n,p) Co-58	1.686E-16	0.68	1.02
Co-59 (n,g) Co-60 [Bare]	2.785E-13	1.84	1.02
Co-59 (n,g) Co-60	1.935E-14	1.01	1.04
Slot EM			
Ni-58 (n,p) Co-58 [Bare]	2.481E-16	0.46	0.98
Ni-58 (n,p) Co-58	2.358E-16	0.49	1.03
Co-59 (n,g) Co-60 [Bare]	4.744E-13	1.08	1.01
Co-59 (n,g) Co-60	3.007E-14	0.65	1.03
Slot EB			
Ni-58 (n,p) Co-58 [Bare]	3.495E-16	0.33	0.96
Ni-58 (n,p) Co-58	3.209E-16	0.36	1.04
Co-59 (n,g) Co-60 [Bare]	8.338E-13	0.62	1.01
Co-59 (n,g) Co-60	5.366E-14	0.36	1.01
Slot FT			
Ni-58 (n,p) Co-58 [Bare]	1.736E-16	0.66	0.99
Ni-58 (n,p) Co-58	1.686E-16	0.68	1.02
Co-59 (n,g) Co-60 [Bare]	2.667E-13	1.92	1.03
Co-59 (n,g) Co-60	1.989E-14	0.98	1.05
Slot FM			
Ni-58 (n,p) Co-58 [Bare]	2.465E-16	0.47	0.97
Ni-58 (n,p) Co-58	2.338E-16	0.49	1.02
Co-59 (n,g) Co-60 [Bare]	4.668E-13	1.10	1.02
Co-59 (n,g) Co-60	3.281E-14	0.59	1.03
Slot FB			
Ni-58 (n,p) Co-58 [Bare]	3.491E-16	0.33	1.00
Ni-58 (n,p) Co-58	3.425E-16	0.33	1.02
Co-59 (n,g) Co-60 [Bare]	8.776E-13	0.58	1.02
Co-59 (n,g) Co-60	6.025E-14	0.32	1.01

*Reactions per second per atom

Table F.3 Calculated and adjusted neutron group fluxes, key 2, position 9, slot J

Group	Group Upper Energy Boundary* [eV]	Neutron Group Fluence Rate Calculated**	Adjusted**
1	2.000E+07	1.057E+06	2.356E+06
2	1.271E+07	4.058E+06	9.059E+06
3	1.013E+07	1.209E+07	2.698E+07
4	8.072E+06	2.755E+07	5.743E+07
5	6.434E+06	2.803E+07	5.791E+07
6	5.523E+06	3.698E+07	7.595E+07
7	4.742E+06	3.932E+07	8.075E+07
8	4.071E+06	3.444E+07	7.089E+07
9	3.495E+06	4.265E+07	8.778E+07
10	3.000E+06	3.055E+07	6.626E+07
11	2.724E+06	1.019E+08	2.229E+08
12	2.038E+06	2.874E+07	6.294E+07
13	1.850E+06	3.674E+07	8.044E+07
14	1.655E+06	3.410E+07	7.464E+07
15	1.480E+06	4.212E+07	9.213E+07
16	1.282E+06	6.662E+07	1.457E+08
17	1.000E+06	6.962E+07	1.520E+08
18	7.653E+05	1.169E+08	2.543E+08
19	4.704E+05	1.194E+08	2.591E+08
20	2.297E+05	1.057E+08	2.269E+08
21	1.000E+05	1.857E+08	3.658E+08
22	1.202E+04	5.333E+07	1.050E+08
23	6.004E+03	5.285E+07	1.041E+08
24	3.000E+03	1.577E+08	3.105E+08
25	3.911E+02	5.434E+07	1.070E+08
26	1.978E+02	5.531E+07	1.089E+08
27	1.000E+02	7.985E+07	1.573E+08
28	3.817E+01	1.147E+08	2.259E+08
29	1.000E+01	4.258E+07	8.386E+07
30	6.178E+00	6.478E+07	1.276E+08
31	3.000E+00	5.089E+07	1.002E+08
32	1.770E+00	1.702E+08	3.351E+08
33	3.970E-01	2.816E+07	5.546E+07
34	3.300E-01	4.975E+07	9.798E+07
35	2.700E-01	1.334E+08	2.627E+08
36	2.150E-01	4.486E+08	8.834E+08
37	1.620E-01	1.859E+09	2.309E+09
38	1.040E-01	5.953E+09	5.228E+09
39	5.000E-02	7.509E+09	6.594E+09
40	1.000E-02	7.402E+08	6.501E+08
	1.000E-05		

*Energy in eV
**Group fluxes in neutrons $cm^{-2}.s^{-1}$
***Lower energy boundary of 40th group

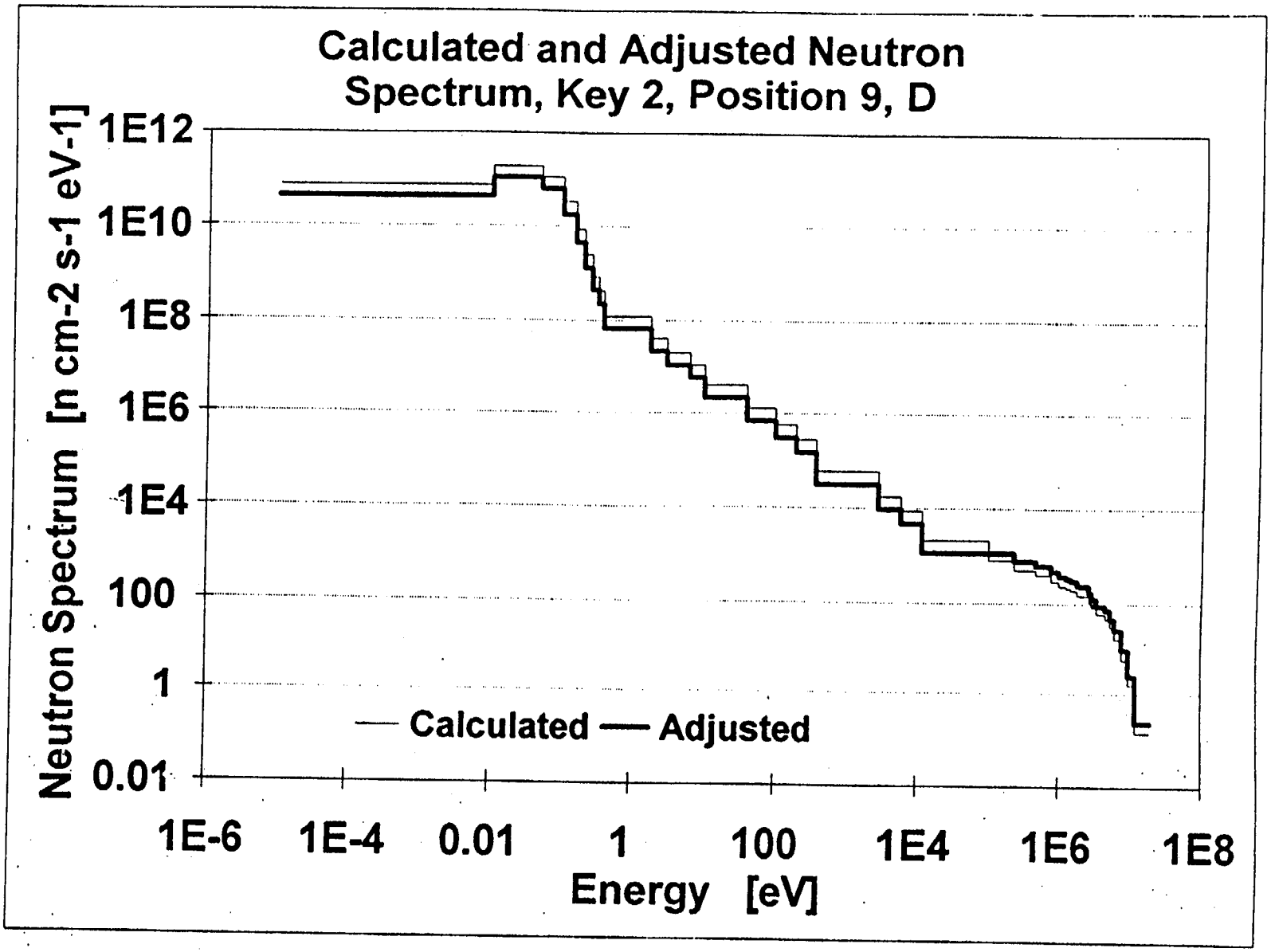

Fig. F.1 Calculated and adjusted neutron spectrum, key 2, position 9, D

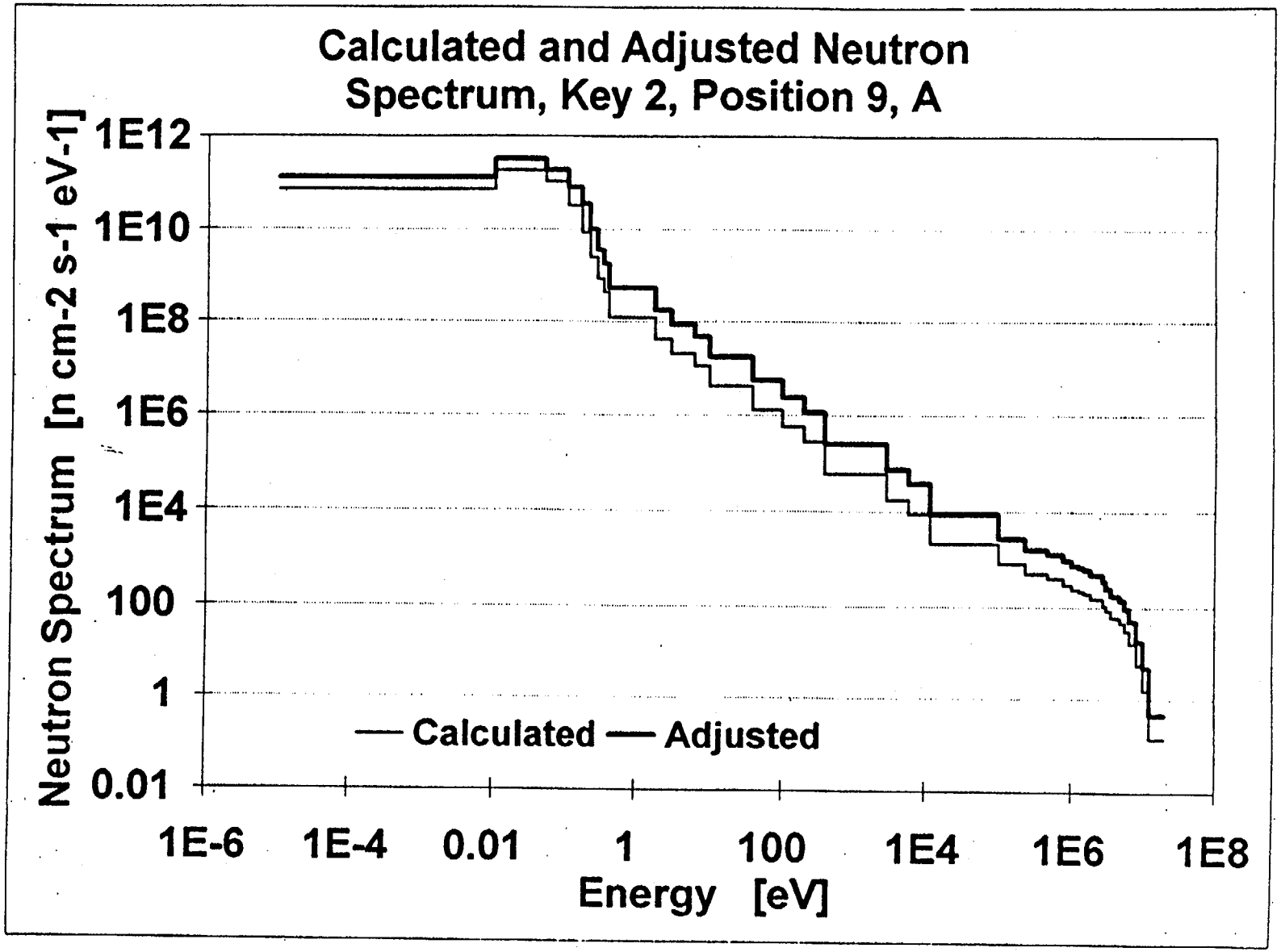

Fig. F.2 Calculated and adjusted neutron spectrum, key 2, position 9, A

APPENDIX G

RESULTS FOR KEY 4, POSITION 2

Table G.1 Calculated and adjusted irradiation parameters, key 4, position 2

	Calculated Value*	Calculated Std.%	Adjusted Value	Adjusted Std. %	Scale Fact.	Adj. Fact.	Adj./ Calc.
Slot D							
F > 1MeV	2.47E+08	± 38	2.43E+08	± 9	0.941	1.048	0.99
F > 0.1MeV	4.96E+08	± 38	4.91E+08	± 13	0.941	1.051	0.99
F < 0.4 eV	3.12E+10	± 139	9.99E+09	± 5	0.941	0.340	0.32
dpa/s	6.46E-13	± 68	4.42E-13	± 5	0.941	0.727	0.68
Slot J							
F > 1MeV	2.47E+08	± 38	3.10E+08	± 10	1.421	0.885	1.26
F > 0.1MeV	4.96E+08	± 38	6.43E+08	± 13	1.421	0.912	1.30
F < 0.4 eV	3.12E+10	± 139	2.33E+10	± 6	1.421	0.525	0.75
dpa/s	6.46E-13	± 68	6.66E-13	± 6	1.421	0.726	1.03
Slot B							
F > 1MeV	2.47E+08	± 38	3.16E+08	± 41	1.432	0.895	1.28
F > 0.1MeV	4.96E+08	± 38	6.54E+08	± 41	1.432	0.920	1.32
F < 0.4 eV	3.12E+10	± 139	2.50E+10	± 39	1.432	0.559	0.80
dpa/s	6.46E-13	± 68	6.90E-13	± 22	1.432	0.746	1.07
Slot A							
F > 1MeV	2.47E+08	± 38	4.30E+08	± 10	2.154	0.812	1.74
F > 0.1MeV	4.96E+08	± 38	9.05E+08	± 13	2.154	0.850	1.82
F < 0.4 eV	3.12E+10	± 139	7.20E+10	± 6	2.154	1.076	2.31
dpa/s	6.46E-13	± 68	1.29E-12	± 5	2.154	0.933	2.00
Slot ET							
F > 1MeV	2.47E+08	± 38	2.39E+08	± 10	1.037	0.936	0.97
F > 0.1MeV	4.96E+08	± 38	4.92E+08	± 13	1.037	0.956	0.99
F < 0.4 eV	3.12E+10	± 139	1.02E+10	± 6	1.037	0.314	0.33
dpa/s	6.46E-13	± 68	4.42E-13	± 5	1.037	0.659	0.68
Slot EM							
F > 1MeV	2.47E+08	± 38	3.14E+08	± 10	1.421	0.898	1.28
F > 0.1MeV	4.96E+08	± 38	6.51E+08	± 13	1.421	0.923	1.31
F < 0.4 eV	3.12E+10	± 139	2.26E+10	± 6	1.421	0.510	0.73
dpa/s	6.46E-13	± 68	6.66E-13	± 5	1.421	0.726	1.03
Slot EB							
F > 1MeV	2.47E+08	± 38	4.35E+08	± 10	2.077	0.850	1.77
F > 0.1MeV	4.96E+08	± 38	9.09E+08	± 13	2.077	0.882	1.83
F < 0.4 eV	3.12E+10	± 139	6.50E+10	± 6	2.077	1.003	2.08
dpa/s	6.46E-13	± 68	1.23E-12	± 5	2.077	0.918	1.91

Table G.1 (continued)

	Calculated Value*	Calculated Std.%	Adjusted Value	Adjusted Std. %	Scale Fact.	Adj. Fact.	Adj./ Calc.
Slot FT							
F > 1MeV	2.47E+08	± 38	2.36E+08	± 10	1.049	0.914	0.96
F > 0.1MeV	4.96E+08	± 38	4.88E+08	± 13	1.049	0.937	0.98
F < 0.4 eV	3.12E+10	± 139	1.10E+10	± 6	1.049	0.336	0.35
dpa/s	6.46E-13	± 68	4.46E-13	± 5	1.049	0.658	0.69
Slot FM							
F > 1MeV	2.47E+08	± 38	3.03E+08	± 10	1.389	0.884	1.23
F > 0.1MeV	4.96E+08	± 38	6.28E+08	± 13	1.389	0.911	1.27
F < 0.4 eV	3.12E+10	± 139	2.33E+10	± 6	1.389	0.537	0.75
dpa/s	6.46E-13	± 68	6.56E-13	± 6	1.389	0.731	1.02
Slot FB							
F > 1MeV	2.47E+08	± 38	4.17E+08	± 10	2.047	0.827	1.69
F > 0.1MeV	4.96E+08	± 38	8.75E+08	± 13	2.047	0.862	1.76
F < 0.4 eV	3.12E+10	± 139	5.83E+10	± 6	2.047	0.913	1.87
dpa/s	6.46E-13	± 68	1.15E-12	± 5	2.047	0.868	1.78

* Units are neutron . cm^{-2}. s^{-1} for F > 1 MeV, F> 0.1 MeV, F > 0.4 eV, and s^{-1} for dpa rate (dpa/s).

Table G.2 Measured reaction rates, C/M, and A/M ratios, key 4, position 2

Reaction	M*	C/M	A/M
Slot D			
Al-27 (n,a) Na-24 [Bare]	8.333E-19	0.99	1.05
Ti-48 (n,p) Sc-48 [Bare]	3.374E-19	0.90	0.94
Ti-48 (n,p) Sc-48	3.191E-19	0.95	0.99
Cu-63 (n,a) Co-60 [Bare]	4.669E-19	0.98	0.98
Cu-63 (n,a) Co-60	4.332E-19	1.05	1.05
Ti-46 (n,p) Sc-46 [Bare]	6.684E-18	1.00	0.95
Ti-46 (n,p) Sc-46	6.220E-18	1.07	1.02
Fe-54 (n,p) Mn-54 [Bare]	2.926E-17	1.20	1.11
Fe-54 (n,p) Mn-54	3.153E-17	1.11	1.03
Ti-47 (n,p) Sc-47 [Bare]	8.127E-18	0.93	0.89
Ti-47 (n,p) Sc-47	7.619E-18	0.99	0.94
Fe-58 (n,g) Fe-59 [Bare]	9.525E-15	3.43	1.06
Sc-45 (n,g) Sc-46 [Bare]	2.167E-13	3.18	0.99
Sc-45 (n,g) Sc-46	7.903E-15	2.33	1.07
Slot A			
Ni-58 (n,p) Co-58 [Bare]	7.278E-17	0.62	1.03
Ni-58 (n,p) Co-58	7.370E-17	0.62	1.01
Co-59 (n,g) Co-60 [Bare]	1.980E-12	0.48	1.04
Co-59 (n,g) Co-60	1.426E-13	0.21	1.03
Slot B			
U-235 (n,f) Ba-140	5.644E-13	0.62	1.06
U-235 (n,f) Zr-95	5.287E-13	0.66	1.14
U-235 (n,f) Ru-103	5.433E-13	0.64	1.11
Slot J			
U-235 (n,f)	5.972E-13	0.58	1.05
Ni-58 (n,p) Co-58 [Bare]	5.506E-17	0.82	0.98
Ni-58 (n,p) Co-58	5.302E-17	0.86	1.02
Co-59 (n,g) Co-60 [Bare]	6.167E-13	1.54	1.06
Co-59 (n,g) Co-60	4.794E-14	0.61	1.17

Table G.2 (continued)

Reaction	M*	C/M	A/M
Slot ET			
Ni-58 (n,p) Co-58 [Bare]	4.145E-17	1.10	1.01
Ni-58 (n,p) Co-58	4.203E-17	1.08	1.00
Co-59 (n,g) Co-60 [Bare]	2.574E-13	3.70	1.08
Co-59 (n,g) Co-60	2.409E-14	1.22	1.19
Slot EM			
Ni-58 (n,p) Co-58 [Bare]	5.400E-17	0.84	1.02
Ni-58 (n,p) Co-58	5.491E-17	0.83	1.00
Co-59 (n,g) Co-60 [Bare]	6.108E-13	1.56	1.05
Co-59 (n,g) Co-60	4.643E-14	0.63	1.11
Slot EB			
Ni-58 (n,p) Co-58 [Bare]	7.652E-17	0.59	0.99
Ni-58 (n,p) Co-58	7.380E-17	0.61	1.03
Co-59 (n,g) Co-60 [Bare]	1.869E-12	0.51	1.02
Co-59 (n,g) Co-60	1.055E-13	0.28	1.03
Slot FT			
Ni-58 (n,p) Co-58 [Bare]	4.223E-17	1.08	0.98
Ni-58 (n,p) Co-58	4.051E-17	1.12	1.02
Co-59 (n,g) Co-60 [Bare]	2.713E-13	3.51	1.10
Co-59 (n,g) Co-60	2.787E-14	1.05	1.20
Slot FM			
Ni-58 (n,p) Co-58 [Bare]	5.612E-17	0.81	0.94
Ni-58 (n,p) Co-58	5.112E-17	0.89	1.03
Co-59 (n,g) Co-60 [Bare]	6.225E-13	1.53	1.05
Co-59 (n,g) Co-60	4.945E-14	0.59	1.11
Slot FB			
Ni-58 (n,p) Co-58 [Bare]	7.235E-17	0.63	1.00
Ni-58 (n,p) Co-58	7.079E-17	0.64	1.02
Co-59 (n,g) Co-60 [Bare]	1.596E-12	0.60	1.04
Co-59 (n,g) Co-60	1.168E-13	0.25	1.05

*Reactions per second per atom

Table G.3 Calculated and adjusted neutron group fluxes, key 4, position 2, slot J

Group	Group Upper Energy Boundary* [eV]	Neutron Group Fluence Rate Calculated**	Adjusted**
1	2.000E+07	5.520E+05	8.033E+05
2	1.271E+07	1.858E+06	2.659E+06
3	1.013E+07	5.141E+06	7.235E+06
4	8.072E+06	1.117E+07	1.310E+07
5	6.434E+06	1.065E+07	1.212E+07
6	5.523E+06	1.386E+07	1.549E+07
7	4.742E+06	1.490E+07	1.665E+07
8	4.071E+06	1.363E+07	1.547E+07
9	3.495E+06	1.668E+07	1.897E+07
10	3.000E+06	1.182E+07	1.523E+07
11	2.724E+06	4.116E+07	5.409E+07
12	2.038E+06	1.289E+07	1.700E+07
13	1.850E+06	1.718E+07	2.260E+07
14	1.655E+06	1.671E+07	2.198E+07
15	1.480E+06	2.182E+07	2.867E+07
16	1.282E+06	3.651E+07	4.778E+07
17	1.000E+06	3.967E+07	5.179E+07
18	7.653E+05	7.020E+07	9.141E+07
19	4.704E+05	7.372E+07	9.586E+07
20	2.297E+05	6.601E+07	9.390E+07
21	1.000E+05	1.205E+08	3.275E+08
22	1.202E+04	3.599E+07	9.783E+07
23	6.004E+03	3.677E+07	9.995E+07
24	3.000E+03	1.167E+08	3.173E+08
25	3.911E+02	4.298E+07	1.168E+08
26	1.978E+02	4.544E+07	1.235E+08
27	1.000E+02	6.854E+07	1.863E+08
28	3.817E+01	1.049E+08	2.853E+08
29	1.000E+01	4.094E+07	1.113E+08
30	6.178E+00	6.436E+07	1.750E+08
31	3.000E+00	5.223E+07	1.420E+08
32	1.770E+00	1.840E+08	5.000E+08
33	3.970E-01	3.543E+07	9.632E+07
34	3.300E-01	7.459E+07	2.028E+08
35	2.700E-01	2.310E+08	6.280E+08
36	2.150E-01	8.234E+08	2.238E+09
37	1.620E-01	3.471E+09	4.003E+09
38	1.040E-01	1.116E+10	6.757E+09
39	5.000E-02	1.404E+10	8.503E+09
40	1.000E-02	1.381E+09	8.364E+08
	1.000E-05***		

*Energy in eV
**Group fluxes in neutrons $cm^{-2}.s^{-1}$
***Lower energy boundary of 40th group

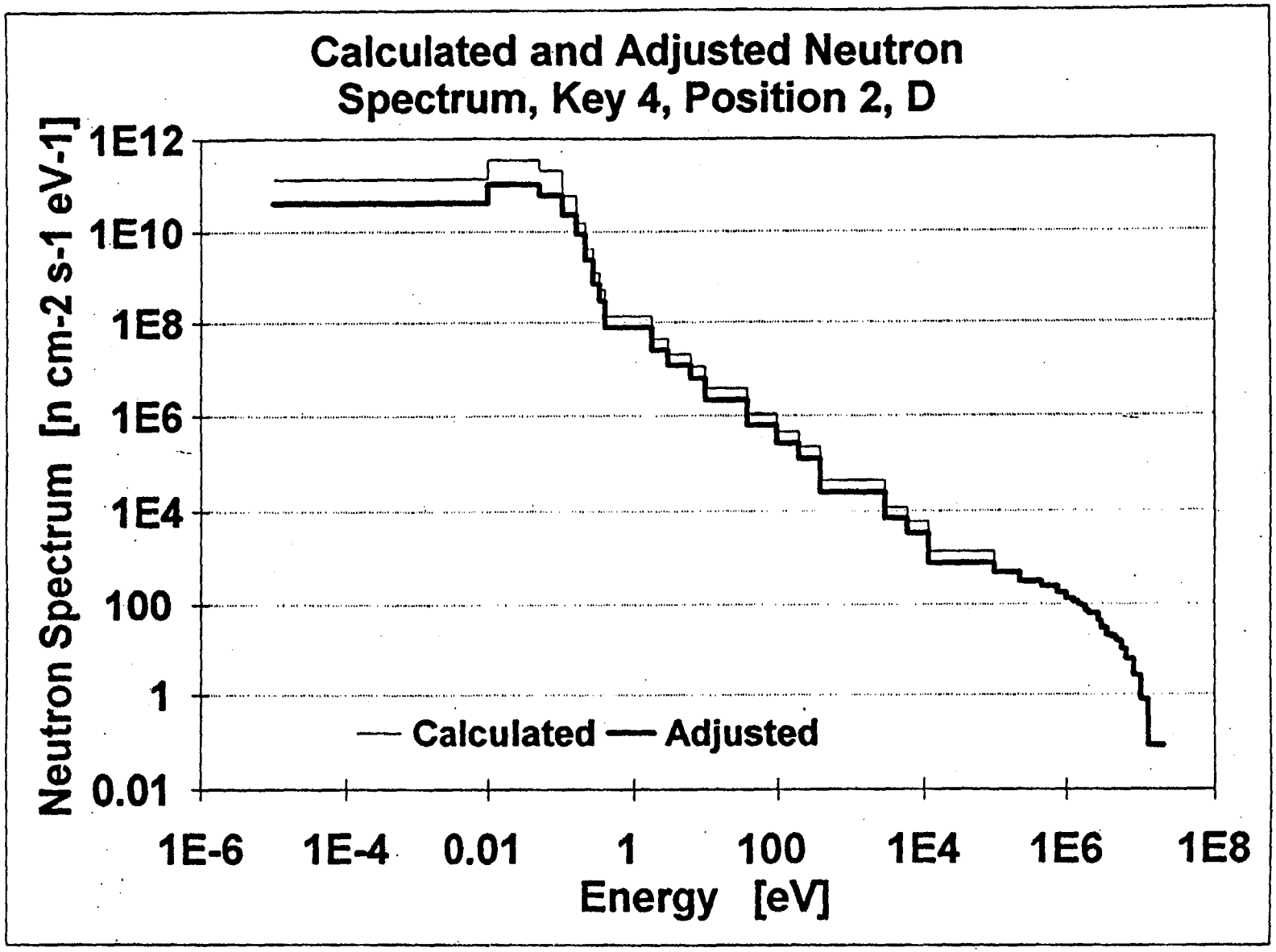

Fig. G.1 Calculated and adjusted neutron spectrum, key 4, position 2, D

Fig. G.1 Calculated and adjusted neutron spectrum, key 4, position 2, D

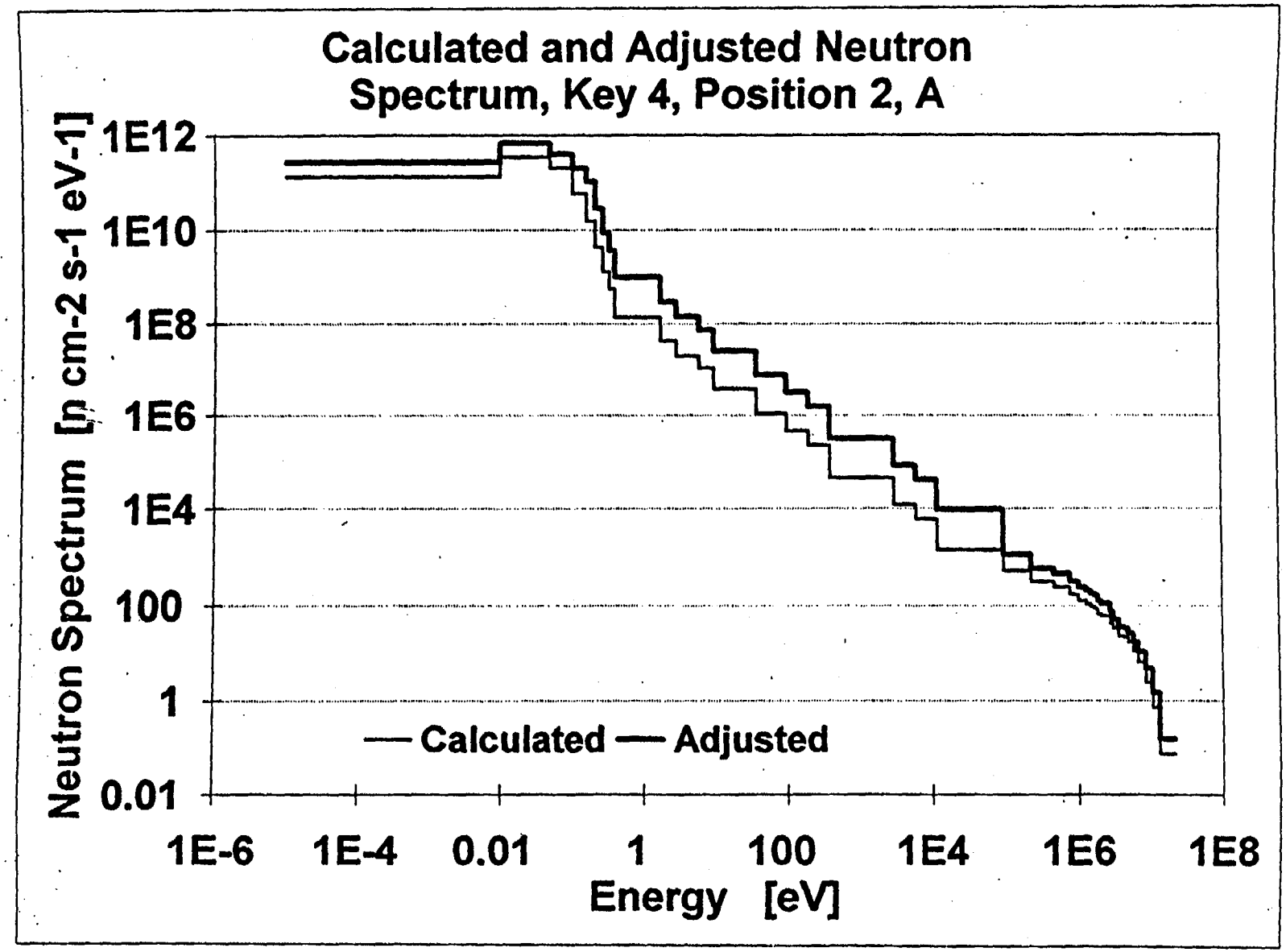

Fig. G.2 Calculated and adjusted neutron spectrum, key 4, position 2, A

APPENDIX H

RESULTS FOR KEY 4, POSITION 10

Table H.1 Calculated and adjusted irradiation parameters, key 4, position 10

	Calculated Value*	Calculated Std.%	Adjusted Value	Adjusted Std. %	Scale Fact.	Adj. Fact.	Adj./ Calc.
Slot D							
F > 1MeV	3.97E+08	± 38	2.95E+08	± 9	0.660	1.127	0.74
F > 0.1MeV	7.56E+08	± 38	5.68E+08	± 13	0.660	1.139	0.75
F < 0.4 eV	3.26E+10	± 139	1.11E+10	± 5	0.660	0.516	0.34
dpa/s	8.94E-13	± 55	5.34E-13	± 5	0.660	0.905	0.60
Slot J							
F > 1MeV	3.97E+08	± 38	4.09E+08	± 10	1.088	0.946	1.03
F > 0.1MeV	7.56E+08	± 38	8.05E+08	± 13	1.088	0.979	1.06
F < 0.4 eV	3.26E+10	± 139	2.75E+10	± 6	1.088	0.775	0.84
dpa/s	8.94E-13	± 55	8.62E-13	± 6	1.088	0.886	0.96
Slot B							
F > 1MeV	3.97E+08	± 38	3.90E+08	± 40	1.021	0.962	0.98
F > 0.1MeV	7.56E+08	± 38	7.66E+08	± 40	1.021	0.992	1.01
F < 0.4 eV	3.26E+10	± 139	2.64E+10	± 40	1.021	0.793	0.81
dpa/s	8.94E-13	± 55	8.22E-13	± 25	1.021	0.900	0.92
Slot A							
F > 1MeV	3.97E+08	± 38	6.00E+08	± 10	1.717	0.880	1.51
F > 0.1MeV	7.56E+08	± 38	1.20E+09	± 13	1.717	0.921	1.58
F < 0.4 eV	3.26E+10	± 139	8.01E+10	± 6	1.717	1.433	2.46
dpa/s	8.94E-13	± 55	1.64E-12	± 6	1.717	1.066	1.83
Slot ET							
F > 1 MeV	3.97E+08	± 38	2.78E+08	± 10	0.70	1.00	0.70
F > 0.1 MeV	7.56E+08	± 38	5.42E+08	± 13	0.70	1.03	0.72
F < 0.4eV	3.26E+10	± 139	1.16E+10	± 6	0.70	0.51	0.36
dpa/s	8.94E-13	± 55	5.19E-13	± 6	0.70	0.83	0.58
Slot EM							
F > 1 MeV	3.97E+08	± 38	3.76E+08	± 10	0.99	0.96	0.95
F > 0.1 MeV	7.56E+08	± 38	7.38E+08	± 13	0.99	0.99	0.98
F < 0.4eV	3.26E+10	± 139	2.56E+10	± 6	0.99	0.80	0.79
dpa/s	8.94E-13	± 55	7.94E-13	± 6	0.99	0.90	0.89

Table H.1 (continued)

	Calculated Value*	Std.%	Adjusted Value	Std. %	Scale Fact.	Adj. Fact.	Adj./ Calc.
Slot EB							
F > 1 MeV	3.97E+08	± 38	5.47E+08	± 10	1.53	0.90	1.38
F > 0.1 MeV	7.56E+08	± 38	1.09E+09	± 13	1.53	0.94	1.44
F < 0.4eV	3.26E+10	± 139	6.20E+10	± 6	1.53	1.25	1.91
dpa/s	8.94E-13	± 55	1.39E-12	± 6	1.53	1.02	1.55
Slot FT							
F > 1 MeV	3.97E+08	± 38	3.26E+08	± 10	0.82	1.00	0.82
F > 0.1 MeV	7.56E+08	± 38	6.37E+08	± 13	0.82	1.02	0.84
F < 0.4eV	3.26E+10	± 139	1.22E+10	± 6	0.82	0.45	0.37
dpa/s	8.94E-13	± 55	5.97E-13	± 6	0.82	0.81	0.67
Slot FM							
F > 1 MeV	3.97E+08	± 38	4.44E+08	± 10	1.17	0.96	1.12
F > 0.1 MeV	7.56E+08	± 38	8.72E+08	± 13	1.17	0.99	1.15
F < 0.4eV	3.26E+10	± 139	2.84E+10	± 6	1.17	0.75	0.87
dpa/s	8.94E-13	± 55	9.22E-13	± 6	1.17	0.88	1.03
Slot FB							
F > 1 MeV	3.97E+08	± 38	6.50E+08	± 10	1.81	0.91	1.64
F > 0.1 MeV	7.56E+08	± 38	1.29E+09	± 13	1.81	0.94	1.71
F < 0.4eV	3.26E+10	± 139	7.40E+10	± 6	1.81	1.26	2.27
dpa/s	8.94E-13	± 55	1.65E-12	± 6	1.81	1.02	1.85

* Units are neutrons . cm^{-2}. s^{-1} for F>1 MeV, F>0.1 MeV, F<0.4 eV, and s^{-1} for dpa rate (dpa/s).

Table H.2 Measured reaction rates, C/M, and A/M ratios, key 4, position 10

Reaction	M*	C/M	A/M
Slot D			
Al-27 (n,a) Na-24 [Bare]	1.102E-18	1.71	1.04
Ti-48 (n,p) Sc-48 [Bare]	4.474E-19	1.53	0.94
Ti-48 (n,p) Sc-48	4.161E-19	1.64	1.01
Cu-63 (n,a) Co-60 [Bare]	6.529E-19	1.57	0.98
Cu-63 (n,a) Co-60	6.119E-19	1.67	1.04
Ti-46 (n,p) Sc-46 [Bare]	9.345E-18	1.54	0.99
Ti-46 (n,p) Sc-C46	8.734E-18	1.65	1.05
Fe-54 (n,p) Mn-54 [Bare]	4.306E-17	1.57	1.05
Fe-54 (n,p) Mn-54	4.485E-17	1.50	1.01
Ti-47 (n,p) Sc-47 [Bare]	1.065E-17	1.33	0.91
Ti-47 (n,p) Sc-47	1.046E-17	1.36	0.93
Fe-58 (n,g) Fe-59 [Bare]	1.143E-14	2.95	0.99
Sc-45 (n,g) Sc-46 [Bare]	2.400E-13	2.97	0.99
Sc-45 (n,g) Sc-46	8.682E-15	2.37	1.05
Slot J			
U-235 (n,f)	6.980E-13	0.56	0.96
Ni-58 (n,p) Co-58 [Bare]	8.540E-17	1.01	0.96
Ni-58 (n,p) Co-58	7.895E-17	1.09	1.03
Co-59 (n,g) Co-60 [Bare]	7.508E-13	1.31	1.04
Co-59 (n,g) Co-60	5.326E-14	0.63	1.15
Slot B			
U-235 (n,f) Ba-140	5.232E-13	0.74	1.11
U-235 (n,f) Zr-95	5.651E-13	0.69	1.02
U-235 (n,f) Ru-103	5.475E-13	0.71	1.06
Slot A			
Ni-58 (n,p) Co-58 [Bare]	1.181E-16	0.73	1.01
Ni-58 (n,p) Co-58	1.169E-16	0.74	1.02
Co-59 (n,g) Co-60 [Bare]	2.261E-12	0.44	1.03
Co-59 (n,g) Co-60	1.507E-13	0.22	1.00

Table H.2 (continued)

Reaction	M*	C/M	A/M
Slot ET			
Ni-58 (n,p) Co-58 [Bare]	5.512E-17	1.57	1.01
Ni-58 (n,p) Co-58	5.574E-17	1.55	1.00
Co-59 (n,g) Co-60 [Bare]	3.133E-13	3.15	1.04
Co-59 (n,g) Co-60	2.489E-14	1.35	1.11
Slot EM			
Ni-58 (n,p) Co-58 [Bare]	7.839E-17	1.10	0.96
Ni-58 (n,p) Co-58	7.191E-17	1.20	1.04
Co-59 (n,g) Co-60 [Bare]	7.171E-13	1.37	1.03
Co-59 (n,g) Co-60	4.878E-14	0.69	1.06
Slot EB			
Ni-58 (n,p) Co-58 [Bare]	1.105E-16	0.78	0.99
Ni-58 (n,p) Co-58	1.054E-16	0.82	1.03
Co-59 (n,g) Co-60 [Bare]	1.756E-12	0.56	1.02
Co-59 (n,g) Co-60	1.145E-13	0.29	1.02
Slot FT			
Ni-58 (n,p) Co-58 [Bare]	6.628E-17	1.31	0.99
Ni-58 (n,p) Co-58	6.428E-17	1.34	1.02
Co-59 (n,g) Co-60 [Bare]	3.170E-13	3.11	1.07
Co-59 (n,g) Co-60	2.940E-14	1.15	1.13
Slot FM			
Ni-58 (n,p) Co-58 [Bare]	9.240E-17	0.94	0.96
Ni-58 (n,p) Co-58	8.599E-17	1.01	1.03
Co-59 (n,g) Co-60 [Bare]	7.844E-13	1.26	1.03
Co-59 (n,g) Co-60	5.774E-14	0.58	1.07
Slot FB			
Ni-58 (n,p) Co-58 [Bare]	1.343E-16	0.64	0.97
Ni-58 (n,p) Co-58	1.240E-16	0.70	1.04
Co-59 (n,g) Co-60 [Bare]	2.105E-12	0.47	1.02
Co-59 (n,g) Co-60	1.332E-13	0.25	1.02

*Reactions per second per atom

Table H.3 Calculated and adjusted neutron group fluxes, key 4, position 10, slot J

Group	Group Upper Energy Boundary* [eV]	Neutron Group Fluence Rate Calculated**	Adjusted**
1	2.000E+07	1.018E+06	8.997E+05
2	1.271E+07	4.031E+06	3.575E+06
3	1.013E+07	1.239E+07	1.102E+07
4	8.072E+06	2.601E+07	2.316E+07
5	6.434E+06	2.306E+07	2.105E+07
6	5.523E+06	2 727E+07	2.533E+07
7	4.742E+06	2.711E+07	2.518E+07
8	4.071E+06	2.205E+07	2.164E+07
9	3.495E+06	2.504E+07	2.473E+07
10	3.000E+06	1.743E+07	1.904E+07
11	2.724E+06	5.955E+07	6.589E+07
12	2.038E+06	1.881E+07	2.083E+07
13	1.850E+06	2.502E+07	2.763E+07
14	1.655E+06	2.406E+07	2.656E+07
15	1.480E+06	3.121E+07	3.438E+07
16	1.282E+06	5.300E+07	5.790E+07
17	1.000E+06	5.657E+07	6.111E+07
18	7.653E+05	1.030E+08	1.106E+08
19	4.704E+05	1.067E+08	1.149E+08
20	2.297E+05	9.266E+07	1.097E+08
21	1.000E+05	1.652E+08	3.942E+08
22	1.202E+04	4.817E+07	1.149E+08
23	6.004E+03	5.000E+07	1.193E+08
24	3.000E+03	1.579E+08	3.768E+08
25	3.911E+02	5.820E+07	1.389E+08
26	1.978E+02	6.196E+07	1.478E+08
27	1.000E+02	9.355E+07	2.232E+08
28	3.817E+01	1.433E+08	3.419E+08
29	1.000E+01	5.581E+07	1.332E+08
30	6.178E+00	8.758E+07	2.090E+08
31	3.000E+00	7.058E+07	1.684E+08
32	1.770E+00	2.343E+08	5.591E+08
33	3.970E-01	4.785E+07	1.142E+08
34	3.300E-01	9.270E+07	2.212E+08
35	2.700E-01	2.704E+08	6.451E+08
36	2.150E-01	9.198E+08	2.195E+09
37	1.620E-01	3.733E+09	4.492E+09
38	1.040E-01	1.174E+10	8.447E+09
39	5.000E-02	1.437E+10	1.034E+10
40	1.000E-02	1.383E+09	9.958E+08
	1.000E-05***		

*Energy in eV
**Group fluxes in neutrons cm^{-2}. s^{-1}
***Lower energy boundary of 40th group

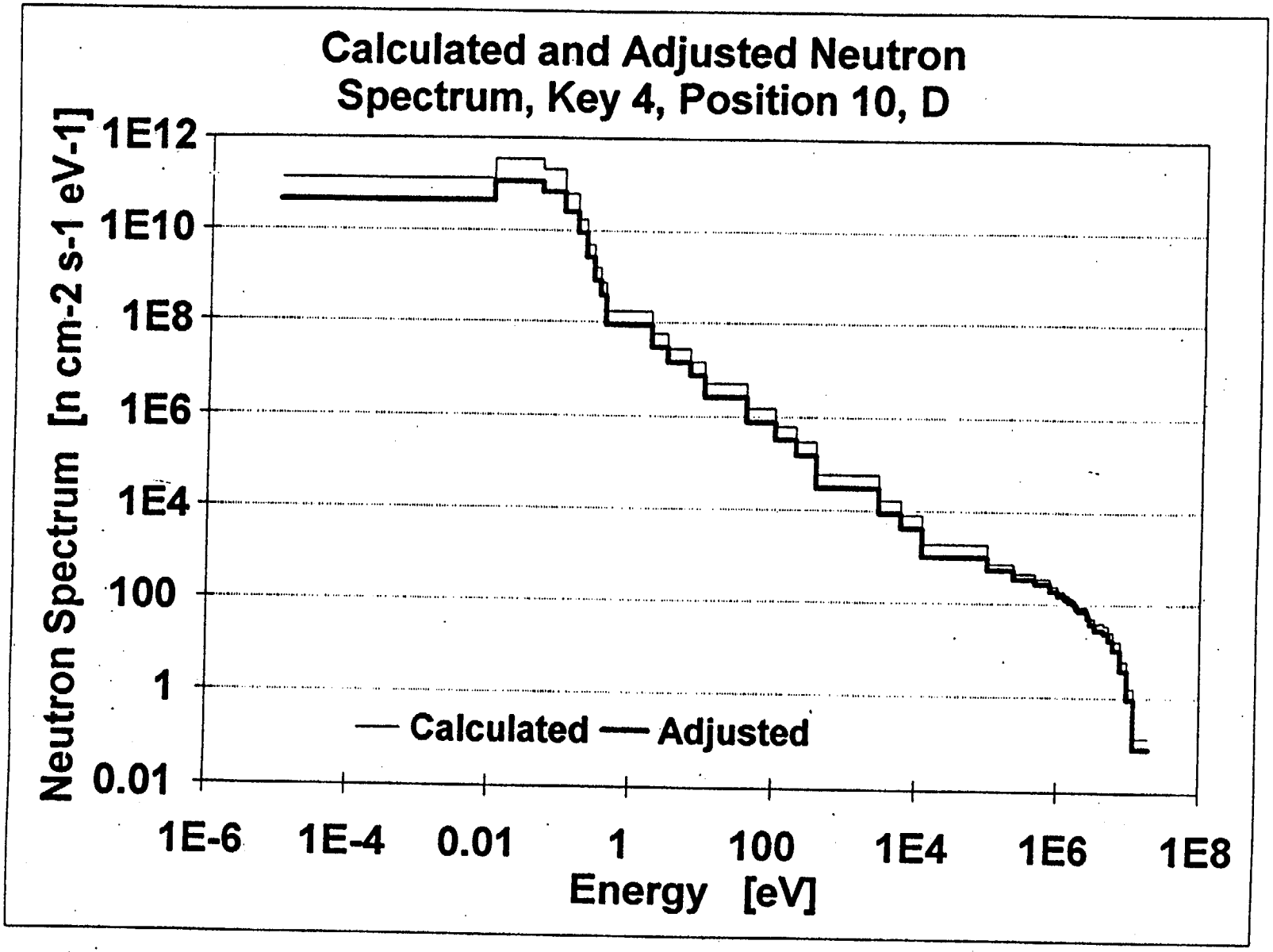

Fig. H.1 Calculated and adjusted neutron spectrum, key 4, position 10, D

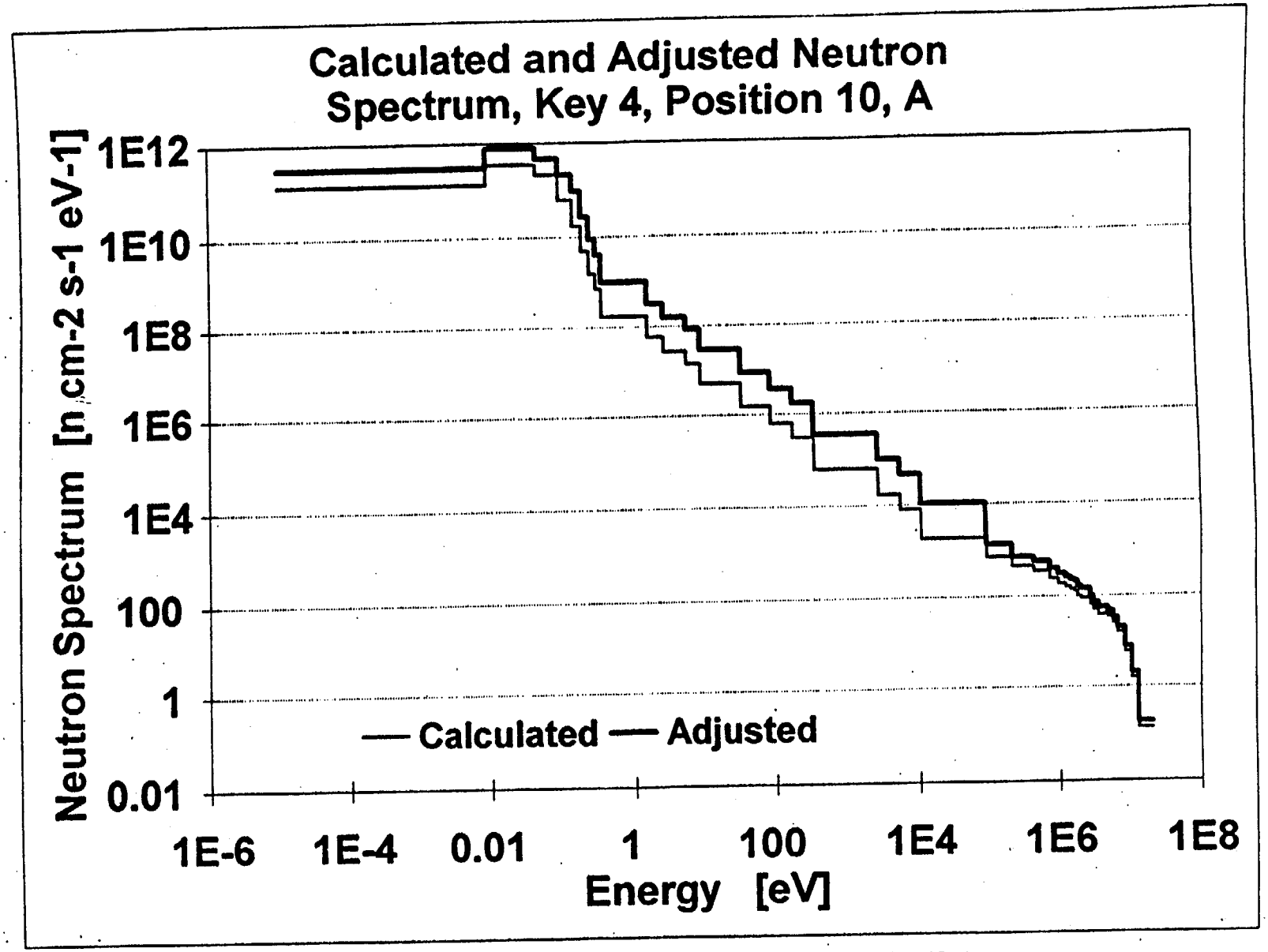

Fig. H.2 Calculated and adjusted neutron spectrum, key 4, position 10, A

APPENDIX I

SCHEMATIC OF DOS3 LOWER SPLIT HALF HOLDER (PART 2-2 DWG. M-11511-OH-001-E-R1) SHOWING SLOT NOMENCLATURE AND DOSIMETER LOADING ASSIGNMENT

ORNL-DWG 93M-14907

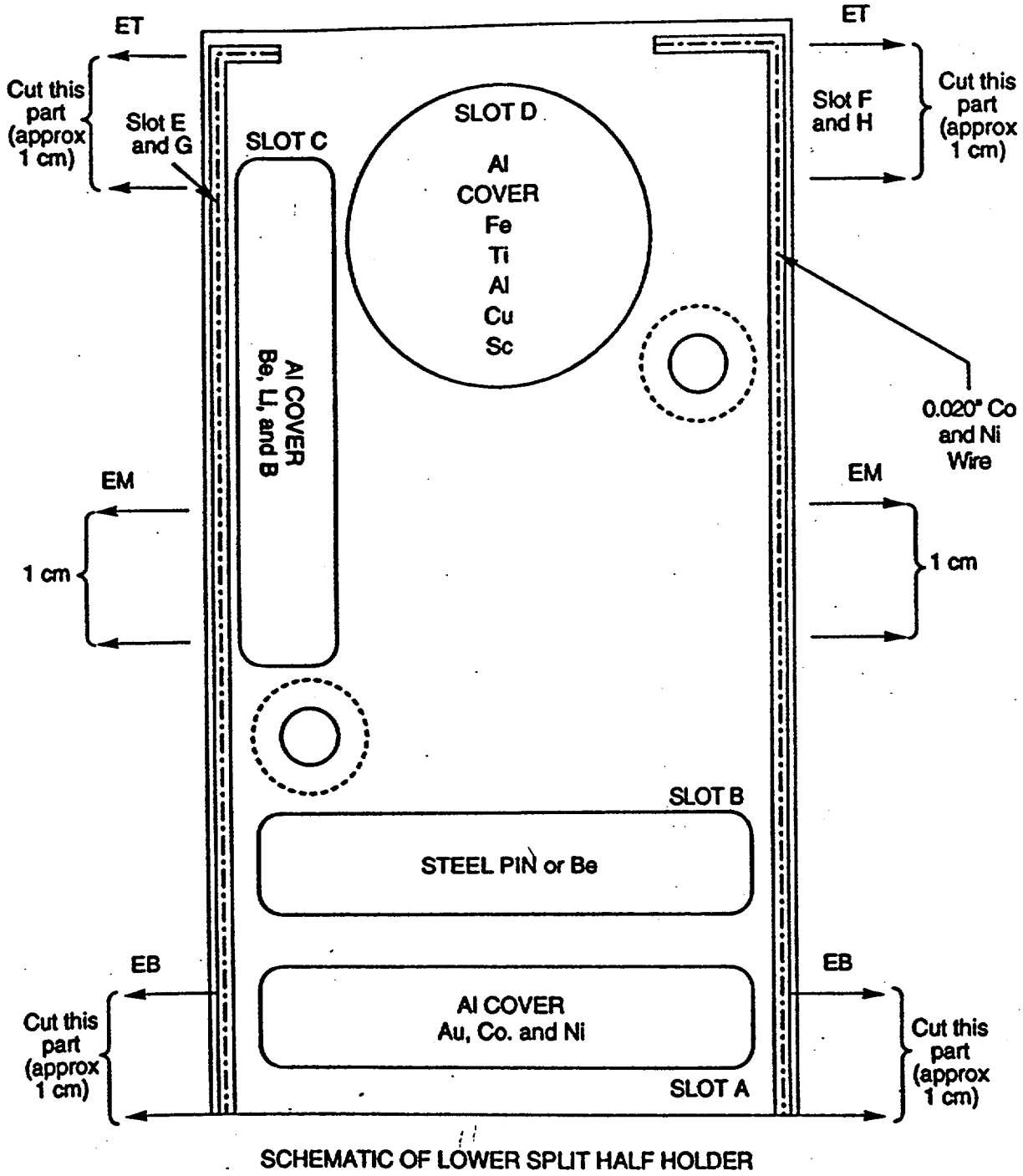

Fig. I. 1 Schematic of dosimetry capsule with slot locations

INTERNAL DISTRIBUTION

1. C. A. Baldwin
2. B. R. Bass
3. E. E. Bloom
4. J. A. Bucholz
5. R. D. Cheverton
6. W. R. Corwin
7. F. Dyer
8. K. Farrell
9. D. Glasgow
10. F. M. Haggag
11. Dennie Heatherly
12. G. Hirtz
13. R. Hobbs
14. R. L. Huddeleston
15. D. J. Ingersol
16. S. K. Iskander
17-21. F. B. K. Kam
22. L. K. Mansur
23. D. E. McCabe
24. J. G. Merkle
25. R. K. Nanstad
26. J. Pace
27. W. E. Pennell
28. C. E. Pugh
29-33. I. Remec
34-36. C. H. Shappert
37. R. E. Stoller
38. K. Thoms
39. J. A. Wang
40. R. M. Westfall
41. G. E. Whitesides
42. Central Research Library
43. ORNL Y-12 Research Library Document Reference Section
44-45. Laboratory Records Department
46. Laboratory Records, ORNL (RC)
47. ORNL Patent Office

EXTERNAL DISTRIBUTION

48. S. T. Byrne, ABB - Combustion Engineering, Windsor, CR 60695

49. Frank C. Cherney, Section Leader, USNRC, Office of Nuclear Regulatory Research, Mail Stop NL/S 302, Washington, D.C. 20555

50. B. J. Elliott, Nuclear Regulatory Commission, NRR/Div. of Engineering Technology, MS704, Washington, DC 20555

51. A. Fabry, CEN/SCK, Belgium, Reactor Physics Department, Boeretang 200, B-2400MOL, Belgium

52. Dr. Bogdan Glumac, Head, Reactor Physics Division, Reactor Center, Brine Jamova 39, 61111 Ljubljana, Slovenia

53. L. R. Greenwood, Pacific Northwest Laboratories, Mail Stop P7-22, P.O. Box 999, Richland, Washington 99352

54. J. Grundl, National Institute of Standards and Technology, Bldg. 235-A155, Gaithersburg, Maryland 20899

55. J. R. Hawthorne, Materials Engineering Associates, 9700B Martin Luther King, Jr. Highway, Lanham, MD 20706

56. C. A. Hrabal, USNRC, Office of Nuclear Regulatory Research, Mail Stop NL/S 302, Washington, D.C. 20555

57. Matt Hutmaker, NE44 Germantown, U. S. Department of Energy, Washington, D.C. 20585

58. R. E. Johnson, USNRC, Division of Engineering, Mail Stop NL S 314, Washington, D.C. 20555

59. N. P. Kadambi, USNRC, Mail Stop 8 D22, Washington, DC 20555

60. Mike Mayfield, USNRC, Division of Engineering, Mail Stop NL S 217 C, Washington, D.C. 20555

61. Jozef Stefan Institute, Library, Jamova 39, 61 111 Ljubljana, Slovenia

62. Dr. G. P. Marino, USNRC, Mail Stop NLS007, Washington, DC 20555

63. E. D. McGarry, National Institute of Standards and Technology, Bldg. 235-A155, Gaithersburg, Maryland 20899

64. Bill McLaughlin, National Institute of Standards and Technology, Bldg. 235-A155, Gaithersburg, Maryland 20899

65. Warren Minners, USNRC, Office of Nuclear Regulatory Research, Mail Stop NL/S 360, Washington, D.C. 20555

66. Joseph A. Murphy, U. S. Nuclear Regulatory Commission, Mail Stop NLS007, Washington, DC 20555

67. P. E. Norian, U. S. Nuclear Regulatory Commission, Mail Stop NLS314, Washington, DC 20555

68. Brian Oliver, Rockwell International, Rocketdyne Div., 6633 Canoga Ave., Canoga Park, California 91309

69. Frank Ruddy, Westinghouse Science & Technology Center, 1310 Beulah Rd., Bldg. 302, Rm. 201, Pittsburgh, Pennsylvania 15235

70. C. Z. Serpan, Jr., U. S. Nuclear Regulatory Commission, Division of Engineering, Mail Stop NLS217C, Washington, D.C. 20555

71. Al Taboada, USNRC, Division of Engineering, Mail Stop NL S 217 C, Washington, D.C. 20555

72. T. J. Walker, USNRC, Division of Engineering, Mail Stop NL S 217 C, Washington, D.C. 20555

73. John Williams, University of Arizona, Tucson, Arizona 85721

74-80. NRC/RES Division of Engineering, Washington, D.C. 20555

81. Ohio State University, Dept. of Metallurgical Engineering, Columbus, Ohio 43210-1179

82. University of Missouri-Rolla, Dept. of Nuclear Engineering, Rolla, Missouri 65401

83. Office of the Deputy Assistant Manager for Energy, Research, and Development, Department of Energy Oak Ridge Operations (DOE-ORO), P.O. Box 2008, Oak Ridge, Tennessee 37831-6269

84-87. Office of Scientific and Technical Information, P.O. Box 62, Oak Ridge, Tennessee 37831

88-216. Given distribution as shown in category RF (NTIS-10)

NRC FORM 335 (2-89) NRCM 1102, 3201, 3202

U.S. NUCLEAR REGULATORY COMMISSION

BIBLIOGRAPHIC DATA SHEET

(See instructions on the reverse)

1. REPORT NUMBER (Assigned by NRC, Add Vol., Supp., Rev., and Addendum Numbers, if any.)
NUREG/CR-6117
ORNL/TM-12484

2. TITLE AND SUBTITLE
Neutron Spectra at Different High Flux Isotope Reactor (HFIR) Pressure Vessel Surveillance Locations

3. DATE REPORT PUBLISHED
MONTH: December
YEAR: 1993

4. FIN OR GRANT NUMBER
L2552

5. AUTHOR(S)
I. Remec,* F. B. Kam

6. TYPE OF REPORT

7. PERIOD COVERED (Inclusive Dates)

8. PERFORMING ORGANIZATION – NAME AND ADDRESS (If NRC, provide Division, Office or Region, U.S. Nuclear Regulatory Commission, and mailing address; if contractor, provide name and mailing address.)
Oak Ridge National Laboratory
Oak Ridge, TN 37831-6370

*Josef Sefan Institute
Ljubljana, Slovenia

9. SPONSORING ORGANIZATION – NAME AND ADDRESS (If NRC, type "Same as above"; if contractor, provide NRC Division, Office or Region, U.S. Nuclear Regulatory Commission and mailing address.)
Division of Safety Issue Resolution
Office of Nuclear Regulatory Research
U.S. Nuclear Regulatory Commission
Washington, DC 20555-0001

10. SUPPLEMENTARY NOTES

11. ABSTRACT (200 words or less)

This project addresses the potential problem of radiation embrittlement of reactor pressure vessel (RPV) supports. Surveillance specimens irradiated at the High Flux Isotope Reactor (HFIR) at relatively low neutron flux levels (about 1.5E+8 $cm^{-2} \cdot s^{-1}$) and low temperature (about 50°C) showed embrittlement more rapidly than expected. Commercial power reactors have similar flux levels and temperatures at the vessel support structures. The purposes of this work are to provide the neutron fluence spectra data that are needed to evaluate previously measured mechanical property changes in the HFIR, to explain the discrepancies in neutron flux levels between the nickel dosimeters and two other dosimeters, neptunium and beryllium, and to address any questions or peculiarities of the HFIR reactor environment.

12. KEY WORDS/DESCRIPTORS (List words or phrases that will assist researchers in locating the report.)
neutron spectra
High Flux Isotope Reactor (HFIR)
radiation embrittlement
reactor pressure supports
pressure vessel surveillance

13. AVAILABILITY STATEMENT
unlimited

14. SECURITY CLASSIFICATION
(This Page)
unclassified
(This Report)
unclassified

15. NUMBER OF PAGES

16. PRICE

NRC FORM 335 (2-89)